

**PHYTO-MEDIATED SYNTHESIS OF ZINC OXIDE NANOPARTICLES,
EVALUATION OF THEIR PHYSICO-CHEMICAL PROPERTIES AND
CELLULAR EFFECTS IN COMPARISON WITH THE CHEMICALLY
SYNTHESIZED COMMERCIAL VERSION**

*Thesis submitted to University of Calicut
in partial fulfillment of the requirement for the award of*

**Doctor of Philosophy
in
Biotechnology**

By

AHLAM ABDUL AZIZ



**DEPARTMENT OF BIOTECHNOLOGY
UNIVERSITY OF CALICUT
2020**

**DEPARTMENT OF BIOTECHNOLOGY
UNIVERSITY OF CALICUT**

Certificate

This is to certify that the Thesis entitled “**Phyto-mediated synthesis of zinc oxide nanoparticles, evaluation of their physico-chemical properties and cellular effects in comparison with the chemically synthesized commercial version**” submitted to University of Calicut, as partial fulfillment of Ph.D. programme for the award of the degree of Doctor of Philosophy in Biotechnology by **Ahlam Abdul Aziz.**, embodies the results of bonafide research work carried out by her under my guidance and supervision at the Department of Biotechnology, University of Calicut. This Thesis has not previously formed the basis for the award of any degree, diploma, associateship, fellowship or other similar titles or recognition. The candidate has passed the course work of the Ph.D. Program in accordance with the UGC regulation.

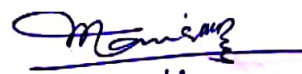
C.U Campus

Date:

Dr. P. R. Manish Kumar
(Research Supervisor)
Professor,
(Former Head and Coordinator)
Department of Biotechnology
University of Calicut
Kerala - 673635

Certificate

It is hereby certified that the Doctoral Thesis of Ms Ahlam Abdul Aziz submitted herewith, following adjudication, does not carry modification/correction(s) since the Evaluation Reports are bereft of any such comments or suggestions.



Prof.(Dr.) P.R. Manish Kumar (Retd.)
Department of Biotechnology
University of Calicut
(Research Supervisor)

09.10.2020
CU Campus, Thenhipalam

DECLARATION

I hereby declare that the work presented in the Thesis entitled “**Phyto-mediated synthesis of zinc oxide nanoparticles, evaluation of their physico-chemical properties and cellular effects in comparison with the chemically synthesized commercial version**” submitted to the University of Calicut, as partial fulfillment of Ph.D. programme for the award of the degree of Doctor of Philosophy in Biotechnology, is original and carried out by me under the supervision of Prof. (Dr.) P. R. Manish Kumar, Department of Biotechnology, University of Calicut. This has not been submitted earlier either in part or full for any degree or diploma of any university.

C.U Campus
Date :

Ahlam Abdul Aziz

ACKNOWLEDGEMENTS

First and foremost, I praise and thank God Almighty, most Gracious, most Merciful, for providing me with this great opportunity and showering me with blessings throughout my research period and beyond. I am grateful to Thee for health, strength, ability, knowledge and perseverance bestowed upon me without which this achievement wouldn't have been possible.

I place on record my heartfelt and sincere thanks to my supervisor, Prof. (Dr.) P. R. Manish Kumar for this precious opportunity to work under him. I express my gratefulness for grooming, guiding, encouraging and moulding me not only to a better researcher but to a better individual. He has been always there as an inspiration throughout my years of research and I thank him profusely, for mentoring and pushing me through all my research hardships. Without his yogic and thoughtful guidance, constructive criticism and timely interferences, Ph.D. would still have been a dream to me. Apart from contributions of time and ideas, his careful editing has enhanced the shaping and presentation of this Thesis.

I express my gratitude to Prof. (Dr.) K. K. Elyas, Head of the department, for his encouragement and kindness. I thank the faculty members, Dr. V. B. Smitha, Mr. Gopinathan and the technical assistant Dr. Tara Menon, for their support.

I am grateful to Department of Science and Technology (Govt. of India) for providing me with financial assistance by way of INSPIRE fellowship which aided me to pursue my doctoral research.

My love and respect to dear Jayasree madam, for her motherly presence and emotional support during the tenure of research. Thank you madam for the epitome of love and support you are in Manish sir's life, motivating each of us to be better and strong individuals and life partners.

I am indebted to my seniors, Lakshmi chechi, Rajettan and Nithya chechi, for their warmth and affection.

Words fail to express my love to Shanibatha and Manju chechi for being the pillars of support and motivation throughout my research period. You both are not just labmates to me, you are like elder sisters and your families hold a special place in my heart for you stood by me through joy and despair.

I also thank my beloved labmates Soumya T, Jobish Joseph and Meghna Sudhesh for their help, love, care and mental support especially during the final strains of this Thesis work. Thank you Soumya, for clearing my doubts and also for your practical advices. Thanks to Meghna for your technical support and Jobish for your timely help.

I owe thanks to all other research scholars of the department for making my research life lively and fun-filled. Thank you Dr. Anusha T, Dr. Manju Mohan, Dr. Deepthi V. C., Dr. Deepthi Madayi, Dr. Megha K. B., Faisal Moosa, Remya Johny, Tancia Rosalin, Nidheesh Roy, Surya P. H., Suhana and Anju V. V. for all the encouragement and academic support as well.

Extending my sincere appreciation to all members of non teaching staff of the department: Iqbalkka - our librarian, Biju sir - section officer, Srikanth sir and Sudheesh sir – section assistants, Lalitha chechi and Shambhu chettan – lab attenders and Shine chettan – office attendant, for all technical help given to me my research tenure. Remembering all the PG students who came and made friends with me and gave me such good memories. I especially thank Mrs. Anjana Ratheesh, former student of our department, for providing plant samples used for my preliminary work .

I am grateful to the research scholars of our sister departments for all kinds of assistance provided to me. I would like to express my thanks to Dr. Sereena, Department of Life Sciences for helping with the microbial strains. Taking names of a hundred friends I made in-and-out of the University during my research would take pages, so, with immense pleasure to have befriended each of you I thank you for all the affection and positivity. I treasure each of you in the depths of my heart.

Words cannot express my affection to my neighbours who are like my family. Thank you Gracy aunty and Cleatus uncle, for taking care of me like a daughter, and Chikku and Kuttan for your sibling-like concern. Thanks to all my acquaintances at Kohinoor.

I acknowledge CSIF – University of Calicut, SEM facility – NIT Calicut, FACS facility – RGCB Trivandrum, STIC facility – CUSAT and the technical assistants for all the help provided. I also acknowledge Mr. Rajesh, Bina Photostat for assistance in formatting, printing and binding preparing this Thesis.

Family is the backbone for my every achievement in my life including the long course of research where I felt all the warmth from them. My dear Vappa Mr. Abdul Aziz, who is no more with us, was always a knowledge-seeker and encouraged his four daughters to be good in person through fruitful education. It was his dream that motivated me in doing research and on this occasion I am in tears to remember how much I am proud of being his daughter!! Ms. Majeetha, my sweet and inspiring Umma, is the firm pillar where I find all levels of support in all my ways of life. My loving sisters Ameena, Amal and Maryam, their husbands and kids are all beyond thanks and formalities for their untiring prayers, support, love and guidance. I am greatly and heavily indebted to my in-laws - Uppa, Umma, brothers, sisters and their huge family for their unconditional support, motivation and love they continue to provide to their daughter-in-law to fulfill her dreams.....Thanks to each and everyone of both families though they are worth much more!!

Words are too insufficient to express my thoughts on my love, my betterhalf, Saifuu, for being patient, calm and tolerant to our busy life at the University. Without your encouragement, I wouldn't have been able to enjoy the long years of research and without your loving concern and unanxious nature; I couldn't have tackle my pains not only in research, but my life in general. Love you my sweetheart for everything and my prayers are with you every moment.....

I can't stop my words without thanking the Almighty again and again for giving me all this precious opportunities to understand your grand design that brings me closer to you.....Alhamdulillah!!

Ahlam Abdul Aziz

CONTENTS

	Page No.
<i>List of Tables</i>	vi
<i>List of Figures</i>	viii
<i>Abbreviations</i>	xii
1. INTRODUCTION	1-9
1.1. Nanotechnology: Revolutionizing and integrating physico-chemical and biological sciences	1
1.2. Nanomaterial-based drug delivery	2
1.3. Nanotechnology in cancer ‘theranostics’ (therapeutics-diagnostics)	3
1.4. Zinc oxide nanoparticles	5
1.5. About this Thesis	6
1.5.1. Aims and Objectives	6
1.5.2. Thesis Layout	9
2. REVIEW OF LITERATURE	10-48
2.1. Nanoparticles : An overview	10
2.2. Zinc and Zinc oxide nanoparticles	12
2.3. Applications of zinc oxide nanoparticles	13
2.4. Synthesis of zinc oxide nanoparticles	17
2.4.1. Physical and chemical methods	18
2.4.2. Biological methods	19
2.4.3. Physico-chemical characterization of zinc oxide nanoparticles	23
2.5. Cancer	25
2.5.1. Hallmarks of cancer	27
2.5.2. Deregulation of cell cycle and apoptosis leads to cancer	28
2.5.3. Genetics and epigenetics in cancer	32
2.5.4. Cancer therapy	34
2.5.5. Cancer nanomedicine	39
2.6. Preliminary screening of plants employed for biosynthesis of zinc oxide nanoparticles	41
2.6.1. Ethnopharmacology of selected plants in brief :	44
2.6.1.1. <i>Spondias pinnata</i> (L. f.) Kurz.	44
2.6.1.2. <i>Manilkara zapota</i> (L.) P. Royen	45
2.6.1.3. <i>Annona muricata</i> (L.)	47

3. PHYTO-MEDIATED BIOSYNTHESIS AND PHYSICO-CHEMICAL CHARACTERIZATION OF ZnONPs	49-71
3.1. Introduction	49
3.2. Materials and methods	50
3.2.1. Biosynthesis of ZnONPs	50
3.2.1.1. <i>Preparation of plant extracts</i>	51
3.2.1.2. <i>Biosynthesis by sol-gel method</i>	51
3.2.2. Characterization	51
3.2.2.1. <i>X-ray diffraction (XRD) analysis</i>	51
3.2.2.2. <i>Field Emission Scanning Electron Microscopy (FESEM) & Energy Dispersive X-ray spectroscopy (EDX)</i>	52
3.2.2.3. <i>Fourier Transform Infrared (FTIR) spectroscopy</i>	52
3.2.2.4. <i>UV-visible (UV-vis) spectroscopy</i>	52
3.2.2.5. <i>Photoluminescence (PL) spectroscopy</i>	53
3.2.2.6. <i>High Resolution Transmission Electron Microscopy (HRTEM)</i>	53
3.3. Results and discussion	53
3.3.1. Phyto-assisted sol-gel synthesis of ZnONPs	53
3.3.2. Physico-chemical characterization	57
3.3.2.1. <i>X-ray diffraction (XRD) analysis</i>	57
3.3.2.2. <i>Field Emission Scanning Electron Microscopy (FESEM) & Energy Dispersive X-ray spectroscopy (EDX)</i>	59
3.3.2.3. <i>Fourier Transform Infrared (FTIR) spectroscopy</i>	62
3.3.2.4. <i>UV-Visible (UV-vis) spectroscopy</i>	66
3.3.2.5. <i>Photoluminescence (PL) spectroscopy</i>	68
3.3.2.6. <i>High Resolution Transmission Electron Microscopy (HRTEM)</i>	69
4. CELLULAR AND MOLECULAR INVESTIGATIONS TO ASSESS THE ANTICANCER POTENTIAL AND BIOCOMPATIBILITY OF PHYTO-DERIVED AND THE CHEMICALLY SYNTHESIZED ZnONPs	72-142
4.1. Introduction	72
4.2. Materials and methods	74
4.2.1. Chemicals and reagents	74
4.2.2. Human cancer cell lines employed in the present study	74
4.2.2.1. <i>Chronic myelogenous leukemic K562 cells</i>	75
4.2.2.2. <i>Colon carcinoma HCT 116 cells</i>	75
4.2.2.3. <i>Lung adenocarcinoma A549 cells</i>	76
4.2.2.4. <i>Culturing and maintenance of cell lines</i>	76

4.2.3. Cytotoxicity evaluation of ZnONPs against human cancer cells	77
4.2.3.1. <i>MTT assay</i>	77
4.2.3.2. <i>Trypan blue dye exclusion assay</i>	77
4.2.4. Clonogenic assay	78
4.2.5. Evaluation of cell death by microscopy	78
4.2.5.1. <i>Light microscopy</i>	78
4.2.5.2. <i>Scanning electron microscopy</i>	79
4.2.5.3. <i>Fluorescence microscopy</i>	79
4.2.5.3.1. <i>Hoechst 33258 staining</i>	79
4.2.5.3.2. <i>Acridine orange-ethidium bromide dual staining</i>	79
4.2.6. Assessment of intracellular biochemical changes: Reactive oxygen species (ROS), mitochondrial membrane potential (MMP) and Ca ²⁺ ion release	80
4.2.7. Flow cytometric analysis of apoptosis	80
4.2.8. Genotoxicity analysis	81
4.2.8.1. <i>Comet assay</i>	81
4.2.8.2. <i>DNA fragmentation</i>	81
4.2.9. Gene expression profiling by reverse transcription-quantitative polymerase chain reaction (RT - qPCR).	81
4.2.10. Protein immunoblot analysis	83
4.2.11. Cytotoxicity evaluation of ZnONPs against normal human cells	84
4.2.11.1. Peripheral blood-derived lymphocytes (hPBLs)	84
4.2.11.1.1. <i>MTT assay</i>	84
4.2.11.1.2. <i>Mitotic index (MI) analysis</i>	84
4.2.11.2. Erythrocytes	85
4.2.11.2.1. <i>Hemolysis</i>	85
4.2.12. Cytotoxicity evaluation of ZnONPs against plant cell model : <i>Allium cepa</i> L. root-tip cells	85
4.2.12.1. <i>Mitotic Index analysis and trypan blue viability assay</i>	85
4.3. Statistical analysis	86
4.4. Ethical statement	86
4.5. Results and discussion	86
I. Evaluation of Cytotoxicity of Phyto-Mediated and The Chemically Derived ZnONPs on Three Human Cancer Cell Lines –HCT 116, A549 AND K562.	86
4.5.1. <i>MTT assay</i>	86
4.5.2. <i>Trypan blue dye exclusion assay</i>	91
4.5.3. <i>Clonogenic assay</i>	91

4.5.4. Microscopic evaluation of cytotoxicity	95
4.5.4.1. <i>Light microscopy</i>	95
4.5.4.2. <i>Scanning electron microscopy (SEM)</i>	98
4.5.4.3. <i>Fluorescence microscopy</i>	101
4.5.4.3.1. <i>Hoechst 33258 staining</i>	101
4.5.4.3.2. <i>AO/EtBr dual-staining</i>	102
4.5.5. Effect of phyto-derived/chemical ZnONPs on release of intracellular Ca ²⁺ , generation of reactive oxygen species (ROS) and loss of mitochondrial membrane potential (MMP)	106
4.5.6. Flow cytometric (FACS) analysis of apoptosis	115
4.5.6.1. <i>Effect of ZnONPs on cell cycle progression</i>	115
4.5.6.2. <i>Effect of ZnONPs on phosphatidyl serine externalization</i>	121
4.5.7. Genotoxic effects of phyto-derived/chemical ZnONPs	124
4.5.7.1. <i>Comet assay</i>	124
4.5.7.2. <i>DNA fragmentation</i>	125
4.5.8. Gene expression analysis by Reverse Transcription-quantitative polymerase chain reaction (RT- qPCR).	127
4.5.9. Protein expression analysis by western blotting	132
II. Evaluation of Cytotoxicity / Biocompatibility of The Phyto-Mediated and The Chemically-Derived ZnONPs Employing Normal Human And Plant Cell Models	135
4.5.10. Effect of ZnONPs on human peripheral blood derived lymphocytes (hPBLs) and erythrocytes	135
4.5.11. Effect of ZnONPs on <i>Allium cepa</i> root-tips	139
5. EVALUATION OF MULTIFACETED PROPERTIES: PHOTOCATALYTIC, ANTIBACTERIAL AND DNA-INTERACTIVE POTENTIAL OF PHYTO-DERIVED AND THE CHEMICALLY SYNTHESIZED ZNONPS	143-159
5.1. Introduction	143
5.2. Materials and Methods	144
5.2.1. Photocatalytic dye degradation	144
5.2.2. Antibacterial activity	145
5.2.2.1. <i>Quantitative MIC-MBC determination</i>	145
5.2.2.2. <i>Qualitative well diffusion assay</i>	146
5.2.3. Biogenic ZnO-DNA interactions	146
5.2.4. Statistical analysis	147
5.3. Results and Discussion	147
5.3.1. Photocatalytic dye degradation	147
5.3.2. Antibacterial potential	151
5.3.2.1. <i>Quantitative MIC-MBC determination</i>	151

5.3.2.2. <i>Qualitative well diffusion assay</i>	152
5.3.3. Biogenic ZnO-DNA interactions	155
6. SUMMARY AND CONCLUSIONS	160-165
FUTURE PROSPECTS	165
REFERENCES	166-247
APPENDIX	i-ii
LIST OF PUBLICATIONS AND CONFERENCES	iii-vi

LIST OF TABLES

Table No.	Title	Page No.
2.1.	Anticancer activity of ZnONPs based nanoplateforms.	16
2.2.	Phyto-mediated biosynthesis of ZnONPs differing in size and morphology.	20
2.3.	Various physico-chemical techniques useful for characterization of nanoparticles.	23
2.4.	Botanical classification of plants used for screening of extracts for phyto-mediated synthesis of ZnONPs	42
3.1.	Optimization of factors affecting biosynthesis of phyto-derived zinc oxide nanoparticles.	54
3.2.	Zn and O atom compositional profile of EDX analysis	61
3.3.	Major FTIR peaks (in cm^{-1}) and vibration modes assigned for phyto-derived and chemical ZnONPs	65
4.1.	RT-qPCR primer sets used for quantification of relative gene expression	82
4.2.	IC ₅₀ values of phyto-derived/chemical ZnONPs against three human cancer cell lines	90
4.3.	Mean percentage fluorescence intensity of cells stained with intracellular Ca ²⁺ indicator Fluo 3-AM	108
4.4.	Dose-dependent variations in mean fluorescence intensity(%) of cells stained with ROS indicator DCFH-DA	110
4.5.	Mean fluorescence intensity of cells (%) stained with Rhodamine-123	114
4.6.	Cell cycle phase-specific distribution of HCT 116 cells following 48 h treatment with phyto-derived/chemical ZnONPs	117
4.7.	Cell cycle phase-specific distribution of A549 cells cycle following 48 h of treatment with phyto-derived/chemical ZnONPs	119
4.8.	Cell cycle phase-specific distribution of K562 cells following 48 h of treatment with phyto-derived ZnONPs	121
4.9.	The relative quantitation of mRNA expression of apoptosis-related genes using RT-qPCR in HCT 116 cells treated with phyto-derived/chemical ZnONPs	129
4.10.	The relative quantitation of mRNA expression of apoptosis-related genes using RT-qPCR in A549 cells treated with phyto-derived / chemical ZnONPs	130

4.11.	The relative quantitation of mRNA expression of apoptosis-related genes using RT-qPCR in K562 cells treated with phyto-derived ZnONPs	131
4.12.	MI and RMI of phyto-derived/chemical ZnONPs treated hPBLs	137
4.13.	MI and RMI of phyto-derived/chemical ZnONPs treated <i>Allium cepa</i> root-tips	139
5.1.	MIC and MBC values of phyto-/chemically derived ZnONPs	152
5.2.	Zone of Inhibition (in mm) demonstrating antibacterial activity	154

LIST OF FIGURES

Figure No.	Title	Page No.
1.1.	An outline of the research work presented in this Thesis	8
2.1.	Hallmarks of cancer	28
2.2.	Schematic representation of eukaryotic cell cycle	29
2.3.	Pathways of apoptosis	31
2.4.	miRNA replacement therapy	36
2.5.	<i>Spondias pinnata</i> (L. f.) Kurz.	45
2.6.	<i>Manilkara zapota</i> (L.) P. Royen	46
2.7.	<i>Annona muricata</i> (L.)	47
3.1.	Phyto-derived zinc oxide nanoparticles placed in a ceramic crucible.	55
3.2.	X-ray diffraction patterns of (a) AmFZnONPs (b) AmRZnONPs (c) AmSZnONPs (d) SpLZnONPs (e) MzLZnONPs and (f) cZnONPs [control NPs]	58
3.3.	FESEM images of (a) AmFZnONPs (b) AmRZnONPs (c) AmSZnONPs (d) MzLZnONPs (e) SpLZnONPs and (f) cZnONPs	60
3.4.	EDX spectrum of (a) AmFZnONPs (b) AmRZnONPs (c) AmSZnONPs (d) MzLZnONPs (e) SpLZnONPs and (f) cZnONPs	61
3.5.	FTIR spectra of (a) AmFZnONPs (b) AmRZnONPs (c) AmSZnONPs (d) MzLZnONPs (e) SpLZnONPs and (f) cZnONPs	64
3.6.	Uv-vis absorption spectrum of (a) AmFZnONPs (b) AmRZnONPs (c) MzLZnONPs (d) SpLZnONPs (e) AmSZnONPs and (f) cZnONPs	67
3.7.	Photoluminescence spectrum of (a) AmFZnONPs (b) AmRZnONPs (c) AmSZnONPs (d) SpLZnONPs (e) MzLZnONPs and (f) cZnONPs	69
3.8.	HRTEM images of (a) AmFZnONPs (b) AmRZnONPs (c) AmSZnONPs (d) MzLZnONPs (e) SpLZnONPs and (f) cZnONPs.	70
4.1.	Cytotoxicity evaluation of phyto-derived/chemical ZnONPs against HCT 116 cells for (a) 24 h (b) 48 h and (c) 72 h treatment period	87
4.2.	Cytotoxicity evaluation of phyto-derived/chemical ZnONPs against A549 cells for (a) 24 h (b) 48 h and (c) 72 h treatment period.	88

4.3.	Cytotoxicity evaluation of phyto-derived ZnONPs/chemical against K562 cells for (a) 24 h (b) 48 h and (c) 72 h treatment period.	89
4.4.	Trypan blue dye exclusion assay employing phyto-derived/chemical ZnONPs against (a) HCT 116 (b) A549 and (c) K562 cells	91
4.5.	Inhibition of colony forming capacity of HCT 116 cells on treatment with phyto-derived / chemical ZnONPs	92
4.6.	Inhibition of colony forming capacity of A549 cells on treatment with phyto-derived / chemical ZnONPs	93
4.7.	Inhibition of colony forming capacity of K562 cells on treatment with phyto-derived ZnONPs	94
4.8.	Light microscopic images showing cytomorphological changes in HCT 116 cells after 48 h treatment with (a) AmRZnONPs (b) SpLZnONPs (c) MzLZnONPs and (d) cZnONPs.	96
4.9.	Light microscopic images showing cytomorphological changes in A549 cells after 48 h treatment with (a) AmRZnONPs (b) SpLZnONPs (c) MzLZnONPs and (d) cZnONPs.	97
4.10.	Light microscopic images showing cytomorphological changes in K562 cells after 48 h treatment with (a) AmRZnONPs (b) SpLZnONPs and (c) MzLZnONPs	98
4.11.	Scanning electron microscopic images of HCT 116 cells treated with (a) AmRZnONPs (b) SpLZnONPs (c) MzLZnONPs and (d) cZnONPs.	99
4.12.	Scanning electron microscopic images of A549 cells after treatment with (a) AmRZnONPs (b) SpLZnONPs (c) MzLZnONPs and (d) cZnONPs.	100
4.13.	Scanning electron microscopic images of K562 cells after treatment with (a) AmRZnONPs (b) SpLZnONPs and (c) MzLZnONPs.	100
4.14.	Fluorescence microscopy images of Hoechst 33258 stained (a) HCT 116 (b) A549 and (c) K562 cells after treatment with (i) AmRZnONPs (ii) SpLZnONPs (iii) MzLZnONPs and (iv) cZnONPs	101
4.15.	Induction of apoptosis in HCT 116 cells on treatment with phyto-derived / chemical ZnONPs and stained with AO/EtBr	103
4.16.	Induction of apoptosis in A549 cells on treatment with phyto-derived / chemical ZnONPs and stained with AO/EtBr	104
4.17.	Induction of apoptosis in K562 cells on treatment with phyto-derived ZnONPs and stained with AO/EtBr	105
4.18.	Measurement of intracellular calcium release in cells treated with phyto-derived / chemical ZnONPs using Ca ²⁺ indicator Fluo 3-AM	107

4.19.	Measurement of ROS in HCT 116 cells treated with phyto-derived / chemical ZnONPs	109
4.20.	Measurement of ROS in A549 cells treated with phyto-derived/chemical ZnONPs	109
4. 21.	Measurement of ROS in K562 cells treated with phyto-derived ZnONPs	110
4. 22.	Measurement of mitochondrial membrane potential in HCT 116 cells treated with phyto-derived/chemical ZnONPs	112
4.23.	Measurement of mitochondrial membrane potential in A549 cells treated with phyto-derived / chemical ZnONPs	113
4.24.	Measurement of mitochondrial membrane potential in K562 cells treated with phyto-derived ZnONPs	113
4.25.	Histograms showing cell cycle distribution of HCT 116 cells following 48 h treatment with phyto-derived / chemical ZnONPs	116
4.26.	Histograms showing cell cycle distribution of A549 cells following 48 h of treatment with phyto-derived / chemical ZnONPs	118
4.27.	Histograms showing cell cycle distribution of K562 cells following 48 h of treatment with phyto-derived ZnONPs	120
4.28.	Apoptogenic effect of phyto-derived /chemical ZnONPs on HCT 116 cells after 48 h treatment and stained with annexin V / PI	122
4.29.	Apoptogenic effect of phyto-derived /chemical ZnONPs on A549 cells after 48 h of treatment at IC ₅₀ concentration and stained with annexin V / PI	123
4.30.	Apoptogenic effect of phyto-derived ZnONPs on K562 cells after 48 h treatment and stained with annexin V/PI	124
4.31.	Alkaline comet assay: Detection of DNA strand breaks following treatment with (i) AmRZnONPs (ii) SpLZnONPs (iii) MzLZnONPs and (iv) cZnONPs on (a) HCT 116 cells and (b) K562 cells.	125
4.32.	Analysis of DNA fragmentation induced by phyto-derived / chemical ZnONPs in HCT 116 and K562 cells	127
4.33.	Western blot analysis of apoptosis-related protein expression in HCT 116 cells following treatment with (a) AmRZnONPs (b) SpLZnONPs (c) MzLZnONPs and (d) cZnONPs	133
4.34.	Western blot analysis of apoptosis-related protein expression in A549 cells following treatment with (a) AmRZnONPs (b) SpLZnONPs (c) MzLZnONPs and (d) cZnONPs	134
4.35.	Western blot analysis of apoptosis-related protein expression in K562 cells following treatment with (a) AmRZnONPs (b) SpLZnONPs and (c) MzLZnONPs	135

4.36.	Cytotoxicity evaluation of phyto-derived / chemical ZnONPs against hPBLs.	136
4.37.	Cytotoxicity against hPBLs studied by preparation of Giemsa stained metaphase spread	137
4.38.	Morphological evaluation of erythrocytes stained with Giemsa	138
4.39.	Cytotoxicity of ZnONPs against <i>A. cepa</i> root-tip cells	140
4.40.	Trypan blue staining of <i>A. cepa</i> roots	141
5.1.	(A) Pictorial and (B) graphical representation of photocatalytic dye degradation of methylene blue by biosynthesized ZnONPs following exposure to sunlight at (a) 0 h (b) 1 h (c) 3 h (d) 5 h and (e) 5 h (methylene blue control)	148
5.2.	Photocatalytic methylene blue dye degradation at time intervals of 1, 3 and 5 h by (a) AmFZnONPs (b) AmRZnONPs (c) AmSZnONPs (d) SpLZnONPs (e) MzLZnONPs and (f) cZnONPs	149
5.3.	Panels of images depicting antibacterial activity of (a) AmFZnONPs (b) AmRZnONPs (c) AmSZnONPs (d) SpLZnONPs and (e) MzLZnONPs against four clinical bacterial isolates employing Kirby-Bauer well diffusion assay.	153
5.4.	Interaction of Plasmid DNA-pUC18 (0.2 µg/µL) with (a) AmFZnONPs (b) AmRZnONPs (c) AmSZnONPs (d) SpLZnONPs (e) MzLZnONPs and (f) cZnONPs	157
5.5.	Interaction of λ DNA (0.3 µg/µL) with (a) AmFZnONPs (b) AmRZnONPs (c) AmSZnONPs (d) SpLZnONPs (e) MzLZnONPs and (f) cZnONPs	158
5.6.	Interaction of 100 bp ladder DNA (0.5 µg/µL) with (a) AmFZnONPs (b) AmRZnONPs (c) AmSZnONPs (d) SpLZnONPs (e) MzLZnONPs and (f) cZnONPs	159

ABBREVIATIONS

4D	:	4 dimension
μm	:	Micrometer
μL	:	Microliter
μg	:	Microgram
ADP	:	Adenosine di-phosphate
AFM	:	Atomic force microscopy
ALK	:	Anaplastic lymphoma kinase
ALP	:	Alkaline phosphatase
AmF	:	<i>Annona muricata</i> fruit
AmFZnONP(s)	:	<i>Annona muricata</i> fruit zinc oxide nanoparticle(s)
AML	:	Acute myeloid leukemia
AmR	:	<i>Annona muricata</i> root
AmRZnONP(s)	:	<i>Annona muricata</i> root zinc oxide nanoparticle(s)
AmS	:	<i>Annona muricata</i> seed
AmSZnONP(s)	:	<i>Annona muricata</i> seed zinc oxide nanoparticle(s)
ANOVA	:	Analysis of variance
AO	:	Acridine orange
APAF1	:	Apoptotic protease activating factor 1
ATM	:	Ataxia telangiectasia mutated
ATP	:	Adenosine tri-phosphate
ATR	:	Attenuated total reflection
a.u.	:	Arbitrary units
B.C	:	Before Christ
BAK	:	Bcl ₂ homologous antagonist/killer
BAX	:	Bcl ₂ associated X protein
BCIP	:	5-Bromo-4-chloro-3-indolyl phosphate
BCIP/NBT	:	5-bromo-4-chloro-3-indolyl-phosphate/nitro blue tetrazolium
BCL ₂	:	B-cell lymphoma 2
BCR/ABL	:	Breakpoint cluster region – Abelson
BER	:	Base excision repair
BET	:	BF-TEM electron tomography
BF – TEM	:	Bright field - Transmission electron microscopy
BH3	:	Bcl ₂ homology 3
BIR	:	Baculovirus IAP repeat
bp	:	base pair
BRCA	:	Breast cancer gene
BSA	:	Bovine serum albumin
Cas-3	:	Caspase-3

Cas-8	:	Caspase-8
Cas-9	:	Caspase-9
CC	:	Carbon – Carbon
CO	:	Carbon – Oxygen
CAD	:	Caspase activated DNase
CAR	:	Chimeric antigen receptor
CCl ₄	:	Carbon tetrachloride
CDK	:	Cyclin dependent kinase
cDNA	:	Complementary DNA
CH	:	Carbon – Hydrogen
Chk	:	Checkpoint kinase
CLSI	:	The clinical and laboratory standards institute
cm	:	Centimeter
CN	:	Carbon – Nitrogen
CNT	:	Carbon nanotube
COOH	:	Carboxyl group
CO ₂	:	Carbon dioxide
CRISPR	:	Clustered regularly interspaced short palindromic repeats
CTL	:	Cytotoxic T lymphocyte
CYT	:	Cyt Immune Sciences
Cyt <i>c</i>	:	Cytochrome <i>c</i>
cZnONP(s)	:	Chemically synthesized zinc oxide nanoparticle(s)
DCFH-DA	:	Dichloro-dihydro-flourescien diacetate
DISC	:	Death inducing signaling complex
DLS	:	Dynamic light scattering
DM	:	Dichloromethane
DMEM	:	Dulbecco’s Modified Eagle’s Medium
DMF	:	N, N-dimethylformamide
DMSO	:	Dimethyl sulfoxide
DNA	:	Deoxyribonucleic acid
dNTP	:	Deoxy-nucleotide triphosphate
DRS	:	Diffuse reflectance spectroscopy
DTT	:	Dithiothreitol
EBV	:	Epstein–Barr virus
EDTA	:	Ethylenediaminetetraacetic acid
EDX	:	Energy dispersive X-ray
EELS	:	Electron energy-loss spectroscopy
EGF	:	Epidermal growth factor
EGFR	:	Epidermal growth factor receptor
ELISA	:	Enzyme-linked immune sorbent assay
EPA	:	Environment protection agency

EPR	:	Enhanced permeability and retention
EPR	:	Enhanced retention and permeation
ER	:	Endoplasmic reticulum
ERK	:	Extracellular signal regulated kinase
EtBr	:	Ethidium Bromide
eV	:	Electron volt
FACS	:	Fluorescence-activated cell sorting
FAK	:	Focal adhesion kinase
FBS	:	Fetal bovine serum
FDA	:	Food and drug administration
FESEM	:	Field-emission scanning electron microscopy
FTIR	:	Fourier-transform infrared spectroscopy
FWHM	:	Full width at half maximum
g	:	Gram(s)
GAE	:	Gallic acid equivalents
GAPDH	:	Glyceraldehyde 3-phosphate dehydrogenase
GLUT	:	Glucose transporter
GRAS	:	Generally recognized as safe
h	:	Hour(s)
H ₂ O ₂	:	Hydrogen peroxide
HAA	:	Heterocyclic aromatic amine
HAADF – STEM	:	High-angle dark-field scanning Transmission electron microscopy
HCl	:	Hydrochloric acid
HCV	:	Hepatitis C virus
HIV	:	Human influenza virus
hPBL	:	Human peripheral blood lymphocyte
HPV	:	Human papilloma virus
HRTEM	:	High resolution transmission electron microscopy
HTLV	:	Human T-cell leukemia-lymphoma virus
IAP	:	Inhibitors of apoptosis proteins
IC	:	Inhibitory concentration
ICDD	:	International centre for diffraction data
ICU	:	Intensive care unit
IFN	:	Interferon
IL	:	Interleukin
JCPDS	:	Joint committee on powder diffraction standards
JNK	:	Janus kinase
KBr	:	Potassium bromide
KCl	:	Potassium chloride
kDa	:	Kilodalton

KSHV	:	Kaposi's sarcoma-associated herpes virus
kV	:	KiloVolt
LB	:	Luria bertani
lncRNA	:	Long non-coding RNA
mA	:	Milliampere
MB	:	Methylene blue
MBC	:	Minimum bactericidal concentration
MCF-7	:	Michigan cancer foundation-7
mcg	:	Microgram
MCV	:	Molluscum contagiosum virus
MDM	:	Mouse double minute
MDR	:	Multiple drug resistance
mg	:	Microgram
MHC	:	Major histocompatibility complex
MI	:	Mitotic index
MIC	:	Minimum inhibitory concentration
min	:	Minutes
miRNA	:	MicroRNA
mL	:	Milliliter
mm	:	Millimeter
mM	:	Millimolar
M-MLV	:	Moloney murine leukemia virus
MMP	:	Mitochondrial membrane potential
MMR	:	Mismatch repair
MMSET	:	Multiple myeloma SET domain
MO	:	Methyl orange
mRNA	:	Messenger RNA
mTOR	:	Mammalian target of Rapamycin
MTT	:	3-(4, 5- dimethylthiazol-2-yl)-2, 5- diphenyltetrazolium bromide
MzL	:	<i>Manilkara zapota</i> leaf
MzLZnONP(s)	:	<i>Manilkara zapota</i> leaf zinc oxide nanoparticle(s)
N	:	Normality
Na ₂ CO ₃	:	Sodium carbonate
NaBH ₄	:	Sodium borohydride
NaCl	:	Sodium chloride
NaOH	:	Sodium hydroxide
NBT	:	Nitro blue tetrazolium
NCCS	:	National Centre for Cell Sciences
ncRNA	:	Non-coding RNA
NER	:	Nucleotide excision repair

NK cells	:	Natural Killer cells
nm	:	Nanometer
nM	:	Nanomolar
NO	:	Nitric oxide
NP	:	Nanoparticle(s)
NSCLC	:	non-small-cell lung carcinoma
°C	:	Degree Celsius
oc	:	Open circular
OD	:	Optical density
OH	:	Oxygen – Hydrogen
O _i	:	Interstitial oxygen
PAGE	:	Polyacrylamide gel electrophoresis
PALB	:	Partner and localizer of BRCA
PANI	:	Polyaniline
PARP	:	Poly (ADP-ribose) polymerase
PBS	:	Phosphate buffered saline
PbS	:	Lead sulphide
PC	:	Prostate cancer
PCR	:	Polymerase Chain Reaction
PEG	:	Poly-ethylene glycol
PHA	:	Phytohaemagglutinins
PI	:	Propidium iodide
PL	:	Photoluminescence
PS	:	Phosphatidyl serine
PTEN	:	Phosphatase and tensin homolog
PUMA	:	p53 upregulated modulator of apoptosis
PVDF	:	Polyvinylidene fluoride or polyvinylidene difluoride
RB	:	Retinoblastoma
RBC	:	Red blood cell
RH-123	:	Rhodamine 123
RIPA	:	Radioimmunoprecipitation assay
RMI	:	Relative mitotic index
RNA	:	Ribonucleic acid
RNS	:	Reactive nitrogen species
ROS	:	Reactive oxygen species
RPMI	:	Roswell Park Memorial Institute medium
RT-qPCR	:	Reverse Transcription-quantitative polymerase chain reaction
SAED	:	Selected area electron diffraction
sc	:	Supercoiled
SD	:	Standard deviation
SDS-PAGE	:	Sodium dodecyl sulfate - polyacrylamide gel electrophoresis

SEM	:	Scanning electron microscopy
siRNA	:	Short interfering RNA
SL	:	Synthetic lethality
SPION	:	Superparamagnetic iron-oxide nanoparticles
SpL	:	<i>Spondias pinnata</i> leaf
SpLZnONP(s)	:	<i>Spondias pinnata</i> leaf zinc oxide nanoparticle(s)
SPR	:	Surface Plasmon Resonance
SPSS	:	Statistical package for the social sciences
SRL	:	Sisco research laboratories
TBA	:	Tert-butyl alcohol
TBS	:	Tris-buffered saline
TBST	:	Tris-buffered saline containing Tween 20
TCA	:	Tri-chloro acetic acid
TE	:	Tris EDTA
TEM	:	Transmission electron microscopy
TG-DTA	:	Thermogravimetric differential thermal analysis
TNF	:	Tumor necrosis factor
TRIS	:	2-amino-2 hydroxy methyl-propane-1-3- diol
USA/US	:	United States of America
UV – Vis	:	Ultra Violet - Visible
UV	:	Ultra violet
V	:	Volt
v/v	:	volume/volume
VEGF	:	Vascular endothelial growth factor
VPT	:	Vapor phase transport
W	:	Watt
w/v	:	Weight/volume
WHO	:	World Health Organisation
XPS	:	X-ray photoelectron spectroscopy
XRD	:	X-ray diffraction
Zn _i	:	Interstitial zinc
ZnONP(s)	:	Zinc oxide nanoparticle(s)

APPENDIX

Annexin V – FITC binding buffer (pH 7.4)

HEPES	10mM
Nacl	140 mM
Cacl ₂ 2 H ₂ O	25 mM

Blotting buffer

Tris base	3.03 g
Glycine	14.4 g
Methanol	200 ml

Cold fresh lysis solution (pH 10)

Nacl	2.5 M
EDTA	100 mM
Tris buffer	10 mM
Triton X-100	1%

Cold electrode buffer (pH > 13)

EDTA	1 mM
NaOH	300 mM

DMEM

DMEM powder	13.4 g
FBS	10 % v/v
Streptomycin	100 µg/ml
Penicillin	100 U/ml
Sodium bicarbonate	3.7 g

Ethidium bromide

0.25 µg/ml

FACS staining solution

Triton X-100	0.1%
DNase free RNase A	2 mg/ml
Propidium iodide	500 µg/ml

LB (Luria Bertani) media

Tryptone (w/v)	10g
NaCl (w/v)	10g
Yeast extract (w/v)	5g
Water to 1 litre	

For LB agar add 2% (w/v) agar

Phosphate buffered saline (PBS)

NaCl	8 g
KCl	0.2 g
Na ₂ HPO ₄	1.44 g
KH ₂ PO ₄	0.24 g

RIPA buffer

NP -40	1 %
Na- deoxycholate	2.5 g
SDS	0.1 %
NaCl	150 mM
EDTA	2 mM
NaF	50 mM

RPMI – 1640 medium

RPMI powder	10.4 g
FBS	10% v/v
Sodium bicarbonate	2 g
Streptomycin	100 µg/ml
Penicillin	100 U/ml

TBE (1000 ml)

Tris base	54 g
Boric acid	27.5 g
EDTA (0.5 M)	20 ml

TE (pH 8)

Tris-Cl	10 mM
EDTA	1 mM

Tris-buffered saline (TBS) (pH 7.5)

Tris – HCl	100 mM
NaCl	0.9%

LIST OF PUBLICATIONS

Publications from doctoral Thesis

1. **Ahlam Abdul Aziz**, V. S. Shaniba, P. R. Jayasree . P. R. Manish Kumar (2019) Physico-chemical, photocatalytic and cytotoxicity evaluation of *Annona muricata* L. fruit extract derived zinc oxide nanoparticles in comparison to the commercial chemical version. **Current Science**, 117(9). 1492 – 1504. [Indian Academy of Sciences, Impact factor-0.756]
2. **Ahlam Abdul Aziz**, V. S. Shaniba, P. R. Jayasree . P. R. Manish Kumar. Enhanced anticancer activity of *Spondias pinnata* leaf-mediated zinc oxide nanoparticles on colon carcinoma HCT 116 cells. **(To be Communicated)**
3. **Ahlam Abdul Aziz**, V. S. Shaniba, P. R. Jayasree . P. R. Manish Kumar. Apoptosis induction on HCT 116 and K562 cells by *Manilkara zapota* leaf-mediated zinc oxide nanoparticles. **(To be Communicated)**

Other Publications

1. Shaniba, V. S., **Aziz A.A.** & Kumar, P.R.M. Phyto-mediated synthesis of silver nanoparticles from *Annona muricata* fruit extract, assessment of their biomedical and photocatalytic potential. IJPSR, Vol 8. Issue 1 (2017) ISSN 0975-8232.
2. Shaniba V.S, **Ahlam Abdul Aziz**, Jayasree, P.R. and Manish Kumar P.R.(2019) ‘*Manilkara zapota*(L.) P. Royen leaf extract derived silver nanoparticles induce apoptosis in human colorectal carcinoma cells without affecting human lymphocytes or erythrocytes’. Biological Trace Element Research (Springer Nature) – Published online on Mar 8. 2019; doi: 10.1007/s12011-019-1653-6. [Thomsun & Reuters IF – 2.361]
3. V. S. Shaniba, **Ahlam Abdul Aziz**, Jobish Joseph, P. R. Jayasree, and P. R. Manish Kumar. Book Chapter (accepted) entitled ‘Selective Targeting of

Human Colon Cancer HCT 116 Cells by PhytoMediated Silver Nanoparticles’ – under Pharmaceutical Science and Technology series – Natural Products Chemistry (Academic Apple Press Inc. USA) – in production – Publ. - May 2020

Conferences

1. **Ahlam Abdul Aziz**, Shaniba V. S and Manish Kumar P.R. Sol-gel synthesis and characterization of zinc nanoparticles from leaves of *Annona muricata*. Kerala Science Congress, Alappuzha, January 27-31, 2015
2. **Ahlam Abdul Aziz**, Shaniba V. S and Manish Kumar P.R. Characterization and in vitro analysis of zinc nanoparticles fabricated using graviola root extracts, International conference on nanostructured polymeric materials and polymer nanocomposites, MG University, kottayam, November 13-15, 2015.
3. **Ahlam Abdul Aziz**, Shaniba V. S and Manish Kumar P.R. Phytomediated synthesis of photocatalytically active zinc oxide nanoparticles from fresh flowers of *Cassia fistula* International conference on advances in functional materials (ICAFM) Anna University, Chennai, Jan 6-8, 2017
4. **Ahlam Abdul Aziz**, Shaniba V. S and Manish Kumar P.R. Photocatalytic dye degradation and enhanced biopotentials of *Annona muricata* mediated zinc oxide nanoparticles National seminar on emerging trends in chemical research, Christ college, Irinjalakuda 28 Feb- 1 Mar 2017
5. **Ahlam Abdul Aziz**, Shaniba V.S. and Manish Kumar P.R. An in vitro evaluation of phyto-derived zinc nanoparticles as a promising anti-cancer drug. National level conference on “Reaching the unreached through science and technology- concepts, principles and application of science and technology for Nation Building” Kongunadu Arts and Science College, Coimbatore, October 9-11, 2017 (**Best paper award**).
6. **Ahlam Abdul Aziz**, Shaniba V S, Jayasree P R and Manish Kumar P. R. Synthesis, characterization and in-lab assessment of biofunctionalized zinc

oxide nanostructures. International Symposium on nanomaterials for clean energy and Health Applications, CIT, Coimbatore December 6-8,2017,

7. **Ahlam Abdul Aziz**, Shaniba V.S. and Manish Kumar P.R. Genomic level interaction of biogenic zinc oxide nanostructures on prokaryotic and eukaryotic cell systems. 3rd International conference on Academic and Industrial Innovations: Transitions in Pharmaceutical, Medical and Biosciences (INNOPHARM 3), Kala Academy, Goa, October 22-23,2018. **(Second Prize)**.
8. **Ahlam Abdul Aziz**, Shaniba V.S., Manish Kumar P.R. Antimicrobial and antiproliferative potential of phyto-mediated zinc oxide nanostructures synthesized employing *Annona muricata* L. CRDB-2019 - International Conference on Research and Development in Biosciences held at Department of Biotechnology and Microbiology, Kannur University on January 17-19, 2019.

Other Conferences

1. Shaniba V. S., **Ahlam Abdul Aziz** and Manish Kumar P. R. (2014). Green synthesis of silver nano particles from *Annona muricata* root extract and its antimicrobial activity. International Conference on Biosciences – State-of-the-art Advancements (Proceedings of the Society for Education and Scientific Research), Sept. 11 – 12. Kottayam. P. 76.
2. Shaniba, V.S., **Aziz A.A.** & Kumar, P.R.M. (2015) Biosynthesis of Silver nanoparticles using *Annona Muricata* fruit extract and assessment of its reducing power, International conference on Nanostructured Polymeric Materials and Polymer Nanocomposites, M.G. University, Kottayam. Nov 13-15.
3. Shaniba V.S, **Ahlam Abdul Aziz.** & Kumar, P.R.M. (2015) Green synthesis and Characterization of silver nano particles from *Manikara zapota* leaf broth. UGC sponsored National level conference on sustainable Biotechnology, E.M.E.A College of Arts and Science, Kondotti. Dec 16-17.

4. Shaniba V.S, **Ahlam Abdul Aziz** & Kumar, P.R.M. (2017). Green synthesis of silver nanoparticles employing Manikara zapota leaf extract and evaluation of their antioxidant activities. International Conference on Advances in Functional Materials (ICAFM 2017). Anna University, Chennai, 6-8th Jan.
5. Shaniba V.S, **Ahlam Abdul Aziz** and Dr. P.R. Manish Kumar (2017) Investigations on the biomedical potential of green synthesized silver nanoparticles. National seminar on emerging trends in chemical research, Christ college, Irinjalakuda 28 Feb- 1 Mar.
6. Shaniba V.S, **Ahlam Abdul Aziz**, Dr. P. R Jayasree and Dr. P.R. Manish Kumar. (2017). Annona muricata root extract-mediated biomimetic synthesis of silver nanoparticles: Characterization and biomedical applications. 27th Swadeshi Science Congress held at Amrita Viswa Vidyapeetham, Amrita University, Kollam. 07-09 November 2017
7. Shaniba V.S, **Ahlam Abdul Aziz**, Dr. P. R Jayasree and Dr. P.R. Manish Kumar. (2018). Green synthesis of silver nanoparticles from Manikara zapota leaf extract and in-vitro evaluation of its biological activities. International conference on emerging trends in agriculture, food processing, engineering and Biotechnology held at Karunya institute of technology & science, Coimbatore, 21-23 February 2018.
8. Shaniba V.S, **Ahlam Abdul Aziz**, Dr. P. R Jayasree and Dr. P.R. Manish Kumar. (2018) Apoptogenic potential of biosynthesized silver nanoparticles on Human colon cancer HCT116 cell line. 30th Kerala Science Congress, Govt. Brennen College, Thalassery, 28-30 January, 2018.

INTRODUCTION

1.1. Nanotechnology: Revolutionizing and integrating physico-chemical and biological sciences

Nanotechnology is a tremendously growing revolution of science dealing with the engineering and manipulating of nanomaterials of distinct size. Nanoparticles (NPs) are particles possessing unique physico-chemical characteristics, different from those of its bulkier counterparts, attributable to its finer size below 100 nm and surface properties. Any substance having one or more dimension in nanoscale is considered to be a nanomaterial (Singh et al., 2017; Khan et al., 2017; Fawcett et al., 2017). The use of nanoparticles with exciting multifaceted properties is known to date back to almost 4500 years in human history. They are generated in living systems or abiotic systems through natural calamities and also can be synthesized chemically/biochemically in laboratories (Heiligtag and Niederberger, 2013). Due to their intrinsic physico-chemical nature, they are utilized in diverse fields such as biomedical, pharmaceutical, energy science, textile, food, health care, opto-electronics, cosmetics and so on (Nasrollahzadeh et al., 2019). This multifunctional particle based technology works on a supra-molecular level enabling creation of novel products useful for man and his environment. The technology is being used advantageously in the realm of therapeutic applications such as tailoring of nanodrugs with functional components and utilization of their unique/selective electromagnetic properties to distinguish between pathological and normal tissues (Wolfram and Ferrari, 2019). Within biological environments, macromolecules such as proteins bind to the surfaces of NPs, leading to the formation of a ‘corona’. These interactions can modify the physico-chemical properties of NPs, which then determine the elicited physiological responses including cellular uptake, distribution, bioavailability and toxicity, thereby regenerating a particle with a ‘new biological identity’ with altered therapeutic efficacy (Roberti et al., 2019).

1.2. Nanomaterial-based drug delivery

The use of intact natural bioactive compounds as drugs is beset with many difficulties such as poor specificity, induction of drug resistance and overdose. Nanodrug delivery platforms overcome these inefficiencies by providing target-specific drug delivery with biocompatibility and enhanced drug loading efficiency. Broadly, the smart nanodrug-carriers can be classified into (i) organic, polymer based and (ii) inorganic, metallic nanocarriers (Lombardo et al., 2019). The former include self-assembly amphiphiles and synthetic nanostructures such as micelles, multilamellar liposomes, solid lipid, dendrimers as well as carbon nanotubes, whilst inorganic carriers comprise of quantum dots, mesoporous silica, gold nanoparticles, superparamagnetic iron-oxide nanoparticles (SPION). Natural biopolymeric nanomaterials like chitosan, alginate, cellulose and xanthan gum are also widely used. Chitosan has found use in ocular drugs with muco-adhesive properties and also possesses good antibacterial activity, whilst alginate nanoparticles have been used as a carrier for venlafaxine, treating depression via intranasal administration (Haque et al., 2012; Patra et al., 2018). Liposomes are also used as promising nanocarriers to deliver hydrophobic, hydrophilic, charged drugs along with ligands such as antibodies anchored to them which enable site-specificity and improve distribution in the cells due to their similarity in membraneous structure. Encapsulation of hydrophobic drugs like camptothecin, paclitaxel in the hydrophobic core of polymeric micelles have been shown to boost drug penetrability due to their small size and hydrophilic shell structure (Wakaskar, 2017). Quantum dots are active semiconductors useful both as drug carriers as well as for fluorescent labeling (Mirza and Siddiqui, 2014). Gold nanoparticles have proven to be an excellent metallic nanocarrier with monolayer tunability capable of covalent and non-covalent interaction with drug (Calixto et al., 2016). However, the advent of DNA as a tool for drug delivery is a great footstep in this emerging technology. DNA is inherently biocompatible and biodegradable which can be used as nanostructures using immobile holiday junction technology as demonstrated by Seeman's oligonucleotide tile-based bottom-up approach, Rothemund's DNA origami approach, as well as Yin's single-stranded tile approach. DNA-modified

magnetic nanoconjugates have been used for detection and suppression of RNA markers recently (Bakshi et al., 2019). DNA nanostructures are not only capable of carrying and delivering small fluorescent molecules for imaging and therapy but can also incorporate molecular entities such as siRNA, microRNA, aptamers, CpG-rich sequences including CRISPR/Cas9 system (Hu et al., 2019). CRISPR/Cas9 is one of the biggest recent biotechnological innovations in precision genome-editing, which has opened up new avenues of drug discovery and therapeutic interventions.

1.3. Nanotechnology in cancer ‘theranostics’ (therapeutics-diagnostics)

Cancer can be briefly explained as a group of diseases caused by immortal growth of healthy cells into tumours due to failure in the inherent control of an individual’s ‘programmed cell death’. Cancer ‘theranostics’ blends therapeutics and diagnostics under a single platform fostering targeted and personalized treatment employing molecular and genetic backgrounds (Arruebo et al., 2011; Aoun et al., 2015). Under the current scenario of increasing global cancer burden of 18.1 million new cases and 9.6 million deaths (incidence - one in 5 of men and 6 of women; death - one in 8 men and 11 women), this combinatorial approach of therapeutics and diagnostics makes perfect sense. The second major cause of global death is due to cancer - the first being cardiovascular diseases - with men afflicted majorly by lung, prostate, colorectal, stomach and liver cancers whilst women are observed to develop breast, colorectal, lung, cervix and thyroid cancers (WHO, 2018).

Conventional cancer treatment regimes comprising of diagnosis, imaging, surgical removal of tumour including radio/chemotherapies, however, have not been found to be completely successful. Therapeutic failure is attributable to poor pharmacokinetics, adverse non-specific side-effects of radiations/chemotherapeutic drugs on healthy cells and even development of multidrug resistance due to heterogeneity of cancer cells. Likewise, complete removal of tumours/cancer cells often becomes practically impossible through surgery which becomes a total failure following onset of metastasis (Pérez-Herrero and Fernandez-Medarde, 2015; Wang et al., 2015; Mansoori et al., 2017; Hamed et al., 2019). Many of these demerits of cancer therapeutic strategies are being addressed by nanotechnological advances

capable of providing targeted drug delivery with its nano-scale carriers and particles. Drug delivery can be achieved by organic (soft) or inorganic (hard) nanoparticles that improve pharmacodynamic profiles with enhanced specificity, reduce harming of healthy tissues, decrease systemic toxicity, enable easy implementation of combination therapies, thereby, providing comforting relief to patients (Bor et al., 2019).

The advantages of nanotherapy emanate from unique characteristics of nanoparticles decorated /functionalized with suitable ligands. *Passive* targeting by ‘enhanced permeation and retention effect’ (EPR) of nanomaterials makes the technology innovative since cancerous tissues are typically characterized by leaky vasculature and impaired lymphatic drainage. *Active* targeting involves receptor specific ligands attached to nanoparticles which enhance easy detection of tumour sites through respective receptors (Tran et al., 2017; Zhao et al., 2018). Nanoparticles also facilitate incorporation of diagnostic agents for precise targeting of affected cells both for release and visualization of the drugs used by imaging systems (Irimie et al., 2017; Jurj et al., 2017). The use of these particles has also proven to overcome radiation resistance due to tumour hypoxia. Nanomaterials having high-Z elements can act as effective radiosensitizers / nanocarriers in delivering therapeutic radioisotopes or chemodrugs to perform a chemo-radiotherapy (Song et al., 2017). An active anticancer biomolecule thymoquinone from *Nigella sativa* essential oil used as thymoquinone nanoparticle formulations showed good bioavailability with enhanced anticancer and anti-inflammatory properties with reduced undesirable cytotoxicity (Ballout et al., 2018). Liposomal formulations of daunorubicin, doxorubicin, cytarabine, vincristine, irinotecan are some of the approved anticancer drugs against Kaposi’s sarcoma, breast cancer, lymphomatous meningitis, leukemia and pancreatic cancer respectively (Bor et al., 2019). Enhanced drug efficiency has also been achieved using protein-based nanoformulations (Gou et al., 2018).

Inorganic metal-based ‘hard’ nanoparticles have captured the burgeoning interest of nanotechnologists on cancer theranostics due to their small size, unique surface features and easy synthesis methods. Gold nanoparticles have proven to be an excellent candidate which is biocompatible, non-toxic and non-immunogenic

with good optical and tunable properties and a negative charge on surface for easy modifications (Singh et al., 2018). Spherical gold nanoconjugates of doxorubicin, paclitaxel, daunorubicin, tamoxifen are some examples of anticancer drugs (Sztandera et al., 2019). Likewise, silver nanoparticles also exhibit anticancer potential against various human cancer cell lines. A recent study using combination of anticancer drug camptothecin with silver nanoparticles was found to induce synergistic cytotoxicity resulting in ROS-mediated apoptosis of human cervical cancer cells (Yuan et al., 2018).

1.4. Zinc oxide nanoparticles

Zinc oxide nanoparticles (ZnONPs) are inexpensive, inorganic semiconductors possessing distinct optical, electrical, physico-chemical characteristics. The wide band gap and large exciton binding energy (60meV) of these nanoparticles makes them a good UV absorber having high photocatalytic efficiency in waste water treatment (Rathore et al., 2015). Biomedical applications of ZnONPs include their use in drug delivery, bio-sensing / imaging due to its non-toxic nature (Kumar et al., 2011; Kalpana and Rajeswari, 2018). ZnONPs are reportedly toxic to gram-positive / negative bacteria (Raghupathi et al., 2011; Reddy et al., 2014). Zinc oxide nanostructures are also known to exhibit enhanced and selective antiproliferative activity against cancer cells like HL60, HeLa, HepG2, breast cancer MDA-MB-231 and MCF-7 (Premanathan et al., 2011; Paino et al., 2016; Biplab et al., 2016; Moghaddam et al., 2017). Physical and chemical methods of ZnONPs synthesis are disadvantageous due to their high cost, increased time-consumption and usage / generation of hazardous chemicals. To address these concerns, several efforts have been focused to develop successfully a cost-effective, eco-friendly ('green'), reliable and sustainable alternative approach of nanoparticle synthesis, employing microbes, plant and plant products which enable generation of nanoparticles through a process of bioreduction. Exploiting plant extracts for this purpose is potentially advantageous over use of microbial cultures due to their easy availability, low or non-hazardous nature and the lack of elaborate processes in ensuring aseptic conditions and culture maintenance (Ahmed et al., 2017). Also, plant extract-mediated nanofabrication is an essential and versatile one-pot bioreduction approach for capping and stabilizing of these elite nanoparticles. Several studies have demonstrated enhanced activity of such biosynthesized

ZnONPs against bacterial and cancer cells emphasizing their superiority over chemically derived particles (Gunalan et al., 2012; Suresh et al., 2015; Chung et al., 2015; Mahendiran et al., 2017; Steffy et al., 2018).

To conclude, recent research has witnessed rapid advancements in applications of nanotechnology in various fields including medicine and healthcare. Besides complementing existing technologies, it also offers a novel set of tools which can contribute significantly towards cancer detection, prevention, diagnosis and treatment.

1.5. About this Thesis

1.5.1. Aims and Objectives

The present study deals with the biosynthesis of pure, crystalline zinc oxide nanoparticles, using a nature-friendly, cost-effective and simple method employing sol-gel technique. To realize this aim, various plant parts (leaves, flowers, fruits, seeds and roots / rhizomes) from 10 different plants were randomly selected to prepare aqueous extracts suitable for lab-scale synthesis of biogenic ZnONPs. Of the multiple plant parts screened, the extracts prepared from leaves of *Spondias pinnata* (L. f.) Kurz and *Manilkara zapota* (L.) P. Royen and those obtained from the roots, fruits and seeds of *Annona muricata* L. were found to successfully support the biosynthesis of ZnONPs through phytoconstituent-assisted bioreduction process. To obtain specific information on the size, shape and chemical nature of the nanoparticles generated, standard physico-chemical techniques such as UV-visible spectrophotometry (UV-vis), Photoluminescence (PL), X-ray diffraction (XRD), Fourier transform infrared spectroscopy (FTIR), Field emission scanning electron microscopy (FESEM), Energy dispersive X-ray spectroscopy (EDX) and High-resolution transmission electron microscopy (HRTEM) were employed. Investigations on anticancer activities of ZnONPs were studied *in vitro* using chronic myelogenous leukemic K562 suspension cells, colon carcinoma HCT 116 and lung adenocarcinoma A549 adherent cell lines. Based on cytotoxicity evaluation of the nanoparticles by the MTT assay, the most potent ZnONP preparations were selected for detailed studies at the cellular and molecular biological levels. The toxicity of these particles were also examined on normal human cells including peripheral blood derived lymphocyte cultures, erythrocytes and a standard plant cell

model, the meristematic root-tip cells of *Allium cepa* L. Further research extensions to evaluate the multifaceted properties of the phyto-derived ZnONPs comprised of studies on their antibacterial and photocatalytic potential including *in vitro* DNA interactions. *Escherichia coli*, *Klebsiella pneumoniae*, *Pseudomonas aeruginosa*, *Staphylococcus aureus* were the four clinical bacterial isolates used to determine bacterial growth inhibition whilst methylene blue was used to assess photocatalysis. ZnONP-DNA interactions were studied using purified pUC18 plasmid, λ phage and 100 bp ladder DNA. To bring out a strict comparison between the properties of phyto-derived ZnONPs produced in the present study, the commercially available chemical version of ZnONPs purchased from Sigma Aldrich (USA) was employed as a control in all experiments. A flowchart outlining the experimental studies reported in this Thesis is given in Fig. 1.1.

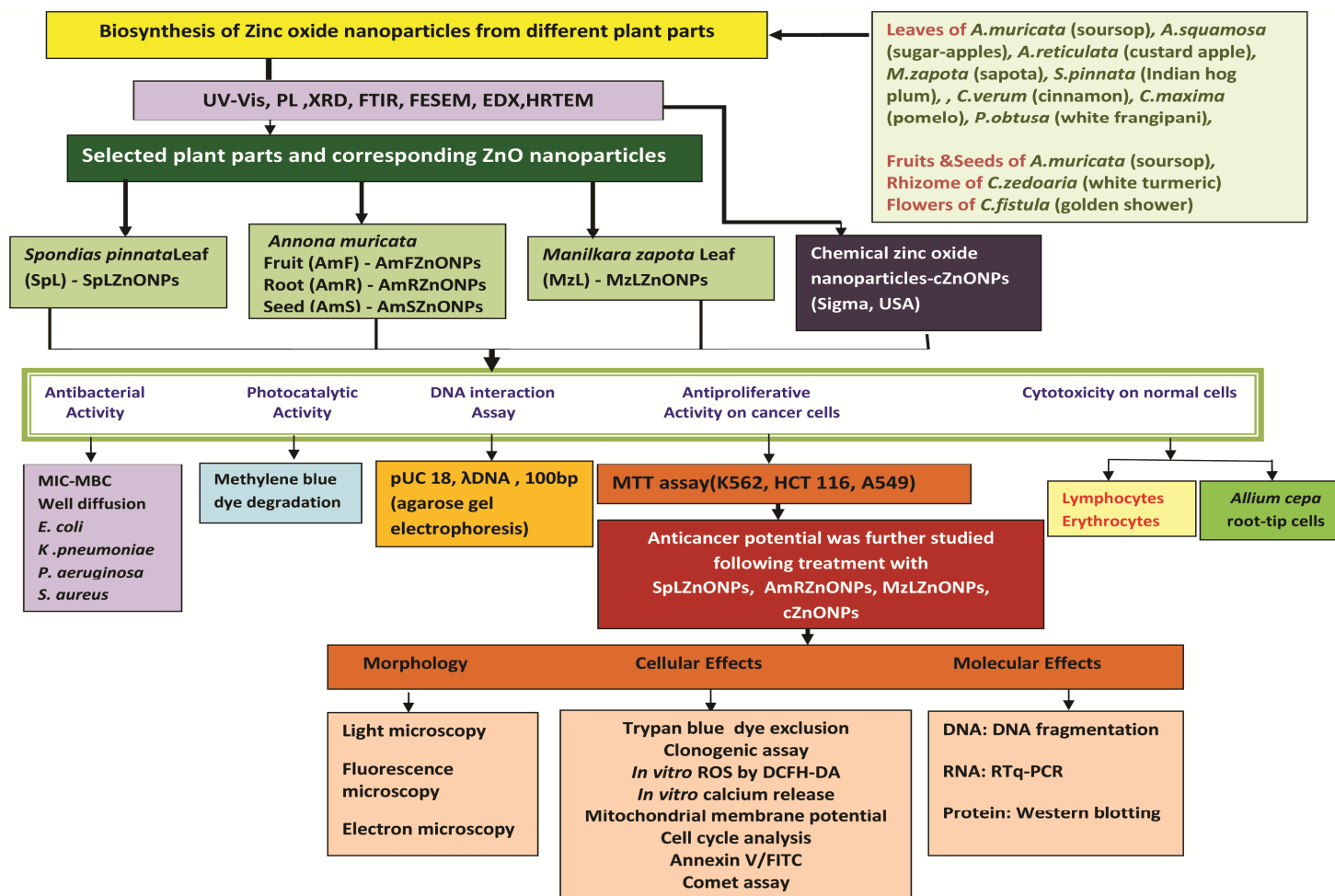


Fig.1.1. An outline of the research work presented in this Thesis

1.5.2. Thesis Layout

This thesis is divided into **six** chapters: the **first chapter** comprises of an introduction to the general theme of nanotechnology highlighting developments in the rapidly growing area of nanomedicine, particularly those involved in drug delivery, cancer diagnostics and therapy. It also provides a comprehensive outline of the doctoral research represented as a flowchart. The **second chapter** presents a review of literature comprising of a historical perspective on nanotechnology with special focus on zinc oxide nanoparticles, their mode of synthesis / characterization and reports on their multi-faceted properties. The chapter also includes a brief mention of the global scenario of cancer incidence, molecular genetics and developments in diagnostics and therapy of cancer; short notes on the plants used in the present study are also furnished. The **third chapter** gives the details of screening of plant extracts and the methodology utilized for biosynthesis of zinc oxide nanoparticles and their characterization. The **fourth chapter** reports on the cellular effects of biogenic versus commercial zinc oxide nanoparticles against eukaryotic cells including human normal / cancer cells and a plant cell model. The **fifth chapter** makes a brief mention on the research extensions exploring the multifunctional potential (antibacterial, photocatalysis, and molecular interactions with DNA) of phyto-derived nanoparticles in comparison to that of the chemically synthesized commercial version. The **sixth chapter** summarizes the highlights and conclusions of the present study followed by a brief note on its future prospectives. A bibliography of all citations and an appendix with recipes for reagent preparation are provided at the end of the Thesis. Prepages enlist all tables, figures and abbreviations used in the Thesis.

REVIEW OF LITERATURE

2.1. Nanoparticles : An overview

Conceptually, the origins of the nanotechnology paradigm can be traced back to the famous lecture by Richard Feynman given on 29th December 1959 at the annual meeting of American Physical Society quoted as “There's Plenty of Room at the Bottom”. However, the term ‘nanotechnology’ was coined in 1974 by Norio Taniguchi of Tokyo University. In modern times the term encompasses design, synthesis and applications of materials/devices engineered at the nanoscale sizes. The use of nanomaterials dates back to 4500 years when ceramic matrices were reinforced with asbestos nanofibres (Colomban and Gouadec, 2005). Other examples include the use of 5nm PbS nanoparticles for hair dye and Egyptian blue synthetic pigment, red glass coloured by copper nanoparticles during late bronze age in Italy, celtic red enamels during 400 B.C and the Lycurgus cups with ruby glass impregnated with gold nanoparticles (Brun et al., 1991, Walter et al., 2006, Artioli et al., 2008, Leonhardt, 2007, Heiligtag and Niederberger, 2013). However, a scientific explanation on quantum sized effects of nanoparticles was put forth in 1857 by Michael Faraday by synthesizing colloidal solution of gold nanoparticles. The US Food and Drug Administration (USFDA) defined nanomaterials as those having at least 1-100 nm in one dimension of the particle which also exhibit dimension-dependent phenomenon (Federal Drug Administration: USA, 2011). According to Environmental Protection Agency (EPA), nanomaterials are those having distinct and dissimilar properties than their bulkier chemical equivalent (United Nations, 2012).

Nanoparticles and nanomaterials can be classified based on their composition, dimension and origin. Composition based classifications include carbon-based, inorganic-based, organic-based and composite-based nanoparticles, whilst the dimension-based include 0D, 1D, 2D and 3D nanoparticles. Origin-based nanoparticles include natural and synthetic nanomaterials (Jeevanandam et al., 2018). Nature is an abundant source of nanomaterials. Nanobacteria, viruses and

fungi produce nanoparticles in their bodies. Nanocages / protein capsids of viruses have been utilized for targeted drug delivery (Saunders et al., 2009). Unique superparamagnetic nanoparticles from magnetotactic bacteria (Li et al., 2011), cellulose nanofibers in plants (Mohammadinejad et al., 2016), superhydrophobic nanostructures on lotus leaves (Barthlott and Neinhuis, 1997), color and fine structures of wings of the grasshopper (*Acrida cinerea cinerea*), dragonfly (*Hemicordulia tau*) and butterfly species (*Papilio xuthus*) (Nguyen et al., 2014), color patterns of peacock's feathers (Zhang et al., 2012) and the nanostructures of bones (Li et al., 2013), proteins (Papazoglou et al., 2007), DNA (Sinden et al., 2012), enzymes (Schaefer, 2010) of human body are all examples of naturally occurring nanoparticles.

Nanoparticles are thus ubiquitous components of our environment essential for the sustenance of life. The technology has now reached its fourth generation comprising of molecular nanodevices like nanorobotics (Ferreira et al., 2013, Soto et al., 2018). Nanostructures like liposomes, nanoemulsions, nanocomposites and flavor-enhancing biopolymers have a great impact on food industry as they help improved packaging, preservation, better transportation and in turn better health benefits. These structures also help to sense and stop food spoilage, increase solubility with bioavailability of health supplements and controlled-target delivery of nutraceuticals (Pathakoti et al., 2017). Jampílek and Král'ová (2015) described that the quality and quantity of transported food can also be analysed by using nanoscale tagging devices. Nanoencapsulation is a smarter option which helps in delivering highly reactive yet unstable compounds like anthocyanins, using ferritin nano-cages enabling extended shelf life and prevention of micro-supplement degradation (Singh et al., 2017). Furthermore, nano zinc oxide and titanium oxide in cosmetic formulations have enhanced dermal spreading and offer protection from UV. Also, nano silver particles in skin cleansers have good antibacterial and antifungal properties (Gajbhiye et al., 2016). Arbutin, solid lipid, polyaminiacid, nanocapsules, native polymers like polyaminoacids and carbon fullerenes are also used nanoforms in cosmeceuticals (Moazzam et al., 2018).

Nanoengineering innovations in textile industry provides the fabric with properties like enhanced durability, anti-wrinkling and anti-static behaviour, hydrophobicity and anti-microbial nature while retaining its texture, colour and comfort (Yetisen et al., 2016). A supercapacitor textile developed using aligned multiwalled carbon nanotube (CNT) / polyaniline (PANI) composite fiber-based textiles as electrodes was integrated with photoelectric conversion function making self powering textile, a great step towards the dream of portable and wearable energy devices (Pan et al., 2014). Sports shoes, clothing, stadium floorings, tennis ball coatings, racquets have all been modified and improved by this novel technology (Harifi et al., 2015). Agricultural needs can also be met through nanotechnology. Nanoencapsulated pesticides promising controlled release with greater stability, solubility and durability with low amount of application is an eco-friendly approach (Bhattacharyya et al., 2016; Nuruzzaman et al., 2016). The development of clay nanotubes as low-cost carriers of pesticides, fabrication of xylem vessels and nanoscale carriers for efficient delivery of herbicides, fertilizers, plant growth regulators are all privileges of nanotechnology in agricultural sector (Dasgupta et al., 2017). Gas-leakage sensing by self-heating of metal oxide nanowires, ZnO-quasi 1D nanostructure in conductometric gas sensing devices are yet other bench marks (Sama et al., 2015; Galstyan et al., 2016). Nanoscale biosensors including quantum dots, noble metal nanoparticles, lanthanide luminescent nanoparticles as well as label-free transduction by nanotubes, nanowires, nanocantilevers and nanopores help early detection of disease causing pathogens and aid in efficient diagnosis and treatment (Sposito et al., 2018). Thus, nanotechnology has an overpowering presence interacting in each and every aspect of human life. However, the exploitation, utilization of these particles and their fate in environment must be thoroughly researched in order to avoid concerns on their toxicity.

2.2. Zinc and Zinc oxide nanoparticles

Studies have revealed that close to 3000 zinc containing proteins reside in human cells. Zinc is an essential trace element for the survival of life as a catalytic,

structural and regulatory cofactor. The very first report on this transition metal ion was published in 1869 by Jules Raulin, further studied by Ananda Prasad on zinc deficiency after two decades. The discovery of Zn containing erythrocyte enzyme carbonic anhydrase is an initiation of research on a biological important key element (Maret et al., 2013). Zinc is a cofactor of many enzymes and is also involved in cellular proliferation, metabolism and even cell death by interaction with biological moieties such as DNA, RNA, proteins and lipids (Maret et al., 2012). ZnO is graded as a “GRAS” (generally recognized as safe) substance (Code of Federal Regulations Title 21, Section 182.8991) by the U.S. Food and Drug Administration (FDA) which makes these nanoparticles much more impressive from the perspective of drug delivery and biocompatibility (Hong et al., 2015; Jiang et al., 2018). The fact that bulk-ZnO possesses unique physico-chemical potential, low cost and easy availability makes it relatively more exploitable (Shamsuzzaman et al., 2017). Of the two main forms of zinc oxide crystals - hexagonal wurtzite and cubic zinc blende - the former is said to be more common and stable under ambient conditions (Purkait et al., 2015). Previous reports have shown that zinc oxide nanoparticles (ZnONPs) have stimulating properties acquired through its bulk form and also due to its mode of synthesis. ZnONPs are promising and versatile II-VI semiconductor inorganic particles. It has direct wide band gap (3.3eV) lying near UV spectrum with high excitation binding energy (60meV) at room temperature. This wide band gap is the reason for its improved electrical conductivity which is enhanceable on doping (Wang, 2004; Kuskovsky et al., 2006; Janotti and de Walle, 2009; Zhang et al., 2012). Based on the mode of synthesis, these nanoparticles attain different shapes such as nanospheres, nanoplates, nanowires, nanoflowers and so on (Kakiuchi et al., 2006; Jang et al., 2008; Ding and Wang, 2009; Moezzi et al., 2011)

2.3. Applications of zinc oxide nanoparticles

Zinc oxide is a unique metal oxide semiconductor due to its surface energy, low toxicity, good electron mobility, wide and direct band gap energy and thermal conductivity (Janotti and de Walle, 2009; Guo, 2017). It is also a good UV absorber and a promising candidate of nano-electronics and photonics (Samuel et al., 2009;

Sagadevan et al., 2018). They also exhibit high catalytic efficiency, strong adsorption capability which is utilized in sunscreens, cosmetics, rubber processing ceramics and for waste water treatments (Parthasarathy et al., 2017). There are several reports on various applications of zinc oxide nanoparticles which exploit their multifaceted potential including photocatalytic, anti-diabetic, anti-inflammatory, antibacterial and anticancer activity.

Photocatalysis is a catalyst-mediated chemical reaction in the presence of light. A photocatalyst can itself absorb either UV, visible light or a combination of both and generate electron-hole pairs (Djurišić et al., 2014). A clean energy source like that of sun for degrading pollutants has been exploited in achieving photocatalysis. Degradation of methyl orange dye as well as paraquat herbicide has been accomplished using spinach-mediated zinc oxide nanocatalysts in the presence of UV and sunlight (Munshi et al., 2018). A 93 % degradation of water contaminants like methyl orange (MO), methylene blue (MB) and methyl red was obtained using ZnO nanoparticles to remove factory contaminants (Alhadhrami et al., 2018). Photodegradation of methylene blue within 30 minutes under UV light was also achieved by *Phyllanthus niruri* leaves extract-mediated ZnONPs (Anbuvannan et al., 2015). Also, green synthesized nanoparticles showed enhanced photocatalytic activity and good photostability since they possess good oxygen vacancies (Archana et al., 2016). First order kinetics governs MO dye degradation by ZnONPs (Bhatia and Verma, 2017). However, this enhanced photo-decomposition depends on the route of preparation of nanoparticles which determines the specific surface sites for advanced reactions. Photocatalytic potential of ZnONPs also showed improvement when grown on porous silica microparticles or doped by nitrogen (Rathore et al., 2015; Azmina et al., 2017; Montero-Muñoz et al., 2017). Biosynthesized nano-ZnO can degrade methylene blue dye completely within 90 min and is also capable of photo-desulfurization (Raja et al., 2018; Sudheer kumar et al., 2018; Khalafi et al., 2019).

ZnONPs also possess greater anti-diabetic activity than silver nanoparticles in streptozotocin-induced diabetic rats due to decrease in blood glucose level caused by increase in insulin level, glucokinase activity, insulin receptor IRA and GLUT2

expression (Alkaladi et al., 2014). Reversal of diabetes by these nanoparticles has been achieved *in vitro* owing to their pleiotropic action (Asani et al., 2016). Several other studies also report on good antidiabetic activity of biosynthesized zinc oxide nanoplateforms (Thatoi et al., 2016; Rehana et al., 2017; Bayrami et al., 2018; Rajkumar et al., 2018; Arvanag et al., 2019; Vinotha et al., 2019).

ZnONPs are also reported to possess antibacterial potential. Studies have shown that reactive oxygen species (ROS) generation, followed by cell wall damage and nanoparticle intake due to enhanced membrane permeability and toxicity of dissolved ions resulted in antibacterial activity (Sirelkhatim et al., 2015). Food-borne pathogens *Salmonella typhimurium* and *Staphylococcus aureus* displayed pitted membrane on treatment with these nanoparticles (Akbar et al., 2019). Reverse transcription-quantitative PCR of stress genes involved in ZnONPs treated *Campylobacter jejuni* cells showed increased expression of stress genes (Xie et al., 2011). The electron-hole pair generated in ZnONPs on exposure to light is also known to improve their antibacterial effect (Sivakumar et al., 2018). ZnONPs synthesized using sol-gel method is known to cause cell death in both gram positive and gram negative bacteria (Khan et al., 2016). Carbapenem resistant *Acinetobacter baumannii*, an opportunistic pathogen was also found susceptible to these inorganic nanoparticles by lipid peroxidation, leakage of reducing sugars and reduced viability (Tiwari et al., 2018). There are several recent reports on antibacterial activity of ZnONPs (Janaki et al., 2015; Kadiyala et al., 2018; da Silva et al., 2019; Sharmila et al., 2018).

ZnONPs exhibited antifungal activity against *Penicillium expansum*, *Botrytis cinerea*, *Candida krusei*, coffee fungus *Erythricium salmonicolor* and many others (He et al., 2011; Esteban-Tejeda et al., 2015; Arciniegas-Grijalba et al., 2017). Surface- modified ZnONPs can potentially modify the infectivity of Herpes-simplex virus type-1 (HSV-1) by exerting their effect on viral particles than by interfering with cellular targets (Farouk and Shebl, 2018). Biocompatible zinc oxide nanoparticles have also showed antihelminthic activity against *Gigantocotyle explanatum* and *Toxocara vitulorum* (Khan et al., 2015; Dorostkar et al., 2017).

Cancer incidence rates have been increasing worldwide. In this scenario, the successful use of ZnONPs as an effective anticancer agent in many *in vitro* studies offers great hope. Biosynthesized nanoparticles have been found to possess enhanced antiproliferative potential against MCF-7, HepG₂, A549 and HT-29 colon cells (Ratney and David, 2017; Anitha et al., 2018; Rajesh Kumar et al., 2018; Hussain et al., 2019). Moon et al. (2016) reported that sustained zinc ion releasing ZnO chips cause selective cytotoxicity against human B lymphocyte-derived Raji cells over normal human peripheral blood mononuclear cells. Table 2.1 summarizes the anticancer activity of ZnONPs based nanoplatforms

Table 2.1. Anticancer activity of ZnONPs based nanoplatforms.

Cancer type	Effect of ZnONPs
Colon cancer	ZnONPs suppressed cell viability in Caco-2 cell line via increased ROS, induced IL-8 release, lysosomal destabilization with fatty acids in addition to increase in intracellular Zn ions. (De Angelis et al., 2013; Cao et al., 2015; Fang et al., 2017). ZnONPs conjugated with peptides had a higher antiproliferative effect on HT-29 colon cancer cells than other gold NPs and iron oxide NPs (Aswathnarayan et al, 2018).
Hepatocarcinoma	ZnONPs caused ROS generation, oxidative DNA damage leading to mitochondria-mediated apoptosis in HepG2 cells (Sharma et al., 2012; Akhtar et al., 2012). Dox-ZnO nanocomplex can act as a drug delivery system to increase the internalization of the anticancer drug Dox in SMMC-7721 cells (Deng and Zhang, 2013) .
Breast cancer	Eco-friendly formulations of ZnONPs arrested cell cycle in G2/M phase and upregulated proapoptotic genes p53, p21, Bax and JNK and downregulated antiapoptotic genes Bcl-2, AKT1, and ERK1/2 in a dose-dependent manner in MCF-7 cells (Moghaddam et al., 2017). RGD (Arg-Gly-Asp) - targeted ZnONPs can target integrin $\alpha\beta3$ receptors to increase the toxicity of the ZnONPs to MDA-MB-231 cells even at lower doses (Othman et al., 2016). ZnO-Fe ₃ O ₄ magnetic composite nanoparticles have no significant toxicity towards non-cancerous NIH 3T3 cells but show obvious toxicity at similar concentration to MDA-MB-

	231 cells (Bisht et al., 2016). Functionalized ZnONPs released ~75% of the paclitaxel payload within six hours in acidic pH, improved chemotherapy tolerance, and increased antitumor efficacy (Puvvada et al., 2015).
Lung cancer	ZnONPs incorporated in liposomes not only rendered pH responsivity to the delivery carrier but also exhibited synergetic chemo-photodynamic anticancer action (Tripathy et al., 2015). Human lung adenocarcinoma cells with an EGFR mutation are sensitive to ZnONP20 and Al-ZnONP20, which resulted in non-autophagic cell death (Bai et al., 2017).
Ovarian cancer	ZnONPs are able to induce significant cytotoxicity, apoptosis and autophagy in SKOV3 cells through reactive oxygen species generation and oxidative stress (Bai et al., 2017).
Cervical cancer	DOX-ZnO/PEG nano-composites exhibited better dose-dependent toxicity towards HeLa cell lines (Hariharan et al., 2012). ZnO nanoparticles showed a dynamic cytotoxic effect in cervical carcinoma cells which induced apoptosis through increased intracellular ROS levels and upregulated p53 and caspase-3 expression (Pandurangan et al., 2016).
Gastric cancer	Conjugated ZnONPs were able to carry a large amount of hydrophobic drug (curcumin) showing high anti-gastric cancer activity (Dhivya et al., 2017; Dhivya et al., 2018).
Human epidermal cancer	ZnONPs induced cell cycle arrest in S and G2/M phase and also caused cell death by intracellular ROS generation in A431 cells (Patel et al., 2016).
Acute promyelocytic leukemia	Hyaluronic acid / ZnO nanocomposite caused G2/M cell cycle arrest and stimulated apoptosis-related increase in caspase-3 and -7 activities of the HL60 cells (Namvar et al., 2016).

(Adapted from Jiang et al., 2018)

2.4. Synthesis of zinc oxide nanoparticles

Synthesis or fabrication of nanoparticles is done mainly by two methods: *top-down* and *bottom-up* approaches. *Top-down* approach involves mechano-synthetic break down of bulk particles to nanoscale in which manual control of its surface characteristics is not possible. Mechanical milling, nanolithography, laser-ablation, sputtering, thermal decomposition and arc-discharge are few of widely

used techniques for *top-down* synthesis (Khandel et al., 2018). On the other hand, *bottom-up* approach employs gradual clustering of small atoms with controlled surface properties and characteristics. Techniques used for *bottom-up* approach are sol-gel, chemical vapour deposition, atomic layer deposition, molecular beam epitaxy, pyrolysis and biological synthesis (Arole and Munde, 2014). Based on a literature scan, zinc nanoparticles synthesis can be broadly classified into physical, chemical and biological methods.

2.4.1. Physical and chemical methods

Pulsed-laser ablation is a physical method of zinc oxide nanoparticle synthesis using zinc metal in deionized water devoid of any surfactant (Kim et al., 2011; Dorranean et al., 2012). Modified ZnO nano-crystalline powder in large quantities was obtained by temperature-independent high energy ball milling technique (Habib, 2009; Salah et al., 2011). Yu et al. (2010) reported advantages of chemical vapour deposition and vapour phase transport (VPT) in nanoparticle synthesis and also proposed a modified VPT for ZnO nanowire synthesis. Chemical synthesis is further classified into liquid phase and gas phase according to the medium of synthesis phase. Pyrolysis and gas condensation methods comprise gas phase mode whilst precipitation / co-precipitation, sol-gel, oil microemulsion, chemical reduction, solvo-thermal and hydrothermal are all included in liquid phase mode (Naveed ul haq et al., 2017). Using various concentrations of zinc acetate dihydrate, nanoparticles with chemical and shape regularity were synthesized using ultrasonic spray pyrolysis technique (Lee et al., 2012). A novel combination of sol-gel and spray pyrolysis methods to achieve fine-sized, less agglomerated ZnO nanoparticles has been proposed by Guo et al. (2014). It was reported that small sized nanoparticles with high yield and increased purity can be synthesized using bicontinuous microemulsion technique (L'opez-Cuenca et al., 2011). There are other successful reports on synthesis of ZnO nanoparticles by wet chemical, co-precipitation, solvo-thermal, sono-chemical and hydrothermal methods (Askarinejad et al., 2011; Kripal et al., 2011; Talam et al., 2012; Ramimoghadam et al., 2013; Elsayed et al., 2014; Bai et al., 2015). Chemical synthesis of ZnO nanoflowers and

rosette-like nanostructures have been reported which employ solutions of zinc acetate dehydrate, zinc nitrate hexahydrate, hydroxylamine hydrochloride and sodium hydroxide as reagents followed by refluxing (Wahab et al., 2007; Wahab et al., 2009).

2.4.2. Biological methods

Although physical and chemical methods have been successful in synthesis of ZnONPs, these are time-consuming, demanding high energy inputs and use of costly chemicals which also generate toxic or hazardous byproducts. Biosynthetic methods based on naturally occurring biomaterials provide an alternative means for obtaining nanoparticles. There are several reports on the synthesis of ZnO nanoparticles employing plant parts, bacteria / fungi, seaweeds and other natural products. Biosynthesis of nanoparticles is unique and reliable not only because of very low levels or complete absence of toxicity in comparison to most of the physico-chemical production methods but also because it can be used to produce large quantities of nanoparticles with defined shapes and sizes (Khandel et al., 2018). Use of plants in nanoparticle synthesis by the 'green chemistry' route is quite novel. Since plants are treasures of known and unknown bioactive compounds, this approach is advantageous since it amenable to scaling-up, is economically viable and safe (Ponarulselvam et al., 2012). Synthesis employing plants and plant extracts includes three main phases: (i) the activation phase (ii) the growth phase and (iii) the process-termination phase. The first phase involves bioreduction and nucleation of the reduced metal atoms followed by Ostwald ripening process, in which small adjacent nanoparticles spontaneously coalesce into particles of a larger size. The final phase involves stabilization of nanoparticles in the presence of phytoconstituents and favourable energetics necessary for shape formation (Makarov et al., 2014). Utilization of microbial systems possess inherent disadvantages due to high cost and aspects related to maintenance of aseptic condition as well as time consumption and monitoring of the entire process (Mahendiran et al., 2017; Das et al., 2018). Table 2.2 lists out a set of recent studies on phyto-mediated biosynthesis of different types of ZnONPs utilizing extracts from various plant parts.

Table 2.2. Phyto-mediated biosynthesis of ZnONPs differing in size and morphology.

Sl. No.	Source	Part	Size (nm)	morphology	Reference
1	<i>Acalypha indica</i>	Leaves	100-200	wurtzite	Gnanasangeetha et al., 2014
2	<i>Achyranthes aspera</i>	Leaves	30-40	Flake-like	Duraimurugan et al., 2018
3	<i>Aegle marmelos</i>	Leaves	18	hexagonal	Fowsiya et al., 2019
4	<i>Agathosma betulina</i>	Dry leaves	12-26	Quasi-spherical agglomerates	Thema et al., 2015
5	<i>Albizia lebbek</i>	Stem bark	66.25	Irregular, spherical	Umar et al., 2019
6	<i>Aloe barbadensis miller</i>	Leaves & gel	25-45	spherical, hexagonal	Sangeetha et al., 2011
7	<i>Aloe vera</i>	Peel	50-220	hexagonal	Chaudhary et al., 2019
8	<i>Anisochilus carnosus</i>	Leaves	56.14	Hexagonal, spherical	Anbuvaran et al., 2015
9	<i>Azadirachta indica</i>	Fresh leaves	18	spherical	Elumalai et al., 2015
10	<i>Bauhinia tomentosa</i>	Leaves	22-94	Hexagonal wurtzite	Sharmila et al., 2018
11	<i>Calotropis procera</i>	Latex	5-40	spherical	Singh et al., 2011
12	<i>Camellia sinensis</i>	Leaves	16	Hexagonal wurtzite	Senthilkumar et al., 2014
13	<i>Citrus aurantifolia</i>	Fruit	50-200	wurtzite	Samat et al., 2013
14	<i>Citrus paradise</i>	Peel	12-72	spherical	Kumar et al., 2014
15	<i>Citrus sinensis</i>	Peel	12.55	polyhedral	Nava et al., 2017
16	<i>Coctus pictus</i>	Leaves	20-80	Spherical, rod, hexagonal	Suresh et al., 2018
17	<i>Cocos nucifera</i>	Coconut water	20-80	Spherical, hexagonal	Krupa and Vimala., 2016
18	<i>Coptidis Rhizoma</i>	Dried rhizome	2.9-25.2	Spherical, rod	Nagajyothi et al. 2014
19	<i>Costus woodsonii</i>	Leaves	20-25	Hexagonal wurtzite	Khan et al., 2019
20	<i>Cucurbita pepo</i>	Leaves	8	Hexagonal wurtzite	Hu et al., 2019
21	<i>Eichhornia crassipes</i>	Leaves	32-36	spherical	Rajiv et al., 2018
22	<i>Euphorbia tirucalli</i>	Leaves	~20	-	Hiremath et al., 2013
23	<i>Ficus racemosa</i>	Leaves	15	Hexagonal	Birusanthi et al., 2018
24	<i>Garcinia Xanthochymus</i>	Fruits	20-30	spherical	Nethravati et al., 2015
25	<i>Glycosmis pentaphylla</i>	Leaves	32-36	Hexagonal wurtzite	Vijayakumar et al., 2018
26	<i>Gossypium</i>	Cellulosic fibre	13	Wurtzite, spherical, nanorod	Aladpoosh and Montazer., 2015

27	<i>Hibiscus sabdariffa</i>	Leaves	9-18	hexagonal	Mahendiran et al., 2017
28	<i>Lycopersicon esculentum</i>	Fruits	20-100	spherical	Sutradhar and Saha., 2016
29	<i>Moringa oleifera</i>	Leaf	24	Spherical, granular	Elumalai et al., 2015
30	<i>Nephelium lappaceum</i>	Peel	50.90	hexagonal	Yuvvakumar et al., 2014
31	<i>Ocimum americanum</i>	Leaves	21	spherical	Kumar et al., 2019
32	<i>Ocimum tenuiflorum</i>	Leaves	13.86	hexagonal	Raut et al., 2013
33	<i>Parthenium hysterophorous</i>	Leaves	16.10-58.60	Spherical	Sri Sindhura et al., 2013
34	<i>Phyllanthus niruri</i>	Leaves	25.61	Hexagonal, wurtzite	Anbuvaran et al., 2015
35	<i>Pisonia grandis</i>	Leaves	50.95	Hexagonal, spherical	Joghee et al., 2018
36	<i>Plectranthus amboinicus</i>	Leaf	50-180	Rod	Fu and Fu., 2015
37	<i>Poncirus trifoliata</i>	Dried fruits	21.12	Spherical	Nagajyothi et al., 2013
38	<i>Pongamia pinnata</i>	Leaves	26	Spherical, hexagonal	Sundararajan et al., 2015
39	<i>Punica granatum</i>	Leaves, Fruit peel	10-30, 32.98 / 81.84	Spherical, Spherical/hexagonal	Singh et al., 2019, Sukri et al., 2019
40	<i>Ruta graveolens</i>	Stem	28	Wurtzite	Lingaraju et al., 2015
41	<i>Santalum album</i>	Leaves	70-140	Nanorods	Kavitha et al., 2016
42	<i>Scadoxus multiflorus</i>	Leaves	31	Irregular spherical	Al-Dhabi and Arasu MV, 2018
43	<i>Sesbania grandiflora</i>	Leaves	15-35	Spherical	Rajendran and Sengodan., 2017
44	<i>Solanum nigrum</i>	Leaves	20-30	Wurtzite, hexagonal	Ramesh et al., 2015
45	<i>Solanum torvum</i>	Leaves	34-40	Non-smooth spherical	Ezealisiji et al., 2019
46	<i>Spathodea campanulata</i>	Leaves	30-50	Spherical	Ochieng et al., 2015
47	<i>Swertia chirayita</i>	Leaves	2-10	Spherical	Akhter et al., 2018
48	<i>Trifolium Pratense</i>	Flower	60-70	Spherical	Dobrucka and Dhugaszewska, 2016
49	<i>Vitex negundo</i>	Flowers	38.17	Hexagonal	Ambika and Sundrarajan, 2015
50	<i>Ziziphus nummularia</i>	Leaves	17.2	Irregular spherical	Padalia and Chanda., 2017
51	<i>Coriandrum sativum</i>	Leaves	34	Spherical aggregates	Singh et al., 2019
52	<i>Nyctanthes arbor-tristis</i>	Flowers	12-32	Polydispersed aggregates	Jamdagni et al., 2018
53	<i>Moringa oleifera</i>	Leaves	12.27-30.51	Wurtzite	Matinise et al., 2017

Besides plant extracts, other natural agents can also be potentially employed to synthesize ZnONPs from metal precursors. Marine resources have largely remained unexplored in this regard. A few reports exist on nanoparticle synthesis using seaweeds such as green *Caulerpa peltata*, red *Hypnea Valencia*, brown *Sargassum myriocystum* and brown macroalga *Sargassum muticum* (Nagarajan et al., 2013; Azizi et al., 2014). Microbial-mediated synthesis of zinc oxide nanoparticles has been carried out employing bacteria, fungi and yeast (Yusof et al., 2019). Microbes act as a bio-factory to reduce metal ions into metal nanoparticles either intracellularly or extracellularly. Fungal-mediated synthesis seems to be a promising approach as it produces biologically active compounds relatively superior to those obtained from bacterial systems. Also, extracellular biosynthesis is advantageous due to simple downstream processing requirements. Extracellular pathway is based on nitrate reductase mediated enzymatic reactions, whilst the intracellular one is based on trapping, bioreduction and capping processes mediated by electrostatic interaction (Kundu et al., 2014, Alamri et al., 2018). Highly potent ZnONPs were synthesized employing bacteria, *Aeromonas hydrophila* (Jayaseelan et al., 2012). Similar reports are available on biogenic synthesis of nanomaterials using *Lactobacillus sporogens*, *Pseudomonas aeruginosa*, *Rhodococcus pyridinivorans*, *Bacillus licheniformis*, *Staphylococcus aureus*, *Sphingobacterium thalpopophilum*, *Streptomyces* and *Serratia* species (Prasad and Jha, 2009; Singh et al., 2014; Kundu et al.,2014; Tripathi et al.,2014; Rauf et al.,2017; Rajabairavi et al., 2017; Balraj et al.,2017; Dhandapani et al.,2014). *Candida albicans*, *Aspergillus terreus* and *Aspergillus niger* are some of the fungal species exploited for the synthesis of zinc oxide nanoparticles (Sangappa et al., 2013; Shamsuzzaman et al., 2015; Kalpana et al., 2018). *Pichia* species of yeast have also been utilized for similar studies (Chauhan et al., 2015; Moghaddam et al., 2017). ZnONPs have also been synthesized by an eco-friendly approach using polysaccharide-like gum tragacanth, protein albumen, silk, polymerizing agent gelatin, uncooked rice and so on (Nouroozi et al., 2011; Zak et al., 2011; Han et al., 2012; Ramimoghadam et al., 2013; Darroudi et al., 2013)

2.4.3. Physico-chemical characterization of zinc oxide nanoparticles

Physico-chemical characteristics and unique properties, if any, of nanoparticles can be studied by various techniques to elucidate their size, shape, topography, charge, thermal, electrical and optical properties (Table 2.3). The most common techniques used for characterization of nanoparticles are (i) UV–visible spectrophotometry, (ii) Photoluminescence/PL spectroscopy, (iii) Dynamic light scattering/DLS, (iv) Fourier transform infrared spectroscopy/FTIR, (v) X-ray diffraction/XRD, (vi) Energy dispersive X-ray spectroscopy/EDX, (vii) Atomic force microscopy/AFM, (viii) X-ray photoelectron spectroscopy/XPS, (ix) Attenuated total reflection/ATR, (x) UV-visible diffuse reflectance spectroscopy/UV-DRS, (xi) Transmission electron microscopy/TEM, (xii) Thermogravimetric-differential thermal analysis/TG-DTA, (xiii) Field emission scanning electron microscopy /FESEM and Raman spectroscopy.

Table 2.3. Various physico-chemical techniques useful for characterization of nanoparticles

Aspect characterized	Techniques used
Morphology (shape/size)	Dynamic light scattering Electron microscopy (scanning/transmission) Atomic force microscopy
Topography (surface)	X-ray diffraction BET
Chemical	UV visible spectroscopy Electron dispersive X-ray spectroscopy Fourier transform infrared spectroscopy/attenuated total reflection
Electrical	Electrokinetics (zeta/cyclic voltammetry studies)
Optical	Microscopy, Double photon correlation spectroscopy, Raman spectroscopy Surface plasmon resonance

(Adapted from *Kumar et al., 2017*)

Assessment of optical properties of nanoparticles is determinable by UV-Vis spectroscopy, wherein the sharp absorption peak denotes monodispersed, nanosized

identity of the particles (Talam et al., 2012). The characteristic absorption peak of ZnO nanoparticles obtained at 370 nm is due to electrical transition of valence and conduction band responsible for intrinsic band gap absorption. The range of UV absorption of ZnO nanoparticles is around 360-380 nm (Zak et al., 2011, Umar et al., 2019). Photoluminescent (PL) spectra of semiconducting ZnO nanoparticles are a good mark of their surface defects in which the emissions at blue region explains the radiative recombination of light-induced electrons and holes (Taunk et al., 2015). Some ZnO nanoparticles have been found to show emissions in the entire visible range; some reports mention emission at UV and green regions as well (Sashtri et al., 2014; Musa et al., 2017). XRD is yet another technique which gives reliable data on particle grain size, crystallinity and crystal phase-lattice parameter. The diffraction peaks help to calculate average size by well known Debye-Scherrer equation and the crystal structure can be referred to the International Centre for Diffraction Data (ICDD) previously known as JCPDS (Mourdikoudis et al., 2018). It has been observed that the peaks of ZnO nanoparticles are slightly broadened compared to the sharp peaks of its bulkier counterpart (Bindu and Thomas, 2014). FTIR spectrum analysis reveals the stretching vibrations of chemical bonds involved in the reduction and stabilization of nanoparticles during synthesis. Previous studies have shown that the Zn-O bond vibrations can be confirmed by the peaks around 400 and 600 cm^{-1} (Parthasathy and Thilagavathy, 2011; Wahab et al., 2011; Yuvvakumar et al., 2015). FESEM allows detailed analysis of size, shape and agglomerating nature of the nanoparticles. The differences in the growing pattern of zinc oxide nanoparticles dependent on the metal precursor can also be analyzed by this microscopic technique (Fakhari et al., 2019). TEM images also provide comprehensive information on the nature of nanoscale materials and are quite advantageous in material studies using its variations such as bright-field TEM (BF-TEM), high-angle dark-field scanning TEM (HAADF-STEM), electron energy-loss spectroscopy (EELS) and BF-TEM electron tomography (BET) [Anjum, 2016]. Images from the latter technique reveal the crystalline nature of the particles as evidenced by bright spots in selected area electron diffraction (SAED) pattern (Taunk et al., 2015). EDX analysis aids in quantifying atomic level composition of

nanoparticles such as that of Zn and O in the case of ZnO nanoparticles (Suresh et al., 2018). EDX analysis of pure ZnO nanoparticles reportedly displayed two major peaks of Zn and O equivalent to 70 and 25 percentage by weight (Brintha and Ajitha, 2015; Shamhari et al., 2018). All these techniques are capable of providing adequate information useful for the identification of specific nanoparticles.

2.5. Cancer

Carcinogenesis is a condition of uncontrolled proliferation of our own cells which develop into tumors/cancers due to the malfunctioning of these cells. The three basic steps include initiation, promotion and progression of carcinogenesis occurs due to defects in the surveillance system inherent to healthy cells. The initiation stage involves accumulation of irreversible genomic mutations and modifications such as transversions, transitions, deletions, methylations and histone acetylations followed by changes in cellular behaviour characterized by aggressiveness and invasive malignant growth (Pitot, 1993; Helfinger et al., 2018). According to GLOBOCAN 2018 database, global pattern of cancer incidence and death is estimated to be high in Asia. The survey also unveils the incidence of the disease in Africa, Asia, Europe and America as 5.8%, 48.4%, 23.4% and 21.0% with the mortality rates being 7.3%, 57.3%, 9.0% and 14.4% respectively.

Cancer is the second leading cause of global mortality after heart disease and a non-communicable disease irrespective of the income or development of a country. The causative factors involved in development of successive mutations leading to cancer include environmental, occupational, exposure to chemical/physical agents, viral infections as well as due to changing lifestyles. Mutagenic environmental factors are a cause of grave concern since they affect large populations. A pioneering report on cancer was documented by Percival Pott in 1775 which revealed the incidence of scrotal cancers in chimney sweeps due to heavy soot exposure (Pott, 1775). The U.S. National Toxicology Program's 14th report (2016) on carcinogens has published a list of such environmental mutagens with explanations on the cause of cancer formation as dependent on the amount, duration and genetic sensitivity of each individual. The list includes aflatoxins,

aristolochic acid, arsenic, asbestos, coal tar, cadmium, mineral oils, nickel compounds and wood soot. Polycyclic aromatic hydrocarbons were identified as the mutagenic agent in coal tar while asbestos, benzene and chlorinated hydrocarbons caused pancreatic cancer (Cook et al., 1933; Antwi et al., 2015). The discovery of DNA structure enhanced research on DNA damaging effects of these mutagens. It was found that specific mutagens produce characteristic patterns of somatic mutations in the DNA of malignant cells designated as 'mutation signatures' as revealed by next generation sequencing techniques (Poon et al., 2014). Studies have shown that endogenous metabolites, environmental and dietary carcinogens, some anti-inflammatory drugs and genotoxic cancer therapeutics can induce damage to DNA, activating thereby cell signalling networks deciding cell fate such as repair, death or survival (Roos et al., 2015). A cohort study by Yu et al. (2018), found out that consumption of hot tea alone or with alcohol and smoking increased risk of esophageal cancer. A detailed study on smokeless tobacco (paan and gutkha) usage by chewing, dipping and snuff leads to oral cancer due to generation of reactive oxygen species by 3-(methylnitrosamino)-proprionitrile, nitrosamines, and nicotine (Niaz et al., 2017). Epidemiologic studies have reported an association between frequent consumption of well-done cooked meats and prostate cancer (PC) risk. The cooking temperature is a critical factor of generating carcinogenic byproducts known to be present in charred red meat and cooked processed meats. These carcinogens include heterocyclic aromatic amines (HAA) such as 2-amino-1-methyl-6-phenylimidazo [4,5-b]pyridine (PhIP) known to cause prostate cancer in rodents (Weight et al., 2017; Pacheco et al., 2016). Lifestyle and obesity is associated with both increased cancer incidence and progression in multiple tumour types, and is estimated to contribute upto 20-25 % of cancer-related deaths. These associations are driven, in part, by metabolic and inflammatory changes in adipose tissue that disrupt physiological homeostasis both within local tissues and systemically (Quail et al., 2019). Although, cancer is non-contagious, there are studies which reveal infectious aetiology of viral cancers. Seven established human cancer viruses include a positively stranded RNA virus (HCV), a complex and stable retrovirus (HTLV-I), small (MCV and HPV) to large DNA viruses (KSHV and

EBV), and a DNA virus with a retroviral component to its life cycle (HBV) [Chang et al., 2017].

2.5.1. Hallmarks of cancer

The six hallmarks of cancer proposed by Hanahan and Weinberg, (2000) were revised due to conceptual progress after a decade to summarize the logical frame work of neoplastic diseases by adding four other hallmarks (Fig. 2.1). Loss of control over the growth of the neoplastic cells makes them replicate uncontrollably and exhibit sustained proliferative signaling leading to cancerous condition. This causes the cancer cells to exhibit more receptors, stimulate neighbouring normal cells to release growth factors thus making them active and proliferating (Amin et al., 2015). Alteration in signaling pathways, deregulation of cell-cycle proteins, hypoxia, altered metabolism resulting from mutations and/or epigenetic changes promote survival and growth of cancer cells by constitutively stimulating signaling pathways (Feitelson et al., 2015). Immuno-editing done by cancer cells as well as a suppressed immunogenicity by genetic instability were selected and promoted to be solid tumours and this was also considered to be a new hallmark (Hanahan and Weinberg, 2011). Genomic instability was reported in hereditary and sporadic cancers. These develop by mutations in DNA repair mechanism which gets multiplied on further cell proliferation. Microsatellite instability, increased base-pair mutations, variations in expression of tumour suppressors such as *P53*, *CDKN2A*, *PTEN*, DNA damage checkpoint gene and cell growth oncogenes *EGFR* and *RAS* also resulted in genomic instability that lead to cancer (Negrini et al., 2010). Patients with familial breast cancer and Fanconi's anemia expressed chromosome instability by mutations in *CHEK2*, *ATM*, *NBS1*, *RAD50*, *BRIP1* and *PALB* (Yao et al., 2014).

Metastasis is a complicated process of spreading and development of cancer through an invasion-metastasis cascade. The cascade starts with angiogenesis followed by detachment of cells from the site of origin, their migration and invasion through basement membrane and movement through blood to settle at a different target site and flourish (Guan, 2015). Most complications and cancer recurrence

occurs due to this invasiveness. Growth factors such as prostaglandin E2, EGF, and VEGF as well as molecular mediators of the epithelial-mesenchymal transition have been identified to potentiate metastatic spread of colorectal carcinoma (Kanthan et al., 2012). The survival of multiplying cancer cells shows an altered metabolic energetics of increased glucose uptake, glutaminolysis and fatty acid synthesis (Fadaka et al., 2017)

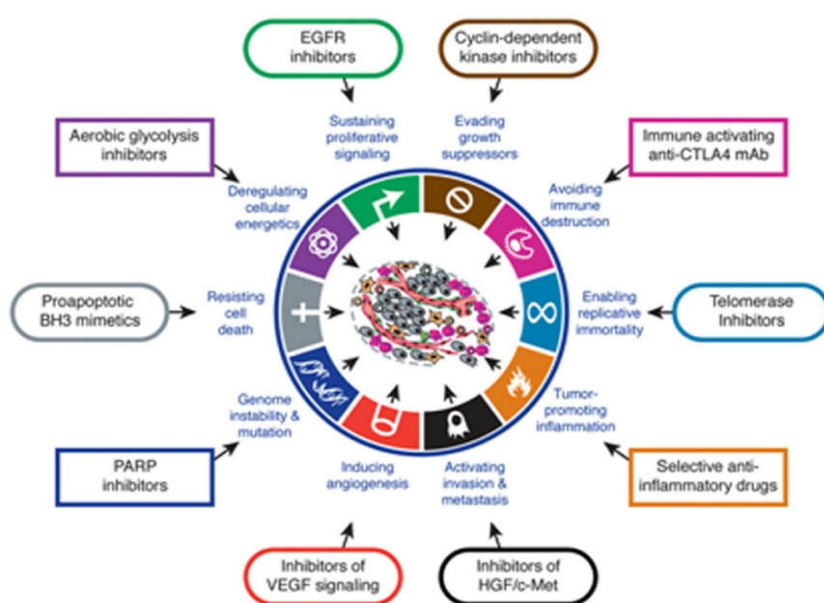


Fig.2.1. Hallmarks of cancer (Hanahan and Weinberg, 2011)

2.5.2. Deregulation of cell cycle and apoptosis leads to cancer

Cell cycle is a highly orchestrated mechanism of the growth and division of mother cells into their healthy daughter cells. Any damage caused to the parent cell is either efficiently repaired or removed in the normal condition of cell cycle. However, a defective eukaryotic cell cycle leads to the world's worst disease of chaos, cancer. Briefly, cell cycle is divided into two major stages (i) a long interphase consisting of two Gap phases G_1 and G_2 flanking the genome synthetic S phase and (ii) a short mitotic (M) phase comprising of mitosis and cytokinesis but with a G_0 or quiescence/resting phase. The entire process is sequentially and carefully scrutinized by cell-cycle engines driven by cyclins, cyclin-dependent kinases (cdks) and cdk inhibitors (Lim et al., 2013). The role of these trio proteins

which is depicted in the Fig. 2.2. explains their unavoidable significance in the mechanism of surveillance. Various checkpoints monitor cell size, DNA damage and microtubule-spindle fibre assemblies during each phase of cell cycle progression (Barnum and O'Connell, 2014). Cdks are members of well conserved serine/threonine protein kinase family and their activity depends on changes in the levels subunits of regulatory proteins such as cyclins according to the necessities of cell cycle phases.

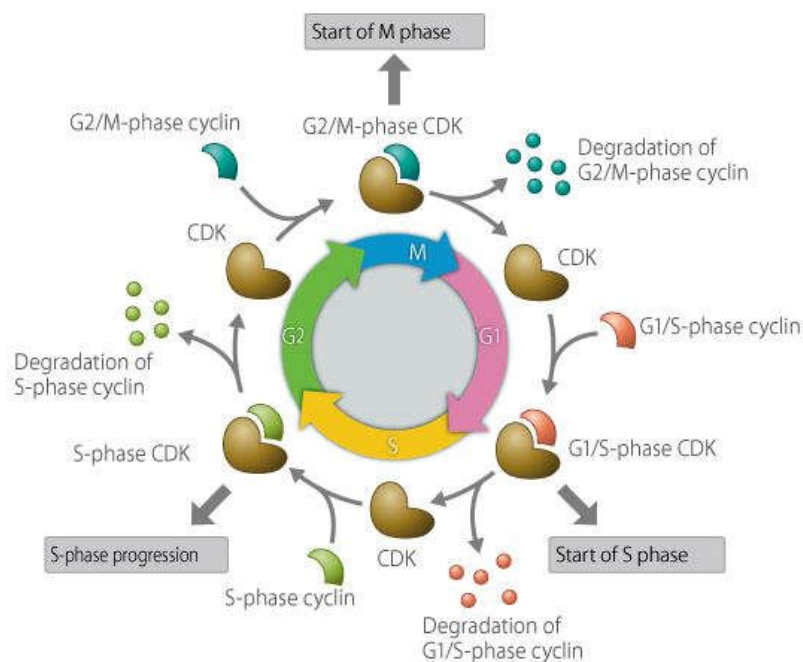


Fig. 2.2. Schematic representation of eukaryotic cell cycle
(courtesy CSLS / The University of Tokyo)

It is clear that, a single disturbance in these highly co-ordinated complex physiological cycles may lead to high risk pathological complications. Deregulation of cell cycle by defective check points - G₁/S, G₂/M and spindle assembly - lead to multiplication of mutated daughter cells and the condition could become irreversible and susceptible to proliferation. For example, RB gene mutation cause misregulation of G₁/S checkpoint which leads to retinoblastoma while cyclin D overexpression also affects the same checkpoint causing breast cancer, skin and esophageal cancer. Also, mutations in RB induce aneuploidy and results in hyperexpression of Mad2, a spindle-assembly checking component.

In the face of any irreparable defect in cell cycle progression or damage in cellular genomic content, cells commit suicide thereby preventing proliferation of cancer cells (Wang et al., 2016). This programmed cell death, technically called apoptosis, is associated with typical morphological and biochemical changes within the cell. Apoptosis is a necessity for a pathogen-infected cell, for wound healing and some developmental processes. Mutations in oncogenes or tumor suppressor genes alter/prevent this highly conserved process leading to development of cancer by avoiding cell death and undergoing proliferation without halt (Pierce, 2012). Apoptosis plays an important role in the treatment of cancer as it is a popular target of many treatment strategies. Cancer cells are more sensitive to apoptotic signals than normal cells due to dual upregulation of pro- and anti-apoptotic genes which make them primed for death (Pfeffer and Singh, 2018). Drugs or treatment strategies that can restore the apoptotic signalling pathways towards normality have the potential to eliminate cancer cells (Wong, 2011).

Apoptosis is categorized as type I classic caspase-dependent apoptosis, type II caspase-independent apoptosis with autophagic appearance and double membrane vacuole and type III caspase-independent with condensed chromatin (Hongmei, 2012). Mechanistically, apoptosis is broadly classified into extrinsic, intrinsic and granzyme B pathways (Martin valet et al., 2005). Fig.2.3. depicts the major pathways of apoptosis. Extrinsic pathway is initiated by cell surface death receptors. The death receptors are mainly tumor necrosis factor (TNF) receptor super family. The major ligands and death receptors of this pathway include FasL/FasR, TNF- α /TNFR1, Apo3L/DR3, Apo2L/ DR4 and Apo2L/DR5. Upon ligand - binding, cytoplasmic adapter proteins are recruited which exhibit corresponding death domains that bind with the receptors. Activation of death inducing signaling complex (DISC) followed by that of procaspase-8 leads to apoptosis triggering (Elmore et al., 2007). The intrinsic pathway is regulated by proapoptotic and antiapoptotic genes of *BCL-2* family. The mitochondrial release of cytochrome *c* into cytosol followed by the formation of apoptosome with Apaf-1 further initiates apoptotic cascade by procaspase-9 activation (Hüttemann et al., 2011). Both extrinsic and intrinsic pathway converge on execution pathway of caspase-3, -6 and -7 resulting in cleavage of poly (ADP-ribose) polymerase (PARP) finally causing

cell death. IAPs (Inhibitor of Apoptosis Protein family), an eight-membered protein family, are the most important negative regulators of caspases. IAP classes including XIAP, c-IAP1, c-IAP2 and survivin share a common structural feature possessing baculovirus IAP repeat (BIR) domain at N terminal and a c-terminal ring finger domain. Survivin is normally absent in non-malignant cells but is aberrantly overexpressed in most cancer cells causing apoptotic resistance and hence is used as a therapeutic target. Human granzyme B are serine proteases released by cytoplasmic granules of cytotoxic T lymphocytes (CTLs) / natural killer (NK) cells introduced through perforin to target cells. These enzymes induce cell killing by mitochondrial pathway via cleavage of BID or direct cleavage of caspase-3 and -7 (Safta et al., 2014). However, granzyme A, also known as tryptase follows a caspase-independent apoptotic pathway involving a novel mitochondria-mediated DNA damage pathway (Chowdhary and Lieberman, 2008).

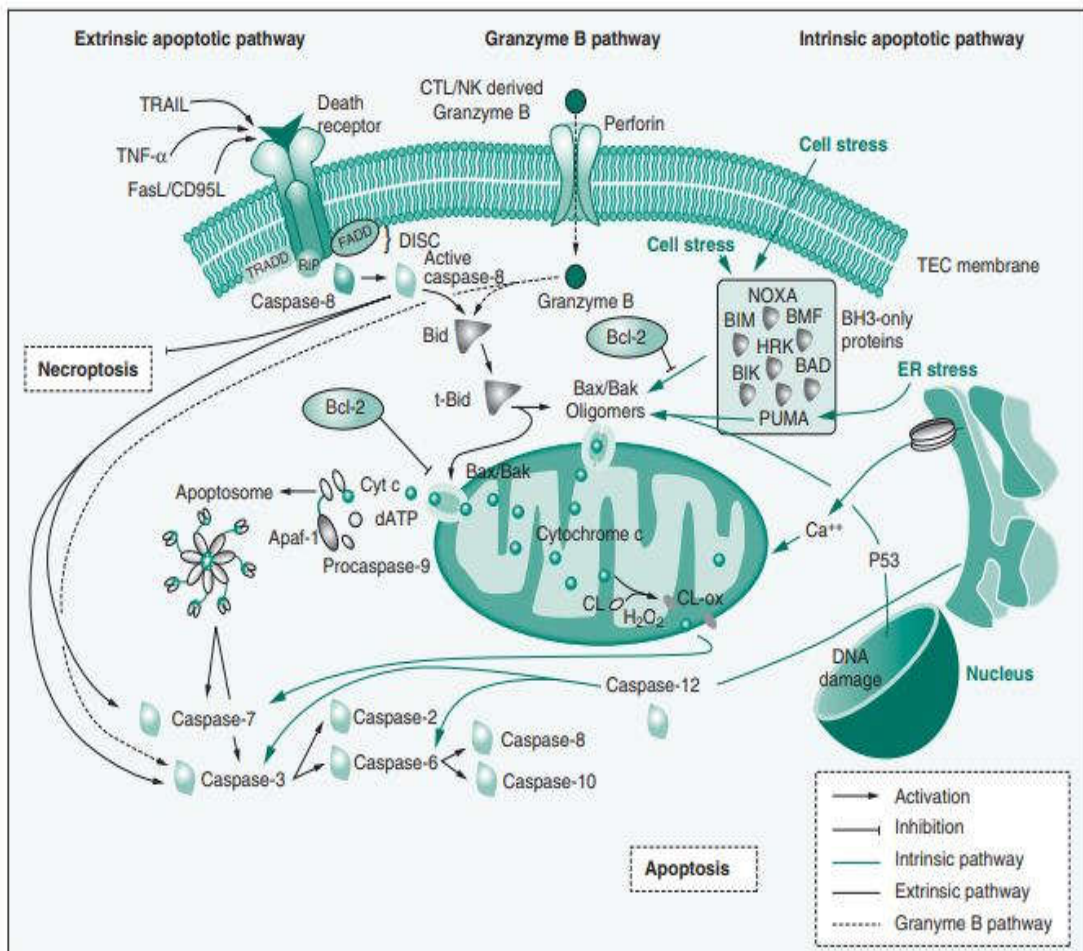


Fig.2.3. Pathways of apoptosis (Kim-Campbell et al., 2019)

The pivotal role of p53, rightly called ‘guardian of genome’ in the control of cell cycle and apoptosis regulation cannot be ignored. This tumor suppressor gene is acclaimed to be the sole guide to decide whether the cell should continue the cycle, arrest or undergo apoptosis. A plethora of external factors causing damage to DNA activate this gene to repair the condition and to prevent further mutations. Also, DNA damage induces activation of kinases like *ATM* (Ataxia telangiectasia mutated protein) and *Chk2* (Checkpoint kinase 2) causing phosphorylation of p53, thus signalling cell cycle arrest/apoptosis. Apoptotic pathway triggered by p53 include trans-activation of pro-apoptotic PUMA (p53 upregulated modulator of apoptosis), FAS (cell surface death receptor) or BAX protein (Vogelstein et al., 2000; Hofseth et al., 2004; Bai and Zhu, 2006; Chiang et al., 2013; Bai and Wang, 2014). Most of the cancers develop due to mutations in p53 resulting in genomic instabilities which leads to tumor progression, drug resistance and metastasis (Joruiz and Bourdon, 2015; Hientz et al., 2017).

2.5.3. Genetics and epigenetics in cancer

Oncogenesis or *tumorigenesis* is a consequence of inappropriate crosstalk between multiple genetic and epigenetic events ultimately culminating in cancer progression. Studies have shown that alterations in genetic and epigenetic factors are the major cause for cancer development. The mutations in genes such as proto-oncogenes, tumor suppressor and genome maintenance genes are termed as ‘driver mutations’ since they drive the development of cancerous conditions. Another class of random ‘passenger’ mutations which do not directly induce disease; instead it occurs due to continuous exposure of mutagenesis and lack of repair, which collectively renders tumors more fragile due to impaired fitness (Wodarz et al., 2018; Salvadores et al., 2019).

Proto-oncogenes code for proteins required for basic cellular survival. However, they become oncogenes on point mutation, chromosomal translocation and amplification. This dominant gain-of-function mutation upregulates proliferation. These genes encode proteins for apoptosis prevention, signal transduction and transcription (eg. *SIS*, *ERB A & B*, *MYC*, *FOS*, *JUN*, *SRC*, *RAS*,

BCL-1). Proto-oncogenes become oncogenes on viral attack by acquiring insertional activation of genes like that of human T-cell lymphotropic virus. *Tumor suppressor gene* mutations also result in hyper proliferation of cells. The loss-of-function by these genes by deletion, point mutation and methylation prevent apoptosis and enhance replication. Some of them for example are cell cycle regulators (p16, RB), transcription factors (p53, WT-1), GTPase activators (NF1) and receptors/signal transducers (TGF- β). The third class of genes mainly consists of *DNA repair components*; on mutation lose their error correcting potential hence proliferate abnormal cells than normal ones. Also, the defective repair genes make normal cuts on genes but remain unrepaired. Defects in nucleotide excision repair and mismatch repair genes results in *Xeroderma pigmentosum*, colorectal, endometrial and stomach cancers.

Epigenetics is the study of heritable phenotype changes in gene expression that do not involve changes to the underlying DNA sequence, which in turn, affects how cells read the genes. Epigenetic change is a regular and natural occurrence but can also be influenced by several factors including age, the environment/lifestyle, and disease state. Epigenetic alteration includes the changes in DNA modification (post-transcriptional control, DNA/promoter methylation) and nucleosome rearrangement (long-range regulation, local nucleosome remodeling, deposition of histone proteins and covalent modification of canonical core histones) [Lund and van Lohuizen, 2004; Ting et al., 2006]. Epigenetic changes also cause genomic instability. The CpG islands hypermethylation related loss-of-function of tumor suppressor gene was reported in colorectal cancer (Hong, 2018). Loss of histone acetylation at lysine 16 methylation in histone H3K4, H3K9, and H3K27 patterns have been spotted in many cancers. EZH2, SETDB1, WHSC1 (MMSET) are some of the histone methyl transferases found to be overexpressed in common epithelial tumors like prostate and breast cancer (Balabhadrapatruni et al., 2016). *MicroRNA* (miRNA) are small non-coding RNAs which act as epigenetic factor(s) by post transcriptional control. They up/down regulate the genes in signaling pathways such as interleukin-6 (IL-6), TGF- β , TGF- β /Smad , Wnt-1 and Wnt-10, Bcl-2, Wnt, Bmi-1, Ccne1, Ccnd1, VEGF , IL-6 in cancer associated fibroblasts of various tumor microenvironments (Du et al., 2016).

2.5.4. Cancer therapy

The main ‘theranostics’ of cancer include surgery, radiotherapy, chemotherapy and their combinations. Randomized clinical trials facilitate assessment of the efficacy (survival frequency) of each treatment method based on a comparison of the tumor size between the treated and control (Damyanov et al., 2018). Surgery is the most commonly used conventional method but the suppression of immune reactivity as well as circulation of tumor cells as a result of post-surgical effect makes the method less acceptable. Wound healing after tumor removal create new issues of neoangiogenesis by vascular endothelial growth factor (VEGF), catecholamines, the wound fluid containing tumor mitogens and angiogenesis of microscopic tumors (Demicheli et al., 2008; Goldstein and Mascitelli, 2011). Radiation therapy depends on type, dose and delivery technique of radiation and also on biological characteristics of cancerous cells to be treated. Mostly, 50% of cancer patients undergo these treatment modalities either alone or in combination with surgery and chemotherapy. A ten year study of treatment of localized prostate cancer proved the inhibition of recurrence of metastasis after surgery and radiotherapy (Hamdy et al., 2016). However, not only tumor cells but also normal cells get mutated or damaged by radiation. Chemotherapy also leads to development of secondary tumors which is to be reduced. Patients with phase III epithelial ovarian cancer were found to survive longer under hyperthermic intraperitoneal chemotherapy during cyto-reductive surgery after their failure with carboplatin and paclitaxel (van Driel et al., 2018). Decline in 21-gene breast cancer mortality was achieved by adjuvant chemotherapy (Sparano et al., 2018). PARP inhibitors combined with chemotherapy helped to reduce tumor relapse by colorectal cancer initiating repaired cells (Jarrar et al., 2019). In patients with previously untreated metastatic non-squamous NSCLC without *EGFR* or *ALK* mutations, the addition of pembrolizumab to standard chemotherapy of pemetrexed and a platinum-based drug resulted in significantly longer survival and progression-free survival than chemotherapy alone (Gandhi et al., 2018). Majority of ovarian cancer were found to relapse and become resistant even after common treatment with a combination of platinum complex and taxane. The efficacy of drug delivery in this

case was obtained by targeting angiotensin signaling with losartan, thus reducing the inhibitory barriers of the tumor microenvironment (Zhao et al., 2018). Hormonal therapy is mainly implemented in the case of prostate and breast cancer. Hormonal therapy with salvage radiation therapy for recurrent prostate cancer was reviewed by Spratt et al, (2017). Chemo-hormonal therapy in prostate cancer improves longevity by adding docetaxel to androgen-deprivation therapy (Kyriakopoulos et al., 2018). Immune blockade checkpoint is a main target of immunotherapy and antibodies against those points were found to be effective in melanoma, renal cell carcinoma and bladder cancer (Hodi et al., 2010; Powles et al., 2014; McDermott et al., 2015). Immunotherapy against programmed death-1 pathway was studied for uro-epithelial bladder cancer (Ghasemzadeh et al., 2015). Chimeric antigen receptor gene-engineered T cell immunotherapy was reported to be an optimistic approach to patients with terminal cancers (Johnson and June, 2017).

The advent of next-generation genomic sequencing tools and biocomputational technologies can give a better understanding of molecular/genetic signatures of each type of cancer and this could pave way to personalized medicine. Personalization increases benefits to large population and decreases cost of therapy (Yeang and Beckman, 2016). Thus based on molecular analysis and tumor microenvironment, personalized cancer therapy can be worthwhile with minimum side effects (Curigliano and Criscitiello, 2014). Charged, small sized non-coding microRNA (miRNA) molecules are promising candidates in cancer therapy as they can effectively silence genes and also target tumor promoting stromal cells thereby delivering potent anticancer activity without immune responses. MiRNA-126 targeting VEGF and EGFL7 showed prognostic value to provide predictive information in relation to the therapeutic outcome of anti-angiogenic agents in metastatic colorectal cancer (Chen et al., 2015).

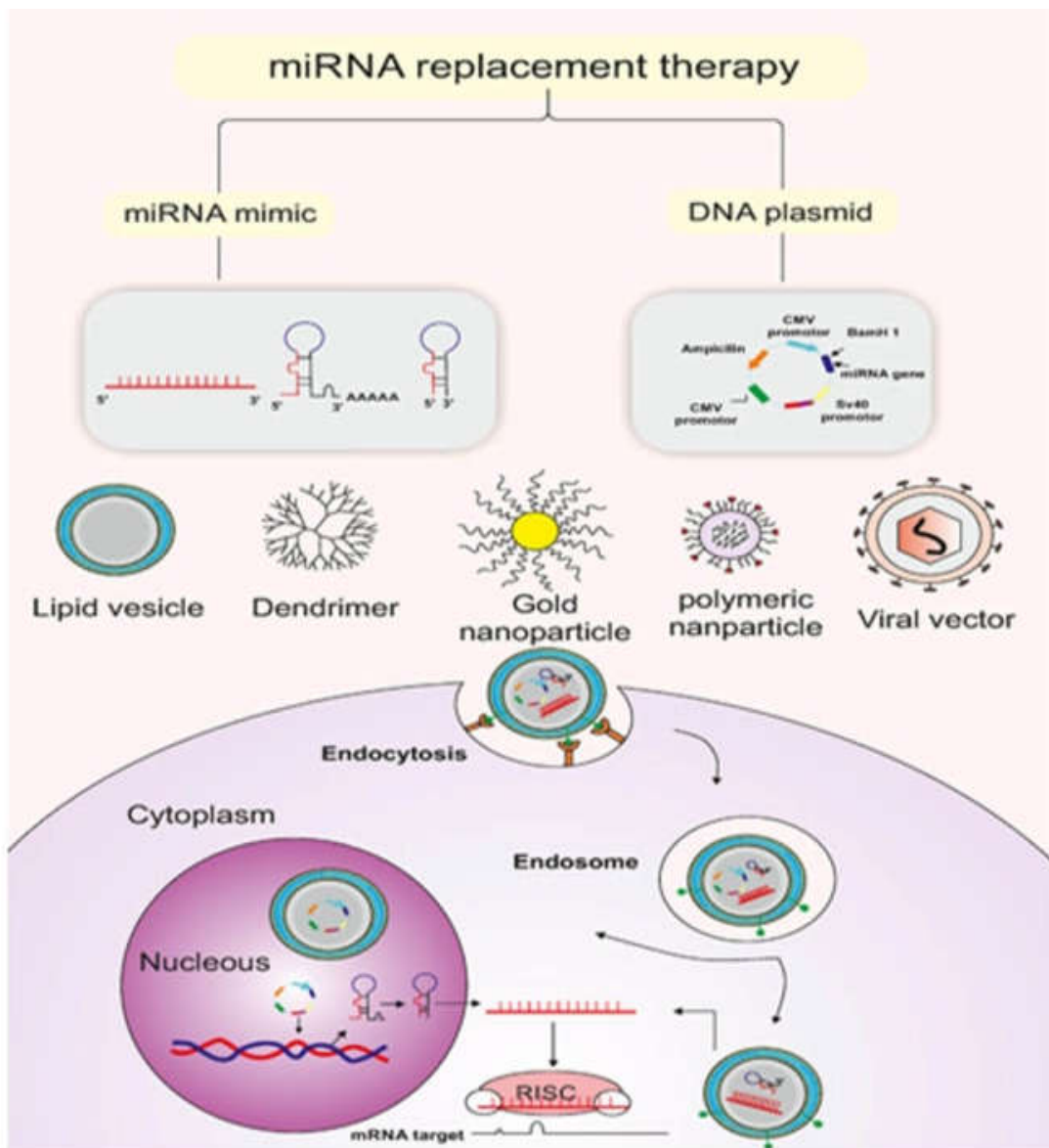


Fig. 2.4. miRNA replacement therapy (Hossenahli et al, 2018).

miRNA replacement therapy (Fig.2.4) involves miRNA mimics or DNA plasmid encoding miRNA genes targeting cancer cells using delivery vector (Hossenahli et al., 2018). Tumor suppressor miRNA mimics such as *145*, *520h*, *Let-7*, *34a* and *29b* are available for colon, pancreas, liver, neuroblastoma and AML respectively (Gregersen et al., 2010; Wang et al., 2010; Lan et al., 2011; Tivnan et al., 2012; Huang et al., 2013). Anti-apoptotic survivin molecule is found to be cancer-inducing and downregulation of this protein is found to be a fruitful approach against squamous cell carcinoma. Dominant-negative survivin mutants, RNA

interference, anti-sense oligonucleotides, small-molecule inhibitors, and peptide-based immunotherapy are recent developments utilized in reducing tumor growth by inactivating survivin (Santarelli et al., 2018). Macrophage-directed immunotherapy is found to be a natural, effective and less toxic method changing M2/repair-type macrophages to M1/kill-type thereby minimizing cancer growth (Mills et al., 2016). Compromising of fork stability mechanism is a good strategy to endure potential cancer therapy by synthetic lethality in chemotherapy and also mutation in replication fork proteins (cancers without BRCA1/2 mutation) which creates alternate pathways for therapy (Liao et al., 2018).

MDM2 inhibitors are used in molecular targeting in advanced triple negative breast cancer, irrespective of p53 status, were found to be appealing. The inhibitors include novel, small molecules such as SP141 reported to reduce cancer growth and metastasis *in vitro* (Qin et al., 2017). It was reviewed that conditionally replicating adenoviral vectors conjugated with short hairpin RNAs produce successful antitumor activities in experimental as well as preclinical trials (Zhang et al., 2016). Tumor necrosis factor- α (TNF α) and interferon- γ (IFN γ) are two cytokines acting as immune modulators and hence have role in cancer therapy. Homing of TNF α and IFN γ to tumor vessels reduce angiogenesis by inhibiting differentiation of tumor associated macrophages and VEGF expression in tumor microenvironment (Shen et al., 2018). Altered energy metabolism of cancer cells was a unique therapeutic intervention of which glutamine metabolism is a good target in cancer prevention (Zhang et al., 2013). Tumor acidosis in colorectal cancer also proves to be a good strategy for precise treatment (Wang et al., 2019). Adjuvant therapy was utilized in randomized clinical trials of metastatic melanoma since 2011 (Ugurel et al., 2017). Targeted medications provide long-term beneficial effect with absence of metastases and reduced tumor burden (Ascierto and Dummer, 2018). A risk based therapy for lethal acute myelocytic leukemia was optimized using *in silico* resources to obtain better results (Yoshinari et al., 2019).

Prokaryotic adaptive immune system containing a programmable single stranded guide RNA attached with a cas9 endonuclease called as Clustered regularly

interspersed short palindromic repeats/cas9 or shortly *CRISPR/Cas9*, opened a plethora of applications in gene editing and engineering as well as in cancer therapy. Synergistic gene interaction, functional gene identification, target validation were possible by using this molecule (Tian et al., 2019). First clinical trial of CRISPR was done in 2016 in China in a non-randomized open label phase I study. In this, engineering T-cells by knock out of programmed cell death protein-1 in *ex vivo* treatment of a metastatic non-small cell lung cancer patient was found to be effective after failures of all standard treatments (Zhan et al., 2019). This editing machinery also has a positive impact on drug discovery and drug target screening. Three genomic libraries are in use (i) CRISPR-based loss-of-function, (ii) CRISPR based-gene activation and (iii) CRISPR based-gene inhibition to screen out positive and negative conditions of drugs (Shalem et al., 2014; Joung et al., 2017; Luo et al., 2016). In cancer therapy, this novel tool can direct endogenous gene expression using guide RNA as well as could alter epigenomic DNA methylation using cas9 tethered to histone modifiers (Martinez-Lage et al., 2018). PD-1 disruption by CRISPR/Cas9 done by Su et al, (2016) improved the efficacy of T cell-based adoptive therapies in Epstein-Barr virus-associated gastric cancer in clinical studies. Although this technology is advantageous, it is not error-free and is also time-consuming. Also, ethical claims were raised after the birth of ‘CRISPR babies’ on November 2018 (Ghosh et al., 2019).

Natural chemopreventive/antiproliferative agents are studied widely on their chemotherapeutic efficiency. Anticancer compounds from different natural sources such as (i) plants - include the microtubule-destabilizing vinca alkaloids (vincristine, vinblastine, vinflunine, vinorelbine, vindesine and eribulin) and microtubule-stabilizing taxanes (paclitaxel, docetaxel, cabazitaxel) (ii) microbes - include doxorubicin, staurosporin, enedyims, daunorubicin (iii) marine biota - include ecteinascidin 743, halichondrin B, dolastatins and (iv) slime molds – include epothilone A & B (Cragg and Pezzuto, 2016; Amaral et al., 2019). According to Amaral et al. (2019), of the 174 compounds approved for commercialization in cancer therapy, 93 (53%) were natural products or their derivatives. Paclitaxel under brand name Taxol[®] from bark of *Taxus brevifolia* Nutt.

(Pacific yew) was acclaimed as a successful story of plant-based chemotherapy. Similarly, curcumin obtained from the rhizome of *Curcuma longa* L. can act on various signaling pathways and can reduce cancer cell proliferation (Seca et al., 2018). Minimally invasive photodynamic therapy utilizes a plant-derived photosensitizer and light to target cancer cells (George and Abrahamse, 2015). Inherited genetic mutations play a major role in about 5 to 10 percent of all cancers (National cancer institute, 2017). Likewise, a small but significant percentage proportion of human cancers, perhaps 15 % worldwide are thought to arise due to involvement of viruses, bacteria or parasites (Alberts et al., 2015). The majority of cancers (≥ 85 %) are rooted in environment and lifestyle (Anand et al., 2008). Therapeutic modalities including lifestyle and dietary changes can influence cancer prevention. Calorie restriction, short-term and prolonged fasting, ketogenic plant-based diets are some of the effective preventive measures (Lettieri-Barbato and Aquilano, 2018). A recent study also highlights alleviation of side-effects and improvement in the quality of life due to physical exercise in breast cancer patients undergoing chemotherapy (Haas et al., 2019).

Since cancer is a disease not confined to a single organ or tissue but affects the entire body system with high heterogeneity, proper cost-effective and low time-consuming therapeutic approaches with fewer side effects must be developed. Optimization of combined therapies along with proper counseling to patients is a hope to successful outcomes. However, the alleviation of risk factors of post-treatment must be a concern for achieving new treatment horizons.

2.5.5. Cancer nanomedicine

Engineering of nanoparticles with necessary tailoring of their properties make them a good candidate for nanomedicine. The enhanced retention and permeation (EPR) effect and selective targeting of nanomaterials are hot topics in therapeutic research. Liposomal doxorubicin (DoxilTM/CaelyxTM) was the first anti-cancer nanomedicine approved by the FDA in 1995 (Barenholz, 2012). Some of the approved anti-cancer nanomedicines include liposome-carried doxorubicin (MyocetTM) / vincristine (MarqiboTM) / daunorubicin (DaunoxomeTM) and

irinotecan (Onivyde™) for metastatic breast cancer, acute lymphoblastic leukemia, HIV-related Kaposi's Sarcoma and second line metastatic pancreatic cancer respectively. Polymeric-conjugated asparaginase [Oncaspar™(PEG)] and polymeric- micelle paclitaxel (Genexol-PM™) have been approved nanomedicines for acute lymphoblastic leukemia and non-small cell lung cancer (Hare et al., 2017). 'Soft and hard' nanomaterials have been shown to accumulate in the lymph nodes / lymphoid tissues and their interaction with immune cells can induce a controlled immune response at the affected site (Björnmalm et al., 2017). Tumour hypoxia is a privilege of tumour cells for the expansion of cancer cells through angiogenesis and metastasis. Development of oxygen-filled nanocarriers and oxygen generators have been shown to improve the efficacy of cancer therapy by modulating tumour hypoxic condition (Jahanban-Esfahlan et al., 2017; Liu et al., 2018). For oral cancer therapy, several plant compounds and chemocompounds designed in nanoforms were introduced as successful drugs by enhancing drug solubility. Natural compounds such as curcumin, naringenin, genistein loaded nanoparticles, colloidal gold NPs, magnetic NPs and UVA-1 activated ZnO NPs were found effective against oropharyngeal squamous cell carcinoma (Marcazzan et al., 2018). Nanoparticles, designed as an ideal candidate for antitumor vaccine delivery with unique composition and surface-charge profiles, can selectively cluster onto lymphoid organs such as spleen and produce desired immunomodulatory effects. Delivery of antitumor vaccine adjuvants via nanoformulations can enhance their potency while reducing side effects by limiting systemic distribution of adjuvants and prolonging their activity in draining lymph nodes (Liu et al., 2018). Fucoidan from brown seaweed based nanocomposites have been used as nanocarriers of drugs like curcumin, paclitaxel and growth factors for delivery (Aquib et al., 2019). A colon cancer-targeted nanomedicine made of pH sensitive polymeric nanoparticles of quercetin was also reported recently (Sunqrot and Abujamous, 2019). The dual role of nitric oxide (NO) in EPR enhancement and cytotoxicity effects has been utilized as an intelligent nano-system involving switchable HSA-NO carrier to adjust NO release for increased drug accumulation and suppress tumor growth (Xu et al., 2019). Functionalized nanogold particles with specific architecture and

characteristics were utilized as drug delivery devices, modulators of angiogenesis, or heat-activated factors destroying tumor tissue (Sztandera et al., 2019). Activatable singlet oxygen generation from lipid hydroperoxide nanoparticles for cancer therapy have been shown to induce efficient apoptotic cancer cell death both *in vitro* and *in vivo* through tumor-specific O₂ generation and subsequent ROS-mediated mechanism (Zhou et al., 2017). Metal nanoparticles were reported to possess a beneficial and powerful role in cancer therapy by means of better targeting, gene silencing and drug delivery. Surface modified particles with targeting ligands offer a better control of energy deposition onto tumours. Besides use as a diagnostic tool for cancer cell imaging, these particles can also allow controlled and targeted drug release for effective cancer treatment and management (Sharma et al., 2017).

2.6. Preliminary screening of plants employed for biosynthesis of zinc oxide nanoparticles

Botanical classification of the plants (Kingdom Plantae) screened for extracts prepared from parts thereof, suitable for lab-scale synthesis of biogenic ZnONPs, is tabulated below:

Table 2.4. Botanical classification of plants used for screening of extracts for phyto-mediated synthesis of ZnONPs

No	Scientific nomenclature	Order	Family	Genus	Species	Plant parts used for extract preparation
1	<i>Annona muricata</i> L. Common name : Soursop, Graviola Vernacular name : Mullanchakka, Mullatha	Magnoliales	Annonaceae	Annona	<i>A. muricata</i>	Leaves Fruits Seeds Roots
2	<i>Annona reticulata</i> L. Common name : Wild sweet sop, Bull's heart Vernacular name : Manilanilam, Aatha	Magnoliales	Annonaceae	Annona	<i>A. reticulata</i>	Leaves
3	<i>Annona squamosa</i> L. Common name : Sugar- apple, Sweet sop Vernacular name : Seethapazham	Magnoliales	Annonaceae	Annona	<i>A. squamosa</i>	Leaves
4	<i>Manilkara zapota</i> (L.) P. Royen Common name : Sapodilla, Chikoo Vernacular name : Sapota	Ericales	sapotaceae	Manilkara	<i>M. zapota</i>	Leaves
5	<i>Spondias pinnata</i> (L. f.) Kurz. Common name : Wild mango, Indian hog plum Vernacular name : Ambazham	Sapindales	Anacardiaceae	Spondias	<i>S. pinnata</i>	Leaves

6	<i>Plumeria obtusa</i> L. Common name : White frangipani Vernacular name : Vellachempakam, Velutharali	Gentianales	Apocynaceae	Plumeria	<i>P.obtusa</i>	Leaves
7	<i>Citrus maxima</i> (Burm.) Merr. Common name : Pomelo, Chinese grapefruit Vernacular name : Kampilinaranga	Sapindales	Rutaceae	Citrus	<i>C.maxima</i>	Leaves
8	<i>Cinnamomum verum</i> J.Presl Common name : Ceylon cinnamon Vernacular name : Karuva, Elavangam	Lurales	Lauraceae	Cinnamomum	<i>C.verum</i>	Leaves
9	<i>Cassia fistula</i> L. Common name : Golden shower, Indian laburnum Vernacular name : Kanikonna	Fabales	Fabaceae	Cassia	<i>C.fistula</i>	Flowers
10	<i>Curcuma zedoaria</i> (Christm.) Roscoe. Common name : White turmeric Vernacular name : Kachcholam, Kua, Pulakizhanna	Zingiberales	Zingiberaceae	Curcuma	<i>C.zedoaria</i>	Rhizomes

2.6.1. Ethnopharmacology of selected plants in brief :

Of the multiple plant parts screened, the extracts prepared from leaves of *Spondias pinnata* (L. f.) Kurz and *Manilkara zapota* (L.) P. Royen and those obtained from the roots, fruits and seeds of *Annona muricata* L. were found to successfully support the biosynthesis of ZnONPs through phytoconstituent-assisted bioreduction process. A brief note on the ethnopharmacological importance of the three selected plants are given below :

2.6.1.1. *Spondias pinnata* (L. f.) Kurz. : *S. pinnata* (Fig.2.5), commonly known as 'hog plum', is a deciduous or semi-evergreen glabrous tree with a pleasant woody smell. They are widely distributed in China, Malaysia, Sri Lanka, Thailand, Myanmar, Andaman Islands and Indian Himalayas. The leaves are compound, pinnate, spirally arranged whilst the fruit is a single seeded drupe (Khomdram et al., 2014). Ethnomedicinally, various parts of this plant are used for different ailments. The bark is traditionally used for treating dysentery, diarrhoea, diabetes mellitus and muscular rheumatism whilst leaves have been found useful for ear-ache. The antiscorbutic fruits are useful for ailments such as bilious dyspepsia, sore throat and cure for bowel disorders (Attanayake et al., 2014; Kamal et al., 2015)

Phytochemically, the tree is a resource for water-soluble polysaccharides (galactose, arabinose), aminoacids (glycine, serine, and alanine), various sterols and terpenoids (Das et al., 2011). The leaves reportedly contain large amount of phenolics and therefore possess good antioxidant activity (Sujarwo et al., 2017). The glycosidic-rich fraction obtained from the bark is known to ameliorate iron overload-induced oxidative stress and hepatic damage in swiss albino mice (Chaudhari et al., 2016). Methyl gallate isolated from bark has been found to induce apoptosis in human glioblastoma (Chaudhari et al., 2015). Other bioactivities reported from the plant include anti-bacterial, ulcer-protective, antihelmintic, anti-diabetic, hepatoprotective and anti-cancerous potential (Bora et al., 2014).



Fig. 2.5. *Spondias pinnata* (L. f.) Kurz.

2.6.1.2. *Manilkara zapota* (L.) P. Royen : The tree is a large, glabrous and evergreen member of the family Sapotaceae comprising of ~79 species. The plant is commonly known as sapodilla (Fig. 2.6.), which grows well under tropical conditions providing edible, sweet and malty flavoured fruits in addition to timber and latex (Uekane et al., 2017). The fruits, rich in nutritional value with high levels of sucrose and fructose, are consumed as fresh or processed as jams and beverages (Shafii et al., 2017). Traditionally, *M. zapota* has been used for several ethnomedical purposes. The medicinal properties of the plant parts have been effective in treating ailments such as diarrhoea, colds, ulcers and fever.



Fig. 2.6. *Manilkara zapota* (L.) P. Royen

M. zapota is also reported to possess a wide range of bioactive constituents including triterpenoids, fixed and saturated oils, hydrocarbons, sterols, enzymes, alkaloids, phenolic compounds, minerals, carbohydrates, amino acids and the saponin known as 'manilkoraside' (Milind and Preeti, 2015). Fruits of this plant are also utilized for cosmeceutical applications (Shafii et al., 2017; Kashif and Akhtar, 2019). Other medicinal properties reported include antinociceptive (Ganguly et al., 2016), anti-inflammatory (Hossein et al., 2012), antipyretic (Ganguly et al., 2013), anti-hypercholesteremic (Fayek et al., 2012), antibacterial (Priya et al., 2014), antifungal (Shanmughapriya et al., 2011) and antihelmintic activities (Kumar et al., 2012). Besides these, several reports on anticancer potential of various extracts of sapota have also been published. These include studies on demonstrating their cytotoxicity against lung carcinoma A549, breast cancer MCF-7, and human cervical HeLa cells (Awasare et al., 2012; Tan et al., 2018; Bashir, 2019).

2.6.1.3. *Annona muricata* (L.) : This tropical tree, also known as soursop, belongs to the family Annonaceae (Fig. 2.7.). Endemic to the warmest areas of the tropics of South and Central America and the Caribbean, it is also distributed widely in tropical and subtropical regions of Central and South America, Western Africa, and Southeast Asia (Abdul Wahab et al., 2018). All parts of the tree including the edible fruit are reported with multiple activities such as anticancer, anticonvulsant, antiarthritic, antiparasitic, antimalarial, hepatoprotective, antidiabetic, analgesic, hypotensive, anti-inflammatory, and immune-enhancing effects (Ferreira et al., 2013; Astirin et al., 2013; Ishola et al., 2014; Patel and Patel, 2016).

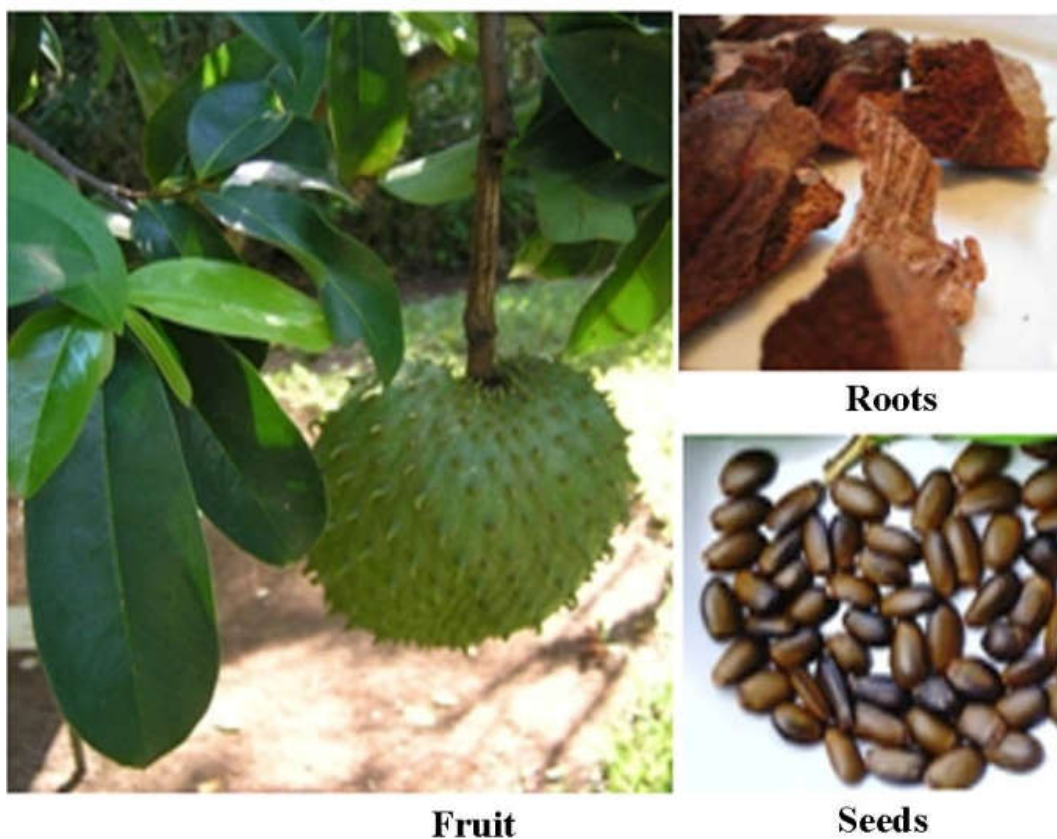


Fig. 2.7. *Annona muricata* (L.)

Traditionally, the leaves are used for treating ailments like headaches, insomnia, cystitis, liver problems and diabetes. Recently, leaves have also been reported to be a source of antioxidant compounds with *in vitro* antidiabetic and inhibitory potential against α -amylase, α -glucosidase, lipase, non-enzymatic glycation and lipid peroxidation (Justino et al, 2018). Leaves are also endowed with

anti-inflammatory, anti-spasmodic and anti-rheumatic activities (de Sousa et al., 2010; Hamizah et al., 2012). Over 400 annonaceous acetogenins isolated from the leaves, seeds, roots, fruits and bark of the tree have been reported to possess cytotoxic and antitumour activities (Rupprecht et al., 1990; Moghadamtousi et al., 2015; Han et al., 2015). Anticancer activity has also been reported against Hep G2, HeLa, A549, HCT 116, MCF-7, leukemic, glioma and pancreatic cancer cells (Liu et al., 2016; Rady et al., 2018; Yajid et al., 2018). The plant extract is also reported to possess the ability to reduce inflammation through inactivation of NALP3 inflammasome (Bitar et al., 2018). Green synthesis of silver and gold nanoparticles employing the extracts of *A. muricata* has been recently achieved (Gavamukulya et al., 2019; Folorunso et al., 2019).

PHYTO-MEDIATED BIOSYNTHESIS AND PHYSICO-CHEMICAL CHARACTERIZATION OF ZnONPs

3.1. Introduction

Biological synthesis of nanoparticles exploit different micro-macroorganisms including bacteria, fungi, microalgae, seaweeds, plants and plant products. Studies have shown that these living systems provide precursors which enable bioreduction of non-metallic and metallic elements/compounds followed by activation/nucleation/coalescence into larger aggregates. Increase in thermodynamic stability and the final shaping of the nanoparticles occurs in the termination phase of synthesis (Makarov et al., 2014). Biological methods have assumed predominance in recent times as they are considered to be ‘green’ or environment-friendly, cost-effective, easier to scale-up and do not entail use of high temperature, pressure, energy, toxic solvents or generate hazardous byproducts.

Phyto-mediated synthesis is an attractive ‘bottom-up’ approach for synthesis of nanoparticles. Bottom-up or self assembly employs atom-by-atom, molecule-by-molecule or cluster-by-cluster construction of a structure into the final material using biological procedures for synthesis. Plants offer a rich, diverse and easily available source of phytochemicals such as ketones, aldehydes, flavonoids, phenolic compounds, alkaloids, sterols, saponins, tannins, amides, terpenoids, carboxylic acids and polysaccharides which can act as reducing, capping and stabilizing agents (Ahmed et al., 2017). Plant based biosynthesis of nanoparticles such as carbon, titanium, cobalt, copper, gold, silver, platinum and palladium, to mention a few, have been successful. Such biogenic nanoparticles have proven to be potentially useful in many biomedical applications including nanomedicine based innovations (Prarthna et al., 2010; Malik et al., 2014; Singh et al., 2018).

This chapter reports on the materials and methods involved in the laboratory scale production of novel zinc oxide nanoparticles and the results obtained thereof.

A total of 10 plants were chosen randomly, following a literature scan, ensuring that the selected plants had not been previously exploited for the purpose. The preliminary screening to select the suitable plant extracts and the methodologies adopted have been described in detail. Confirmation of successful generation of phyto-derived ZnONPs was ascertained by X-ray diffraction (XRD) and Field emission scanning electron microscopy (FESEM) techniques. Subsequent characterization was carried out employing an array of physico-chemical techniques to obtain additional information on their optical, morphological and chemical features. These were [i] UV-visible spectroscopy (UV-vis) [ii] Photoluminescence (PL) [iii] Fourier transform infrared spectroscopy (FTIR) [iv] Energy dispersive X-ray spectroscopy and [v] High resolution transmission electron microscopy (HRTEM). *The commercially available, chemically synthesized zinc oxide nanoparticles (denoted as 'cZnONPs') purchased from Sigma-Aldrich (USA) was also characterized in parallel, using the above mentioned techniques. This was found necessary since the commercial version of nanoparticles was used as controls in all experiments for a strict comparative (biogenic versus chemically synthesized) evaluation of the nanoparticles.*

3.2. Materials and methods

3.2.1. Biosynthesis of ZnONPs

Of a total of ten plants selected for the present study from Malappuram and Thrissur districts in Kerala state (section 2.6; Table 2.5), the plants and parts thereof used for extract preparation were:

1. **Leaves** of (i) *Annona muricata* L., (ii) *Annona reticulata* L., (iii) *Annona squamosa* L., (iv) *Manilkara zapota* (L.) P. Royen, (v) *Spondias pinnata* (L. F.) Kurz., (vi) *Plumeria obtuse* L., (vii) *Citrus maxima* Merr., (viii) *Cinnamomum verum* J. Presl,
2. **Fresh flowers** of (ix) *Cassia fistula* L.,
3. **Rhizome** of (x) *Curcuma zedoaria* Mangaly & M.Sabu and
4. **Roots, fruits & seeds** of *Annona muricata* L.

3.2.1.1. *Preparation of plant extracts*

Plant parts were washed thoroughly in tap water and then with distilled water to remove all traces of dust and impurities. They were then finely chopped, shade-dried and ground into a coarse powder. For plant extract preparation, 10 g of powder was boiled in 200 ml of deionized distilled water for 30 min. The decoction was cooled and pre-filtered through muslin cloth prior to filtration using Whatman No.1 paper. They were then stored in refrigerator for future use.

3.2.1.2. *Biosynthesis by sol-gel method*

Varying amounts (25 - 75 ml) of the individual extracts prepared from the different plant parts were warmed-up. The metal precursor, zinc nitrate hexahydrate (HiMedia Laboratories Pvt Ltd. India), was then added to the extracts at different concentrations, ranging from 4 - 12 % (w/v). The solution was allowed to boil by continuous magnetic stirring for 1 h until it became thicker and turned yellow to golden yellow colored with a gel-like consistency. The semi-solid gel was then subjected to calcination in a ceramic crucible at temperatures ranging from 400-800 °C, for time duration of 1- 3 h, in an air-heated muffle furnace. The calcined product obtained as flakes was then ground into a fine powder before proceeding for characterization.

3.2.2. Characterization

To ascertain whether the attempted biosynthesis resulted in the formation of ZnO nanoparticles, the finely ground calcined products were individually subjected to a primary screening employing XRD and FESEM techniques. Based on the results of this screening, subsequent to confirmation of the successful formation of biogenic ZnONPs, each of the samples was evaluated by other aforementioned techniques.

3.2.2.1. *X-ray diffraction (XRD) analysis*

The purity, crystallinity and average grain size of both of the chemical and biosynthesized versions of nanoparticles were analyzed by X-ray Diffraction studies

using X-ray diffractometer (Rigaku miniflex) with Cu-K α radiation ($\lambda = 0.15406$ nm) scanning in a 2θ ranging from 20-80°. The pattern of XRD peaks obtained was then compared with those of the standard JCPDS card Nos. 36-1451 and 80-0075 to evaluate morphology of nanoparticles. The average particle size was calculated using Debye-Scherrer's formula, $D = 0.89 \lambda / \beta \cos\Theta$: wherein, D represents the crystal size, 0.89 denotes Scherrer's constant, λ is the wavelength of X-rays used and β is the full-width-at-half-maximum (FWHM) of the diffraction peak (Ali et al., 2016; Shamhari et al., 2018).

3.2.2.2. *Field Emission Scanning Electron Microscopy (FESEM) & Energy Dispersive X-ray spectroscopy (EDX)*

The overall morphology and structural characterization of both types of nanoparticles were carried out using FESEM analysis; elemental analysis was accomplished by EDX technique. The data was procured using Hitachi SEM instrument-S46600 connected to Horiba EDX system and CARL-Zeiss Gemini 300. For FESEM, samples were mounted on a stub with adhesive carbon tape and sputtered with gold for analysis (Parthasarathy and Thilagavathi, 2011). EDX data confirmed the sample chemistry and purity in terms of the elemental percentage composition. The data is dependent on X-ray beam energy and the atomic number of sample constituents within a restricted area ($1.0 \mu\text{m}^3$) (Scimeca et al., 2018).

3.2.2.3. *Fourier Transform Infrared (FTIR) spectroscopy*

FTIR analysis was carried out using Jasco 4100 spectrophotometer at wavelengths ranging from 4000-400 cm^{-1} . The spectrum thus obtained reveals the presence of functional groups, adsorbed onto the surface of nanomaterial, involved in the reduction, capping and stabilization of nanoparticles. For this, each sample of ZnO nanomaterial was mixed and pelletized with spectroscopic grade potassium bromide and the percentage transmittance was recorded (Khalil et al., 2014).

3.2.2.4. *UV-visible (UV-vis) spectroscopy*

The surface Plasmon resonance (SPR) of ZnONPs was determined from the absorption peak of UV-Vis spectrum of each ZnONPs. For this, the biosynthesized

particles were subjected to brief pulses of sonication using a Branson-150 Sonifier to achieve a homogeneous aqueous dispersion. SPR was then recorded using a λ 25 - Perkin Elmer UV-Vis spectrophotometer in a wavelength range of 200-700 nm and band gap energy was calculated using the formula, $E=hc/\lambda_{(\text{absorption})}$, where h is Planck's constant (6.626×10^{-34} Js), c is the velocity of light (3×10^8 ms⁻¹) and λ is the absorption wavelength of the biogenic ZnONPs. The intensity of absorption was also indicative of its monodispersity (Talam et al., 2012; Mahamuni et al., 2019; Singh et al., 2019).

3.2.2.5. *Photoluminescence (PL) spectroscopy*

The luminescence of ZnONPs is yet another optical property which is determinable in the UV and visible region at room temperature. This property is dependent on the surface defects of the particle (Rauwel et al., 2016). Biosynthesized and chemical ZnONP powders were subjected to PL analysis with an excitonic wavelength of 340 nm in Perkin-Elmer LS-55 luminescence spectrometer and the emission peaks were analyzed.

3.2.2.6. *High Resolution Transmission Electron Microscopy (HRTEM)*

This microscopic technique is utilized to gather information on the fine structure and morphology of nanoparticles. Utilizing a water bath sonicator, the nanoparticles were dispersed in isopropanol for 15 minutes and the samples were then mounted on a copper grid and dried. The analysis was done using Joel/JEM 2100 equipped with 'selected area electron diffraction' (SAED) setup. The crystallinity is determined from the SAED pattern based on the image resulting from the interaction of electrons through the specimen (Wahab et al., 2007).

3.3. Results and discussion

3.3.1. Phyto-assisted sol-gel synthesis of ZnONPs

The calcined powders obtained from individual plant extracts using sol-gel method (section 3.2.1.3.) were subjected to XRD and FESEM to confirm the presence of biosynthesized ZnONPs. Using a trial and error method, the factors

affecting phyto-mediated biosynthesis were empirically determined for 10 plants and parts thereof. The results obtained have been summarized in Table 3.1.

Table 3.1. Optimization of factors affecting biosynthesis of phyto-derived zinc oxide nanoparticles.

	Parameters tested	Range tested	Optimized conditions	Occurrence of biosynthesis using plants and parts thereof (?)	
				Yes	No
Factors affecting biosynthesis	Concentration of Zn(NO ₃) ₂ . 6H ₂ O	4 – 12 % (w/v)	5 % (w/v)	<i>A. muricata</i> (roots*, fruits and seeds*) <i>S. pinnata</i> (leaves) <i>M. zapota</i> (leaves)	<i>P. obtuse</i> (leaves) <i>C. maxima</i> (leaves) <i>C. verum</i> (leaves) <i>C. fistula</i> (fresh flowers) <i>A. squamosa</i> (leaves) <i>A. reticulate</i> (leaves) <i>C. zedoaria</i> (rhizome)
	Temperature of calcination	400 – 800 °C	600 °C		
	Duration of calcination	1 – 3 h	2 h		

* indicates coarse texture of nanoparticles relative to the finer and softer preparation obtained with the remaining plant parts.

Based on the optimization of parameters involved in the sol-gel method adopted, it was found that successful synthesis of phyto-derived nanoparticles could be obtained at a concentration of 5 % (w/v) of the metal precursor, calcination at 600 °C for 2 h. Incidentally, all these three parameters were found to be independent of external pH regulation. Attempts to optimize pH in acidic/alkaline range resulted in total failure of biosynthesis. Presumably, the inherent pH conditions prevalent in the individual aqueous extracts with their specific phytochemical compositions play a critical role in the bioreduction/redox and capping reactions underlying nanoparticle biosynthesis.



Fig. 3.1. Phyto-derived zinc oxide nanoparticles placed in a ceramic crucible.

The abbreviations used to denote the respective nanoparticles are - AmFZnONPs, AmRZnONPs, AmSZnONPs, SpLZnONPs and MzLZnONPs – wherein the first two letters represent the genus and species (Am: *A. muricata*, Sp: *S. pinnata*, Mz: *M. zapota*) followed by the third letter representing the plant part (F: fruit, R: root, S: seed, L: leaf) and ZnONPs represent zinc oxide nanoparticles as mentioned elsewhere.

Successful biosynthesis of ZnONPs by the sol-gel method employing fruits of *Citrus aurantifolia* and *gum tragacanth* have been previously reported (Samat and Nor, 2012; Darroudi et al., 2013). It has been observed that sol-gel chemistry critically influences morphology and size of complex inorganic particles in the presence of biopolymers (Danks et al., 2016). Plant based ‘green’ synthesis of zinc oxide nanoparticles enjoys better public acceptance as it is deemed to be safe biological method devoid of the usage of harmful chemicals used in nanoparticle fabrications by the conventional chemical route (Mohammadi and Ghasemi, 2018). Plants are highly enriched in various phyto-biomolecules capable of effecting reduction of zinc ions to nanoparticles and functioning as capping agents. The role

of different proteins present in plant extracts in stabilization of formed nanoparticles has also been highlighted (Happy et al., 2019). The variation in composition and concentration of these active biomolecules between different plants and their subsequent interaction with aqueous metal ions are believed to be the main contributing factors to the diversity of nanoparticle sizes and shapes produced (Shah et al., 2015). For example, *Trifolium pratense* flower extract is a rich source of anthocyanins, phenolic acids, tannins, carotenes, essential oil which induce small agglomerated ZnONPs, whilst the flower extract of *Anchusa italic* possessing triterpenes, saponins and flavonoids cause reduction of zinc ions to form hexagonal nanoparticles (Dobrucka et al., 2015; Azizi et al., 2016). Although the exact mechanism of biosynthesis ZnONPs is not completely understood, it is thought that synthesis involves reduction of a zinc salt into Zn^{2+} , followed by the formation of a complex with the most active and abundant phytochemicals present in the plant. Hydrolysis then results in the separation of the phytochemical and Zn^{2+} , wherein the ion forms $Zn(OH)_2$ which on calcination ultimately leads to the formation of ZnO nanoparticles (Basnet et al., 2018). A plethora of several aqueous plant extracts have been used for the biosynthesis of ZnO nanoparticles (Yuvakkumar et al., 2016; Rajeshkumar et al., 2018; Kumar et al., 2019).

As mentioned above, the temperature and duration of calcination greatly influences the surface properties of biogenic zinc oxide nanoparticles. In the present study, a temperature of 600 °C for 2 h was found to be the optima for the formation of ZnONPs beyond which a drastic increase in the crystalline size of the particle was observed. This is in line with several recent reports (Al Hada et al., 2014; Kayani et al., 2015; Baharudin et al., 2018; Belay et al., 2018). Ashraf et al. (2015) have shown that decrement in particle size occurs below 300 °C whilst size increment occurs above the latter temperature. Contrastingly, Mornani et al. (2016) on the other hand, reports that increase in calcination temperature resulted in decrease in particle size. ZnO nanoparticles calcined at 600 °C exhibited the highest conversion efficiency because of its higher dye adsorption ability and lower recombination rate compared to the others was also recently reported (Golsheik et al., 2017). Likewise, the dependence of morphology of ZnONPs has been shown to be highly sensitive to

the concentration of reducing agent and calcination temperature (Raji and Gopchandran, 2017). Yet another study on ZnONPs biosynthesis reported increase in integrity of crystalline structure on calcination at 600 °C for 3 h (Hussain et al., 2019).

3.3.2. Physico-chemical characterization

3.3.2.1. X-ray diffraction (XRD) analysis

XRD technique generates reliable data on particle grain size, crystallinity and crystal phase-lattice parameter. The diffraction peaks assist in computation of average size by well known Debye-Scherrer equation and the crystal structure can be referred from International Centre for Diffraction Data (ICDD) previously known as JCPDS (Mourdikoudis et al., 2018). XRD pattern obtained for all samples could be indexed as the *ZnO wurtzite hexagonal structure* which agreed well with standard bulk ZnO using JCPDS card and the broadening of peaks observed indicated that the particles were in the nanoscale size range (Cao et al., 2019). Fig.3.2a-e shows XRD profile for characteristic diffraction peaks of various plant derived ZnONPs at 2-theta corresponding to the planes (100), (002), (101), (102), (110), (103), (200), (112) and (201). The slight variations in peak intensities showing polycrystalline nature were attributable to differences in the plant constituents involved in synthesis. However, the chemically synthesized cZnONPs taken as controls showed additional peaks at (004) and (202) planes (Fig.3.2f).

The average crystalline size calculated by Scherrer's formula based on the first four intense diffraction peaks fitted to the Lorentzian peak shapes at the plane 100, 002, 101 and 102 (Panda et al.,2017). Thus the mean size of biosynthesized AmFZnONPs, AmRZnONPs, AmSZnONPs, SpLZnONPs and MzLZnONPs obtained were 28±2nm, 46±2.5 nm, 61±3.5nm, 30±1.4 nm and 31±0.5nm respectively whilst the crystal size of cZnONPs was found to be 48.5±2.1 nm.

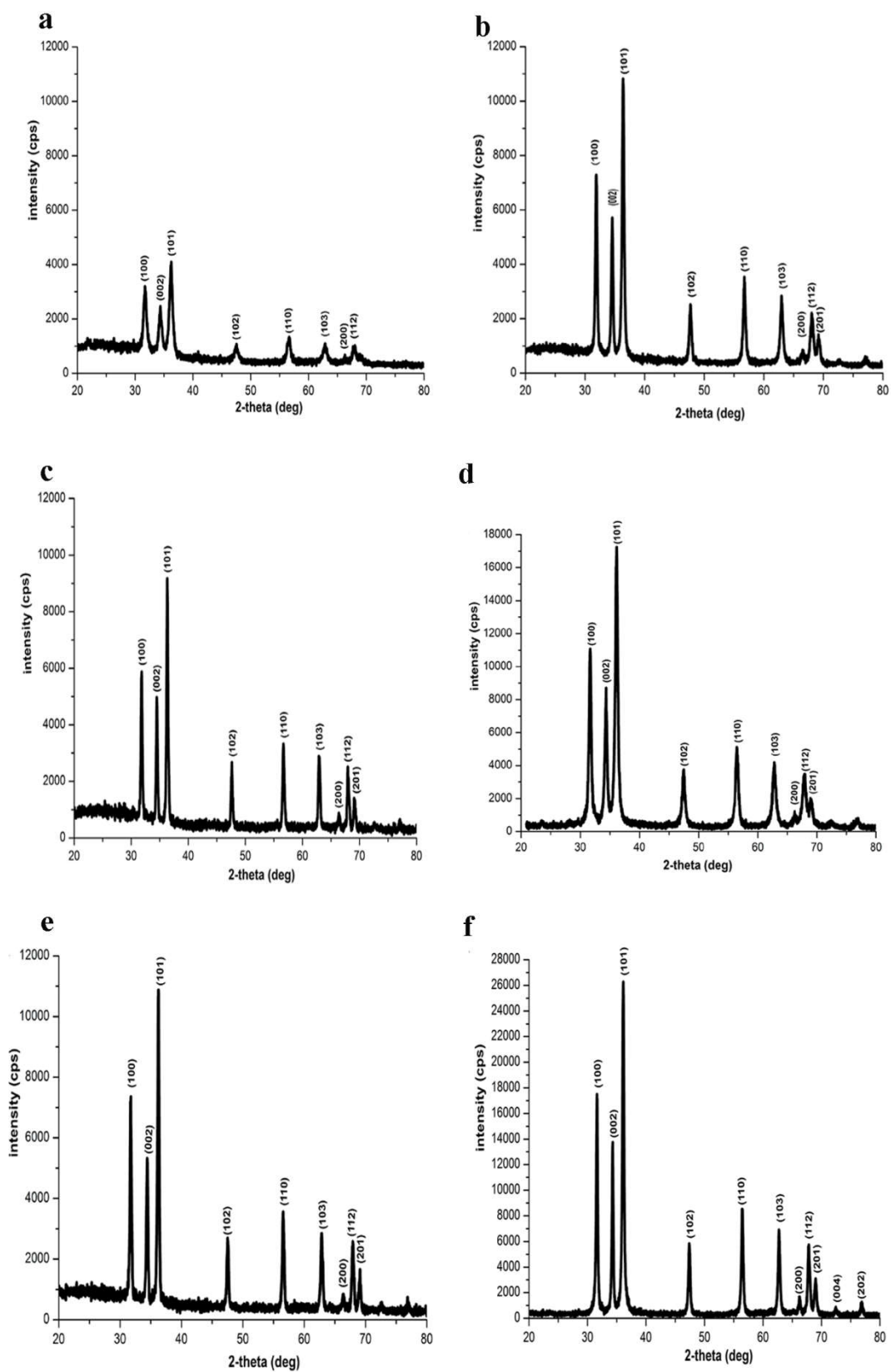


Fig. 3.2. X-ray diffraction patterns of (a) AmFZnONPs (b) AmRZnONPs (c) AmSZnONPs (d) SpLZnONPs (e) MzLZnONPs and (f) cZnONPs [control NPs]

All the nanoparticles displayed a preferred plane of orientation along (101) with a d-spacing in lattice fringes belonging to the same plane (Vimala et al., 2014; choudhary et al., 2019). The characteristic strong and narrow peaks devoid of any other interfering (unwanted) peaks demonstrated the purity of the phyto-derived ZnONPs as well as those of the commercial samples both displaying their crystalline hexagonal structure (Vanathi et al., 2014).

3.3.2.2. *Field Emission Scanning Electron Microscopy (FESEM) & Energy Dispersive X-ray spectroscopy (EDX)*

Fig. 3.3 a–f represents the FESEM micrographs obtained from the individual preparations of the different biosynthesized samples and the chemical version of ZnONPs taken as control. The picture clearly depicts the discrete/embedded/particle nature of ZnONPs with an average size similar to that obtained with XRD computations. A mixture of polycrystalline morphologies could be observed with a predominance of hexagonal structure which matched with the XRD data. This is in line with the observations made by previous researchers (Akhtar et al., 2017; Das and Rabeca, 2017; Khatami et al., 2018). Interestingly, the image of AmSZnONPs clearly showed formations of nanostructures such as hexagonal rods having the biggest size in comparison to all other biosynthesized and the control nanoparticles. The AmR and SpL derived ZnONPs were notable due to their well defined polygonal and hexagonal particle shapes. The presence of phyto-derived material was also evident as bulkier particles associated with the smaller nanoparticles indicative of capping agents adsorbed. A recent report by Alves et al. (2019) discusses the influence of charged phytomolecules on nanocrystal nucleation involving negatively charged sugars leading to formation of rod-like zinc nanoparticles and the presence of high density sugars resulting in platelet-like particles. In the present study, the use of three different extracts prepared from the roots, fruits and seeds of the same plant *A.muricata* resulted in three morphologically distinctive particle types. This clearly emphasizes on the influence of specific cocktails of phyto-derived bioreductants in shaping and tuning of the nanoparticles.

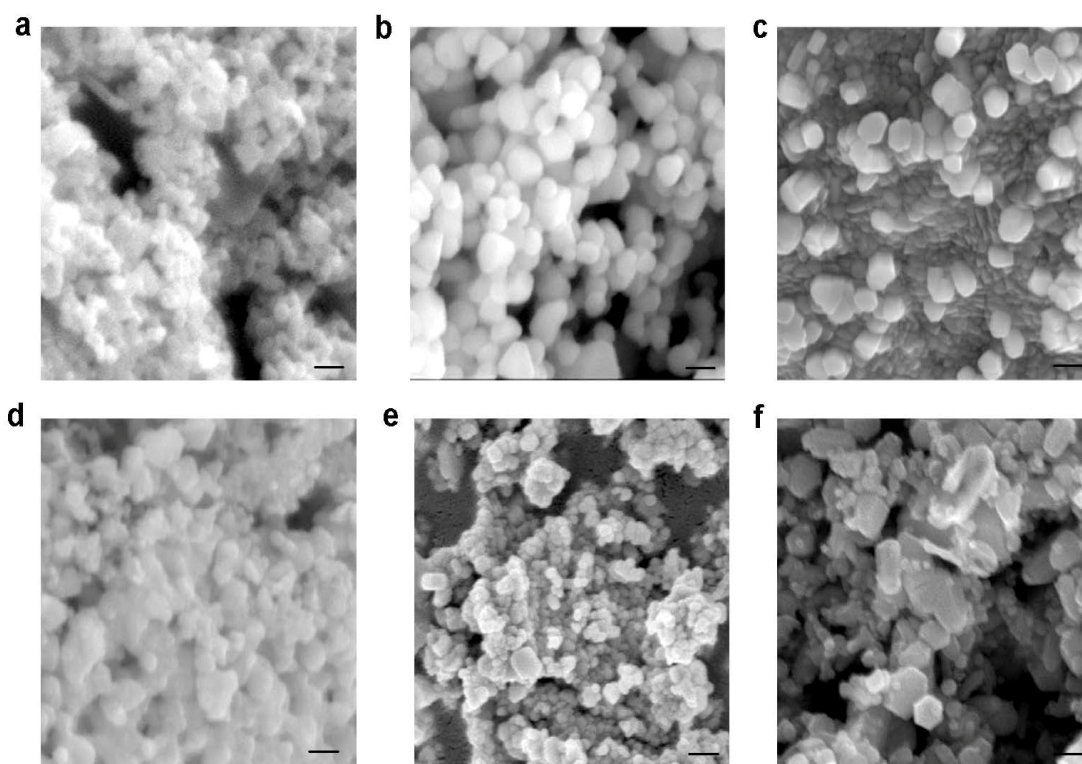


Fig. 3.3. FESEM images of (a) AmFZnONPs (b) AmRZnONPs (c) AmSZnONPs (d) MzLZnONPs (e) SpLZnONPs and (f) cZnONPs (scale bars represent 50 nm).

The elemental compositions of the biosynthesized and the purchased chemical version of ZnONPs were determined by EDX analysis to confirm their purity as evidenced by the signals emanating from elemental zinc and oxygen (Fig 3.4). Notably, AmRZnONPs and AmSZnONPs showed the presence of minute amounts of potassium ion, a vital plant macronutrient likely to have been adsorbed from the plant extract. Table 3.2 gives a profile of the percentage weight of individual elements in the different types of nanoparticles used in this study. The highest percentage of atomic Zn was found to be present in SpLZnONPs followed by that in cZnONPs and MzLZnONPs. All of the three types of *A. muricata* based nanoparticles were found to possess relatively lower amounts of Zn with minor variations. A concomitant variation in the amounts of elemental oxygen is also evident from the EDX profile.

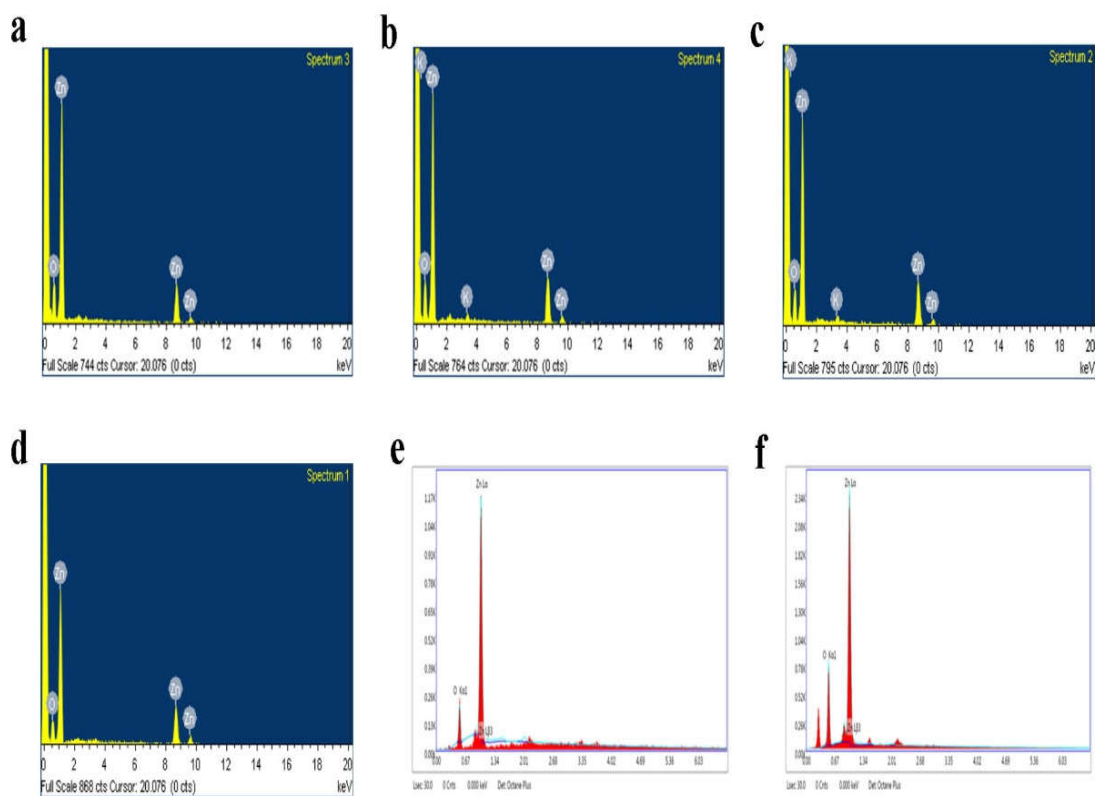


Fig. 3.4. EDX spectrum of (a) AmFZnONPs (b) AmRZnONPs (c) AmSZnONPs (d) MzLZnONPs (e) SpLZnONPs and (f) cZnONPs

Table 3.2. Zn and O atom compositional profile of EDX analysis

Sample	Weight% (Zn)	Weight%(O)	Atomic% (Zn)	Atomic% (O)
AmFZnONPs	74.34	25.66	41.49	58.51
AmRZnONPs	74.84	23.65	43.01	55.53
AmSZnONPs	74.87	23.41	43.18	55.16
MzLZnONPs	82.03	17.97	52.77	47.23
SpLZnONPs	90.59	9.41	70.20	29.80
cZnONPs	83.13	16.87	54.67	45.33

3.3.2.3. *Fourier Transform Infrared (FTIR) spectroscopy*

FTIR spectrum reveals the molecular fingerprint of the sample components based on absorption and transmission of infrared radiations. The unique spectrum with absorption peaks corresponding to the frequencies of vibrations between the bonds of the atoms making up the material provides useful information to identify the unknown compounds. Since the sol-gel method of ZnONP synthesis in this study was carried out in the presence of individual extracts with distinctive phyto-chemical composition, FTIR was carried out to analyze the extract-derived compounds such as those involved in stabilizing/ capping or still others adsorbed or associated with the nanoparticles. Such a recorded spectrum gives the position of bands related to the strength and nature of bonds, and specific functional groups, thus providing valuable information concerning molecular structures and interactions (Mourdikoudis et al., 2018). Fig. 3.5. is a graphical representation of the results of the FTIR analysis of the biosynthesized as well as that of chemical version of ZnONPs. The stretching vibrations below 600 cm^{-1} are characteristic of the spectral representation of metal-oxygen bonding; hence the sharp peaks observed below 500 cm^{-1} are attributable to Zn-O bond bending as reported in previous studies (Yuvakkumar et al., 2014; Parthiban and Sundaramurthy, 2015; Sundrarajan et al., 2015).

In the case of the chemically synthesized ZnONPs, apart from the main fingerprint peak of Zn-O below 500 cm^{-1} mentioned above, very few other functional peaks were observed - those at 3455 cm^{-1} , 1616 cm^{-1} , 1375 cm^{-1} and 700 cm^{-1} corresponding to the vibrations of OH group, alkenyl CC stretch, CN of aromatic amines and phenyl group respectively. However, all phyto-assisted nanoparticles were found to exhibit the presence of abundant organic moieties decorating them (Table 3.3). Broad and intense peaks between 3420 cm^{-1} – 3443 cm^{-1} in biogenic ZnONPs represented OH stretching. AmFZnONPs, AmRZnONPs, AmSZnONPs. SpLZnONPs and MzLZnONPs showed vibrational peaks around $2921\text{-}2923\text{ cm}^{-1}$, $2304\text{-}2363\text{ cm}^{-1}$ and $1022\text{-}1023\text{ cm}^{-1}$ apparently due to OH

stretching of carboxylic acid and symmetric/asymmetric stretch of CH in alkyl groups, CH stretching of aromatic aldehydes and CN stretch of primary amine. The band observed at 1541 cm^{-1} and 1508 cm^{-1} in AmRZnONPs denoted CO groups of flavonoids whilst sharp peaks around 1630 cm^{-1} in AmFZnONPs, AmSZnONPs, SpLZnONPs and MzLZnONPs were attributable to NH bend of primary amine. The moderate absorption peak in the region between 1457 cm^{-1} to 1384 cm^{-1} implicated the presence of aromatic ring on all biosynthesized ZnONPs. Except AmFZnONPs, other green nanoparticles showed a good stretching peak of polypeptide amide bond around 1633 cm^{-1} . Mono and poly-fluorinated compounds accounted for the peaks around 1110 cm^{-1} in all particles except SpLZnONPs. AmFZnONPs, AmRZnONPs and SpLZnONPs displayed aliphatic phosphate stretches around 800 cm^{-1} (Samzadeh-Kermani et al., 2016; Salari et al., 2017; Suresh et al., 2018; Mourdikoudis et al., 2018). The bands centered at and around 1730 cm^{-1} in AmR, AmS and MzL derived ZnONPs are attributable to free –COOH whereas the peak at 2854 cm^{-1} denote the presence of methyl or methoxy groups (Kumar et al., 2014).

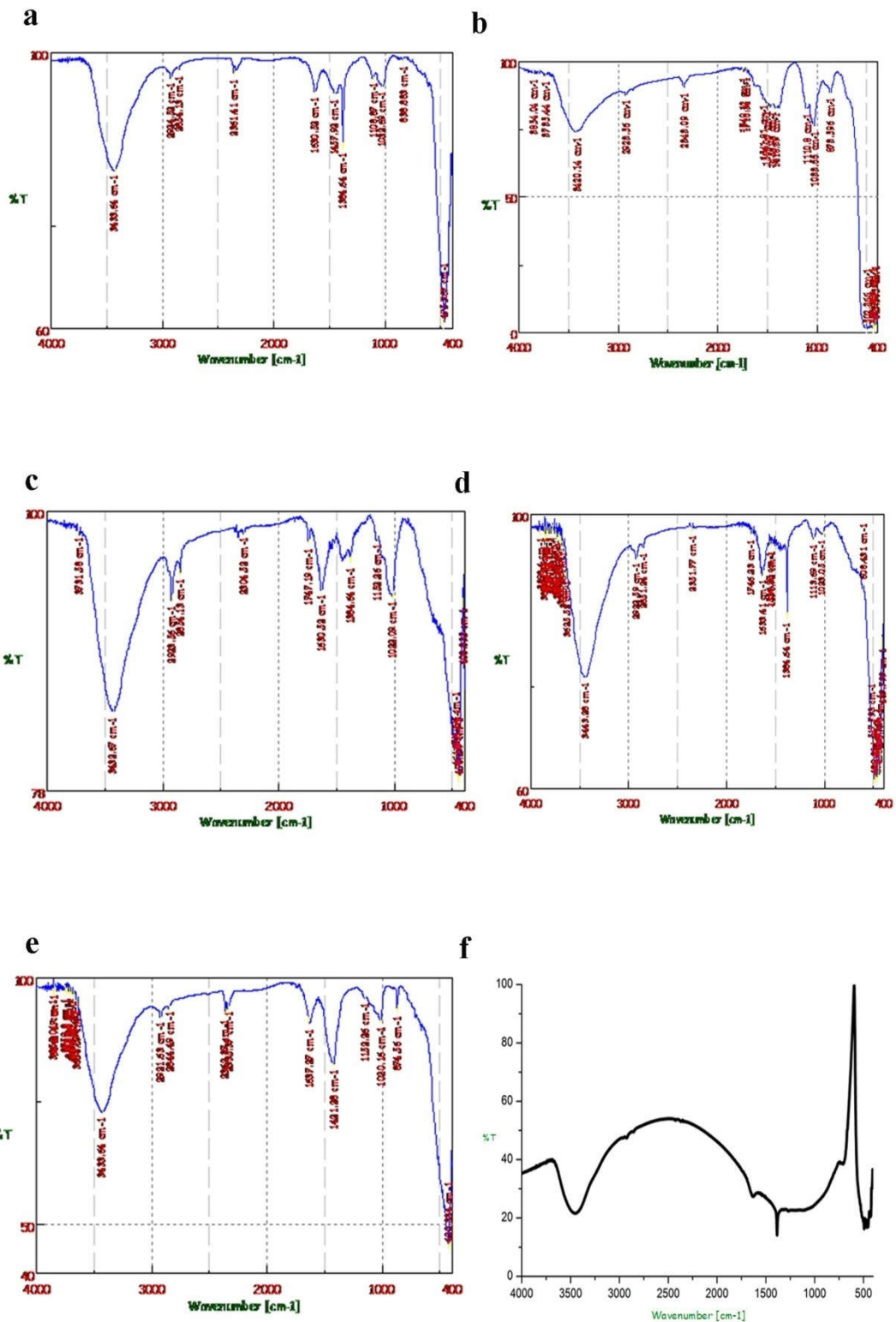


Fig. 3.5. FTIR spectra of (a) *AmFZnONPs* (b) *AmRZnONPs* (c) *AmSZnONPs* (d) *MzLZnONPs* (e) *SpLZnONPs* and (f) *cZnONPs*

Table 3.3. Major FTIR peaks (in cm⁻¹) and vibration modes assigned for phyto-derived and chemical ZnONPs

Vibration mode	AmFZnONPs	AmRZnONPs	AmSZnONPs	SpLZnONPs	MzLZnONPs	cZnONPs
OH stretching	3433	3420	3432	3433	3443	3455
CH stretch in alkyl group	2924	2923	2923	2921	2922	-
CH stretch in methyl or methoxy group	2854	-	2854	2844	2851	-
CH stretch in aromatic aldehydes	2361	2343	2304	2363,2333	2356	-
CO stretching	-	1749	1747	-	1746	-
	-	1716	-	-	-	-
CO-NH bond in polypeptide	1630	-	1630	1637	1633	-
CC stretch, NH ₂ deformation	-	-	-	-	-	1616
Aromatic skeletal CO stretching	-	1541,1508	-	-	-	-
CH ₂ stretching of aromatic rings	1457	1456, 1418	-	1421	-	-
Aliphatic CH stretch	1384	-	1384	-	1384	-
CN stretch of aromatic amines	-	-	-	-	-	1375
COC, CO stretch in fluorinated compounds	1108	1110	1152	-	1113	-
CN stretch of primary amine	1032	1033	1022	-	-	1023
Aliphatic phosphate	838	873	-	874	-	-
Phenyl group	-	-	-	-	-	700
Zn-O bond stretching	475	448,414	456	422	485	478

FTIR spectrum of the biosynthesized ZnONPs thus provides evidence of the presence of plant derived compounds in these nanoparticles which are conspicuous by their absence in the case of the chemically derived particles (Table 3.3). In this context, it is relevant to point out that Lukman et al. (2011) has reported that the adsorption of reducing agents on the surface of metallic nanoparticles is due to the presence of π -electrons and the carbonyl groups present in their molecular structures. Ebadi et al. (2019) has proposed that nanoparticle is synthesized and stabilized by replacing the acids with methyl and hydroxyl groups. The aforementioned FTIR analysis of the biosynthesized nanoparticles is in agreement with several recent reports on biosynthesized zinc oxide nanoparticles (Ezealisiji et al., 2019; Ogunyemi et al., 2019).

3.3.2.4. *UV-visible (UV-vis) spectroscopy*

The absorbance spectra of biogenic and non-biogenic nanoparticles are shown in Fig. 3.6. The area under *surface plasmon resonance* (SPR) peaks depends on shape, size, dielectric constant and surrounding medium. Conducting electrons oscillate at a certain wavelength range due to the SPR effect and this excitonic absorbance clearly demonstrates the quantum confinement effect of small nanoparticles (Rao et al., 2015; Kumar and Dixit, 2017; Mohammadi and Ghasemi, 2018). The intrinsic band gap absorption of biosynthesized AmFZnONPs, AmRZnONPs, AmSZnONPs, SpLZnONPs and MzLZnONPs was obtained at 374-384 nm, 373 nm, 372 nm, 372 nm and 384 nm respectively due to their electron transitions from valence to conduction band (O2p to Zn3d). The band gap energy was calculated as 3.31 & 3.23 eV, 3.33 eV, 3.33eV and 3.23 eV and this red shift in band gap is also shown by other biosynthesized ZnONPs (Saha et al., 2018; Yadav et al., 2019). The sharp peaks obtained at this UV absorption region corresponded to zinc oxide nanoparticles and is indicative of their monodispersity. cZnONPs, however, showed a less intense blue shift absorption peak at 334 nm followed by a red shift at 384 nm.

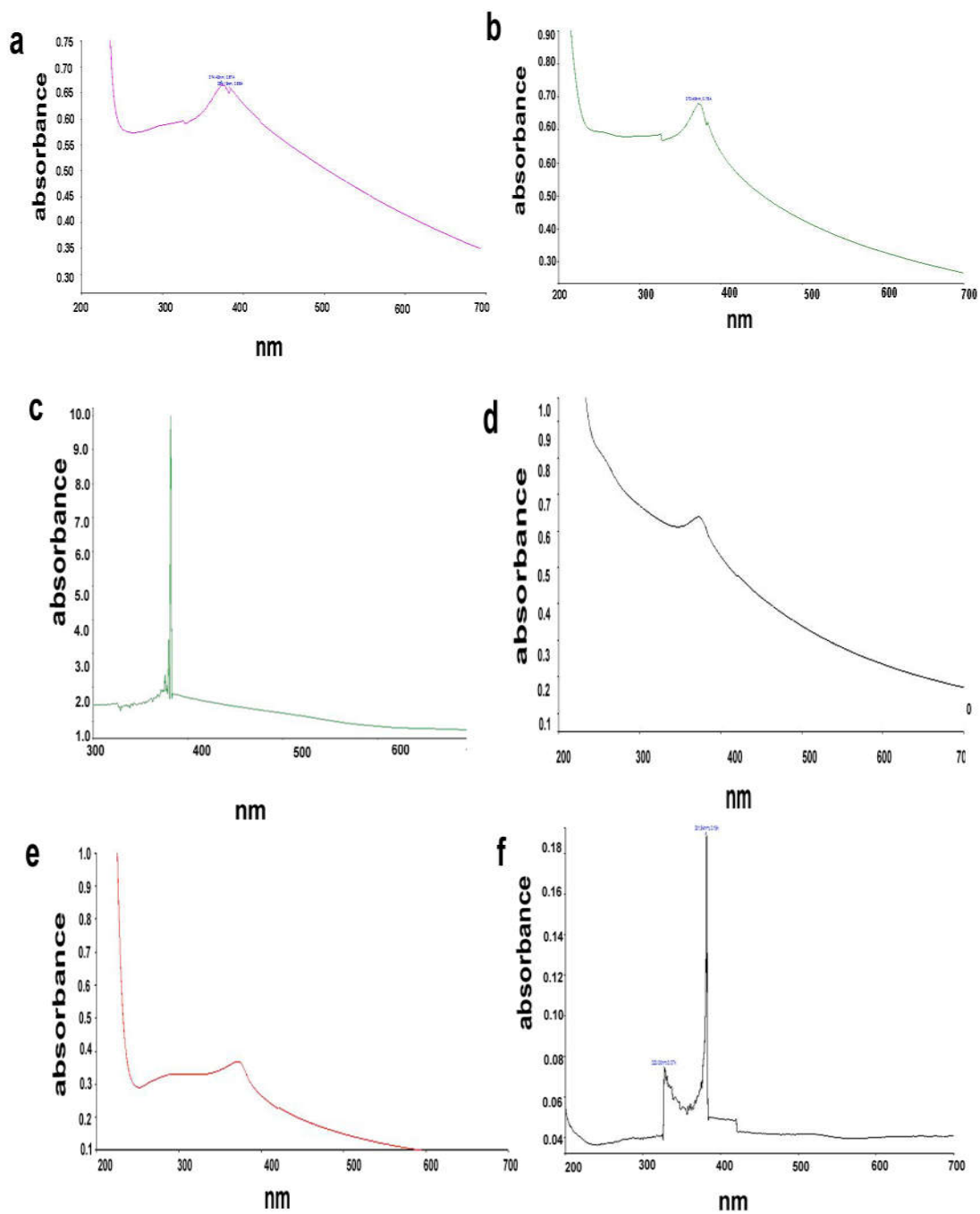


Fig. 3.6. *Uv-vis absorption spectrum of (a) AmFZnONPs (b) AmRZnONPs (c) MzLZnONPs (d) SpLZnONPs (e) AmSZnONPs and (f) cZnONPs*

3.3.2.5. Photoluminescence (PL) spectroscopy

PL is the emission of light as a result of excitation of the sample material by a monochromatic light source. The sample absorbs photons from a source such as laser resulting in electron excitation from valence to conduction band. Excited electrons may lose their energy either by a non-radiative or a radiative recombination process. The radiative recombination of free carriers results in photoluminescence. Semiconductor ZnO can itself luminesce in UV and visible regions which strongly depends on the excitonic recombination and intrinsic defects. According to a previous study by Rauwel et al. (2016), luminescence emission at visible region of a substance is a characteristic of the method used for synthesis and the structural complexities associated with the surface defects. However, in the present study, the results of PL spectroscopy revealed that all five biosynthesized as well as the commercial ZnONPs displayed an emission spectrum only in the visible region which is in agreement with some previous reports (Hazra et al., 2012; Ansari et al., 2013) [Fig. 3.7]. The absence of UV emission in both types of nanoparticles may be due to the short lifespan of free exciton arising from the high oscillator strength of the transition and the fast non-radiative trapping of excited charge carriers (Bindu and Thomas, 2014). Fu and Fu (2014) showed both UV and visible range emission in *P.amboinicus* leaf extract assisted-ZnO nanoparticles.

AmFZnONPs showed only blue emission at 480 nm whilst all others displayed multiple peaks showing broad blue emissions around 420 nm and 480 nm. However, cZnONPs showed an additional green emission band at 540 nm. This green emission is attributed to singly ionized oxygen vacancy resulting from the recombination of a photo-generated hole with a singly ionized charge state (Zhou et al., 2006). The peaks around 420 nm indicated the presence of interstitial zinc (Zn_i) as well as shallow donors and acceptors. A weak band at 460nm in PL spectra of SpLZnONPs and cZnONPs indicated Zn vacancies, interstitial oxygen (O_i) and Zn_i which is similar to the case of fenugreek-derived and seaweed-based ZnONPs (Alshehri et al., 2019; Itrotwar et al., 2019). According to Velsankar et al. (2020), the weak emission band at 480 nm emerges due to the surface defects and also the passage of the electron from shallow donor Zn_i to valence top band. The emission observed at the visible range is also

caused by the decrease in surface to volume ratio as a result of by huge flaws in the surface (Gupta et al., 2018). These aspects of nanoparticles have greatly contributed towards several biomedical and photocatalytic applications.

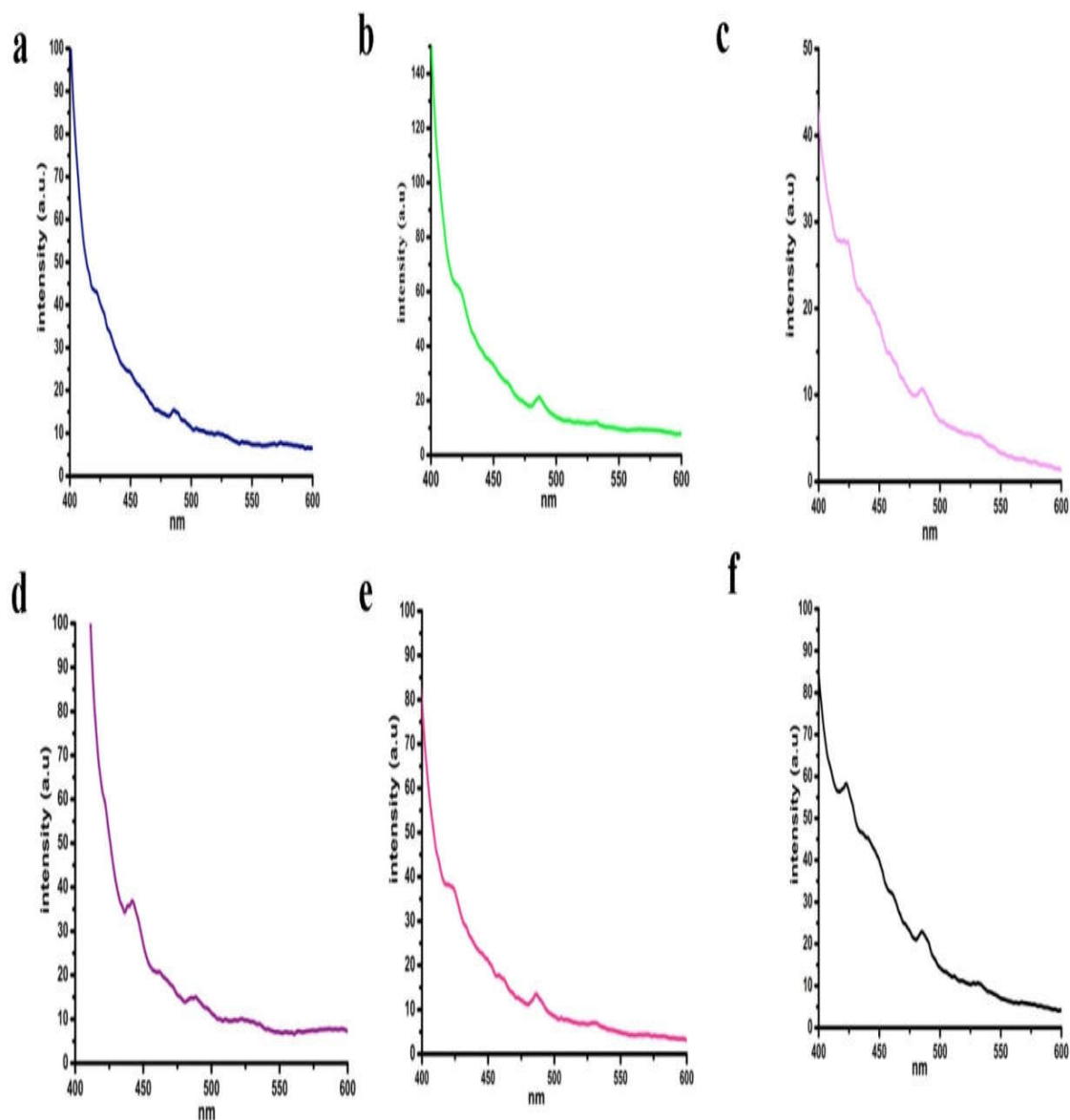


Fig. 3.7. Photoluminescence spectrum of (a) AmFZnONPs (b) AmRZnONPs (c) AmSZnONPs (d) SpLZnONPs (e) MzLZnONPs and (f) cZnONPs

3.3.2.6. High Resolution Transmission Electron Microscopy (HRTEM)

The images obtained with HRTEM technique were found to be in agreement with and a reconfirmation of the results obtained with FESEM and XRD analysis. Monodispersed and polycrystalline nature of both types of ZnONPs could be observed

both in the micrographs as well as the SAED pattern (Fig. 3.8.). Also, the presence of thin hazy cappings of phyto-constituents was observed as a dark thin layer over clustered nanocubes, nanorods, polyhedral and hexagonal crystal structures of biogenic nanoparticles. The average particle size obtained from TEM analysis of AmFZnONPs, AmRZnONPs, AmSZnONPs, SpLZnONPs, MzLZnONPs and cZnONPs were 33 ± 0.8 nm, 42.77 ± 3.1 nm, 58 ± 4.5 nm, 39.23 ± 3.0 , 34.89 ± 2.3 nm and 32.48 ± 4.2 nm respectively. The minor size variations observed here compared with the results of XRD may be due to the nature of sample preparation and presentation associated with the individual instrumental set up. The SAED ring pattern showed bright spots which displayed polycrystallinity with randomly oriented ZnONPs as reported by previous researchers (Khalil et al., 2014; Suresh et al., 2016). The distinct lattice fringes (0.24 nm in biogenic ZnONPs and 0.28 nm for cZnONPs) corresponding to (101) plane supported the XRD analysis and hence distance between crystalline planes are consistent with standard pattern of wurtzite ZnO structure in agreement with some recent reports (Asik et al., 2019; Kadam et al., 2019).

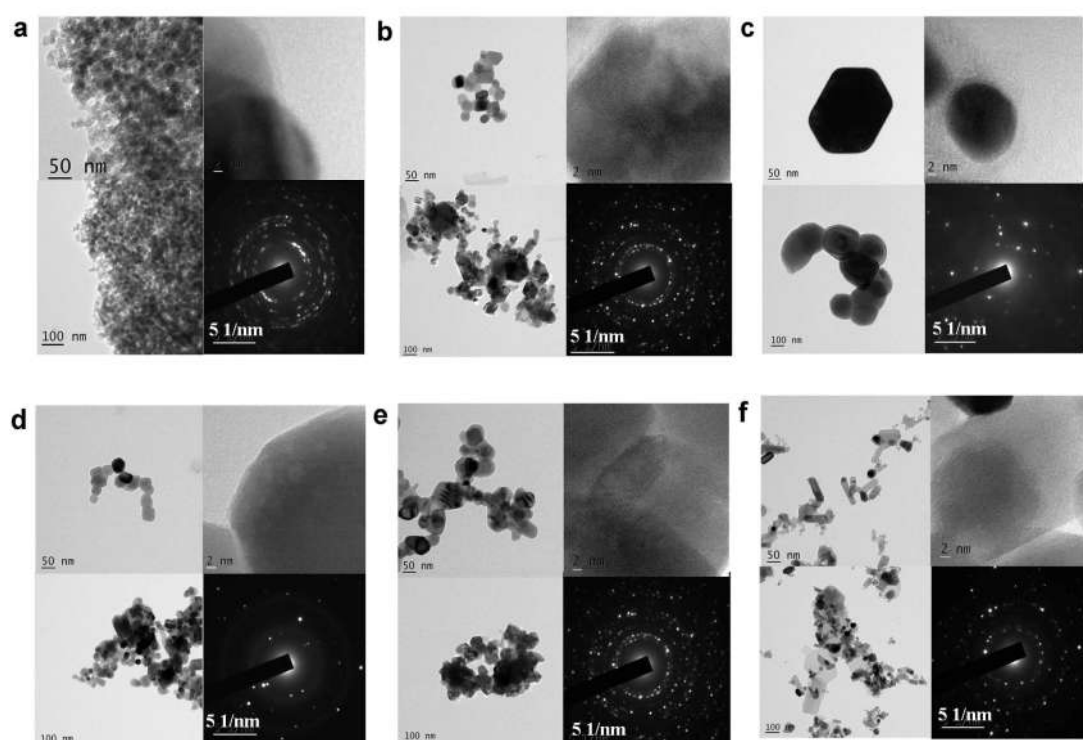


Fig. 3.8. HRTEM images of (a) AmFZnONPs (b) AmRZnONPs (c) AmSZnONPs (d) MzLZnONPs (e) SpLZnONPs and (f) cZnONPs. Scale bars for lattice fringes and SAED patterns are 2 nm and 5 1/nm respectively.

Taken together, the above results revealed that pure and crystalline ZnONPs can be biosynthesized *in situ* in a simple, sol-gel procedure with the aid of suitable aqueous plant extracts and metal precursors using an environmental-friendly manner devoid of the use of any perilous chemicals. The characterization of these particles further lends credence to the fact that nanoparticles can be moulded and packed without any assistance from external chemical stabilizers. It was also interesting to note that the biofunctionalized nanoparticles showed structural properties similar to that of the chemically synthesized commercial version. The following chapters of this Thesis scientifically document a comparison of the multifaceted potential of these phyto-derived zinc oxide nanoparticles with their chemical counterparts, in the light of interesting results obtained during the course of the present study.

CELLULAR AND MOLECULAR INVESTIGATIONS TO ASSESS THE ANTICANCER POTENTIAL AND BIOCOMPATIBILITY OF PHYTO-DERIVED AND THE CHEMICALLY SYNTHESIZED ZnONPs

4.1. Introduction

Nanomedicine embodies nanotechnology based applications in medicine, such as the use of nanoparticles with variable surface chemistry and architecture for cancer imaging and treatment. Numerous investigations have shown that both tissue and cell distribution profiles of anticancer drugs can be controlled by their entrapment in submicronic nanoparticle systems. The rationale behind this approach is to increase antitumor efficacy, while reducing systemic side-effects (Wang et al., 2010; Brigger et al., 2012). Recently, inorganic metal oxides like ZnONPs have received much attention for their implications in cancer therapy, due to their well-defined physico-chemical nature that enhances interactive potential with biological components (Kang et al., 2015; Jiang et al., 2018; Limo et al., 2018; Ebadi et al., 2019). Studies have shown that ZnONPs induce cytotoxicity in a cell-specific and proliferation-dependent manner, with rapidly dividing cancer cells being the most susceptible and quiescent cells the least sensitive (Premanathan et al., 2011; Akhtar et al., 2012). Controlled synthesis and variations in capping agents of these nanoparticles with specific morphological and surface properties are known to contribute towards improved activities relevant to biomedical applications including differences in cytotoxicity (Siddiquah et al., 2018). The latter report also mentions the role of capping agents in increasing the shelf life of nanoparticles upto several hours thereby extending their bioavailability. Recently, several studies were published on the anticancer potential of ZnONPs synthesized in the presence of various plant extracts (Prashanth et al., 2017; Ngoepe et al., 2018; Rauf et al., 2019). Interestingly, the selective nature of cytotoxicity of seaweed derived-ZnONPs against cancer cells without affecting normal cells has been reported by Namvar et al. (2015), which assumes significance of these particles in cancer therapeutics.

A critical approach in cancer therapy involves activation of key genes responsible for induction of apoptotic death. Apoptosis is a highly conserved mechanism by which eukaryotic cells commit suicide, thereby preventing cancer. The ability of cancer cells to bypass this molecular mechanism underlies cancerous transformation of cells and their metastatic progression. Induction of caspase-mediated apoptosis by zinc oxide nanoparticles in cancer cells has been recently reported (Bai et al., 2017; Kadhem et al., 2019). ZnONPs have been shown to affect cellular redox homeostasis by inducing formation of 'reactive oxygen species' (ROS) leading to oxidative stress. This stress, in turn, harms mitochondrial membrane potential causing release of cytochrome *c* and activation of intrinsic apoptotic pathway. The elevated ROS levels pose severe threat to DNA resulting in cell cycle arrest or apoptosis (Bisht et al., 2016).

In view of the above, a set of experiments was conducted to assess the comparative cytotoxicities of the phyto-derived zinc oxide nanoparticles with that of the chemically synthesized commercial version, against selected human cancer cell lines such as chronic myelogenous leukemic K562, colon carcinoma HCT 116 and lung adenocarcinoma A549 cells. Normal human peripheral blood lymphocytes, erythrocytes and a plant cell model - root tip cells of *Allium cepa* L., were also employed to evaluate the biocompatibility and selective action of both types of nanoparticles. The cytotoxicity screening of individual nanoparticle types was based on 3-(4, 5-dimethylthiazolyl-2)-2,5-diphenyltetrazolium bromide (MTT) assay. It is relevant to note here that previous reports on cytotoxic effects of biogenic ZnONPs on HCT 116 and K562 cells were found lacking in published literature. Of the four reports encountered on the action of phyto-derived ZnONPs against the third cell line, A549, by Zhang et al. (2017), Ngoepe et al. (2018), Dobrucka et al. (2018) and Hussain et al. (2019), barring the first, the latter furnished only scanty information on their cellular toxicity. In this context, detailed investigations were undertaken at the cellular and molecular levels to unravel the mode of action of the biosynthesized and characterized zinc oxide nanoparticles on selected cancer cell types. The experimental methodology adopted and the results obtained have been included in the subsequent sections of this chapter.

4.2. Materials and methods

4.2.1. Chemicals and reagents

Dulbecco's Modified Eagle's Medium (DMEM), Roswell Park Memorial Institute (RPMI-1640) medium, HiKaryoXL™ RPMI(PHA-P), 3-(4,5-dimethylthiazolyl-2)-2,5-diphenyltetrazolium bromide (MTT), Bovine serum albumin (BSA), penicillin, streptomycin and acetocarmine were procured from Himedia Laboratories Pvt. Ltd., Mumbai, India. Zinc oxide nanopowder designated as cZnONPs (<50nm), 5-Bromo-4-chloro-3-indolyl phosphate/nitro blue tetrazolium (BCIP/NBT), dimethyl sulfoxide (DMSO), dichloro-dihydro-fluorescein-diacetate (DCFH-DA), Rhodamine123, Flou-3AM, Hoechst 33258, propidium iodide, TRI® reagent, and crystal violet were purchased from Sigma-Aldrich (USA). Alexa Fluor®488-Annexin V/Dead cell apoptosis kit, fetal bovine serum (FBS) and 0.25 % Trypsin-EDTA were obtained from Gibco (Thermo Fisher Scientific, USA). Positively charged nylon membrane was purchased from BDH laboratory supplies, England. SYBR Green PCR Master Mix was purchased from TAKARA (Japan). Tris base, glycine, RNase, acridine orange (AO), ethidium bromide (EtBr), colchicine and heparin were purchased from SRL Pvt. Ltd., (Mumbai, India). Primary rabbit monoclonal antibodies against β -actin, cleaved caspase-3, cleaved PARP, cleaved caspase-8, cyclin B1, cytochrome *c* were purchased from Cell Signalling Technology, USA. Goat anti-rabbit IgG-alkaline phosphatase (ALP)-conjugate, agarose powder, RNase inhibitor, oligo-(dT)18 primer, DTT, and reverse transcriptase enzyme were purchased from Bangalore Genei (Merck Life Sciences, Mumbai, India). All the other reagents used were of analytical grade.

4.2.2. Human cancer cell lines employed in the present study

Three human cell lines - chronic myelogenous leukemic K562, colon carcinoma HCT 116 and lung adenocarcinoma A549 - used in this study were obtained from National Centre for Cell Sciences (NCCS), Pune, India. The salient features of these cell lines have been outlined in the subsections given below.

4.2.2.1. *Chronic myelogenous leukemic K562 cells*

This cell line has been derived from pleural fluid of a 53-year old female patient during terminal blast crisis. It is the first human immortalized myelogenous leukemia cell line of erythroleukemia type (Lozzio and Lozzio, 1975; Drexler, 2000). K562 cells grow as suspension cells and have no B markers of immune globulins, traces of Epstein-Barr virus and Herpes virus (Koeffler and Golde, 1980). K562 resembles undifferentiated and granulocytic leukemic round and smooth cells and also narrow ridge like and small ruffles in some cells with some T cell properties. Karyotyping of K562 cells revealed the presence of 68 to 73 chromosomes, a near triploid state (Klein et al., 1976). These myeloid cells lack MHC complex and are also found to have downregulated bcr: abl gene that reduces adhesiveness (Drexler, 2000; Jongen-Lavrencic, 2005). A major hallmark of this cancer cell line is the presence of t(9;22)(q34;q11) ‘Philadelphia reciprocal translocation’. This genetic abnormality creates a fusion gene BCR-ABL1, expressed as a hybrid protein tyrosine kinase which signals constitutively resulting in genomic instability and uncontrolled cell division (Luchetti et al., 1998). In these cells, death occurs mainly due to activation of mitochondrial apoptosis (Chunhui et al., 2016).

4.2.2.2. *Colon carcinoma HCT 116 cells*

HCT 116 is a human colon cancer cell line having pseudo-diploid karyotype is used highly in cancer research, immunity and inflammatory studies of intestine and drug screening. According to American Cancer Society, 1 in 22 men and 1 in 24 women are at risk of colorectal cancer and it has become the third most common type of cancer in American society. The cells have a mutation in codon 13 of KRAS proto-oncogene and are potentially useful for studies on targeted gene therapy (Rajput et al., 2008). Under *in vitro* conditions, these cells are adherent, epithelial, growth factor independent, invasive, highly motile and tumorigenic (Jiang et al., 1998; Howell et al., 1998; Sawhney et al., 2002; Awwad et al., 2003). Cell signaling molecules like inositol pyrophosphate crammed around an eight carbon inositol scaffold, InsP₈, was found in higher levels in HCT 116 cell variants compared to other mammalian cell lines (Gu et al., 2016). CRISPR/Cas9-mediated knock out of membrane-associated RING-CH

protein 2 (MARCH2) in these cells caused endoplasmic reticulum - mediated stress followed by suppressed cell proliferation, apoptosis, autophagy and also increased sensitivity towards drugs such as etoposide and cisplatin (Xia et al., 2017). Metastasis and invasion of HCT 116 cells was reportedly inhibited by 5-Fluorouracil-loaded pluronic P85 copolymer micelles in *in vitro* and *in vivo* studies (Zhu et al., 2016).

4.2.2.3. Lung adenocarcinoma A549 cells

This is a human, non-small lung cancer-derived alveolar cell line developed from a 58-year old Caucasian male cancerous lung tissue (Giard et al., 1973). The cells possess type II alveolar phenotype with a diameter averaging 10.59 μm (Jiang et al., 2010). A549 cells are known to harbour K-RAS mutation, epidermal growth factor receptor gene amplification, morphological heterogeneity with varying proliferative activity (Kondo et al., 2015). Long term culture of these cells induces multilamellar body formation following differentiation into an alveolar, type II pneumocyte phenotype. Also, SOX2, SOX9 and NANOG progenitor cell marker expression is found increased in these cells indicative of cancer stem cell population (Cooper et al., 2016). It was reported that survivin protein expression could improve sensitivity of A549 to vincristine therapy (Zhou et al., 2017). An intravenous anesthetic drug, propofol, was found to induce apoptosis by upregulation of p53 and p16 expression, downregulation of cyclin D1, Bcl-2 and increase in expression of Bax, cleaved caspase-3,-9 in these cells. Also, inhibition of metastasis and invasion of these lung cancer cells was found to be inhibited by propofol through decreased expression of MMP-9 and vimentin. Downregulation of miR-372 by the same drug also caused inactivation of Wnt/ β -catenin and mTOR pathways, thereby inhibiting their proliferation (Vasileiou et al., 2009, Sun and Gao, 2018).

4.2.2.4. Culturing and maintenance of cell lines

K562 cells were cultured as a suspension in RPMI 1640 medium whilst the adherent HCT 116 and A549 cells were grown as monolayer in DMEM medium in T25 tissue culture flasks. The growth medium was supplemented with 10% (v/v) FBS, streptomycin (100 $\mu\text{g}/\text{mL}$) and penicillin (100 U/mL) and maintained in 5% CO_2 humidified incubator at 37 $^\circ\text{C}$. The medium was replenished based on cell growth and

also was monitored regularly for any possibility of contamination. Trypsinization was done to release the adherent cells in order to collect them for subculturing and seeding whilst suspension cells required only simple harvesting by centrifugation.

4.2.3. Cytotoxicity evaluation of ZnONPs against human cancer cells

4.2.3.1. MTT assay

This rapid and convenient colorimetric assay was performed to assess the cytotoxicity of biogenic and chemical zinc oxide nanoparticles against all the three cell lines, essentially as described previously by Florento et al. (2012). For this, HCT 116, A549 cells (2.5×10^4 no./mL) and K562 cells (5.0×10^4 no./mL) were seeded individually into 96-well microtitre plates and grown for 24 h. After attaining enough growth, all cell types were individually treated with varying concentrations (25 $\mu\text{g/mL}$ - 150 $\mu\text{g/mL}$) of each of the phyto-derived nanoparticles - AmFZnONPs, AmRZnONPs, AmSZnONPs, MzLZnONPs and SpLZnONPs - along with the chemically derived cZnONPs, from a stock solution (5 mg/mL). Similar aliquots of untreated cells of each type as well as those treated with appropriate concentrations of the different plant extracts were also maintained as controls. Following treatment of cells for a period of 24, 48 and 72 h, the culture medium was replaced with MTT (500 $\mu\text{g/mL}$) solution and incubated in the dark for 3 h at 37 °C. The purple formazan crystals resulting from reduction of MTT by mitochondrial dehydrogenase within viable cells were dissolved in DMSO and the absorbance was then measured at 570 nm using a Multiskan EX plate reader (Thermo Scientific, USA). Percentage cell death was determined based on the difference in absorbance values of the treated and control samples (Namvar et al., 2015). The half-maximal inhibitory concentration (IC_{50}) for each type of nanoparticle was experimentally derived from the dose-response curve. All subsequent experiments were carried out at three different concentrations - below, at and above the IC_{50} concentrations – were determined for individual cell and nanoparticle types.

4.2.3.2. Trypan blue dye exclusion assay

This cell viability assay was performed as described by Piccinini et al. 2017. Trypan blue is a cell impermeable dye that enters the cell only when membranes are

compromised in their integrity, thus distinguishing live and dead ones. Briefly, all three cell types were seeded separately at a density of 1×10^5 cells /mL. Following a 24 h growth period, the cells were treated with the nanoparticles for a further 48 h. The cells were then collected by centrifugation (1200 rpm, 5 min) and resuspended in culture medium. A 1:1 dilution of cell suspension was made with 0.4 % trypan blue stain and observed under a light microscope to determine percentage viability; the non-viable cells stained blue whilst the viable intact cells remained colorless due to exclusion of dye.

4.2.4. Clonogenic assay

Ability of cancer cells to form colonies can be assessed under *in vitro* conditions by clonogenic assay. In brief, 500 cells/mL each of HCT 116, A549 and 300 cells/mL of K562 were separately seeded into 6-well plates along with the different nanoparticle types and then incubated for a period of 48 h. Following replacement of culture medium, the cells were grown further for 7 days in a CO₂ incubator. The colonies were then stained using crystal violet (0.5%w/v in 6 % glutaraldehyde) for 30 minutes. Excess stain was rinsed out and the air-dried colonies were counted to obtain the survival percentage (Franken et al., 2006). Survival fraction was determined as percentage of the plating efficiency of the treated cells in comparison to the untreated controls (Wang et al., 2017).

4.2.5. Evaluation of cell death by microscopy

Cytomorphological changes of both of the treated and untreated cells were analyzed employing light, scanning electron and fluorescence microscopy.

4.2.5.1. Light microscopy

The culture plates containing the untreated control and ZnONP-treated cells (1×10^5 cells/mL) were observed under a phase contrast, inverted microscope (Carton N100 FS) following a 48 h exposure period.

4.2.5.2. *Scanning electron microscopy*

Electron microscopy was carried out using a CARL-Zeiss Gemini 300 scanning electron microscope to study the cytomorphological alterations induced by nanoparticles in cancer cells. For this, all the three cancer cell types (1×10^5 cells/mL) were treated with biogenic / chemical ZnONPs for 48 h. The control and treated cells were then fixed in 4 % gluteraldehyde prepared in PBS for 3 min. Following two washes with PBS, the cells were then dehydrated by passing through an ascending series of 75-100% acetone (Sreekanth et al., 2007). The dried cells were then spread onto a carbon tape and sputtered with gold for observation through microscope.

4.2.5.3. *Fluorescence microscopy*

4.2.5.3.1. *Hoechst 33258 staining*

Nuclei-specific Hoechst 33258 staining (1mg/mL) was carried out essentially as described by Sahu et al. (2013). Briefly, both control and treated cells were harvested by centrifugation, washed and re-suspended with PBS and stained for 15 min at 37 °C. The enhanced fluorescence of fragmented chromatin within nuclei was observed and photographed on a fluorescence microscope.

4.2.5.3.2. *Acridine orange-ethidium bromide dual staining*

Apoptotic cells can be visualized by differential staining using 100µg/mL of acridine orange (AO) and ethidium bromide (EtBr). Following a treatment period of 48 h, the control and treated cells (1×10^5 cells/mL) were washed with cold PBS and dual-stained with AO-EtBr for 5 min prior to observation under a fluorescence microscope. Non-apoptotic cells were detectable due to the presence of characteristic green nuclei under a blue filter whilst the apoptotic cells displayed orange to red nuclei (Kang et al., 2015). Percentage of apoptotic cells were then quantified with respect to the untreated control cells.

4.2.6. Assessment of intracellular biochemical changes: Reactive oxygen species (ROS), mitochondrial membrane potential (MMP) and Ca²⁺ ion release

The levels of cellular reactive oxygen species (ROS), mitochondrial membrane potential (MMP) and Ca²⁺ ion release are some of the well established biochemical parameters useful for the assessment of apoptotic induction. Dyes such as dichloro-dihydro-fluorescein diacetate (DCFH-DA), rhodamine 123 and fluo-3AM have been successfully employed for the purpose. The oxidation of non-fluorescent DCFH-DA by intracellular ROS generates, a green, membrane permeable molecule - 2,7, dichloro fluorescein (DCF) - which fluoresces at 530 nm (Eruslanov et al., 2009). All three types of cells were seeded and treated as described earlier followed by incubation with DCFH-DA (10µM) at 37 °C for 30 minutes in the dark. Images of cellular fluorescence were captured. Likewise, variations in green fluorescence intensity of cationic, lipophilic rhodamine 123 (10µg/mL) dye following incubation with ZnONPs indicated depolarization of mitochondrial membranes of cells undergoing apoptosis (Mathuram et al., 2016). Calcium release is also another key event triggering apoptosis induction which is quantifiable by the fluorescence resulting from binding of Ca²⁺ ions to fluo-3AM. Briefly, both control and treated cells were incubated with 5 µM of this dye for 30 minutes at 37 °C and green fluorescence was monitored and photographed.

4.2.7. Flow cytometric analysis of apoptosis

Cell cycle distribution of control and treated cell population was carried out by propidium iodide staining followed by flow cytometric (FACS) analysis. Alexa fluor conjugated annexin V fluorescent staining was carried out according to manufacturer's protocol for detection of externalized phosphatidylserine, characteristic of apoptotic cells emitting green fluorescence. The results obtained with both these techniques were recorded on a BD Bioscience FACS ARIA II cytometer. The cell populations used to analyze cell cycle phase distribution were washed with PBS and fixed in 70% ethanol. Traces of ethanol were eliminated by two washings with PBS, a 30 min RNase A treatment to remove interfering RNA followed by propidium iodide staining (Wang et al., 2016).

4.2.8. Genotoxicity analysis

The damaging effects of both types of ZnONPs on the cellular genome was carried out by using (i) ethidium bromide staining following single cell gel electrophoresis (comet assay) and (ii) observation of DNA breaks on agarose gels.

4.2.8.1. Comet assay

DNA strand breaks can be visualized as a comet tail by nuclear staining with ethidium bromide under fluorescence microscope. This assay was carried out as described by Ng et al. (2017) by mixing the treated cells with low melting agarose followed by electrophoresis under alkaline conditions. The fragmented DNA, a hallmark of apoptosis, is observable as a ‘comet tail’ emanating from the affected nuclei (Aviello et al., 2011).

4.2.8.2. DNA fragmentation

The harvested control and treated cells were incubated in the lysis buffer for 3 h at 37 °C. The reaction mixture was then purified by organic solvent extraction and the DNA was finally precipitated using distilled ethanol by standard procedures (Sahu et al., 2013). The genomic samples were then mixed in TE buffer and electrophoresed on 2.0 % agarose gels at 100 V following detection and photography on a gel documentation system.

4.2.9. Gene expression profiling by reverse transcription-quantitative polymerase chain reaction (RT - qPCR).

RT-qPCR was performed to detect changes in the expression of genes involved in apoptotic induction on exposure to ZnONPs in HCT 116, A549 and K562 cells. Relative expression of a set of key transcripts involved in apoptosis induction, including pro- and anti-apoptotic genes, was studied using ten pairs of primers (Table 4.1.). Using SYBR green dye-detection method, quantitative assessment of the transcripts of these selected genes was carried out relative to the expression of glyceraldehyde-3-phosphate dehydrogenase (GAPDH), which is conventionally

employed as a representative of a housekeeping gene (Chandra et al.,2002; Ahamed et al., 2011; Kuppusamy et al., 2016).

Table 4.1. RT-qPCR primer sets used for quantification of relative gene expression

Primers	Oligonucleotides 5'-3' sequence
GAPDH	Forward: AATCCCATCACCATCTTCCA Reverse: CCTGCTTCACCACCTTCTTG
p53	Forward: CCCAGCCAAAGAAGAAACCA Reverse: TTCCAAGGCCTCATTGAGCT
PUMA	Forward: GACCTCAACGACAGTACGA Reverse: GAGATTGTACAGGACCCTCCA
Caspase-8	Forward: CATCCAGTCACTTTGCCAGA Reverse: GCATCTGTTTTCCCCATGTTT
Caspase-9	Forward: TTCCCAGGTTTTGTTTCCTG Reverse: CCTTTCACCGAAACAGCATT
Caspase-3	Forward: TGGCATACTCCACAGCACCTGGTTA Reverse: CATGGCACACAAAGCGACTGGATGAA
Cytochrome <i>c</i>	Forward: TTTGGATCCAATGGGTGATGTTGAG Reverse: TTTGAATTCCTCATTAGTAGCTTTTTTTGAG
Bax	Forward: TGCTTCAGGGTTTCATCCAG Reverse: GCGGCAATCATCCTCTG
Bcl-2	Forward: TATAAGCTGTTCGAGAGGGGCTA Reverse: GTACTCAGTCATCCACAGGGCGAT
Survivin	Forward: AGAACTGGCCCTTCTTGAGG Reverse: CTTTTTATGTTCTCTATGGGGTC
PARP-1	Forward: GCGCCCGCTCTTAGCGTACT Reverse: CGACACGTTAGCGGAGCGGAC

The levels of individual gene transcripts were determined essentially as described by Khazaei et al. (2017) using the $2^{-\Delta\Delta C_t}$ method, wherein

$$2^{\Delta\Delta C_t} = 2^{C_t(\text{treated cells}) - C_t(\text{control cells})}$$

factor 2 denotes amplification efficiency of template doubling in each cycle during exponential amplification.

Briefly, total RNA was isolated using TRI[®] reagent from the control and the treated cells according to the manufacturer's protocol. RNA was then quantified using a microvolume spectrophotometer (Eppendorf Biospectrometer[®]). For cDNA synthesis, a 5.0 μL reaction containing 1.0 $\mu\text{g}/\mu\text{L}$ RNA, 1.0 μL of oligo dT(100 $\text{ng}/\mu\text{L}$)

and RNAase-free water was incubated at 65 °C for 10 min. The mixture was then made upto 10 µL with sterile nuclease-free water containing 1.0 µL of 10 mM dNTP mix, 2.0 µL of 10x M-MLV reverse transcriptase buffer, 1.0 µL of M-MLV reverse transcriptase, 0.5 µL of RNasin and 0.5 µL DTT (20 mM),. The reaction mixture was incubated at 37 °C for 1 h, heated to 95 °C for 10 min and the cDNA obtained was stored at -20 °C until use. The RT-qPCR was performed on an real-time PCR machine, Illumina Eco™.

4.2.10. Protein immunoblot analysis

Immunostaining of key apoptosis-related proteins was carried out by western blot analysis essentially as described previously (Lakshmipriya et al., 2018) to monitor their expression in HCT 116, A549 and K562 cells. The untreated control and ZnONP-treated cells were washed with cold PBS, lysed in RIPA buffer and incubated on ice for 30 min. The cellular lysates were centrifuged at 10,000×g for 10 min and their protein concentrations determined using Bradford method. Protein samples (50 µg) in 2x sample buffer were electrophoresed on a 12.5% SDS-PAGE gel and then transferred onto positively charged nylon membrane at 15 V overnight. Membranes were washed with Tris-buffered saline Tween-20 (TBST) and blocked with 5% BSA in TBST for 1 h. They were then separately incubated overnight at 4°C with rabbit-derived primary monoclonal antibodies (dilution 1:1000) against cleaved caspase-3, -8 and PARP, cyclin B1, cytochrome *c* and the house-keeping protein - β actin - as the loading control. Following three washes with TBST, the membranes were further incubated with ALP- conjugated secondary antibody (1:2000 dilutions) for 1h. The primary and secondary antibodies were both diluted in blocking buffer. Following washes with TBST, the blots were exposed to BCIP/NBT solution to visualize the immunostained, purple colored, polypeptide bands.

4.2.11. Cytotoxicity evaluation of ZnONPs against normal human cells

4.2.11.1. Peripheral blood-derived lymphocytes (hPBLs)

4.2.11.1.1. *MTT assay*

Lymphocytes offer an inexpensive surrogate cell culture system amenable to analysis of cytotoxicity of various natural and synthetic agents (Montoro et al., 2012). Self-donated blood (5.0 mL) collected in a heparinised centrifuge tube, was used to check cytotoxicity of nanoparticles on hPBLs by MTT assay. For this, 200 µl of plasma was added to 5.0 mL RPMI HiKaryo medium containing PHA (phytohemagglutinin). Following completion of 48 h of incubation at 37 °C, hPBLs were treated with nanoparticles (20 – 100 µg/mL); untreated lymphocyte culture served as control. The MTT assay was carried out as described for cancer cells (subsection 4.2.3.1.) and percentage cell survival was calculated from optical density values at 570 nm using the formula,

$$\text{Cell viability (\%)} = [\text{OD}_{\text{treated}} / \text{OD}_{\text{control}}] \times 100$$

4.2.11.1.2. *Mitotic index (MI) analysis*

Lymphocytes were cultured by adding 200 µl of blood to 5.0 mL RPMI HiKaryo medium and incubated for 48 h. Following incubation, the hPBLs were treated with nanoparticles for further 24 h. To arrest cells at metaphase, colchicine (10 µg/mL) was added 2 h prior to harvest. The cells were then fixed in methanol: acetic acid (3:1 v/v) following hypotonic treatment with pre-warmed 0.075 M KCl and dropped onto clean, frozen and labeled slides. Air-dried slides were stained with Giemsa for 30 min and viewed under a light microscope. MI was calculated by scoring 500 cells of both control and treated samples using the formula,

$$\text{MI (\%)} = (\text{Total metaphases} / \text{Total cells counted}) \times 100$$

The Relative Mitotic Index was also determined as

$$\text{RMI (\%)} = [\text{MI treated} / \text{MI control}] \times 100$$

4.2.11.2. Erythrocytes

4.2.11.2.1. Hemolysis

Cytotoxicity on erythrocytes was spectrophotometrically determined based on release of hemoglobin from the lysed plasma membranes. Blood was centrifuged with an equal volume of PBS (pH 7.4) to remove the buffy coat which was further washed thrice with PBS at 3000 rpm for 5 min. An aliquot of the resultant RBC suspension (0.6 mL) was treated individually with nanoparticles for 90 min at 37 °C. Distilled water and PBS served as positive and negative controls respectively. Following treatment, samples were centrifuged and optical densities of the supernatants were measured at 540 nm (Khan et al., 2015; Raguvaran et al., 2015) and percentage hemolysis was calculated using the formula,

$$\text{Hemolysis (\%)} = [\text{OD}_{\text{test sample}} - \text{OD}_{\text{PBS}} / \text{OD}_{\text{distilled water}} - \text{OD}_{\text{PBS}}] \times 100$$

Morphological examination of treated erythrocytes was then carried out using May-Grunwald-Giemsa method (Junqueira and Carneiro, 2004; WHO, 2016). Briefly, a thin blood smear was prepared on a clean slide, air-dried, fixed in methanol and stained with Giemsa for 30 min and observed under 40 x magnifications.

4.2.12. Cytotoxicity evaluation of ZnONPs against plant cell model : *Allium cepa* L. root-tip cells

4.2.12.1. Mitotic Index analysis and trypan blue viability assay

Allium cepa root tips, an easily available plant source of dividing apical meristematic cells, have been commonly used to evaluate cellular/genotoxic effects of various physico-chemical and biological agents (Pandey et al., 2014; Taranath et al., 2015; Obute et al., 2016). Briefly, after removal of dry scales, healthy bulbs of *A. cepa* were soaked in distilled water for root initiation. On reaching a root length of 1-2 cm, the seedlings were placed individually in distilled water containing ZnONPs at concentrations of 20, 60 and 100 µg/mL. Roots grown in distilled water alone were taken as control. After an overnight exposure to nanoparticles, the root tips were fixed in Carnoy's solution (3:1 v/v of absolute alcohol: glacial acetic acid). The roots were then hydrolyzed with 1.0 N HCl for 10 min followed by acetocarmine staining, destaining with 45 % acetic acid to remove excess dye and further rinsed with distilled water (Bhagyanathan and Thoppil, 2015). A squash preparation of the root-tip

meristem on a clean glass slide was visualized under 40 x objectives. MI was scored as percentage of dividing cells in a total of 500 cells.

For assessment of cell death, control and treated bulbs with intact roots were placed in 0.25 % (w/v) aqueous solution of trypan blue for 15 min. The roots were then washed in running tap water, stained and photographed. Blue coloration in root tips was indicative of the presence of dead cells (Bhagyanathan and Thoppil, 2015).

4.3. Statistical analysis

All results are expressed as the mean \pm S.D from independent experiments carried out in triplicate. Significance was analyzed by one-way ANOVA using SPSS software (version 20.0) by Dunnett's multiple comparison tests. Differences with $P < 0.05$ with respect to control were considered as significant. The levels of significance are denoted as * $P \leq 0.05$, # $P \leq 0.01$, \$ $P \leq 0.001$).

4.4. Ethical statement

Self-donated blood samples of the researcher were used for culturing of peripheral blood derived lymphocytes for assessment of cytotoxicity and hemolysis. Ethical approval for this study was not necessary according to guidelines (Chapter-II, page no. 11-12) of the Indian Council for Medical Research (New Delhi, India) which grants exemption from ethical review of proposals presenting less than minimal risks.

4.5. Results and discussion

I. Evaluation of cytotoxicity of phyto-mediated and the chemically derived ZnONPs on three human cancer cell lines –HCT 116, A549 and K562.

4.5.1. MTT assay

A total of five phyto-derived ZnONPs synthesized in the present study - AmFZnONPs, AmRZnONPs, AmSZnONPs, SpLZnONPs and MzLZnONPs - along with the chemically synthesized commercial version (cZnONPs) taken as the control nanoparticle were subjected to cytotoxicity evaluation using the MTT method. Nanoparticle concentrations ranged from 25-150 $\mu\text{g/mL}$ for a period of 24, 48 and 72 h (Fig. 4.1 – 4.3). All IC_{50} values computed have been given in Table. 4.2. Of the above, three particle types - AmRZnONPs, SpLZnONPs and MzLZnONPs – were

found to exhibit consistent cytotoxicity against all the three cell lines tested in a time and dose-dependent manner. However, AmFZnONPs displayed toxicity only against HCT 116 and K562 cells but failed to kill A549 even at the highest concentration tested. AmSZnONPs, on the other hand, displayed relatively poor cytotoxicity on both adherent cells (HCT 116, A549) while being toxic only to leukemic K562 suspension cells. Notably, the chemical nanoparticles not only displayed a dose-independent cytotoxicity against HCT cells, their IC₅₀ values against K562 cells were also beyond the tested range (>150 µg/mL). However, IC₅₀ concentrations in respect of AmR, SpL and MzL-derived nanoparticles against HCT 116 and A549 cells was found to reduce drastically following 24 h to 48 h treatment beyond which no appreciable change was observed. SpLZnONPs showed highest activity against colon carcinoma cells with a reduction of ~73 % in IC₅₀ value from 24 to 48 h followed by an additional reduction of ~12 % for a further 24 h treatment period (Fig. 4.1.a, b and c). AmRZnONPs and MzLZnONPs also showed significant dose-dependent cytotoxicity against HCT cells.

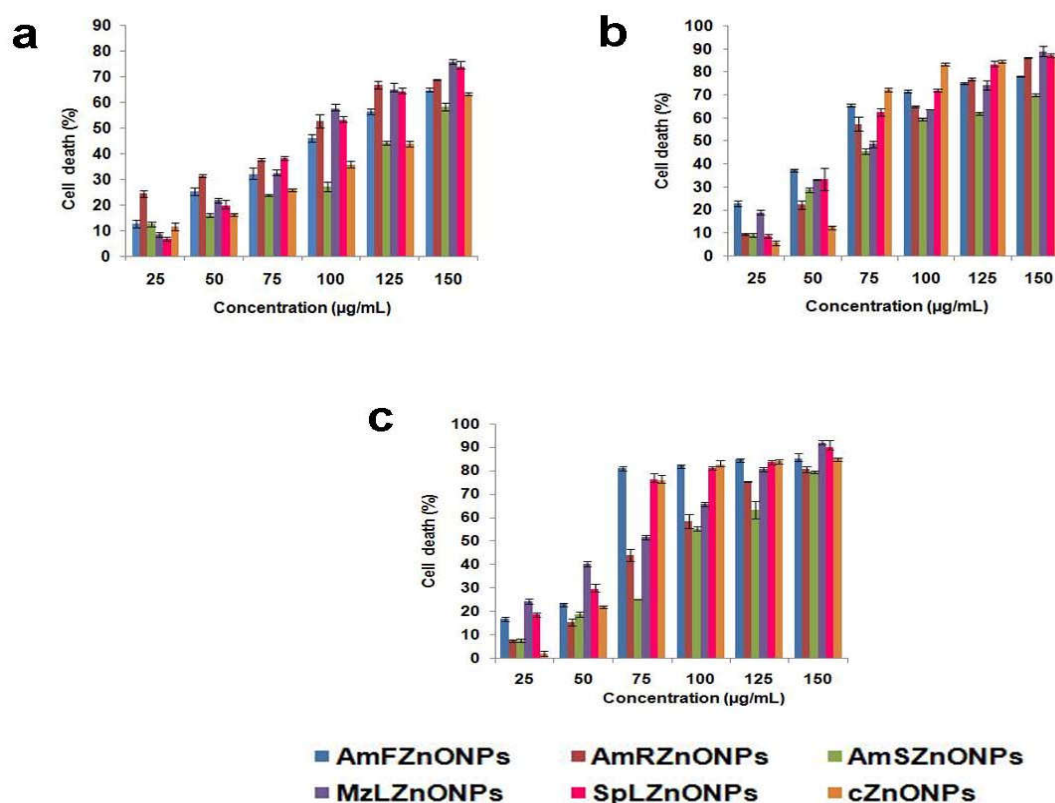


Fig. 4.1. Cytotoxicity evaluation of phyto-derived/chemical ZnONPs against HCT 116 cells for (a) 24 h (b) 48 h and (c) 72 h treatment period. Values represent mean \pm S.D. of three experiments; $p < 0.05$.

In the case of adenocarcinoma cells, both SpLZnONPs and cZnONPs showed a decrement of ~69 % in IC₅₀ value for a 48 h treatment period with a further reduction of ~15 % for 72 hours of exposure to nanoparticles. The decrease in cytotoxicities was also observed in respect of AmRZnONPs and MzLZnONPs as evidenced by increasing IC₅₀ values (Fig. 4.2 a, b and c). Against the suspension cultures of K562, SpL-derived particles exhibited the lowest IC₅₀ values at the 48th and 72nd hour compared to all other phyto-derived particles (Fig. 4.3 b and c.).

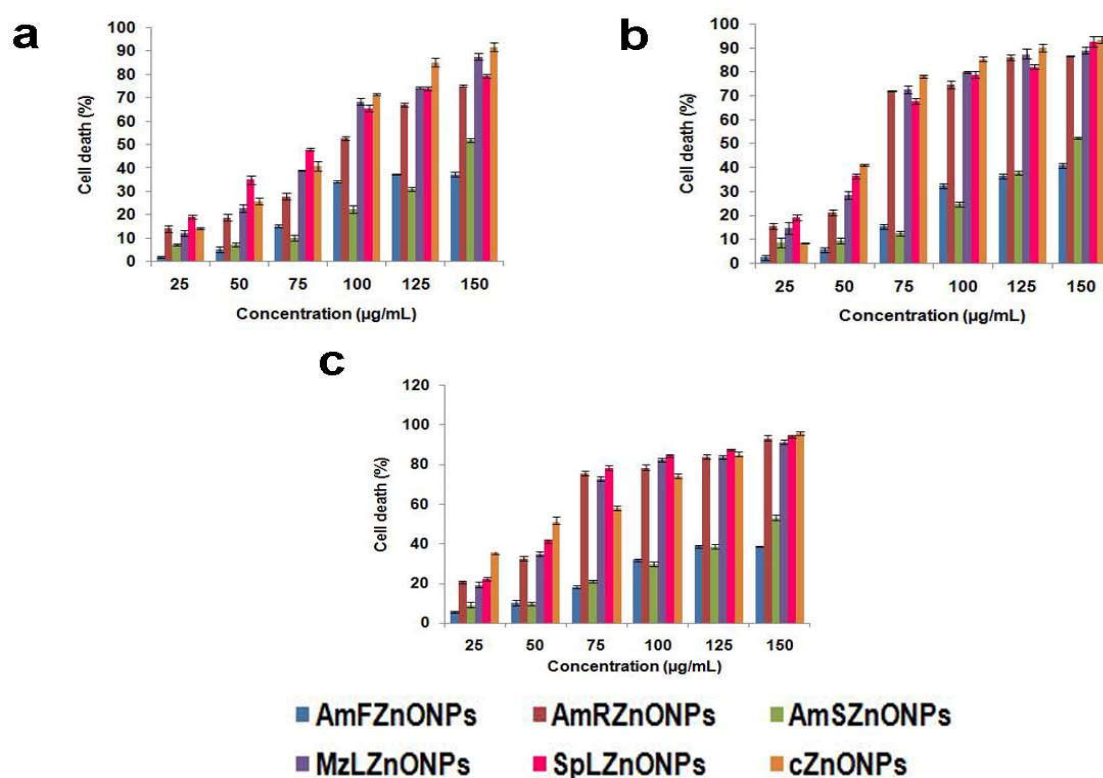


Fig. 4.2. Cytotoxicity evaluation of phyto-derived/chemical ZnONPs against A549 cells for (a) 24 h (b) 48 h and (c) 72 h treatment period. Values represent mean \pm S.D. of three experiments; $p < 0.05$.

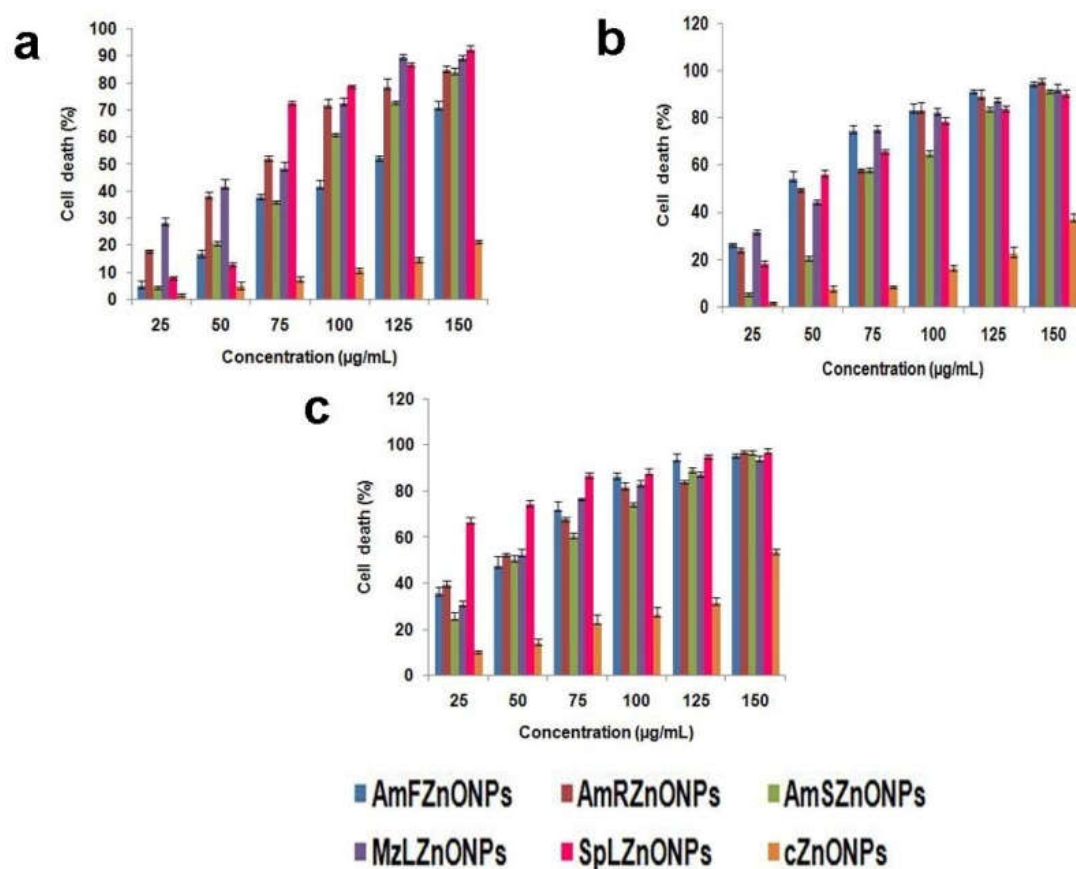


Fig. 4.3. Cytotoxicity evaluation of phyto-derived ZnONPs/chemical against K562 cells for (a) 24 h (b) 48 h and (c) 72 h treatment period. Values represent mean \pm S.D. of three experiments; $p < 0.05$.

It is worth mentioning that the results of cytotoxicity evaluation of individual plant extracts *per se*, within the concentration range of 25 -150 µg/mL against all the three cell lines, were found to be negative. All cells exposed to the different extracts were found to be viable and observed to be cytomorphologically normal. This clearly indicated that the phytochemical composition of the extract, when administered alone, failed to kill the cells. In other words, the recruitment of all or most likely a subset of phytoconstituents responsible for capping and stabilization of the biogenic ZnONPs, apparently play a critical role in conferring cytotoxicity to the nanoparticles. Variabilities in their penetrance and surface interactions have been highlighted in several published reports (Rasmussen et al., 2010; Tso et al., 2010; Geetha et al., 2013; Venkatesan et al., 2016; Biplab et al., 2016). This also gives a logical explanation to

the lack of effective cytotoxicity observed in the case of chemically synthesized cZnONPs.

Table 4.2. IC₅₀ values of phyto-derived/chemical ZnONPs against three human cancer cell lines

Cancer cells	Types of ZnONPs treated (µg/mL)	Treatment duration (h)		
		24	48	72
HCT 116	AmFZnONPs	110 ± 1.4	68.5 ± 0.9	60 ± 0.78
	AmRZnONPs	97 ± 1.8	61 ± 2.1	52 ± 1.3
	AmSZnONPs	137.5 ± 1.0	88 ± 1.6	83 ± 0.56
	SpLZnONPs	82 ± 0.75	60 ± 0.3	53 ± 1.2
	MzLZnONPs	88 ± 1.5	68 ± 0.63	61 ± 1.0
	cZnONPs	140 ± 1.5	60 ± 0.5	60 ± 1.6
A549	AmFZnONPs	>150	>150	>150
	AmRZnONPs	91 ± 0.25	64 ± 0.8	56 ± 1.4
	AmSZnONPs	>150	138 ± 2.2	130 ± 1.2
	SpLZnONPs	85 ± 1.0	59 ± 1.6	50 ± 2.1
	MzLZnONPs	87 ± 1.0	63 ± 0.5	57 ± 0.4
	cZnONPs	89 ± 1.5	58 ± 1.0	49 ± 1.0
K562	AmFZnONPs	124 ± 0.8	70 ± 1.2	64 ± 0.98
	AmRZnONPs	62 ± 1.3	58 ± 0.75	30 ± 1.5
	AmSZnONPs	85 ± 0.5	68 ± 0.5	62 ± 1.5
	SpLZnONPs	55 ± 0.5	35 ± 0.65	24 ± 2.0
	MzLZnONPs	77 ± 1.8	56 ± 2.1	33 ± 1.2
	cZnONPs	>150	>150	143.8 ± 1.8

(Values represent mean ± S.D. of three experiments; $p < 0.05$)

In all subsequent experiments, conducted to evaluate the anticancer potential, only three phyto-derived particles, namely, AmRZnONPs, SpLZnONPs and MzLZnONPs were used since they displayed significant cytotoxicity against all the cancer cell lines tested in this study. Although cZnONPs showed anticancer activity only against two cell lines HCT 116 and A549, it still served as a strict control for a comparative evaluation of cytotoxicity between the biosynthesized versus chemically derived particles. Here, it may be noted that K562 cells were found to be completely refractory / insensitive to cZnONPs. For both HCT 116 and A549 cells, the doses

selected were 40, 60 and 80 $\mu\text{g}/\text{mL}$ whilst for K562 cells, the doses applicable were 20, 40 and 60 $\mu\text{g}/\text{mL}$ for a period of 48 h.

4.5.2. Trypan blue dye exclusion assay

The percentage of non-viable cells in each cell type following 48 h treatment below, at and above- IC_{50} concentration of nanoparticles showed dose-dependent cytotoxicity similar to that observed with MTT assay. However, at IC_{50} concentration, the cell death percentage was found to be marginally higher than those observed with MTT assay in all three cell types. The results are graphically represented in Fig. 4.4.

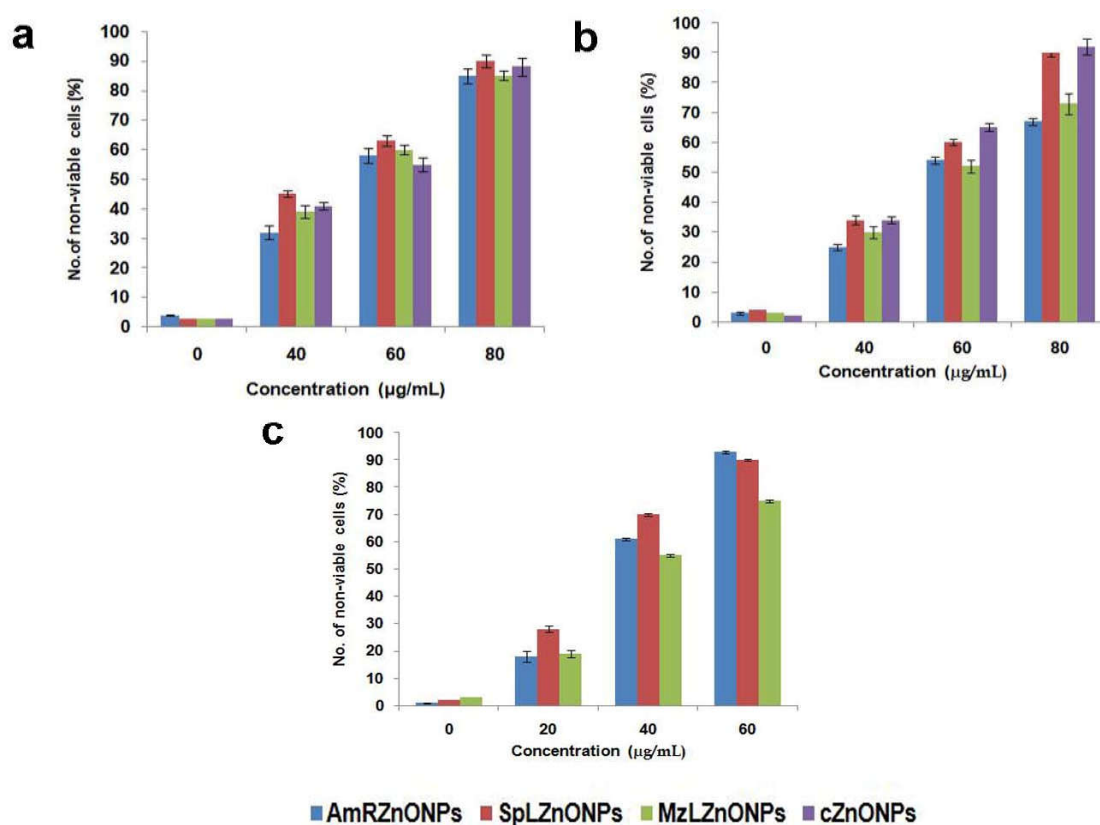


Fig. 4.4. Trypan blue dye exclusion assay employing phyto-derived/chemical ZnONPs against (a) HCT 116 (b) A549 and (c) K562 cells. Values represent mean \pm S.D. of three experiments; $p < 0.05$.

4.5.3. Clonogenic assay

Cellular senescence is an irreversible stopping of mitotic cell division which inhibits colony forming capability of cancer cells. Such inabilities are conventionally

expressed as percentage survival of plated cells following crystal violet staining of culture plates incubated for a long time after exposure to nanoparticles. In the present study, a concentration-dependent decrease in cancer cell colonies was observed compared to those found in untreated controls. In HCT 116 cells, 60 - 70 % of reduction in the colony survival rate was observed at an IC₅₀ value of 60 µg/mL following treatment with all three biogenic nanoparticles compared to only 40 % observed with cells treated with cZnONPs (Fig. 4.5. a and b). At the highest dose tested, about 20 % colony viability was observed in all particle types except those treated with AmRZnONPs showing only ~ 10 % colony survival.

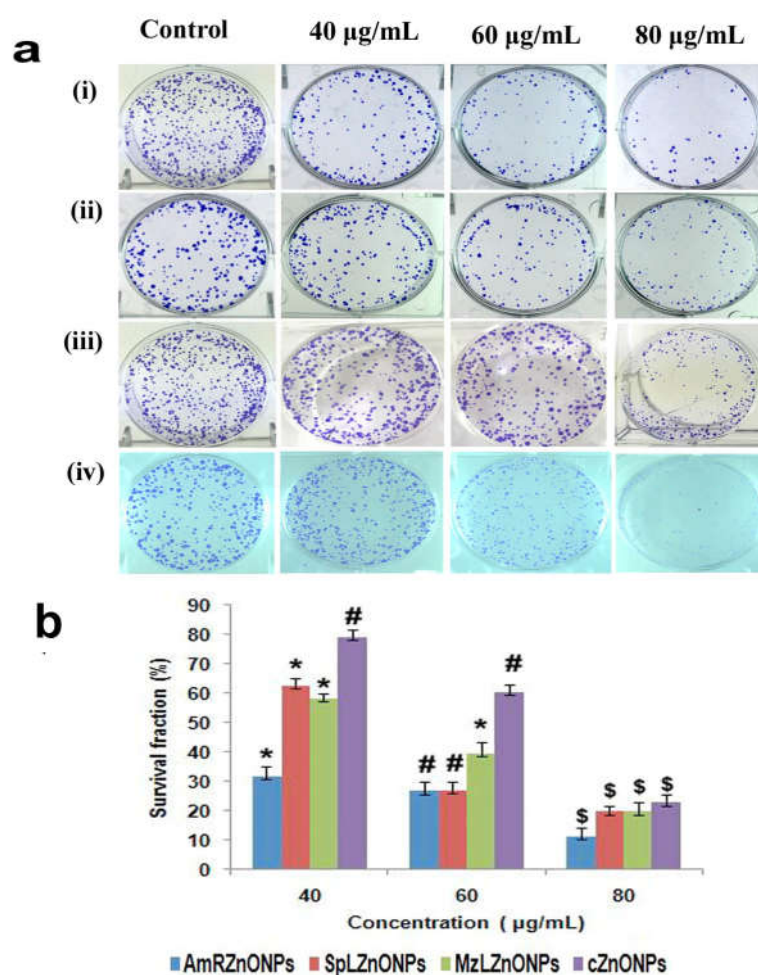


Fig. 4. 5. Inhibition of colony forming capacity of HCT 116 cells on treatment with phyto-derived / chemical ZnONPs (a) Crystal violet stained colonies after treatment with (i) AmRZnONPs (ii) SpLZnONPs (iii) MzLZnONPs and (iv) cZnONPs and (b) histogram showing percentage reduction in colony survival. *P≤0.05, #P≤0.01, \$P≤0.001

In the case of A549 lung cancer cells, MzLZnONPs showed least reduction in colony survival compared to that observed following treatment with the biogenic and the chemically synthesized nanoparticles even at the highest concentration tested (Fig. 4.6 a and b). These cells were also found to exhibit the highest sensitivity to chemical ZnONPs with 21.9 % viability at the IC₅₀ value. However, with K562 cells, the extent of inhibition of colony formation was found to be relatively lower than that observed in HCT 116 and A549 cells. A gradual dose-dependent reduction in colony count was apparent in K562 cells treated with all three biogenic nanoparticles (Fig. 4.7 a and b).

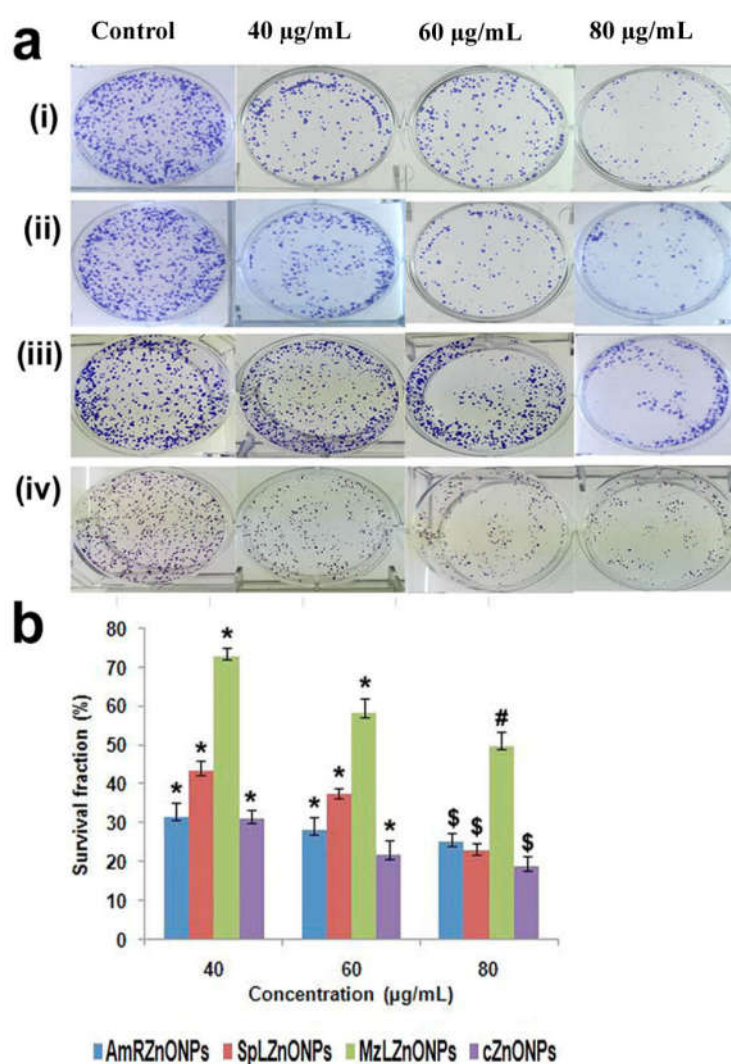


Fig. 4.6. Inhibition of colony forming capacity of A549 cells on treatment with phyto-derived / chemical ZnONPs (a) Crystal violet stained colonies after treatment with (i) AmRZnONPs (ii) SpLZnONPs (iii) MzLZnONPs and (iv) cZnONPs and (b) histogram showing percentage reduction in colony survival. *P ≤ 0.05, #P ≤ 0.01, \$P ≤ 0.001

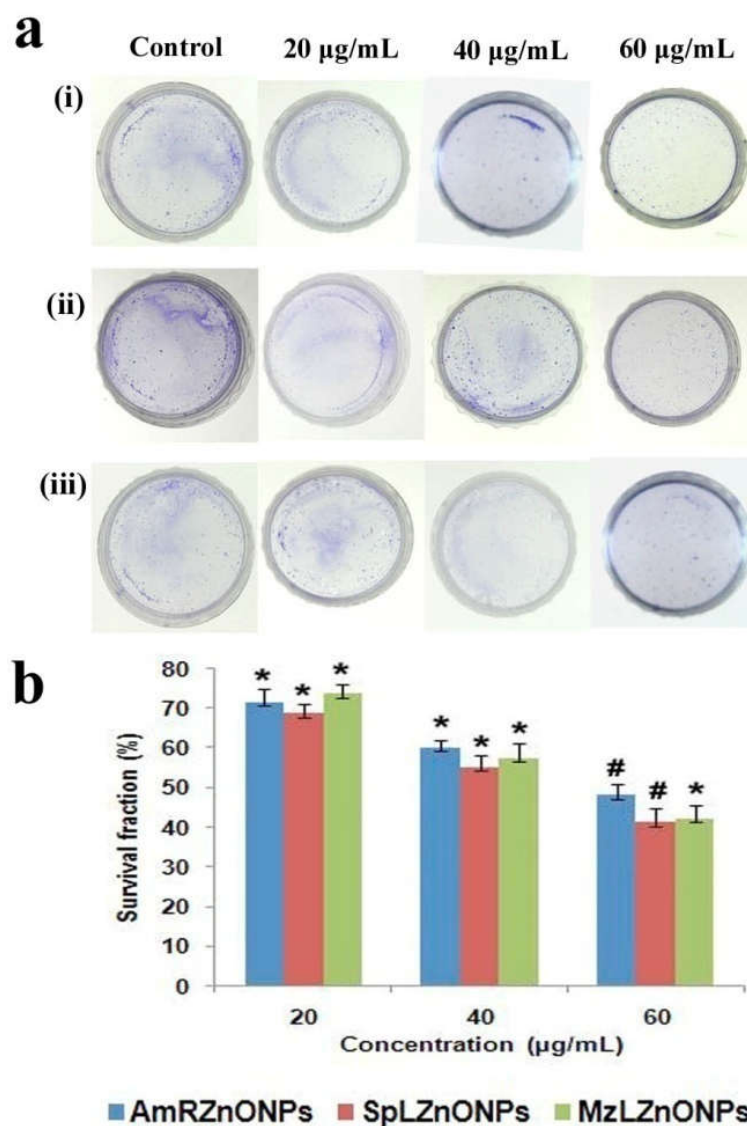


Fig. 4.7. Inhibition of colony forming capacity of K562 cells on treatment with phyto-derived ZnONPs (a) Crystal violet stained colonies after treatment with (i) AmRZnONPs (ii) SpLZnONPs and (iii) MzLZnONPs and (b) histogram showing percentage reduction in colony survival. * $P \leq 0.05$, # $P \leq 0.01$.

It is interesting to note that for the two adherent cancer cells, treatment with sub- IC_{50} concentration of AmRZnONPs also resulted in a significant decrease in their colony forming ability. The dose and duration of exposure to the cytotoxic agent is apparently a critical determinant of the outcome of this assay (Baek et al., 2011).

4.5.4. Microscopic evaluation of cytotoxicity

4.5.4.1. Light microscopy

Cytomorphological alterations followed by treatment with both types of nanoparticles were easily visualized through light microscopy. The adherent colon HCT 116 cells showed a near complete detachment from the culture flasks (Fig. 4.8). This phenomenon called ‘anoikis’, the Greek term meaning ‘homeless’ (Frisch and Francis, 1994; Rouslahti and Reed, 1994) occurs due to loss of cell-matrix interactions resulting from disassembly of focal adhesions, which in turn occurs due to dephosphorylation of a non-receptor tyrosine kinase named focal adhesion kinase (FAK/PTK2). Both endothelial and epithelial cell survival is critically mediated through focal adhesion interactions, which when disrupted, trigger *anoikis*, a class of apoptosis characterized by caspase-3 dependent cleavage of FAK (Kabir et al., 2002; Thuret et al., 2003). In a previous report by Porter et al. (1999), the apoptotic death for adherent monolayer culture occurs simply by the detachment process itself. It has recently been shown that the dissociation of membrane bound integrin with FAK induces *anoikis* via Rho A-JNK-Bim pathway (Haun et al., 2018). Another recent report by Guha et al. (2019) links *anoikis* resistance to integrin and epidermal growth factor receptor (EGFR) related signaling in colon cancer cells. In this context, loss of anchorage of the colon epithelial HCT 116 cells observed following 48 h treatment with both biogenic/chemical ZnONPs is indicative of the occurrence of apoptosis. This was also evident in the phase contrast micrographs displaying the presence of deformed and shrunken cells including those with distorted / fragmented nuclei which is in line with previous observations (Johnson et al., 2000; Hessler et al., 2005; Hattori et al., 2015).

In the present study, the induction of conspicuously large, single bubble-like colon cancer cells following treatment with ZnONPs was clearly observable under the phase contrast microscope. An earlier study on HeLa cells treated with the photosensitiser zinc (II)-phthalocyanine, showed induction of many small evaginations or bubbles, converging later into a macrobubble, finally detaching from the cell surface. The loss of control of water influx has been reported to be the cause of these membrane evaginations (Rello et al., 2005). Similar observations of single enlarged bubbles have been shown to be induced in HCT 116 cells by alismol, a compound purified from

Curcuma zedoaria (Abdul Rahman et al., 2013). Extensive organelle/cell swelling, dilatation of nuclear membrane and condensation of chromatin are well established characteristics of cell necrosis.

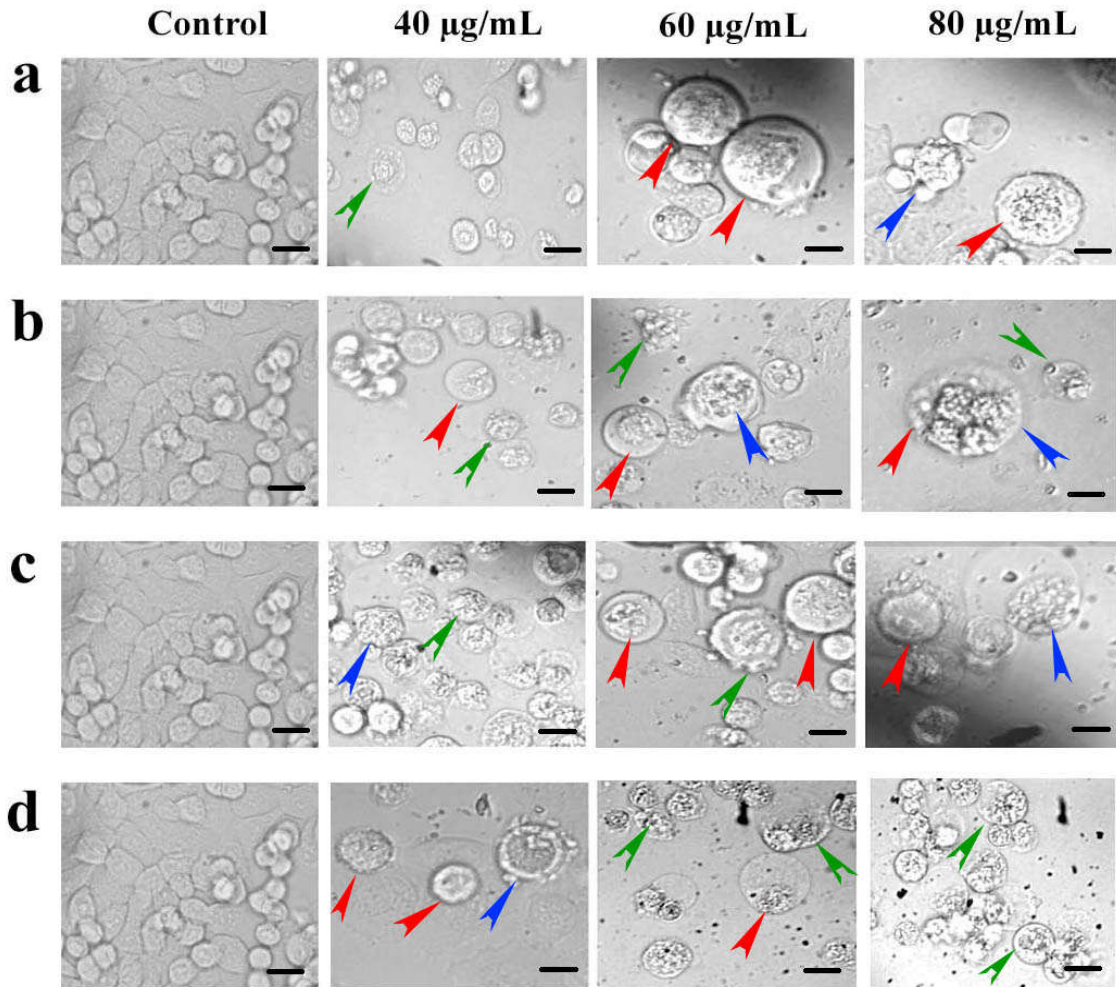


Fig. 4.8. *Light microscopic images showing cytomorphological changes in HCT 116 cells after 48 h treatment with (a) AmRZnONPs (b) SpLZnONPs (c) MzLZnONPs and (d) cZnONPs. Scale bars represent 20 µm. Coloured arrows indicate cell swelling (red), membrane bubbling (blue) and condensed chromatin (green).*

Taken together, the cytomorphological changes observed in ZnONP-treated HCT 116 cells in the present study is highly suggestive of the occurrence of both apoptosis and necrosis as evidenced by massive loss of cell anchorage and the presence of many extensively swollen cells. In this context, it is relevant to note the mounting evidence of a common biochemical network of highly regulated and genetically controlled apoptosis-necrosis continuum ('necroptosis') (Rello et al., 2005; Berghe et al., 2014; Lin et al., 2016; Han et al., 2018). In agreement with the results obtained in

the present study, Farasat et al., 2019 also provides compelling evidence of induction of necroptosis in MCF-7 cells by zinc oxide nanoparticles.

Unlike the above mentioned effects of biogenic ZnONPs, the observations made in respect of the adherent lung carcinoma A549 cells and the suspension culture of leukemic K562 cells were distinctive. A549 cells exhibited anchorage loss only in response to AmRZnONP treatment (Fig. 4.9.). Cellular damage as evidenced by reduction in cell number, deformations in cell membrane and nuclear morphologies were observed to be dose-dependent in this cell type. On the other hand, the scenario was quite different with the K562 cells which showed signs of increased granularity apparently due to chromatin condensation following treatment with SpLZnONPs and MzLZnONPs (Fig. 4.10). The cells were also found to display rough and irregular surface morphology similar to observations associated with grandisin-induced apoptosis reported in K562 cells by Cortez et al. (2017).

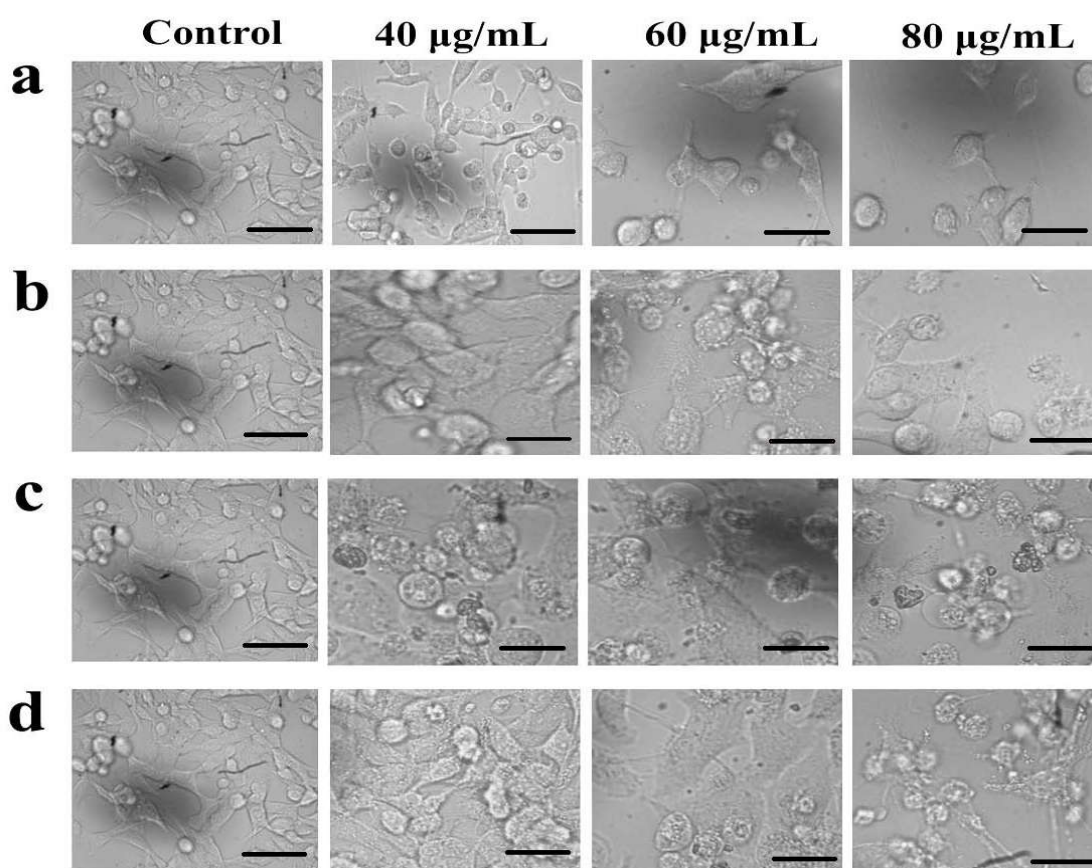


Fig. 4.9. Light microscopic images showing cytomorphological changes in A549 cells after 48 h treatment with (a) AmRZnONPs (b) SpLZnONPs (c) MzLZnONPs and (d) cZnONPs. Scale bars represent 30 μm .

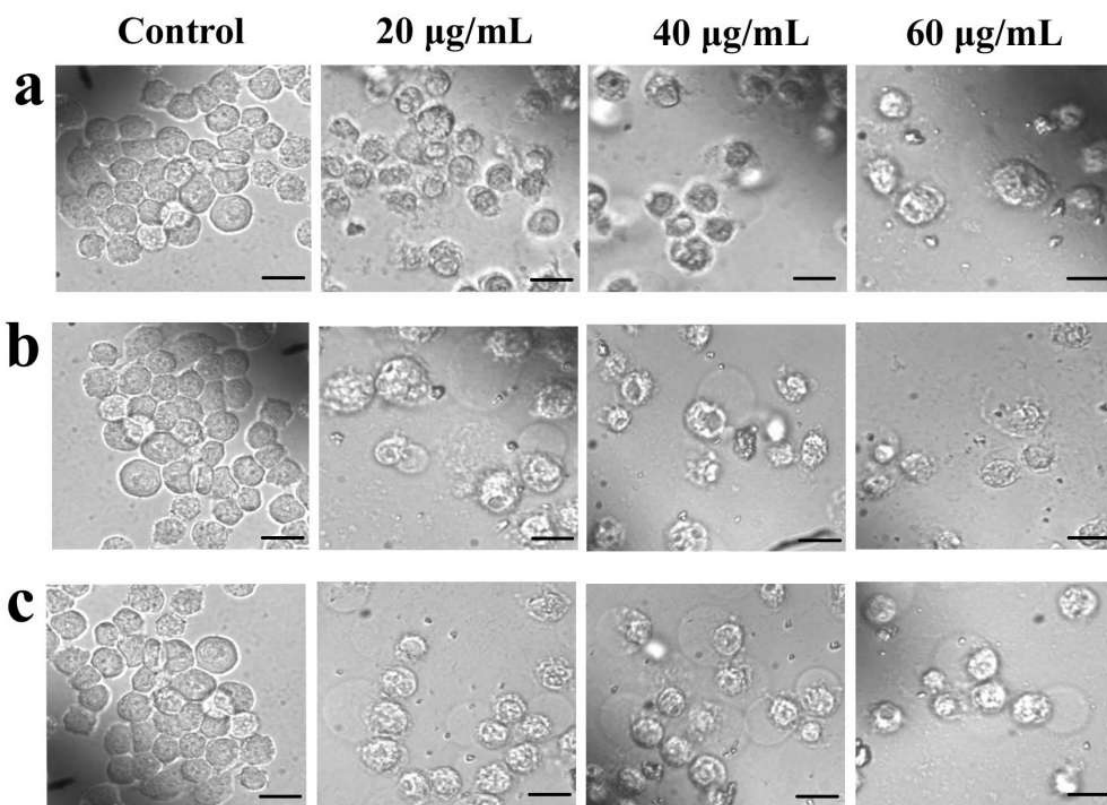


Fig. 4.10. Light microscopic images showing cytomorphological changes in K562 cells after 48 h treatment with (a) AmRZnONPs (b) SpLZnONPs and (c) MzLZnONPs. Scale bars represent 15 μm .

4.5.4.2. Scanning electron microscopy (SEM)

The three types of cancer cells were subjected to SEM technique to obtain high-resolution surface images for a detailed analysis of cytomorphological changes induced by exposure to the different types of ZnONPs. Fig. 4.11. shows images of dose-dependent changes in HCT 116 cells, exposed to varying concentrations of nanoparticles. Small evaginations (bubbles) and invaginations were clearly visible in cells treated with AmRZnONPs, MzLZnONPs and SpL-derived particles at sub-IC₅₀ concentration (40 $\mu\text{g/mL}$). Cells treated with chemical cZnONPs displayed numerous cavities on the plasma membrane surface. A progressive size reduction due to shrinkage was apparent in cells treated with higher concentrations (60 and 80 $\mu\text{g/mL}$) of all nanoparticle types, providing a visual clue of apoptosis induction. Cavities/perforations were also observed on cellular surfaces which are known to result

from ruptured bubbles or evaginations caused during the process of regulated necrosis or ‘necroptosis’ mentioned earlier (sub-section 4.5.4.1.).

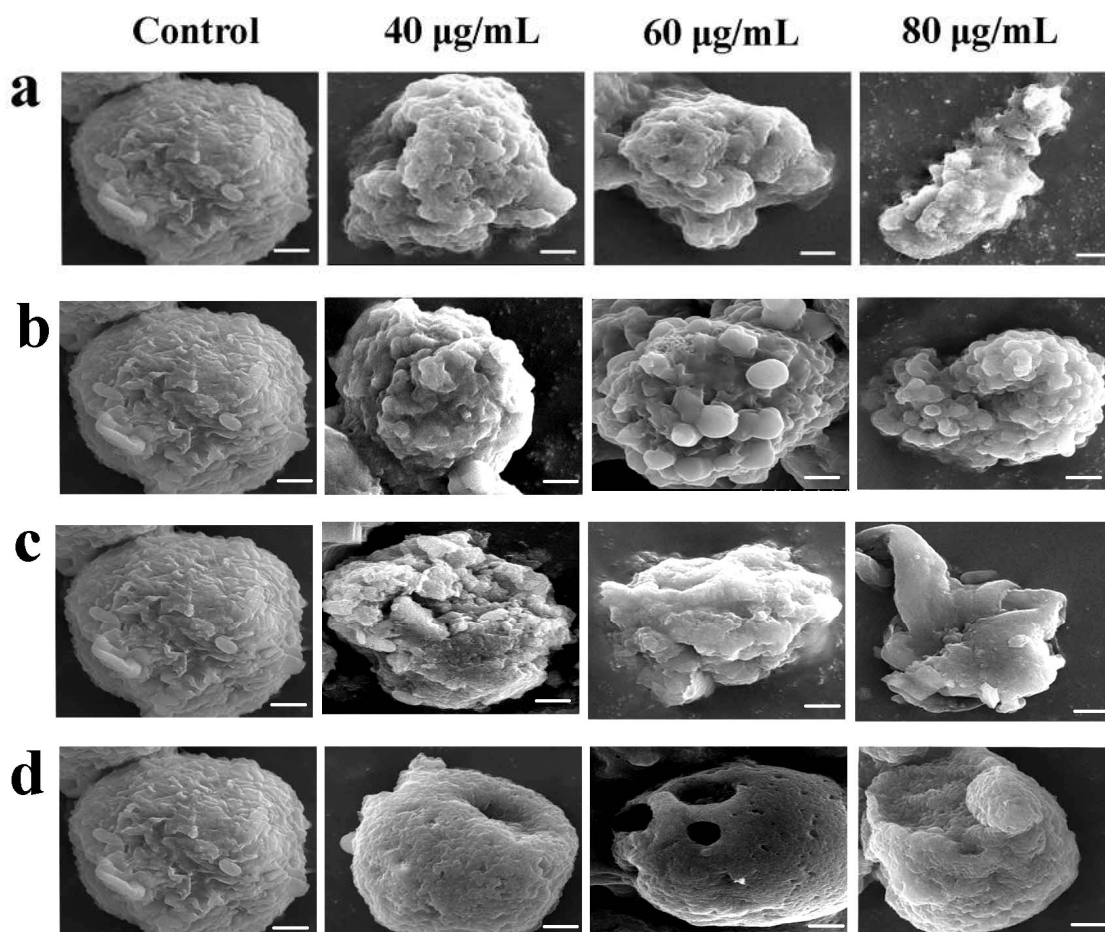


Fig. 4.11. Scanning electron microscopic images of HCT 116 cells treated with (a) AmRZnONPs (b) SpLZnONPs (c) MzLZnONPs and (d) cZnONPs. Scale bars represent 2 μm .

The SEM images of adherent lung cancer cells A549 and the suspension cultures of leukemic K562 cells exposed to different types of nanoparticles exhibited distinctive changes in cellular morphology (Fig. 4.12, 4.13). For instance, an overall dose-dependent shrinkage of cells was apparent with extreme reduction in size and integrity. Membrane perforations and cavities were also clearly visible on cell surfaces. Taken together, the SEM images provided ample evidence to support the occurrence of both necrosis and apoptosis.

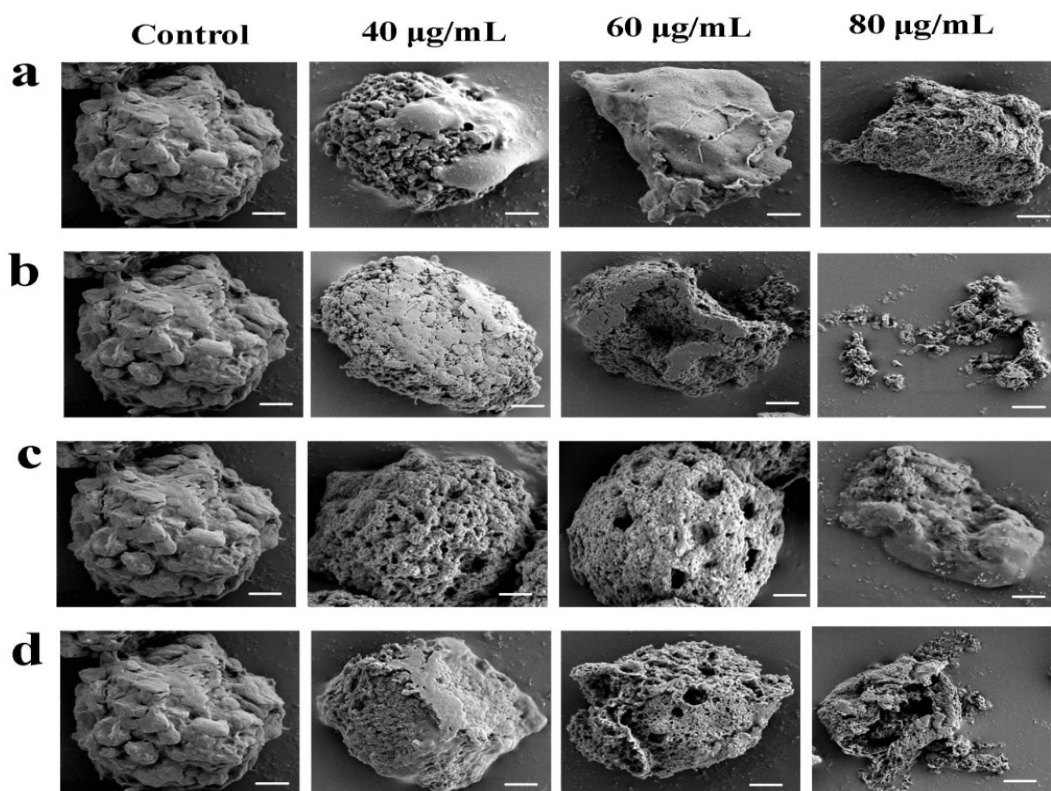


Fig. 4.12. Scanning electron microscopic images of A549 cells after treatment with (a) AmRZnONPs (b) SpLZnONPs (c) MzLZnONPs and (d) cZnONPs. Scale bars represent 2 μm .

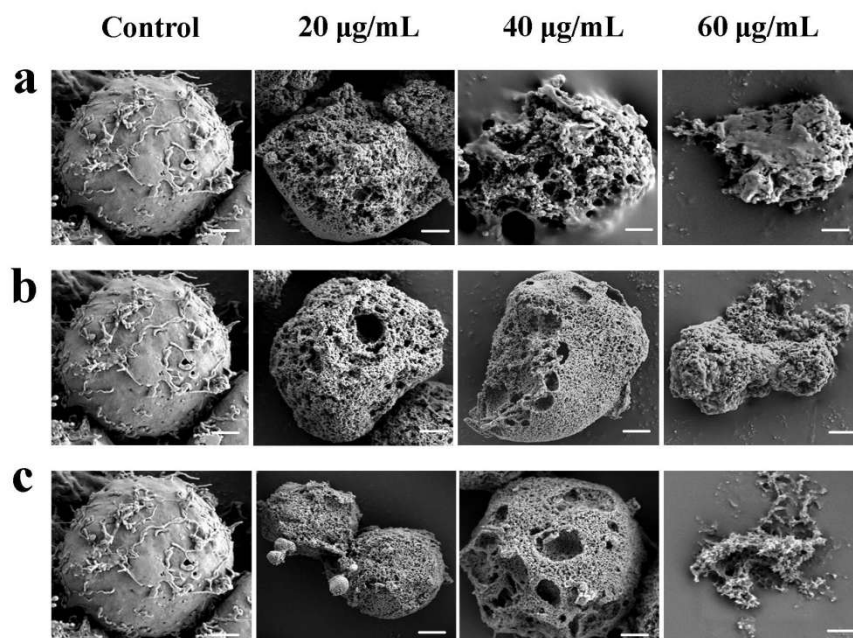


Fig. 4.13. Scanning electron microscopic images of K562 cells after treatment with (a) AmRZnONPs (b) SpLZnONPs and (c) MzLZnONPs. Scale bars represent 2 μm .

4.5.4.3. Fluorescence microscopy

4.5.4.3.1. Hoechst 33258 staining

Hoechst 33258 is a membrane permeable blue dye that stains condensed/fragmented chromatin characteristic of cells undergoing apoptosis. Cells treated with phyto-derived and chemical ZnONPs were stained with the dye and observed under a fluorescence microscope. Nuclear fragmentation associated with apoptosis induction was found to occur in a dose dependent manner in all the three cell types exposed to ZnONPs (Fig. 4.14). The chromatin condensation was clearly evident in HCT 116 and K562 cells at and above the IC₅₀ concentrations. However, in A549 cells, except those treated with SpLZnONPs, this phenomenon was observable only at a concentration above the IC₅₀ value (Fig. 4.14 b).

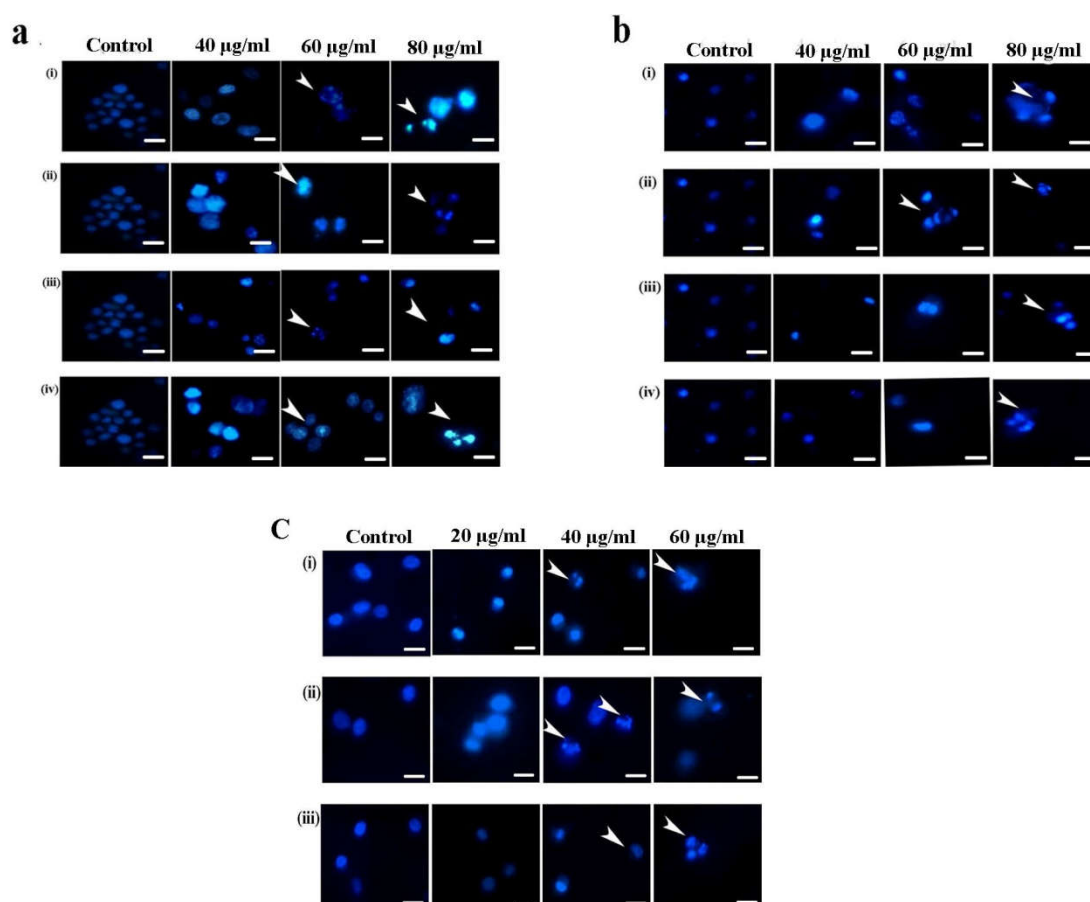


Fig. 4.14. Fluorescence microscopy images of Hoechst 33258 stained (a) HCT 116 (b) A549 and (c) K562 cells after treatment with (i) AmRZnONPs (ii) SpLZnONPs (iii) MzLZnONPs and (iv) cZnONPs (arrow heads indicate apoptotic nuclear condensation and DNA fragmentation). Scale bars represent 20 µm.

4.5.4.3.2. *AO/EtBr dual-staining*

In AO/EtBr dual-staining method, the fluorescence visualized can be used to distinguish / identify different stages of apoptosis-associated cells (Liu et al., 2015). The uniform bright green nuclear fluorescence due to AO is emitted from the intact nuclei of live cells whilst nuclei with irregular green fluorescence denote early phase of apoptotic chromatin condensation. During late apoptosis, EtBr-stained nuclei display irregular orange fluorescence due to nuclear fragmentation; uniform orange to red nuclei are indicative of necrosis (Kosmider et al., 2004). Dual-stained HCT 116 cells exposed to ZnONPs exhibited a dose dependent increase in the number of apoptotic/necrotic cells (Fig. 4.15). Cells treated at 80 $\mu\text{g/mL}$, above- IC_{50} value, of the chemically synthesized cZnONPs and the biogenic AmR and SpL-derived ZnONPs, showed a drastic increase in the percentage of necrotic cells (~90 %) whereas exposure to MzLZnONPs resulted in increase of late apoptotic cells (~75 %).

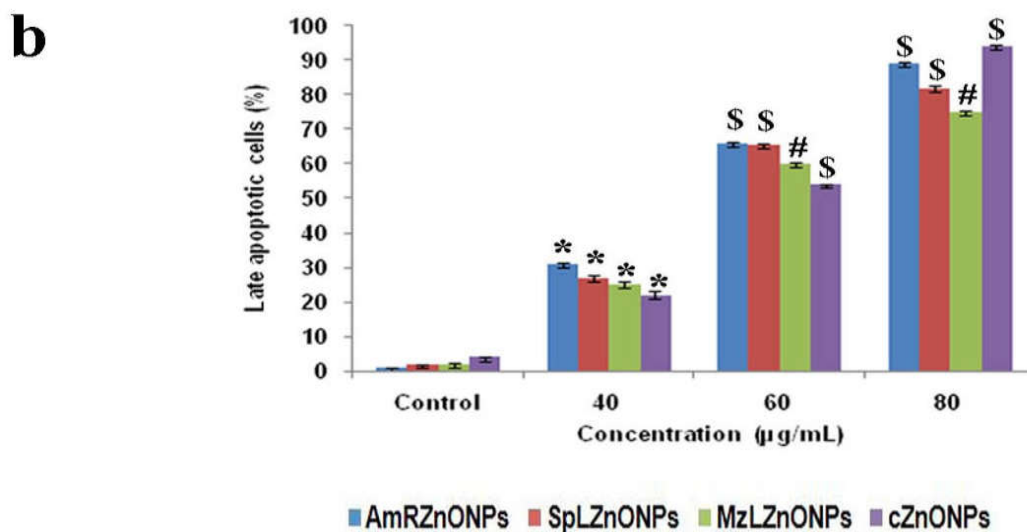
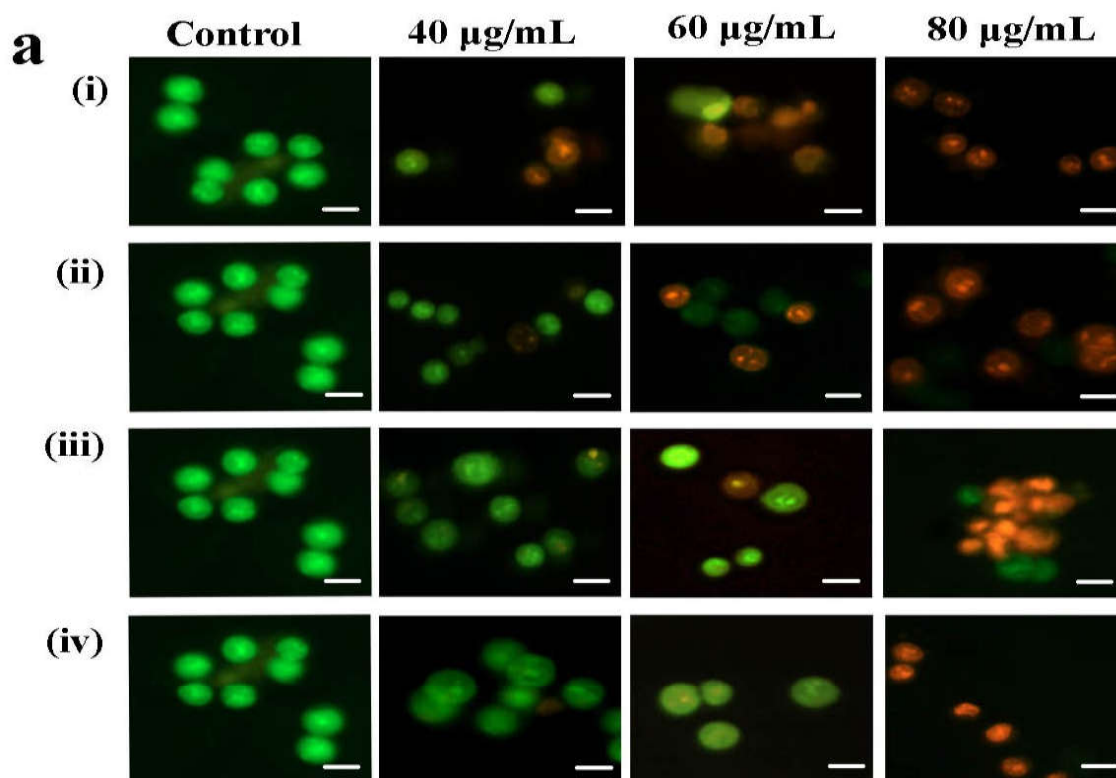


Fig. 4.15. Induction of apoptosis in HCT 116 cells on treatment with phyto-derived / chemical ZnONPs and stained with AO/EtBr (a) Fluorescence microscopic images of AO/EtBr stained cells after treatment with (i) AmRZnONPs (ii) SpLZnONPs (iii) MzLZnONPs and (iv) cZnONPs and (b) histogram showing quantification of late apoptotic cell percentage. Scale bars represent 20 μm . * $P \leq 0.05$, # $P \leq 0.01$, \$ $P \leq 0.001$

Interestingly, A549 cells treated with SpLZnONPs and AmRZnONPs showed high numbers of large, swollen cells with characteristic membrane blebbings and apoptotic bodies (Fig. 4.16). These observations are in agreement with an earlier report on colon cells treated with methanolic extract of *L.vulgare* (Ćurčić et al., 2012). Although cells treated with either cZnONPs or MzL-derived particles showed signs of apoptosis induction, they failed to display increase in size.

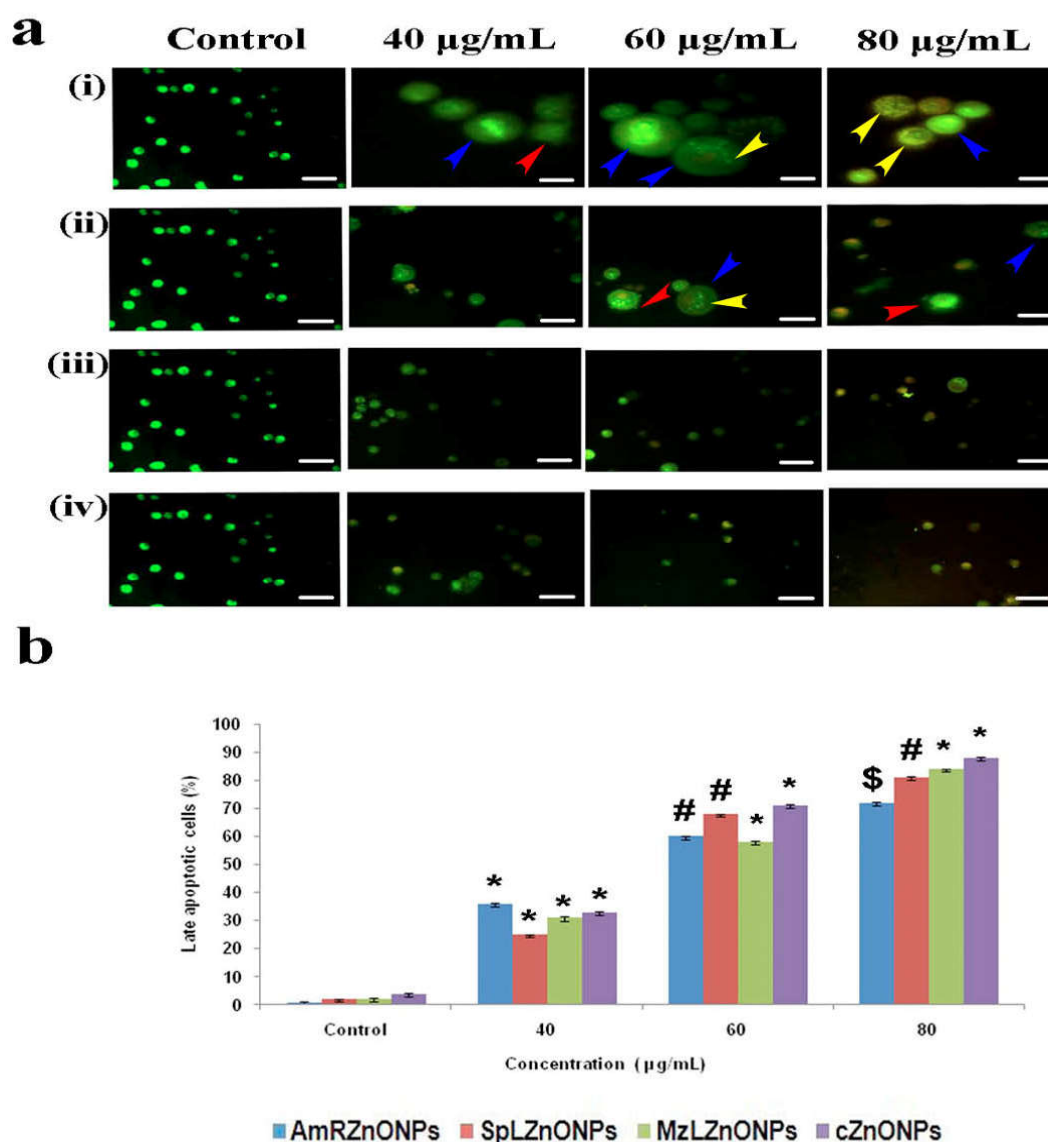


Fig. 4.16. Induction of apoptosis in A549 cells on treatment with phyto-derived / chemical ZnONPs and stained with AO/EtBr (a) Fluorescence microscopic images of of AO/EtBr stained cells after treatment with (i) AmRZnONPs (ii) SpLZnONPs (iii) MzLZnONPs and (iv) cZnONPs and (b) histogram showing quantification of late apoptotic cell percentage. Scale bars represent 20 μm . * $P \leq 0.05$, # $P \leq 0.01$, \$ $P \leq 0.001$. Arrow heads in colour indicate membrane blebbings (red); apoptotic bodies (yellow); swollen cells (blue).

In the case of K562 cells, treatments with AmRZnONPs and SpLZnONPs at 40 and 60 $\mu\text{g}/\text{mL}$ resulted in induction of apoptosis (Fig. 4.17) which was in agreement with the results obtained previously researchers with chemically derived zinc oxide nanoparticle treated Caco-2 cells by Kang et al. (2015). MzLZnONPs were found to induce apoptosis only at the highest concentration of 60 $\mu\text{g}/\text{mL}$ (Fig. 4.17). However, cells treated with the phyto-derived AmRZnONPs and MzLZnONPs at low concentration failed to induce apoptosis as evidenced by their display of green nuclear fluorescence emanating from viable cells.

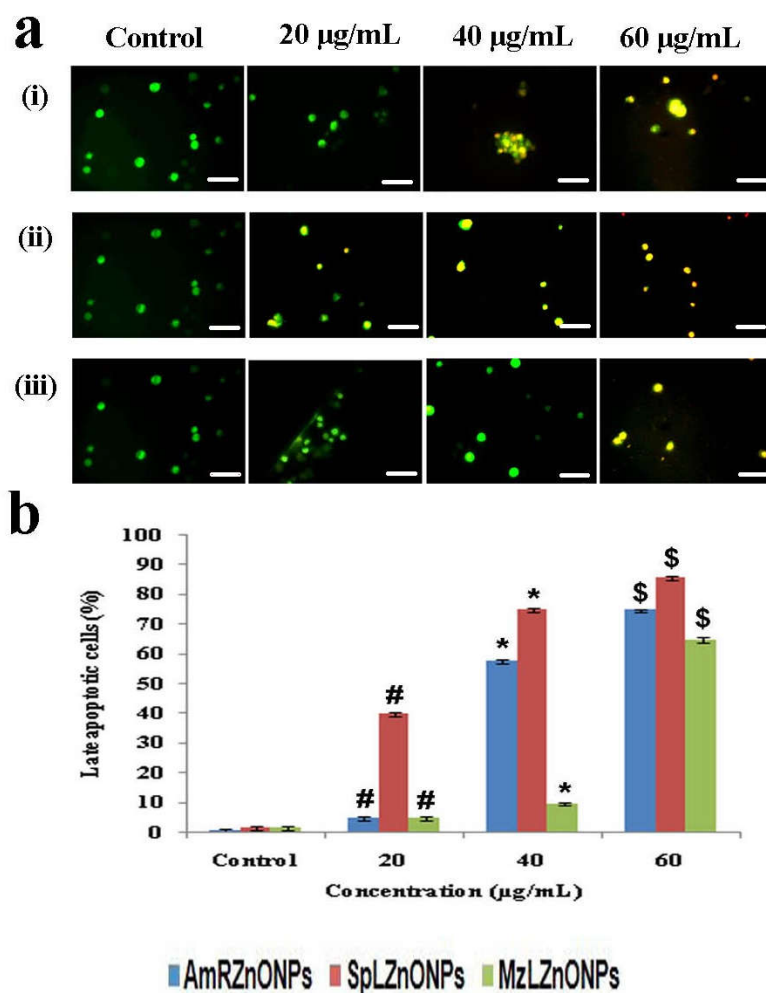


Fig. 4.17. Induction of apoptosis in K562 cells on treatment with phyto-derived ZnONPs and stained with AO/EtBr (a) Fluorescence microscopic images of AO/EtBr stained cells after treatment with (i) AmRZnONPs (ii) SpLZnONPs and (iii) MzLZnONPs and (b) histogram showing quantification of late apoptotic cell percentage. Scale bars represent 30 μm . $*P \leq 0.05$, $^{\#}P \leq 0.01$, $^{\$}P \leq 0.001$

4.5.5. Effect of phyto-derived/chemical ZnONPs on release of intracellular Ca²⁺, generation of reactive oxygen species (ROS) and loss of mitochondrial membrane potential (MMP)

Intracellular Ca²⁺ maintains proper cell function and signal transduction between the endoplasmic reticulum (ER) and the mitochondria for normal cell physiology. Perturbation of this homeostasis causes calcium ions to act as a second messenger to trigger a series of downstream signals in the cell. Calcium overload induced production and accumulation of ROS in mitochondria is known to result in either apoptosis or necrotic cell death (Smaili et al., 2003). In this context, levels of intracellular calcium ions were assessed in the present study employing the Ca²⁺ indicator Fluo-3AM. This dye when cleaved by non-specific intracellular esterases to Fluo-3 which fluoresces green on binding to cellular calcium ions. In all the three cell lines treated with both types of ZnONPs a dose-dependent increase in green fluorescence was clearly evident. Fig. 4.18. includes a common representative image of cells exposed to different concentrations of all types of ZnONPs along with separate histograms depicting results obtained with the three cell types. Table 4.3 shows dose-dependent increase in the percentage of fluorescing cells in all the three cell types treated with different ZnONPs. SpLZnONPs induced Ca²⁺ release was found to be highest in HCT 116 (93 %) and K562 (79 %) cells whereas in A549 cells, treatment with cZnONPs displayed the maximum fluorescence intensity (88%). Increased intracellular calcium levels and disrupted homeostasis leading to cell death has been reported by Guo et al. (2013) in rat retinal ganglion cells treated with ZnONPs. Likewise, zinc oxide nanoparticle-induced calcium signaling dependent lysosomal apoptosis and autophagy was also reported recently in MCF-7 and MDA-MB-468 cells (Mozdoori et al., 2017). Treatment with silver nanoparticles also reportedly induced dose-dependent calcium ion overload in various cell lines (Zhang et al., 2016; Mameneh et al., 2019).

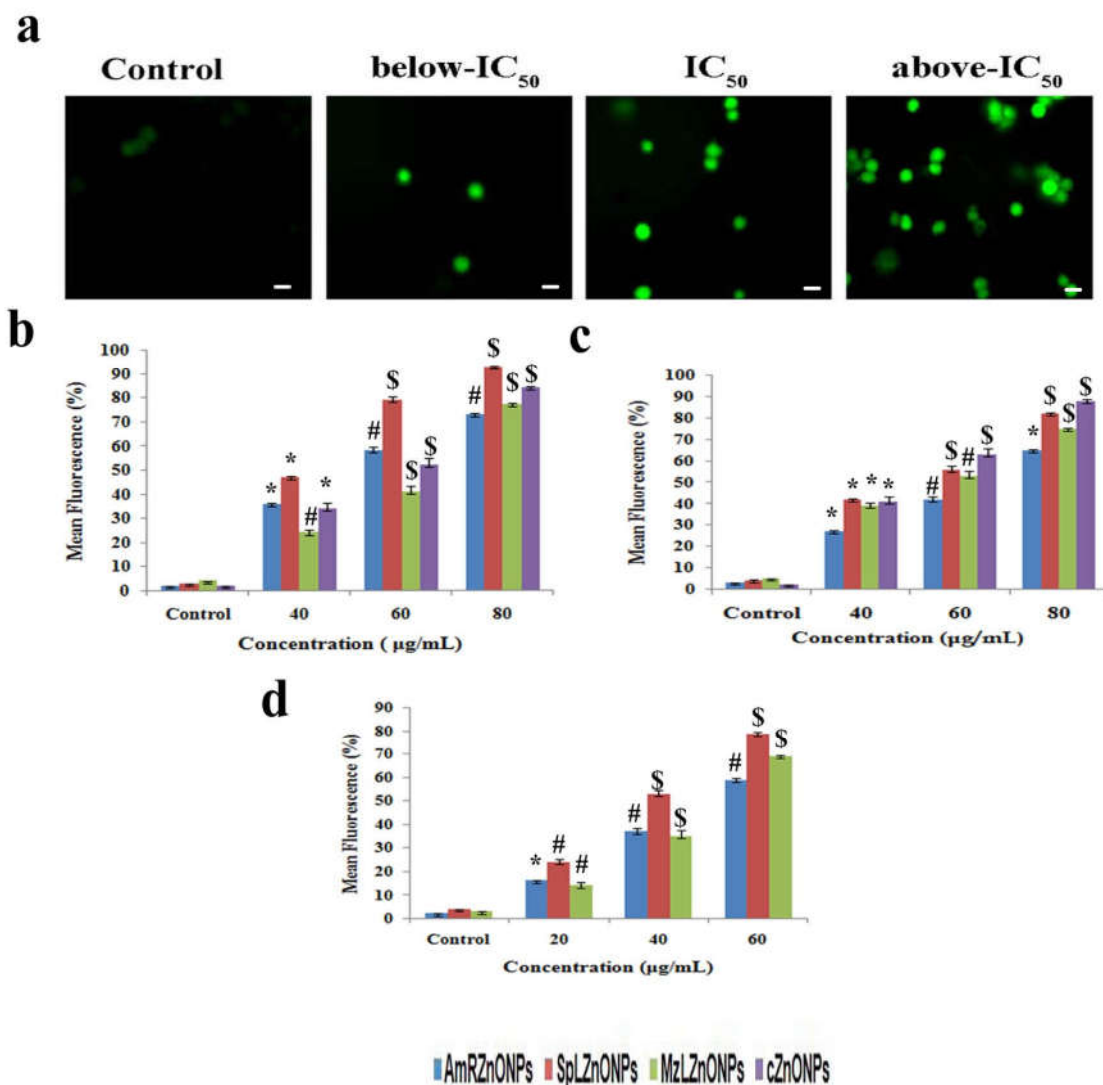


Fig. 4.18. Measurement of intracellular calcium release in cells treated with phyto-derived / chemical ZnONPs using Ca^{2+} indicator Fluo 3-AM (a) representative fluorescence microscopic image of cells exposed to different concentrations of all types of ZnONPs. Histograms represent mean fluorescence intensity of ZnONP-treated (b) HCT 116 (c) A549 and (d) K562 cells. Scale bars represent 20 µm. * $P \leq 0.05$, # $P \leq 0.01$, \$ $P \leq 0.001$.

Table 4.3. Mean percentage fluorescence intensity of cells stained with intracellular Ca²⁺ indicator Fluo 3-AM

Type of ZnONPs	Concentration (µg/mL)	HCT 116 cells	A549 cells	Concentration (µg/mL)	K562 cells
AmRZnONPs	40	36 ± 0.4	27 ± 0.6	20	16 ± 0.4
	60	58 ± 1.4	42 ± 1.2	40	37 ± 1.4
	80	73 ± 0.5	65 ± 0.7	60	59 ± 0.5
SpLZnONPs	40	47 ± 0.5	42 ± 0.5	20	24 ± 1.2
	60	79 ± 1.6	56 ± 1.8	40	53 ± 1.6
	80	93 ± 0.5	82 ± 0.5	60	79 ± 0.8
MzLZnONPs	40	24 ± 1.4	39 ± 1.3	20	14 ± 1.4
	60	41 ± 2.4	53 ± 2.6	40	35 ± 2.4
	80	77 ± 0.4	75 ± 0.6	60	69 ± 0.4
cZnONPs	40	34 ± 2.3	41 ± 2.0	-	-
	60	52 ± 2.7	63 ± 3.1	-	-
	80	84 ± 0.5	88 ± 1.1	-	-

(The values highlighted in blue boxes denote maximal cell-specific intracellular Ca²⁺ release. Values represent mean ± S.D. of three experiments,)

Free radicals such as reactive oxygen species (ROS) and reactive nitrogen species (RNS) are short-lived, unstable and highly reactive atoms and molecules containing one or more unpaired electrons in valency shell. The cellular sites of their generation include mitochondria, peroxisomes, endoplasmic reticulum and phagocytic cells (Phaniendra et al., 2014). These radicals can alter the redox status of nucleic acids, lipids and proteins, thereby increasing oxidative stress causing cellular injuries and a wide array of diseases including various cancers. Various types of nanoparticles including zinc oxide have been reported to cause ROS-mediated oxidative stress which in turn triggers apoptotic cell death (Ma and Yang, 2016; Patel et al., 2016; Bai et al., 2017; Aswathnarayan et al., 2018).

In the present study, following a 48 h exposure to both biogenic and the chemical cZnONPs, a dose-dependent increase in ROS production was observed in all the three cell lines (Fig. 4.19 - 4.21) even at the lowest concentration tested. The maximum ROS production (~90 %) in HCT 116 and K562 cells was induced by SpLZnONPs and in A549 cells following treatment with both the biogenic MzL-derived and the chemically synthesized ZnONPs (Table 4.4). However, lowest ROS production was induced by AmRZnONPs in all the three cell types.

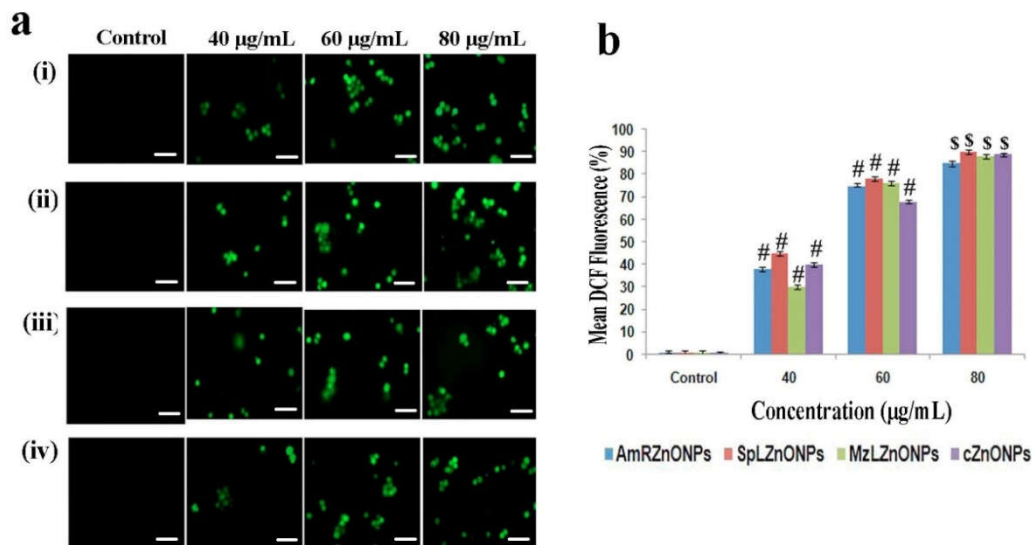


Fig. 4.19. Measurement of ROS in HCT 116 cells treated with phyto-derived / chemical ZnONPs (a) Fluorescence microscopic images of cells treated with (i) AmRZnONPs (ii) SpLZnONPs (iii) MzLZnONPs and (iv) cZnONPs and (b) histogram showing mean fluorescence intensity of cells stained with ROS indicator DCFH-DA. [#] $P \leq 0.01$, ^S $P \leq 0.001$. Scale bars represent 20µm

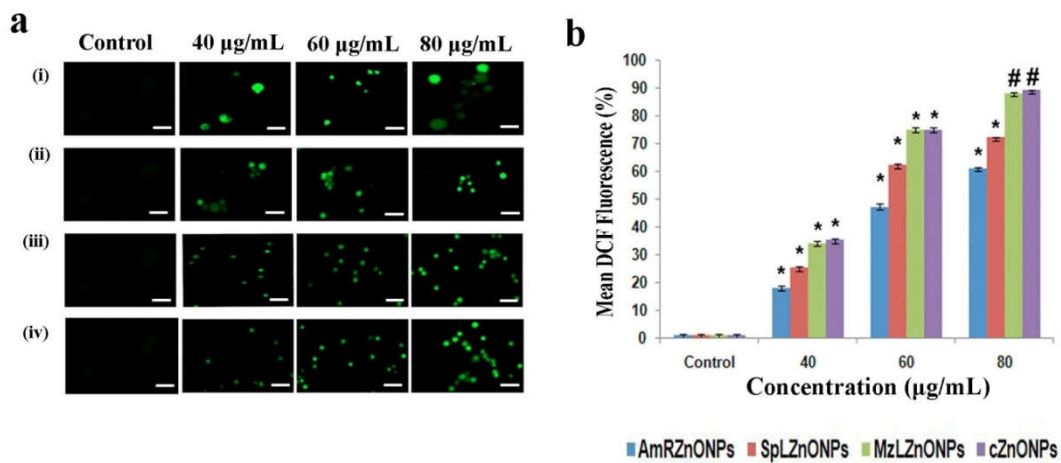


Fig. 4.20. Measurement of ROS in A549 cells treated with phyto-derived/chemical ZnONPs (a) Fluorescence images of cells treated with (i) AmRZnONPs (ii) SpLZnONPs (iii) MzLZnONPs and (iv) cZnONPs and (b) histogram showing mean fluorescent intensity of cells stained with ROS indicator DCFH-DA. ^{*} $P \leq 0.05$, [#] $P \leq 0.01$. Scale bars represent 20 µm

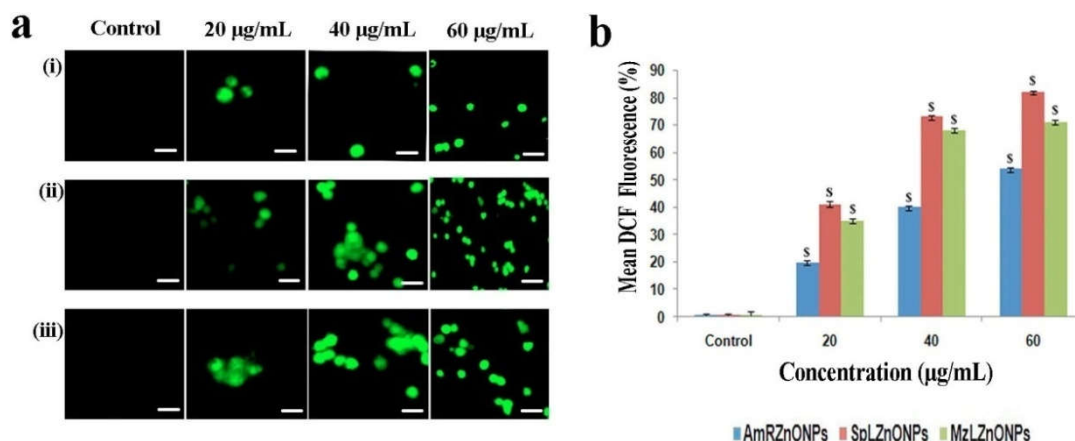


Fig. 4.21. Measurement of ROS in K562 cells treated with phyto-derived ZnONPs (a) Fluorescence microscopic images of cells treated with (i) AmRZnONPs (ii) SpLZnONPs (iii) and MzLZnONPs and (b) histogram showing mean fluorescence intensity of cells stained with ROS indicator DCFH-DA. ^S*P* ≤ 0.001. Scale bars represent 20 µm.

Table 4.4. Dose-dependent variations in mean fluorescence intensity(%) of cells stained with ROS indicator DCFH-DA

Types of ZnONPs	Concentration (µg/mL)	HCT 116 cells	A549 cells	Concentration (µg/mL)	K562 cells
AmRZnONPs	40	38 ± 1.2	18 ± 0.6	20	20 ± 0.5
	60	75 ± 0.5	47 ± 1.1	40	40 ± 0.4
	80	82 ± 0.4	61 ± 0.5	60	54 ± 0.7
SpLZnONPs	40	45 ± 0.6	25 ± 0.7	20	41 ± 1.0
	60	78 ± 1.5	62 ± 0.5	40	73 ± 0.5
	80	90 ± 1.6	72 ± 0.4	60	82 ± 0.6
MzLZnONPs	40	30 ± 0.8	34 ± 0.8	20	35 ± 1.5
	60	76 ± 0.3	75 ± 0.6	40	68 ± 0.8
	80	85 ± 0.9	88 ± 0.3	60	71 ± 0.2
cZnONPs	40	40 ± 0.9	35 ± 0.5	-	-
	60	68 ± 0.8	75 ± 0.8	-	-
	80	85 ± 0.7	88 ± 0.2	-	-

(The values highlighted in blue boxes denote maximal cell-specific ROS production. Values represent mean ± S.D. of three experiments)

The entry of lipophilic, cationic dye Rhodamine-123 (RH-123) into the mitochondrial matrix and its association with the inner membrane is reflective of the mitochondrial transmembrane potential (MMP). Mitochondrial energization induces quenching of RH-123 fluorescence and the rate of decay of green fluorescence is proportional to the loss of MMP (Baracca et al., 2003). ZnONP-treated HCT 116, A549 and K562 cells showed a concentration dependent reduction in fluorescent intensity/ MMP compared with that observed in the untreated control cells (Fig. 4.22-4.24). HCT 116 and K562 cells exhibited the highest reduction in MMP following treatment with SpLZnONPs indicative of a high vulnerability of the cells towards these particles (Table 4.5). A549 cells, on the other hand were found to be relatively more susceptible to loss of MMP when exposed to chemically derived cZnONPs. A dose-dependent decrease in green fluorescence due to loss of MMP in A549 cells following exposure to *Sesuvium portulacastrum* L. derived gold nanoparticles, recently reported by Ramalingam et al. (2016) is in line with the results mentioned above.

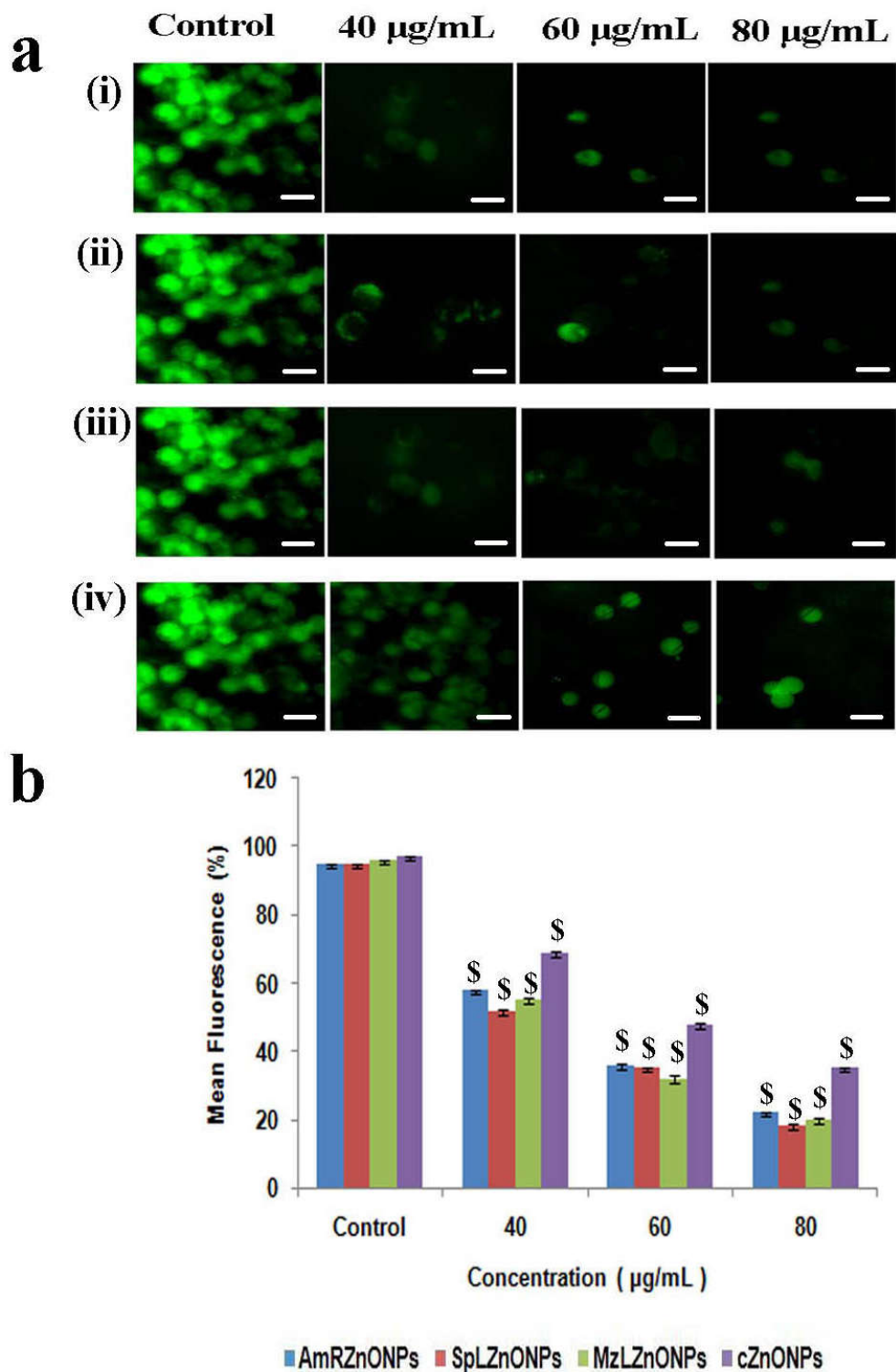


Fig. 4. 22. Measurement of mitochondrial membrane potential in HCT 116 cells treated with phyto-derived/chemical ZnONPs (a) Fluorescence microscopic images following treatment with (i) AmRZnONPs (ii) SpLZnONPs (iii) MzLZnONPs and (iv) cZnONPs. and (b) histogram showing mean fluorescent intensity of cells stained with Rhodamine-123. $^5P \leq 0.001$. Scale bars represent 20 μm .

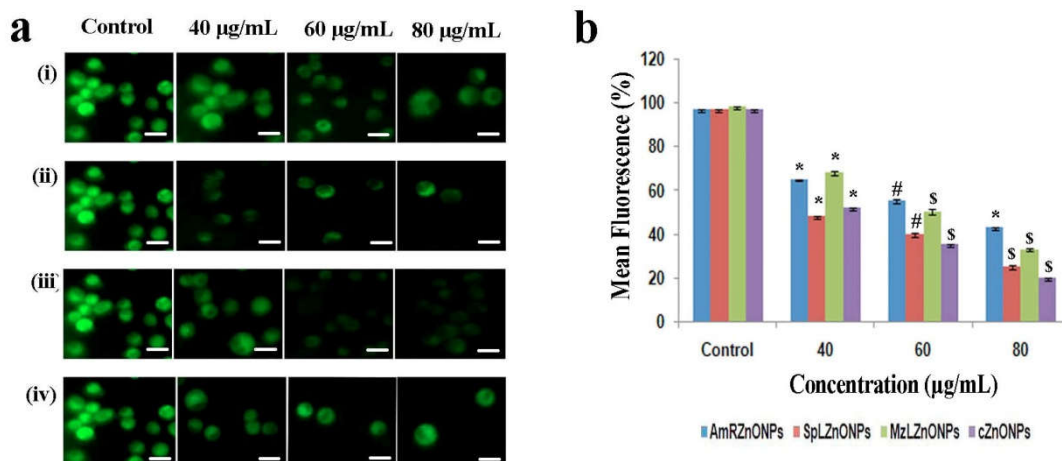


Fig. 4.23. Measurement of mitochondrial membrane potential in A549 cells treated with phyto-derived / chemical ZnONPs (a) Fluorescence microscopic images following treatment with (i) AmRZnONPs (ii) SpLZnONPs (iii) MzLZnONPs and (iv) cZnONPs and (b) histogram showing mean fluorescent intensity of cells stained with Rhodamine-123. * $P \leq 0.05$, # $P \leq 0.01$, $^{\$}P \leq 0.001$. Scale bars represent 20 µm.

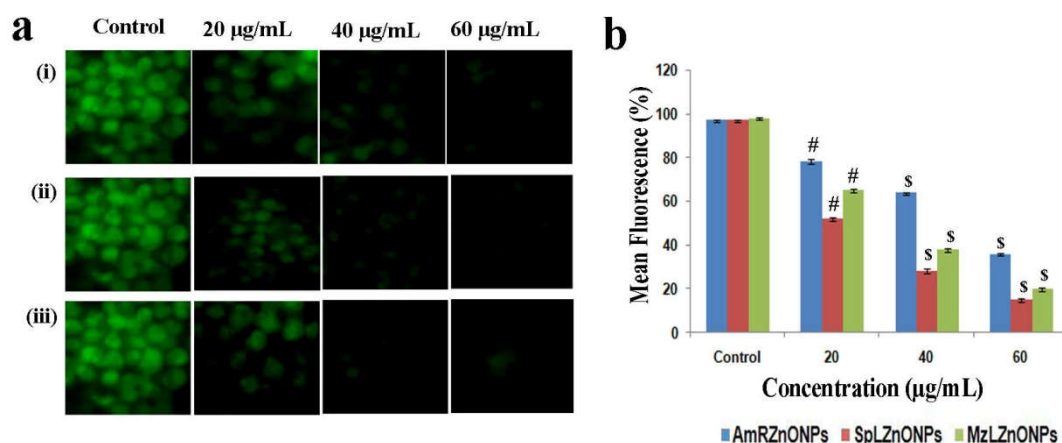


Fig. 4.24. Measurement of mitochondrial membrane potential in K562 cells treated with phyto-derived ZnONPs (a) Fluorescence microscopic images following treatment with (i) AmRZnONPs (ii) SpLZnONPs (iii) and MzLZnONPs and (b) histogram showing mean fluorescent intensity of cells stained with Rhodamine-123. # $P \leq 0.01$, $^{\$}P \leq 0.001$. Scale bars represent 20 µm.

Table. 4.5. Mean fluorescence intensity of cells (%) stained with Rhodamine-123

Types of ZnONPs	Concentration (µg/mL)	HCT 116 cells	A549 cells	Concentration (µg/mL)	K562 cells
AmRZnONPs	40	58 ± 0.2	65 ± 0.2	20	78 ± 1.2
	60	36 ± 0.8	55 ± 0.8	40	34 ± 0.2
	80	22 ± 0.4	43 ± 0.4	60	36 ± 0.5
SpLZnONPs	40	52 ± 0.5	48 ± 0.5	20	52 ± 0.9
	60	35 ± 0.6	40 ± 0.6	40	28 ± 1.3
	80	18 ± 0.9	25 ± 0.9	60	15 ± 0.7
MzLZnONPs	40	55 ± 0.6	68 ± 0.6	20	65 ± 0.7
	60	32 ± 1.2	50 ± 1.2	40	38 ± 0.5
	80	20 ± 0.6	33 ± 0.6	60	20 ± 0.6
cZnONPs	40	69 ± 0.3	52 ± 0.3	-	-
	60	48 ± 0.5	35 ± 0.5	-	-
	80	35 ± 0.4	20 ± 0.4	-	-

(The values highlighted in blue boxes denote maximal cell-specific reduction in mitochondrial membrane potential. Values represent mean ± S.D. of three experiments)

It is evident from the results mentioned above that the phyto-derived SpLZnONPs were relatively more effective against colon and leukemic cells and chemical cZnONPs against lung cancer cells. Taken together, all the three crucial inter-related biochemical determinants of the cell fate analyzed in the present study – levels of intracellular Ca²⁺ / ROS and loss of MMP - were indicative of cell-specific induction of apoptosis by phyto-derived and chemical ZnONPs. Nanoparticles including ZnO reportedly induce oxidative stress, sensitization of calcium storage compartments (ER and mitochondria) leading to apoptosis induction. Nanoparticle size, concentration and the target cell type are factors influencing this phenomenon (Zhang et al., 2012; Chen et al., 2016; Cao et al., 2017).

4.5.6. Flow cytometric (FACS) analysis of apoptosis

4.5.6.1. Effect of ZnONPs on cell cycle progression

Cell cycle is a set of highly ordered, complex series of events involving duplication and division of its contents for cell growth and reproduction. Most of the currently used anti-cancer drugs perturb cancer cells either by inhibiting or by disrupting cell cycle related events including checkpoint activation, arrest cells and induce apoptosis (Chan et al., 2012; Senese et al., 2014; Wenzel and Singh, 2018; Mills et al., 2018). In this context, an analysis of the cell cycle phase-specific distribution of cancer cell populations treated with the different ZnONPs was carried out. The treated cancer cell population at various stages of cell cycle, permeabilized with 70 % ethanol and stained with propidium iodide, was subjected to DNA content quantification by flow cytometric analysis. FACS data representing the DNA profiles, showing the variations in percentage of cells in G₁, S and G₂/M phases with hypodiploid apoptotic cells represented by a sub G₁ population (Kajstura et al., 2007), are graphically represented as histograms. Fig. 4.25 and Table 4.6 show data pertaining to HCT 116 cells treated with AmRZnONPs, SpLZnONPs, MzLZnONPs and chemical cZnONPs. Exposure to the highest dose of phyto-derived AmRZnONPs and the chemically synthesized cZnONPs resulted in 5 and 3-fold increase in the apoptotic sub-G₁cell-fraction compared to that found in the untreated (control) cell population. On the other hand, treatment with SpL and MzL-derived ZnONPs within the 40 - 80 µg/mL dose range tested was found to induce G₂/M phase arrest in ~38 and 54 % cells respectively preventing entry into a new division cycle.

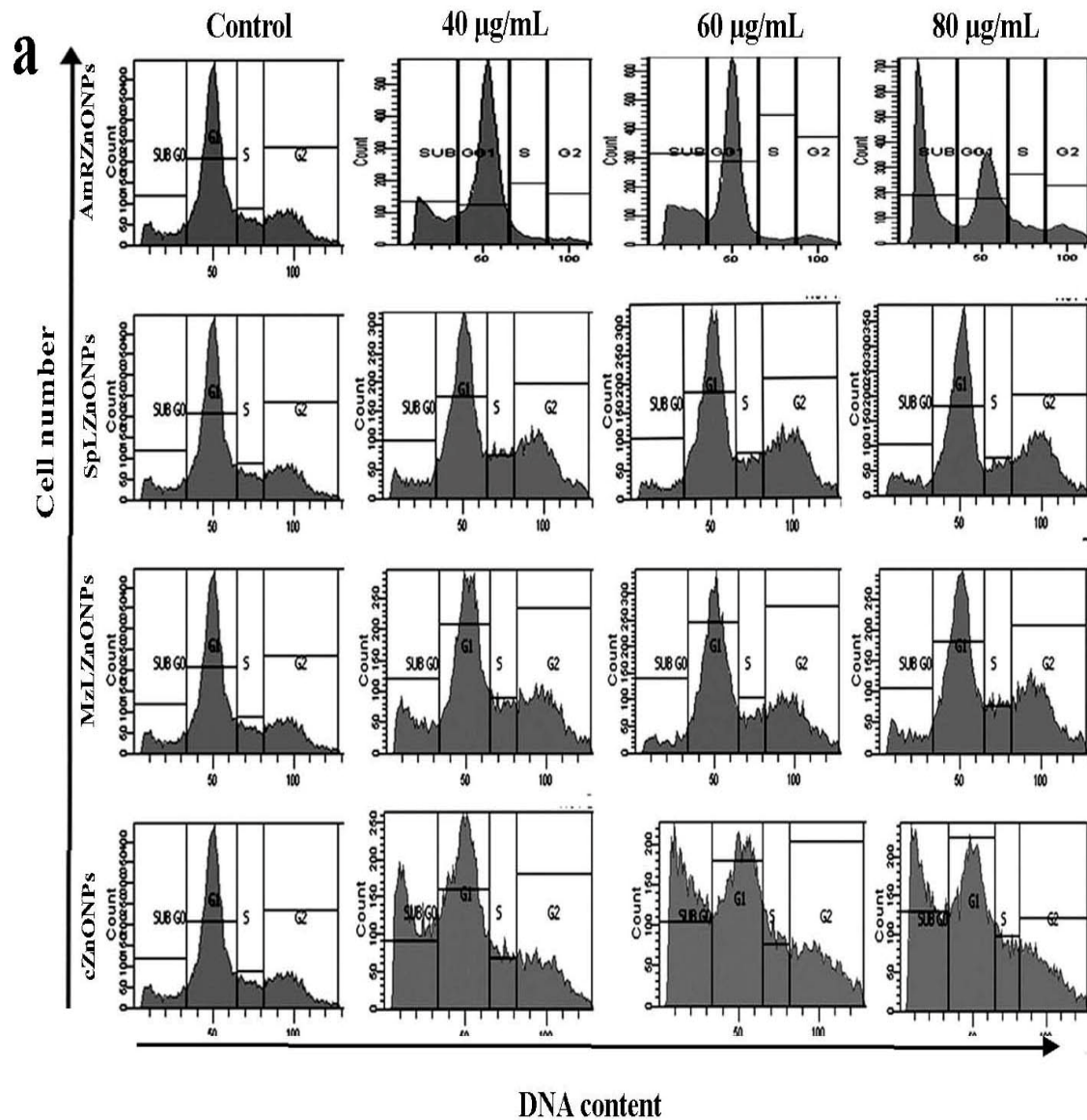


Fig. 4.25. Histograms showing cell cycle distribution of HCT 116 cells following 48 h treatment with phyto-derived / chemical ZnONPs

Table 4.6. Cell cycle phase-specific distribution of HCT 116 cells following 48 h treatment with phyto-derived/chemical ZnONPs

Types of ZnONPs	Concentration (µg/mL)	Sub G ₁ (%)	G ₀ /G ₁ (%)	S (%)	G ₂ /M (%)
Control (HCT 116)	0	9.0 ± 0.5	60.6 ± 1.2	20.6 ± 0.7	9.0 ± 1.3
AmRZnONPs	40	21.1±0.6	67.6±2.5	5.6±1.0	3.4±1.4
	60	24.5±1.5	63.3±1.6	4.0±0.5	5.0±1.3
	80	42.5±0.5	35.2±1.8	9.9±1.5	9.1±1.6
SpLZnONPs	40	8.2 ± 0.3	50.8 ± 0.5	12.1 ± 0.4	28.9 ± 0.7
	60	7.7±1.1	52.1±1.4	9.5±2.2	30.6±0.9
	80	6.0±2.4	51.6±1.3	10.7±2.5	31.7±0.8
MzLZnONPs	40	12.0±2.3	47.7 ±0.5	26.8±1.3	13.4±0.5
	60	6.3±1.8	48.5±0.5	12.5±1.7	28.8±0.5
	80	8.4±1.4	53.7±1.5	11.1±2.0	30.6±0.5
cZnONPs	40	27.9±0.7	44.6±1.9	10.1±1.0	17.4±1.0
	60	31.2±0.6	38.3±2.7	11.7±0.9	18.8±1.6
	80	32.4±0.2	38.4±2.5	11.5±0.8	17.6±0.7

Values given in blue colour denote the highest percentage of cells at a given phase of the cell cycle. Values represent mean ± S.D. of three experiments; $p < 0.05$.

The cell cycle distribution pattern of A549 cells treated with zinc oxide nanoparticles showed arrest in multiple phases of cell progression (Fig. 4.26, Table 4.7). Treatment with phyto-derived and commercial ZnONPs resulted in a dose-dependent increase in cell fractions undergoing S-phase and sub-G₁ sub population. An increase in G₂/M arrest in comparison to the control cell population was observed in treated A549 cells. AmRZnONP treated cells displayed 2-fold increase in the number cells found in S and a 3-fold increase in cells undergoing G₂/M transition without any increase in the percentage of apoptotic cells. In cells treated with MzLZnONPs and cZnONPs, at a concentration above IC₅₀ value, a 3 - 4 fold increase in the apoptotic cell population was observed whereas the latter nanoparticle type was also found to induce arrest in S and G₂/M phase. SpLZnONP-treatment induced maximal G₂/M arrest in cells, which was about 4-folds higher than that found in the untreated control cell population besides inducing a 3-fold increase in the percentage of A549 cells at the S and sub-G₁ phase. Hence, both types of ZnONPs were found to induce cell cycle arrest in the DNA synthetic and the G₂/M phases concomitant with induction of apoptosis in a sub-population of cells.

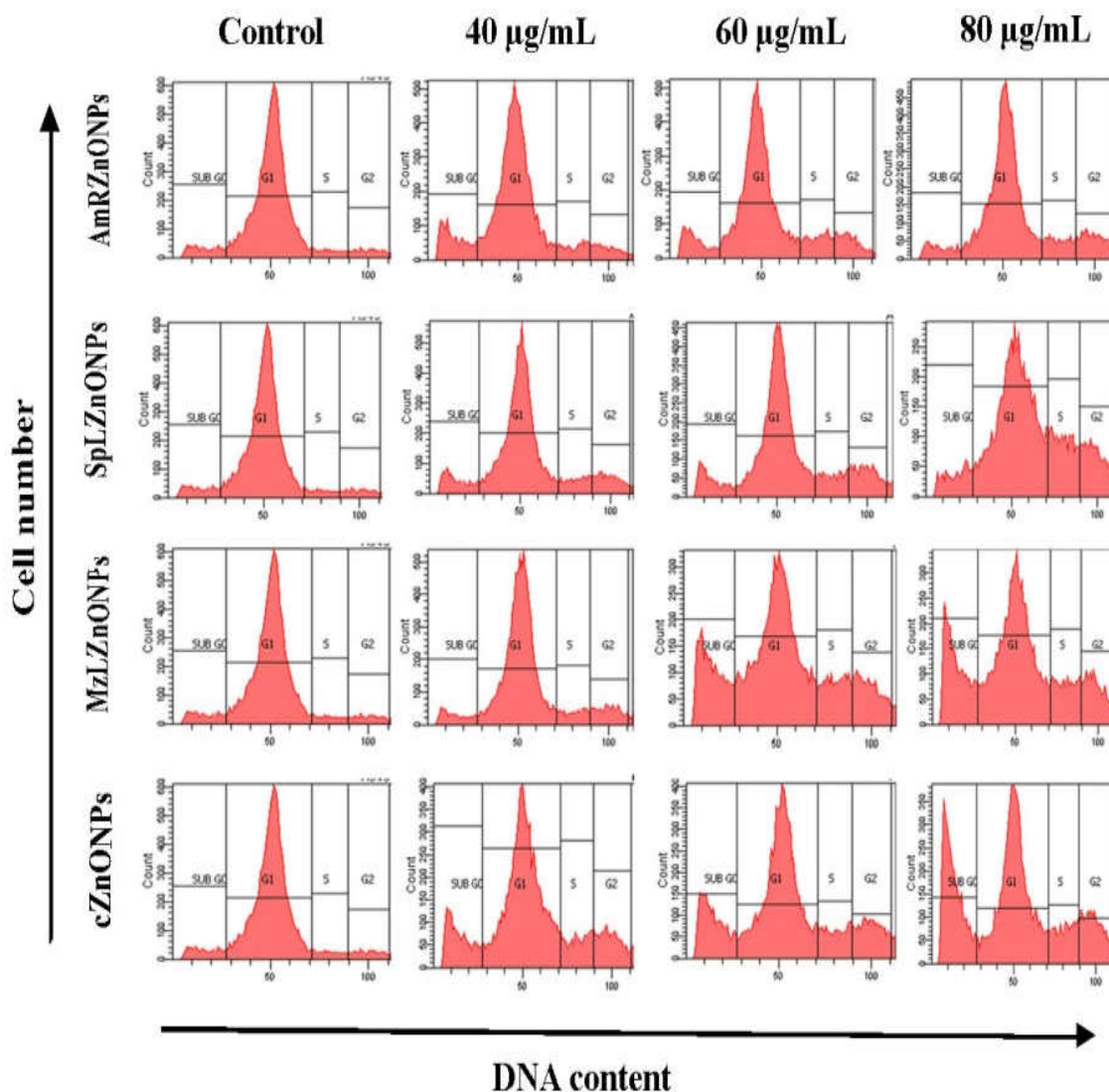


Fig. 4.26. Histograms showing cell cycle distribution of A549 cells following 48 h of treatment with phyto-derived / chemical ZnONPs

ZnONPs-induced G₂/M arrest has been reported recently in human epidermal keratinocytes, HaCaT cells, breast cancer cell lines and human tenon fibroblasts (Gao et al., 2016; Sanad et al., 2018; Vallabani et al., 2019; Yin et al., 2019). Yeast-derived ZnO nanoparticles have also been reported to induce S phase arrest and increase in apoptotic sub-G1 population in MCF-7 (breast cancer) cells (Moghaddam et al., 2017). A natural flavonoid, biochanin A-induced S-phase arrest and apoptosis was reported recently in A549 lung cancer cells by Li et al. (2018). Biogenic gold nanoparticle-induced arrest of A549 cells in multiple phases was also reported recently (Ramalingam et al., 2016)

Table 4.7. Cell cycle phase-specific distribution of A549 cells cycle following 48 h of treatment with phyto-derived/chemical ZnONPs

Types of ZnONPs	Concentration (µg/mL)	Sub G ₁ (%)	G ₀ /G ₁ (%)	S (%)	G ₂ /M (%)
Control (A549)	0	6.5±0.1	83.6±0.4	4.1±1.3	4.7±0.9
AmRZnONPs	40	12.6±0.5	73.7±1.2	6.3±0.9	6.1±0.7
	60	9.8±1.1	70.4±1.5	9.6±1.4	9.2±0.9
	80	6.2±1.5	70.7±1.8	8.9±0.2	11.9±0.9
SpLZnONPs	40	8.9±0.4	72.2±0.8	7.6±0.8	9.7±0.4
	60	9.1±1.7	66.1±0.8	9.5±0.6	12.8±0.5
	80	13.2±2.5	57.4±0.7	11.3±0.4	15.3±0.1
MzLZnONPs	40	6.0±0.5	76.5±1.0	6.7±1.4	9.1±1.0
	60	18.5±1.4	54.8±1.3	11.9±1.1	11.5±0.3
	80	21.1±0.7	52.9±1.5	11.9±0.3	11.8±0.4
cZnONPs	40	13.5±1.5	61.5±2.0	9.8±0.5	11.7±0.6
	60	17.2±0.9	9.8±1.9	9.8±0.5	13.1±0.6
	80	26.4±0.3	11.7±0.5	10.2±0.2	13.1±1.0

Values given in blue colour denote the highest percentage of cells at a given phase of the cell cycle. Values represent mean ± S.D. of three experiments; $p < 0.05$

K562 cells exposed to all the three phyto-derived nanoparticles for 48 h displayed a dose-dependent increase in the percentage of apoptotic sub-G₁ cell population (Fig. 4.27, Table 4.8). These leukemic cells on exposure to AmRZnONPs displayed a 5-fold increase in the number of apoptotic sub-G₁ cells with a 2-fold hike in G₂/M cells when treated at a concentration above IC₅₀ value. Cells treated with SpL and MzL-derived particles exhibited 4-fold and 3-fold increase in apoptotic cell fraction respectively. Interestingly, the overall results derived from FACS data revealed that the cellular effects of each type of nanoparticle were distinctive with respect to all cell cycle phases except G₁. Patel et al. (2016) reported that the uptake of ZnONPs by A431 cells was reduced in G₀/G₁ phase but was found to be highest during G₂/M phase followed by S phase, an observation which is in agreement with the results discussed above. Well known chemotherapeutic agents such as docetaxal and paclitaxel were also reported to arrest cells in G₂/M phase (Hernández-Vargas, 2007; Han and Lee, 2016) lending credence to the drug potential of phyto-derived ZnONPs generated in the present study.

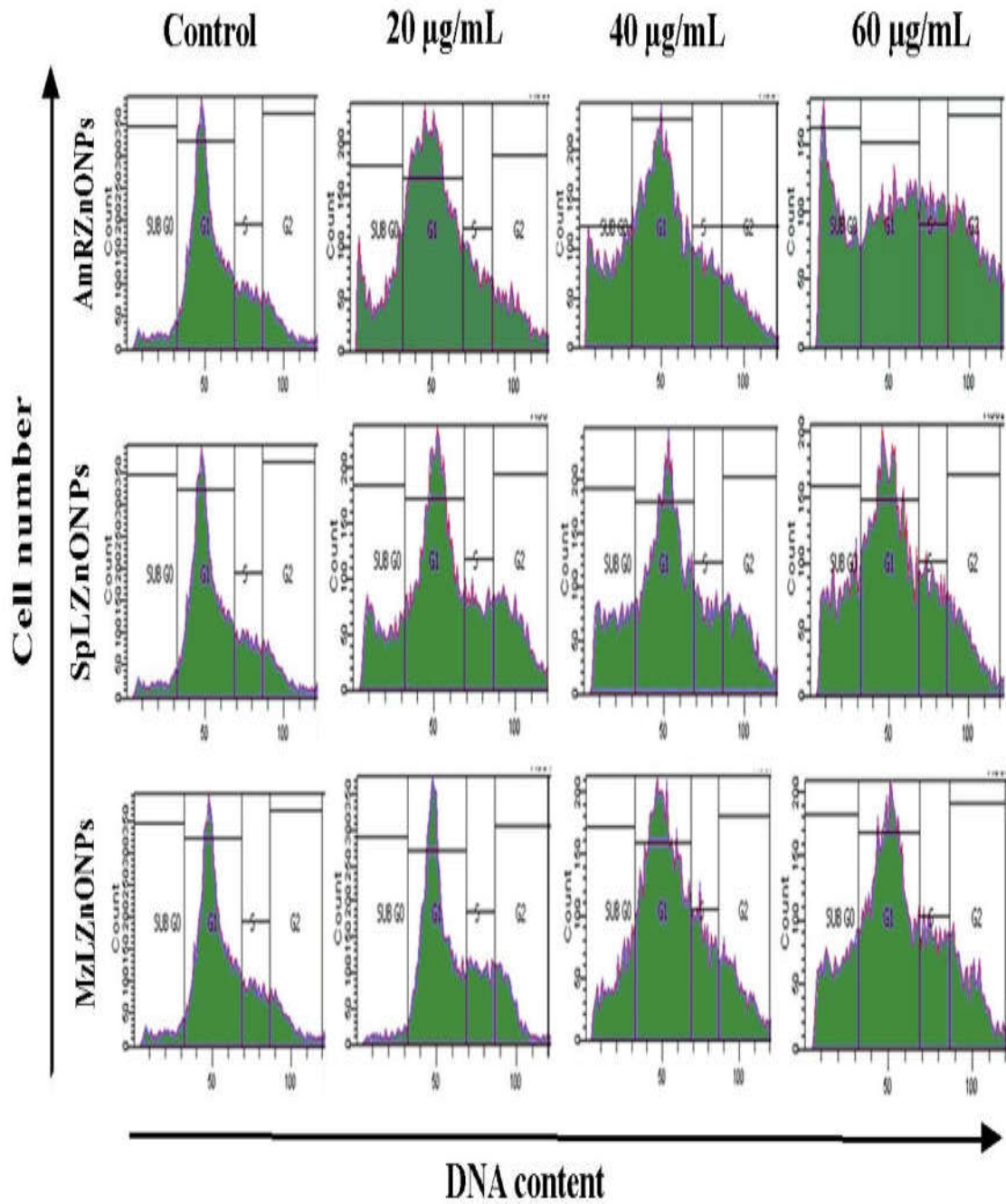


Fig. 4.27. Histograms showing cell cycle distribution of K562 cells following 48 h of treatment with phyto-derived ZnONPs

Table 4.8. Cell cycle phase-specific distribution of K562 cells following 48 h of treatment with phyto-derived ZnONPs

Types of ZnONPs	Concentration (µg/mL)	Sub G ₁ (%)	G ₀ /G ₁ (%)	S (%)	G ₂ /M (%)
Control (K562)	0	5.7±0.2	65.1±0.5	15.5±0.4	12.2±0.3
AmRZnONPs	40	16.2±0.4	57.3±0.1	13.2±0.5	11.5±1.1
	60	22.1±0.3	51.3±0.3	13.4±0.5	11.8±0.7
	80	23.7±0.7	31.5±0.2	15.7±0.5	22.4±0.5
SpLZnONPs	40	15.0±0.4	49.7±1.2	14.1±1.2	18.6±0.3
	60	17.8±0.5	48.9±1.5	13.9±1.3	17.0±0.5
	80	20.7±0.9	49.8±0.9	15.1±0.6	13.1±0.5
MzLZnONPs	40	3.4±0.3	60.8±0.3	18.6±0.1	15.8±0.3
	60	13.8±0.6	55.4±0.8	15.6±0.4	13.7±0.6
	80	17.4±0.5	49.1±1.0	15.8±0.3	15.6±0.7

Values given in blue colour denote the highest percentage of cells at a given phase of the cell cycle. Values represent mean ± S.D. of three experiments; $p < 0.05$

4.5.6.2 Effect of ZnONPs on phosphatidyl serine externalization

One of the hallmarks of cellular apoptosis is an early translocation of inner phosphatidylserine (PS) to the outer leaflet of the cell membrane, which flags the cells for clearance by phagocytosis (Birge et al., 2016). The cellular protein, annexin V binds to externalized PS with high affinity in the presence of calcium ions. For detection, Annexin V tagged with green fluorescent dye Alexa® Fluor 488 was used along with propidium iodide (PI) staining. Dead cells with increased membrane permeability allow entry of propidium iodide which fluoresces red when bound to DNA (Namvar et al., 2015).

All the three cancer cell types, treated with phyto-derived and chemical ZnONPs, showed dose-dependent increase in annexin V positive apoptotic cells emanating green fluorescence. Fig. 4.28 summarizes the results obtained following staining with annexin V/PI, wherein the percentage of fluorescing HCT 116 cells treated with ZnONPs is included. An overwhelming induction of apoptosis was detected in ~97 % cells exposed to SpLZnONPs the highest concentration (80 µg/mL) tested, in comparison with ~32 % of apoptotic cells following treatment with AmRZnONPs and MzLZnONPs. Notably, the percentage of apoptotic cells was found to be the lowest, at ~26 %, following treatment with the commercial cZnONPs.

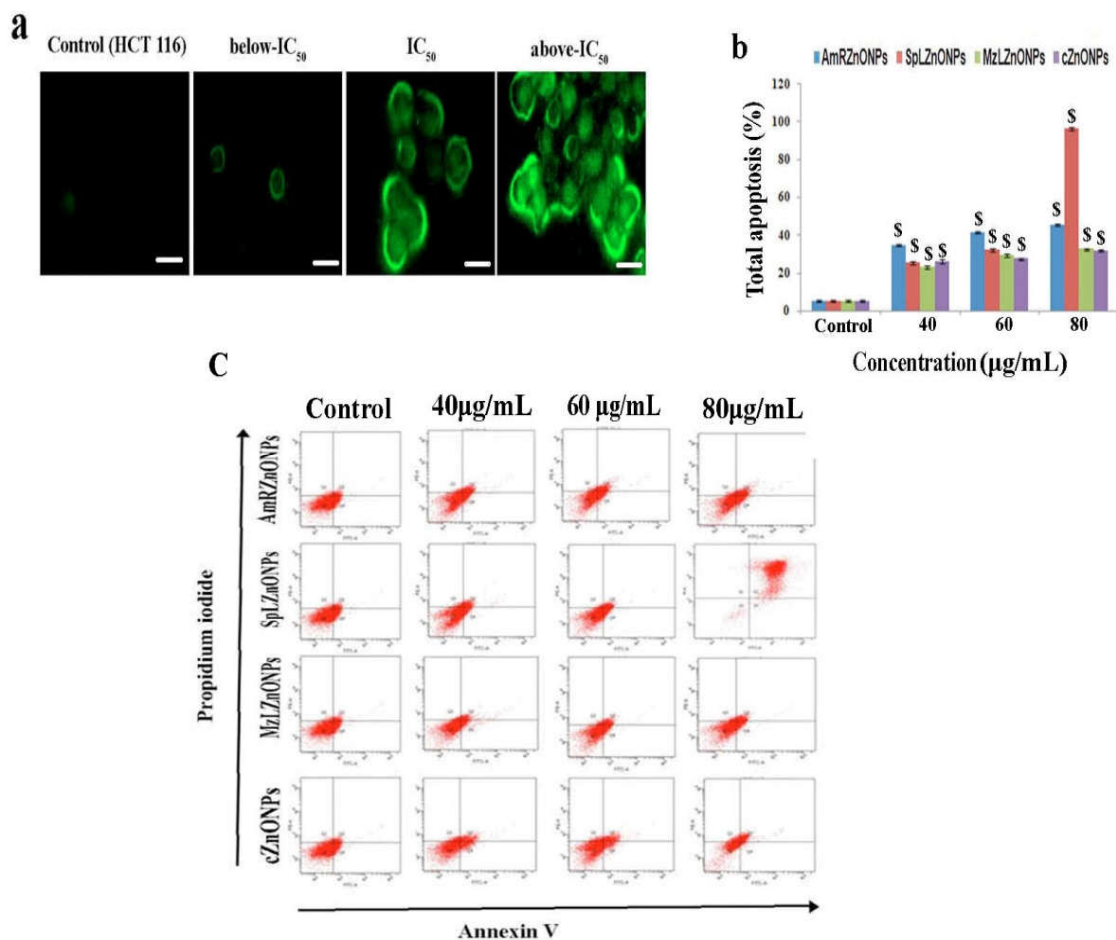


Fig. 4.28. Apoptogenic effect of phyto-derived /chemical ZnONPs on HCT 116 cells after 48 h treatment and stained with annexin V / PI (a) Representative fluorescence microscopic images of cells exposed to all ZnONP types (b) quantitative analysis of total apoptotic cells and (c) flow cytometric analysis of cells. Scale bars represent 20µm. ^S*p* ≤ 0.001

A549 cells treated with AmRZnONPs and cZnONPs at the IC₅₀ concentration of 60 µg/mL, were found to display apoptosis in a staggering majority of cells (~97 %) with the lowest percentage of ~16 % apoptosis found in the cell population exposed to MzLZnONPs (Fig.4.29). A dose-dependent increase in the number of apoptotic cells was found in leukemic K562 cells treated with phyto-derived particles with the highest induction at ~ 76 % observed on exposure to SpLZnONPs followed by incidence of ~60 % and ~34 % on exposure to MzLZnONPs and AmRZnONPs respectively (Fig.4.30). The results are in line with several recent reports on the action of biosynthesized ZnONPs (Sanaeimehr et al., 2018) as well as chemically derived ZnO

particles against various cell types (Ryu et al., 2014; Kim et al., 2015; Jain et al., 2019; Vallabani et al., 2019).

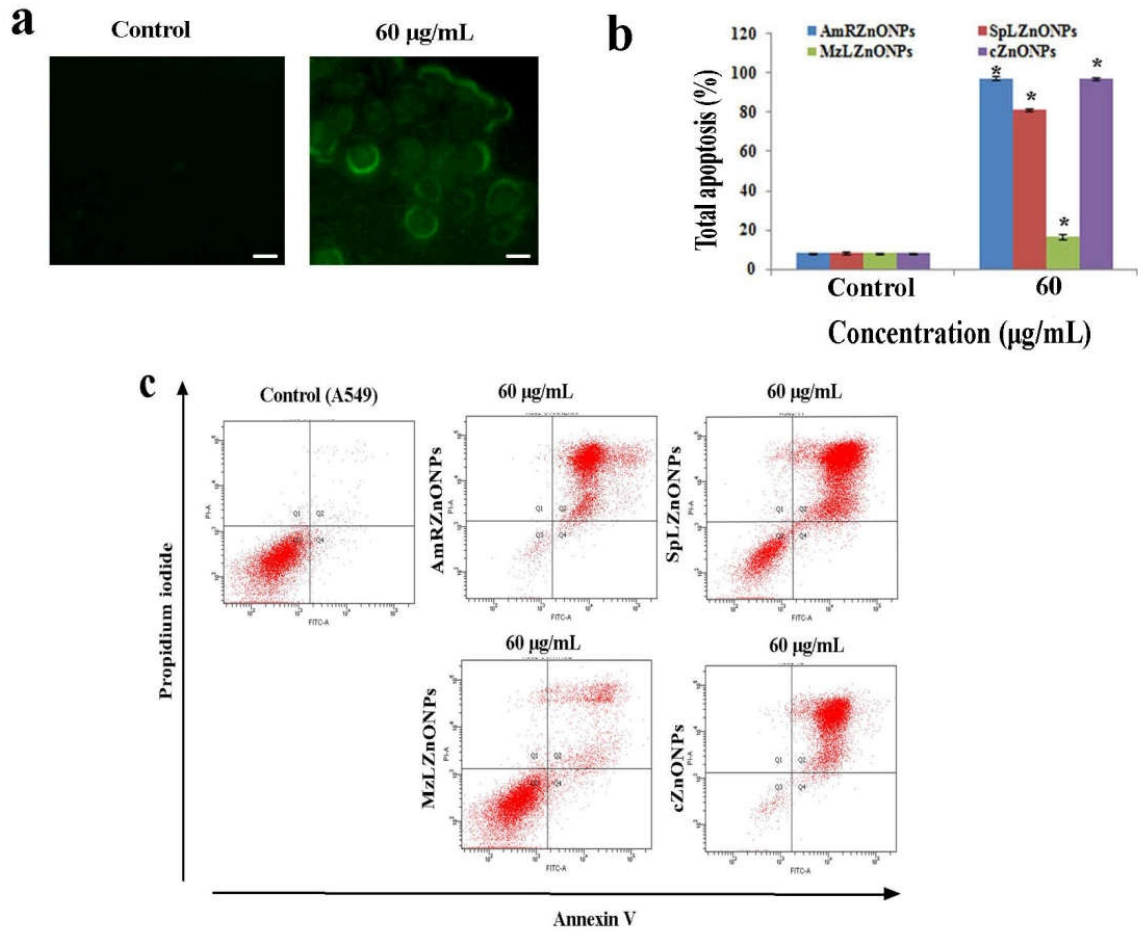


Fig. 4.29. Apoptogenic effect of phyto-derived /chemical ZnONPs on A549 cells after 48 h of treatment at IC_{50} concentration and stained with annexin V / PI (a) Representative fluorescence microscopic images of A549 cells exposed to all ZnONP types (b) quantitative analysis of total apoptotic cells and (c) flow cytometric analysis of cells. Scale bars represent $20\mu\text{m}$. * $p \leq 0.05$

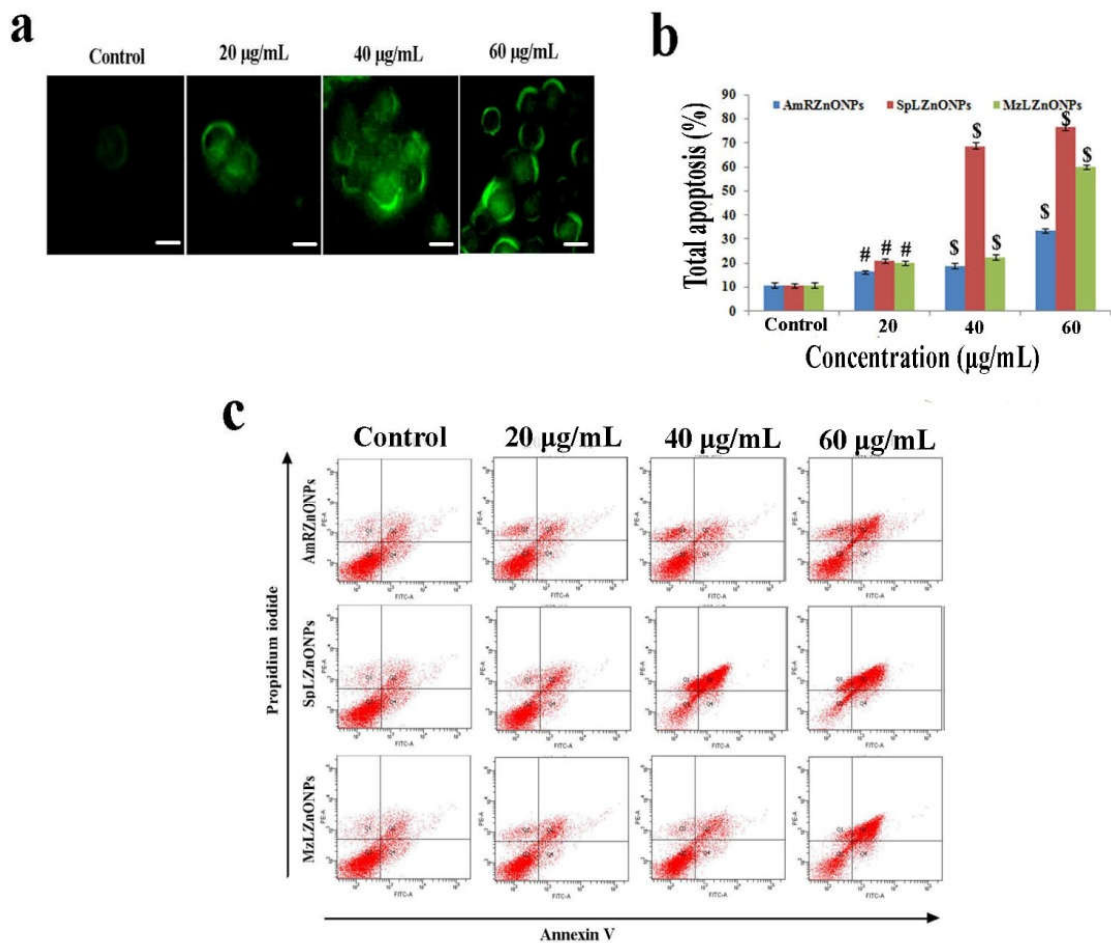


Fig. 4.30. Apoptogenic effect of phyto-derived ZnONPs on K562 cells after 48 h treatment and stained with annexin V/PI (a) Representative fluorescence microscopic images of K562 cells exposed to all ZnONP types (b) quantitative analysis of total apoptotic cells and (c) flow cytometric analysis of cells. Scale bars represent 20µm. # $p \leq 0.01$, \$ $p \leq 0.001$.

4.5.7. Genotoxic effects of phyto-derived/chemical ZnONPs

4.5.7.1. Comet assay

This ‘single cell gel electrophoresis’ assay is a sensitive method to determine DNA damage at the level of individual cells. When subjected to an electric field, the cell harbouring a damaged genome displays single strand breaks/fragments in DNA migrating out of the nucleus as a ‘comet tail’ oriented towards anode. The extent of DNA migration depends directly on the amount of cellular DNA damage (Kumaravel et al., 2009). Increases in comet tail length were observed in a dose-dependent manner in

HCT 116 and K562 cells, following treatment with ZnONPs, indicating the genotoxic effect of nanoparticles. However, A549 cells, treated with both types of ZnONPs, failed to display any comet tails. In HCT 116 cells treated with SpLZnONPs, the extent of DNA damage was apparently higher than that elicited by cZnONPs treatment (Fig.4.31a). In the case of K562 cells, exposure to all the three biogenic nanoparticle types induced relatively prominent comets in a concentration dependent manner (Fig. 4.31b). A similar observation of extensive DNA damage caused by *Marsdenia tenacissima*-derived ZnONPs in laryngeal Hep-2 cancer cells has been recently reported (Wang et al., 2019).

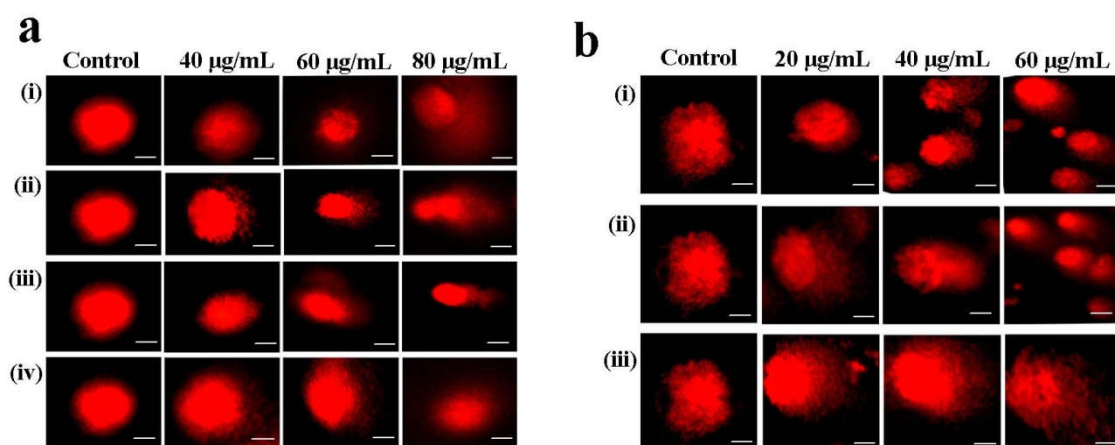


Fig. 4.31. Alkaline comet assay: Detection of DNA strand breaks following treatment with (i) AmRZnONPs (ii) SpLZnONPs (iii) MzLZnONPs and (iv) cZnONPs on (a) HCT 116 cells and (b) K562 cells. Scale bar represents 5 µm.

4.5.7.2. DNA fragmentation

DNA extracted from HCT 116, A549 and K562 cells, treated with ZnONPs, were electrophoresed and visualized under UV light after ethidium bromide staining. In cells undergoing apoptosis/necroptosis, DNA is cleaved by an endonuclease - caspase-activated DNase (CAD) - at internucleosomal linker sites that fragments the chromatin into nucleosomal units of 180 – 200 bp oligomers (Matassov et al., 2004; Larsen and Sorensen, 2016). Appearance of such ‘nucleosomal ladders’ were observed in DNA isolated from treated colon and leukemic cells (Fig. 4.32). It was interesting to note that ZnONP-treated A549 cells failed to display DNA fragmentation very similar

to the lack of induction of comet tails in these cells as mentioned earlier. The electrophoresed DNA, isolated from HCT 116 cells treated with SpLZnONPs, showed a higher intensity band at 500 bp position. Such a disparity in the band intensity was also observed at 700 bp positions in the DNA obtained from colon cells exposed to AmR and MzL-derived particles (Fig. 4.32a). The DNA ladders obtained from HCT 116 cells treated with chemically derived cZnONPs were observed to be bereft of such high intensity bands. DNA laddering was observed to be well defined in the case of SpLZnONPs and MzLZnONP- treated K562 cells (Fig.4.32 b). Notably, along with the DNA laddering, a background smear indicative of non-specific DNA degradation was also evident on the gels. Likewise, DNA isolated from shikonin-induced glioma cells were also found to produce a smear as reported recently by Ding et al. (2019) attributing it to a process of necroptosis triggered by chromatinolysis. Interestingly, DNA isolated from tanshinone A treated Hep G₂ cells were also reported to display both laddering and smearing on agarose gels suggestive of the co-occurrence of apoptosis and necroptosis (Lin et al., 2016). In yet another latest report, Yousef et al. (2019) discusses on the mixed pattern of smearing and laddering of DNA. This observation relates to DNA isolated from rat liver and kidney tissues exposed to ZnONPs resulting in non-specific degradation and inter-nucleosomal cleavage. Necrotic DNA degradation is thought to be a later event following injury / rupture of cells leading to proteolytic digestion of chromatin proteins including histones thereby exposing DNA to endonucleases. ZnONP-induced genotoxic effects on cultured macrophages isolated from mouse as well as on brain tissue of rat have been recently reported (Pati et al., 2016; Attia et al., 2018). Oral squamous carcinoma cells treated with adrenergic agonists have also been found to display DNA smearing following necrotic cell death (Uchida et al., 2019).

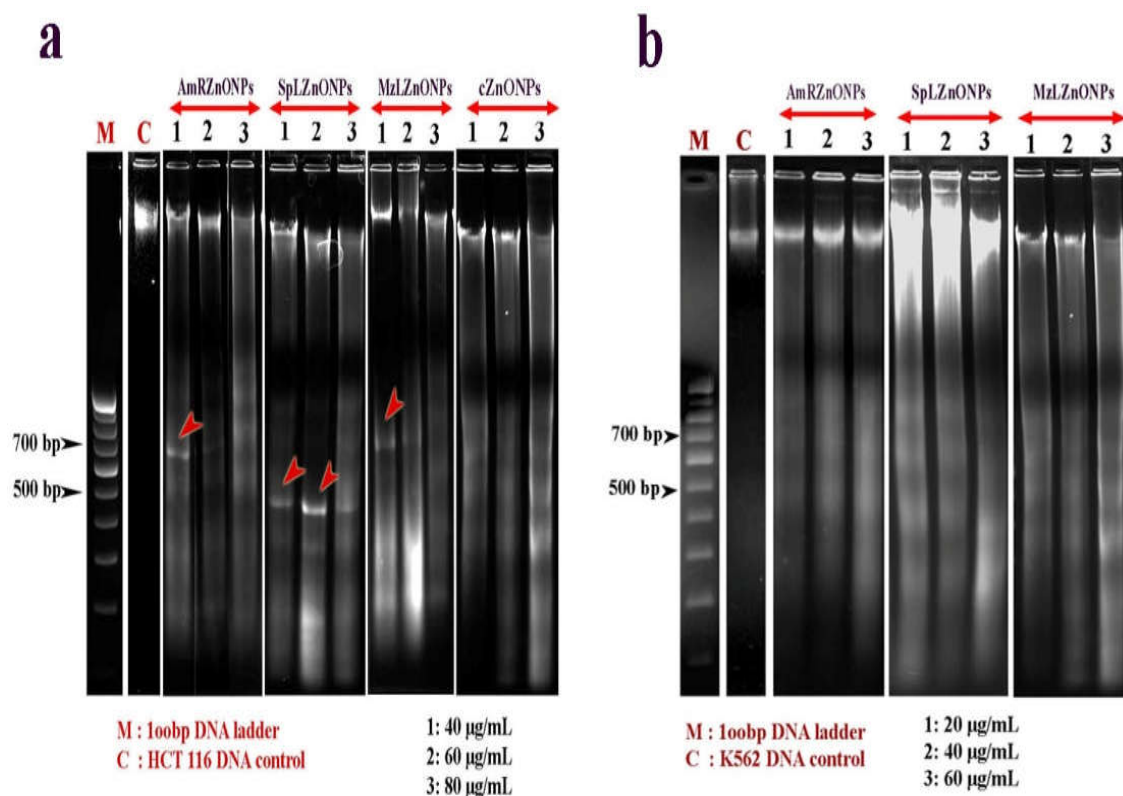


Fig. 4.32. Analysis of DNA fragmentation induced by phyto-derived / chemical ZnONPs in HCT 116 and K562 cells. Red arrow heads denote bands with higher intensity.

4.5.8. Gene expression analysis by Reverse Transcription-quantitative polymerase chain reaction (RT- qPCR).

RT-qPCR is a rapid, sensitive and robust method of gene expression profiling capable of quantifying mRNA levels to study differentially expressed genes (Amatori et al., 2017). Cells undergo apoptosis through two major pathways, the death receptor extrinsic pathway or the mitochondrial intrinsic pathway. Apoptosis is interplay between a set of various pro- and anti-apoptotic molecules as detailed in section 2.5.2. Hence, a selection of eight pro-apoptotic [caspase-8, caspase-9, caspase-3, cytochrome *c* (Cyt *c*), DNA repair enzyme Poly(ADP-ribose) polymerase (PARP), tumour suppressor gene - p53, p53-upregulated modulator of apoptosis (PUMA) and Bax] and two anti-apoptotic (Bcl-2 and survivin) genes were taken up for assessment. ZnONP-induced changes in the transcription levels of the above-mentioned genes, expressed as fold-changes relative to that of the housekeeping gene, GAPDH, has been

determined individually and tabulated for all the three cell types studied (Tables 4.9 – 4.11). The transcriptional variations beyond 3 folds of the values computed for the control gene have been considered for analysis.

In HCT 116 cells, maximum number of pro-apoptotic genes (6 out of 8) were upregulated on treatment with SpLZnONPs followed by AMRZnONPs (4 out of 8) and MzLZnONPs (3 out of 8) (Table 4.9). Notably, the lowest number was recorded with the use of chemically derived cZnONPs upregulating only 2 out of the 8 genes assessed. Although the highest upregulation by 24-folds was observed in the case of the executioner caspase-3, the *Cyt c* transcription was found to be consistently upregulated by treatment with all categories of ZnONPs including the chemical version. Incidentally, treatment with all particle types elicited a minimal downregulation of the two anti-apoptotic genes assessed; control cZnONPs were found to induce maximal downregulation of both Bcl-2 (19-folds) and survivin (8-folds) genes. However, the highest downregulation of Bcl-2 gene transcription (23-folds) was observed following treatment with SpLZnONPs.

In the case of A549 and K562 cells, phyto-derived ZnONP treatment resulted in upregulation of *Cyt c* (Table 4.10 and 4.11) as observed above in colorectal cells. Interestingly, exposure to SpLZnONPs resulted in maximal expression of pro-apoptotic genes (7 out of 8) in these two cell lines. Again, in both cell types, the highest transcriptional hike was observed in the case of caspase-3 gene. In A549 cells, treatment with biogenic and chemical ZnONPs showed increased expression of PARP but phyto-derived ZnONPs induced transcriptional upregulation of caspase-8. However, in K562 cells, treatments with all ZnONP types failed to express p53 and PUMA genes. A minimal downregulation of anti-apoptotic genes was found in ZnONP-treated A549 and K562 cells; the latter cell type also displayed the highest inhibition of survivin expression by ~4 folds when treated with MzLZnONPs. Incidentally, a similar depression of survivin expression has been previously reported by Tomicic et al. (2010) in p53 null cells undergoing mitochondrial apoptosis.

Table 4.9. The relative quantitation of mRNA expression of apoptosis-related genes using RT-qPCR in HCT 116 cells treated with phyto-derived/chemical ZnONPs

Fold Changes in mRNA expression											
ZnONPs	Conc. (µg/mL)	Pro-apoptotic genes								Anti-apoptotic genes	
		p53	PUMA	Bax	Cyt <i>c</i>	Cas-9	Cas-8	Cas-3	PARP	Bcl-2	Survivin
AmRZnONPs	40	0.5±0.1	1.35±0.20	1.1±0.2	2.3±0.2	3.2±1.6	1.3±0.64	0.6±0.3	1.8±.9	1.8±.7	1.7±0.6
	60	0.85±0.3	2.10±0.32	1.8±0.6	3.1±0.3	4.7±0.8	1.5±0.75	0.8±0.4	2.2±1.0	1.9±0.4	1.8±0.53
	80	1.30±0.2	3.80±0.50	2.1±0.9	3.8±0.4	4.9±0.9	1.7±1.0	1.6±0.7	3.3±1.0	2±0.32	1.8±0.4
SpLZnONPs	40	1.32±0.75	2.94±0.62	1.14±0.3	3.8±1.0	1.8±0.2	2.3±1.1	5.4±2.1	2±1.2	10.5±.9	0.63±0.2
	60	2.63±0.9	5.89±0.22	4.05±1.2	8.8±1.1	3.1±0.7	2.3±0.8	23.5±.8	5.8±.3	23.4±.4	1.08±0.6
	80	2.80±1.0	9.58±1.31	7.36±0.4	8.9±0.5	4.0±2.2	2.3±1.2	24.1±.1	6.7±.4	4.9±.2	1.9±0.54
MzLZnONPs	40	0.93±0.2	1.32±0.32	1.7±0.5	0.5±0.4	0.9±0.1	1.3±0.1	3.8±0.5	1.4±.2	0.66±.22	0.6±0.1
	60	1.30±0.21	1.91±0.56	2.8±0.32	1.7±0.4	1.7±0.3	1.5±0.1	7.2±0.2	1.9±.7	1.2±.0.5	0.5±0.1
	80	1.80±0.33	2.30±0.72	3.6±0.41	3.1±0.4	2.9±0.1	1.5±0.1	13.5±1	2.5±.6	1.4±0.5	0.5±0.1
cZnONPs	40	1.20±0.12	1.30±0.32	0.32±0.2	3.8±0.5	0.9±0.3	0.54±0.4	1.8±0.7	6.1±1	8.5±.9	6.4±0.31
	60	1.50±0.15	1.50±0.18	0.86±0.5	4.3±0.6	0.95±0.1	0.75±0.3	1.8±0.1	7.7±.5	19.4±.4	8.4±0.52
	80	2.20±0.23	2.00±0.45	0.92±0.7	4.5±0.2	0.95±0.3	0.75±0.4	2.2±0.4	8.2±.4	6.4±.2	8.4±1.2

Values are expressed as mean ± S.D. $p < 0.05$. Green boxes indicate downregulation of gene expression and boxes devoid of colour represent upregulation. Highest folds of up/down regulated gene expressions are indicated in bold numbers

Table 4.10. The relative quantitation of mRNA expression of apoptosis-related genes using RT-qPCR in A549 cells treated with phyto-derived / chemical ZnONPs

Fold changes in mRNA expression											
ZnONPs	Conc. (µg/mL)	Pro-apoptotic genes								Anti-apoptotic genes	
		p53	PUMA	Bax	Cyt c	Cas-9	Cas-8	Cas-3	PARP	Bcl-2	Survivin
AmRZnONPs	40	0.61±0.2	1.3±0.1	0.5±0.2	2.45±0.7	1.2±0.5	2.3±0.45	0.55±0.3	2.6±1.2	1.25±0.6	1.8±0.3
	60	0.8±0.2	1.0±0.00	0.9±0.1	3.5±1.1	1.3±0.2	2.8±0.32	0.75±0.0	3.2±0.9	1.5±0.3	2.1±0.4
	80	1.0±0.12	0.9±0.1	0.9±0.0	5.0±1.2	1.3±0.2	3.5±0.12	2.5±0.2	3.8±1.0	1.54±0.2	2.3±0.6
SpLZnONPs	40	2.12±0.31	2.24±0.62	1.20±0.5	3.15±0.9	2.49±0.7	3.12±0.2	4.13±0.7	3.8±1.3	1.2±0.2	0.92±0.1
	60	3.14±0.51	5.60±1.5	3.24±0.33	7.39±1.5	2.58±0.2	4.13±0.11	5.25±0.6	4.6±0.8	1.3±0.5	0.95±0
	80	4.12±0.85	7.4±1.3	3.76±0.7	8.52±0.3	2.75±0.2	4.4±1.0	12.2±0.8	6.1±1.2	1.3±0.1	1.5±0.2
MzLZnONPs	40	1.62±0.3	1.9±0.2	1.8±0.2	2.2±1.0	1.95±0.4	1.5±0.34	1.0±0.2	1.8±0.4	0.56±0.1	1.5±0.6
	60	1.8±0.21	2.2±0.3	2.2±0.14	3.2±1.1	2.4±0.3	1.8±0.18	1.5±0.3	2.1±0.2	1.6±0.5	1.5±0.2
	80	2.2±0.3	3.9±0.7	2.4±0.1	3.8±0.5	3.8±0.1	3.2±0.15	3.6±0.1	3.4±0.5	2.1±0.4	1.9±0.1
cZnONPs	40	1.3±0.6	0.81±0.1	1.2±0.3	1.4±0.1	1.5±0.4	0.8±0.0	1.6±0.2	3.4±1.2	0.23±0.0	0.5±0.1
	60	2.5±0.3	0.67±0.3	1.8±0.4	1.7±0.5	2.6±1.1	1.2±0.3	1.9±0.3	4.8±0.6	0.89±0.2	1.1±0.34
	80	3.8±0.2	0.72±0.1	1.8±0.1	2.1±0.1	2.9±0.8	1.5±0.2	6.0±0.4	5.4±0.3	1.88±0.4	1.3±0.43

Values are expressed as mean ± S.D. p < 0.05. Green boxes indicate downregulation of gene expression and boxes devoid of colour represent upregulation. Highest folds of up/down regulated gene expressions are indicated in bold numbers

Table 4.11. The relative quantitation of mRNA expression of apoptosis-related genes using RT-qPCR in K562 cells treated with phyto-derived ZnONPs

Fold changes in mRNA expression									
ZnONPs	Conc. (µg/mL)	Pro-apoptotic genes						Anti-apoptotic genes	
		Cyt <i>c</i>	Cas-9	Cas-3	Cas-8	PARP	Bax	Bcl-2	Survivin
AmRZnONPs	20	2.1±0.3	0.75±0.3	0.95±0.1	-	1.8±0.4	0.78±0.0	0.31±0	1.1±0.2
	40	2.5±0.5	1.4±0.2	1.7±0.5	-	2.1±0.3	1.5±0.3	0.95±.1	1.3±0.3
	60	3.5±0.2	2.4±0.1	2.4±0.8	-	2.8±0.2	1.5±0.1	1.3±.2	1.9±0.1
SpLZnONPs	20	2.31±.8	9.18±1.2	17.5±1.2	1.23±.6	1.5±0.2	1.34±0.1	1.15±.5	2.62±0.2
	40	2.14±.4	8.51±.42	30±2.0	1.59±.2	1.5±0.5	2.34±.21	0.72±.9	2.6±0.5
	60	3.7±.21	8.5±0.66	30±1.5	1.65±.3	1.5±0.5	3.2±.42	0.72±.4	2.6±0.5
MzLZnONPs	20	2.2±1.2	4.5±0.3	1.5±0.8	1.23±.1	1.3±0.1	0.53±0.1	0.8±.1	1.8±0.42
	40	3.1±0.5	5.5±1.2	3.9±1.2	1.4±0.6	1.8±0.2	0.81±0.1	0.9±.6	3.8±0.3
	60	4.5±0.3	9.4±0.4	11.3±.9	1.3±0.4	2.8±0.3	0.9±0.1	0.9±0	3.85±0.2

Values are expressed as mean ± S.D. p < 0.05. Green boxes indicate downregulation of gene expression and boxes devoid of colour represent upregulation. Highest folds of up/down regulated gene expressions are indicated in bold numbers

Overall, transcript quantification revealed that biogenic ZnONPs treatment was found to be cytotoxic to HCT 116, A549 and K562 cells since it triggered mitochondrial apoptosis involving elevated expression of Cyt *c*, cas-9, and cas-3 in a dose-dependent manner. Briefly, the key events of the intrinsic apoptotic pathway comprise of release of mitochondrial cytochrome *c* to the cytosol, apoptosome formation and activation of caspase-9, processing of caspase-3 eventually leading to programmed cellular death (Jin and El-Deiry, 2005). It may be relevant to note here that several reports exist on biogenic and non-biogenic ZnONP-induced intrinsic apoptosis in various cell lines (Akhtar et al., 2012; Namvar et al., 2015; Kavithaa et al., 2016; Wang et al., 2018). A recent study by Katifelis et al. (2018) and Shaniba et al. (2019) have reported that apoptosis induction by silver nanoparticles in HCT 116 colon cells occurs via p53, Bax/Bcl-2, caspase pathway. ZnO nanorod induced apoptosis in A549 cells through ROS and oxidative stress via p53, survivin, bax/bcl-2 and caspase pathways was also reported by Ahmed et al., (2011). However, in the present study, apoptotic gene expressions in A549 cells treated with phyto-derived ZnONPs is indicative of the involvement of extrinsic pathway as evidenced by the significant upregulation in caspase-8 expression. It may be recalled that caspase-8 is activated by dimerization inside a death receptor complex, cleaved by auto-proteolysis and subsequently released into the cytosol. This fully processed form of caspase-8 is thought to cleave caspase-3, thereby inducing cell death (Beaudouin et al., 2013). Induction of apoptosis by these two pathways in A549 cells exposed to plant based cytotoxic agents has already been reported recently (Zhou et al., 2017; Lee et al., 2019). Finally, the effects of chemically derived commercial ZnONPs in the present study were found to be relatively insignificant when compared to the effects of biogenic ZnONPs on HCT 116 and A549 cells already mentioned earlier.

4.5.9. Protein expression analysis by western blotting

Profiling of protein expression by SDS-PAGE was carried out to confirm induction of apoptosis in the three cell types exposed to phyto-derived/chemical ZnONPs. Cytomorphological observations using light, fluorescence and electron microscopy along with flow cytometric and quantitative transcriptomic data analysis provided ample evidence of apoptosis induction in the above-mentioned cells. Hence, immunostaining was carried out using monoclonal antibodies against typical apoptosis-related proteins, namely, cleaved PARP, cleaved caspase-3, -8,

cytochrome *c* and cell cycle regulatory protein, cyclin B1. Increased expression of cytochrome *c*, cleaved caspase-3 and PARP in immunoblots of ZnONP-treated HCT 116 cells confirmed the induction of ROS-mediated mitochondrial apoptotic pathway (Fig.4.33). Dose-dependent downregulation of mitotic marker cyclin B1 observed in SpLZnONPs and MzLZnONPs (Fig. 4.33 b and c) treated colon cells corroborated well with the FACS data on cell cycle distribution including G₂/M arrest (sub-section 4.5.6.1). Cyclin B1 is known to play a crucial role in G₂/M transition and its decreased or near complete lack of expression provides a rationale to the potent antiproliferative efficacy of the particles observed in earlier experiments. Interestingly, the absence of the active form of caspase-8 (an initiator caspase of the extrinsic pathway) in colon cells, in line with the observed failure of amplification of the gene transcript, confirms occurrence of cellular death through the intrinsic pathway.

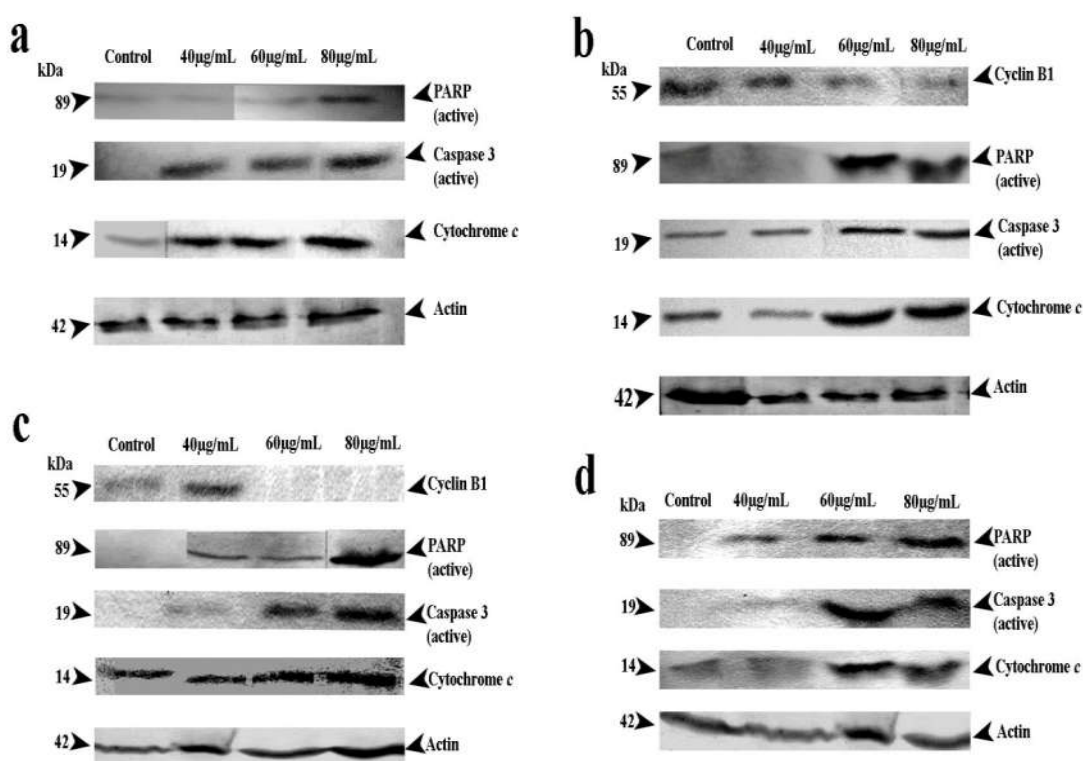


Fig. 4.33. Western blot analysis of apoptosis-related protein expression in HCT 116 cells following treatment with (a) AmRZnONPs (b) SpLZnONPs (c) MzLZnONPs and (d) cZnONPs

In the protein profile of A549 adenocarcinoma cells exposed to all particle types, a dose-dependent increase in the amount of cleaved PARP was observed (Fig. 4.34). A dose-dependent increment in the level of active caspase-8 was also evident in protein profiles obtained from cells treated with phyto-derived ZnONPs, thereby reconfirming involvement of the activated extrinsic apoptotic pathway as already observed and discussed during RT-qPCR analysis. Treatment with both types of ZnONPs caused decrease in cyclin B1 expression which thus provides a valid explanation to the FACS data showing G₂/M arrest. Incidentally, the failure of expression of cleaved caspase-3 and cytochrome *c* on the western blots, despite the observed presence of high levels of these gene transcripts (Section 4.5.8) could either be due to transcript or protein instability. Schwanhäusser et al. (2011) have also observed that the proteins involved in cellular homeostasis and defense responses may have stable mRNA and unstable proteins, which may be the reason for the absence of the concerned protein bands. Mathuram et al. (2016) attributes such a discrepancy between the relative mRNA and protein expression levels to degradation of apoptotic proteins.

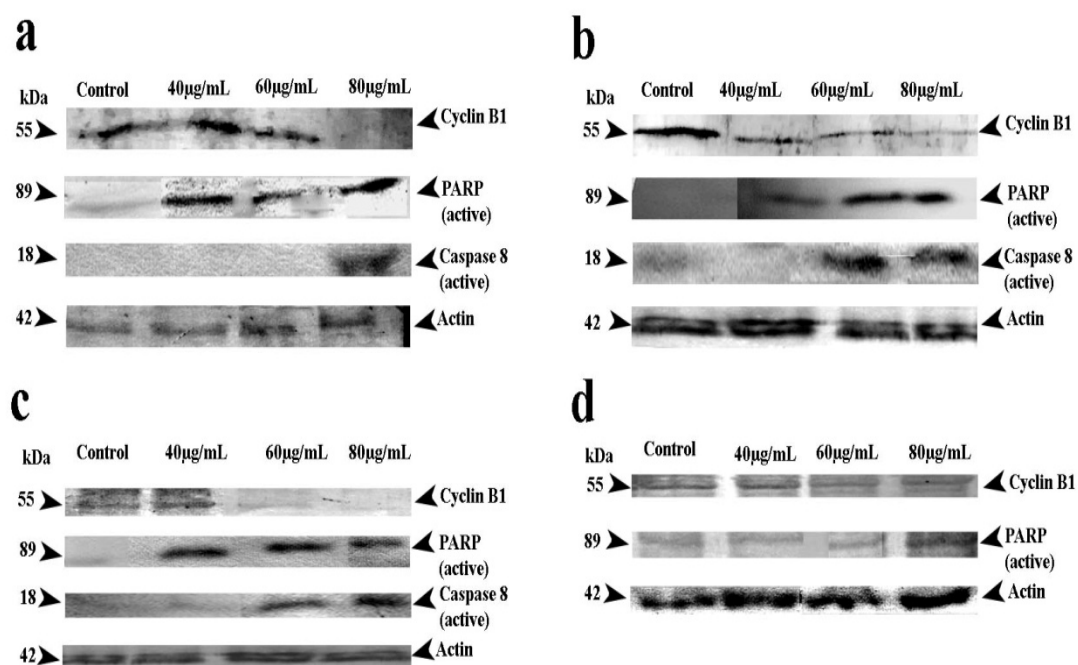


Fig. 4.34. Western blot analysis of apoptosis-related protein expression in A549 cells following treatment with (a) AmRZnONPs (b) SpLZnONPs (c) MzLZnONPs and (d) cZnONPs

Exposure of suspension cultures of K562 to ZnONPs resulted in dose-dependent increase in the expression of cytochrome *c*, cleaved caspase-3 and PARP (Fig. 4.35). These results also confirmed occurrence of cell death through mitochondrial pathway thereby lending credence to the conclusions drawn during the analyses of transcription (RT-qPCR) and cell cycle (FACS) data.

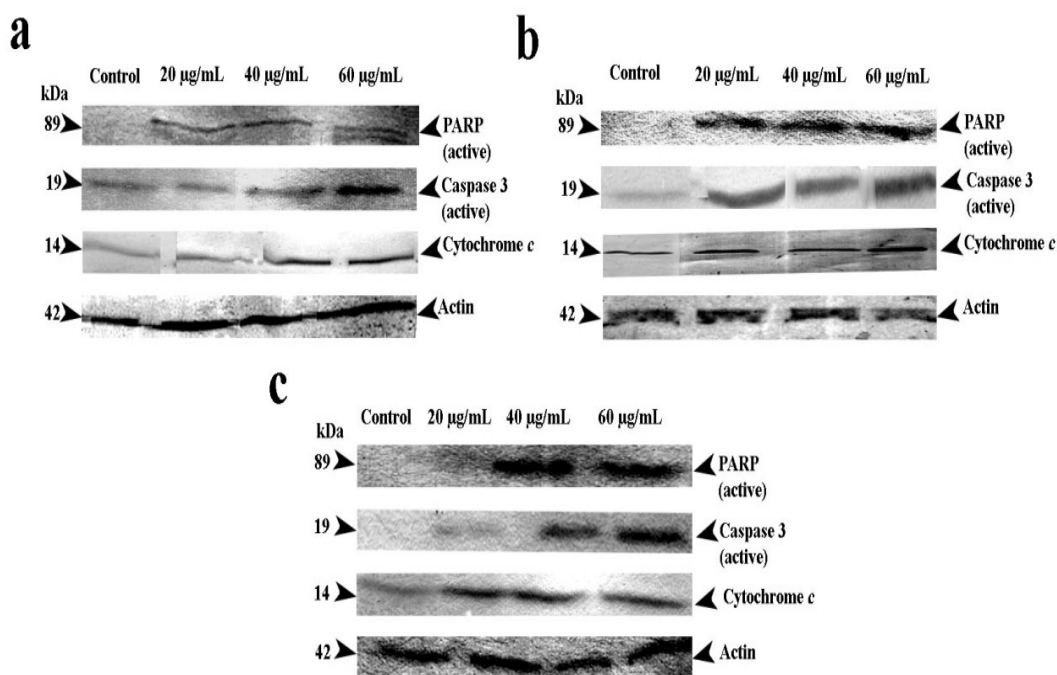


Fig. 4.35. Western blot analysis of apoptosis-related protein expression in K562 cells following treatment with (a) AmRZnONPs (b) SpLZnONPs and (c) MzLZnONPs

II. Evaluation of cytotoxicity / biocompatibility of the phyto-mediated and the chemically-derived ZnONPs employing normal human and plant cell models

4.5.10. Effect of ZnONPs on human peripheral blood derived lymphocytes (hPBLs) and erythrocytes

MTT assay: This assay was performed using hPBLs to evaluate the cytotoxicity of all of the five phyto-derived ZnONPs synthesized (Chapter 3) during the present study along with that of the commercial version of ZnONPs. The results given in Fig. 4.36 showed that predominantly the phyto-derived particles are non-toxic to normal human lymphocytes with only marginal cytotoxicity, at and below

the IC₅₀ concentration. Beyond the IC₅₀ value, following treatment with AmSZnONPs at the highest concentration tested (100 µg/mL), the cell viability was found to decrease to 42 %. It is worth mentioning that even at the highest test concentration, all of the other four biogenic ZnONPs could elicit only upto about 20 % reduction in cell viability. In comparison, the chemical ZnONPs showed relatively very high cytotoxicity inducing cellular death ranging from ~ 40 to 88 % at or above the IC₅₀ value (60, 100 µg/mL) .

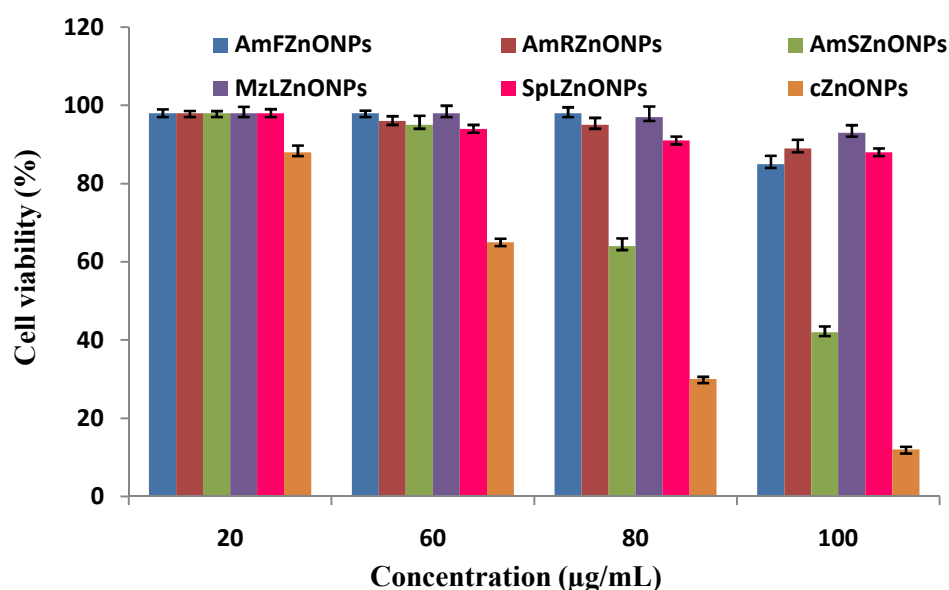


Fig. 4.36. Cytotoxicity evaluation of phyto-derived / chemical ZnONPs against hPBLs. Values represent mean \pm S.D. of three experiments. $p < 0.05$

Determination of Mitotic Index (MI): The chromosome spreads, prepared as described earlier (sub-section 4.2.11.1.2.) were examined to determine the MI and relative mitotic index (RMI) of treated and untreated control lymphocytes. A reduction of 50% and above in RMI values is considered to be indicative of cytotoxicity (Health effects test guidelines, USA, 1998). The results showed that hPBLs treated with biogenic nanoparticles except AmSZnONPs, showed a dose-dependent decrease in RMI ranging from ~7% - 36% as against a drastic reduction of ~ 46% - 94% observed in cells exposed to the chemically-derived cZnONPs (Table 4.12). Lymphocytes treated with AmS-derived nanoparticles displayed a depression in RMI ranging from ~ 22 % - 52 %. In other words, biogenic

nanoparticles were well within the biosafety limits even at the highest concentration tested (100 µg/ml) compared to their chemically derived counterparts which were found to be highly toxic beyond 20 µg/ml.

Table 4.12. MI and RMI of phyto-derived/chemical ZnONPs treated hPBLs

Type of ZnONPs	MI (%)			RMI (%)		
	Concentration (µg/mL)			Concentration (µg/mL)		
	20	60	100	20	60	100
AmFZnONPs	6.95 ± 0.32	6.40 ± 0.58	5.80±0.21	93.8	86.4	78.3
AmRZnONPs	7.00±0.2	6.00±0.5	4.80±1.0	94.6	81.08	64.8
AmSZnONPs	5.8± 0.5	5.40±0.4	3.6±1.2	78.4	73	48.6
SpLZnONPs	6.6±0.5	6.2±0.4	5.6±0.7	89.2	83.7	75.7
MzLZnONPs	6.00±1.1	5.6±0.5	5.2±0.3	81.08	75.7	71
cZnONPs	4.8±0.78	2.1±0.55	0.5±0.32	64.8	28.3	6.7

MI of untreated control cells (7.41 ± 0.93) was taken as 100% to compute the RMI values. Values are expressed as mean \pm S.D., $P < 0.05$ compared to controls. Values shown in blue colour denote the lowest MI / RMI.

Light microscopy of cZnONPs treated cells clearly revealed extensive damage to cellular morphology as evidenced by the loss of well defined cell shape, apparently due to membrane disruption with near complete absence of metaphase chromosomes (Fig. 4.37).

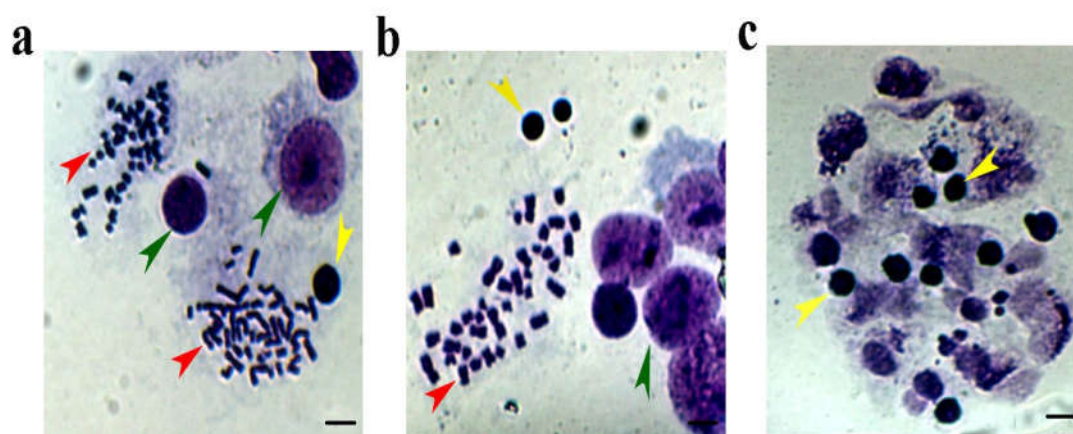


Fig. 4.37. Cytotoxicity against hPBLs studied by preparation of Giemsa stained metaphase spread (a)untreated control cells (b)phyto-derived ZnONP (60 µg/mL) and (c) chemically derived cZnONP (60 µg/mL) treated cells. Red arrow heads denote metaphase spread, yellow for interphase and green for blast cells. Scale bar represents 15 µm.

These observations are in line with earlier studies on ZnONP-induced cellular and genotoxic effects such as decrease in MI accompanied with chromosomal aberrations including chromosomal breaks in hPBLs (Mussarat et al., 2009; Gümüş et al., 2014). Lipid peroxidations leading to alterations in cell membrane, oxidative DNA damage and induction of mitochondria-mediated apoptosis have also been reported (Rikans and Hornbrook., 1997; Lin et al., 2009; Horie and Fujita., 2011).

Hemolysis of erythrocytes : Given the fact that 5% hemolysis is permissible for biomaterials (Das et al., 2011), significant hemolytic activity was not observed in cells treated with either of the two types of nanoparticles tested. However, cZnONPs treatment resulted in a marginal increase of hemolytic index up to 7% at the highest dose tested. Noticeably, erythrocytes exposed to cZnONPs when stained with Giemsa, were observed to be relatively shrunken size-wise displaying sharp angular membrane distortions, but with minimal hemolysis (Fig. 4.38), similar to those described by Shirsekar et al. (2016). Incidentally, similar structurally distorted erythrocytes with lost concavity, typical of echinocytes have been reportedly induced on exposure to certain aqueous plant extracts. This may be attributed to the inherent nature of these agents to modify erythrocyte membrane-related ionic/osmotic transport balance (Maiworm et al., 2008). However, such morphological

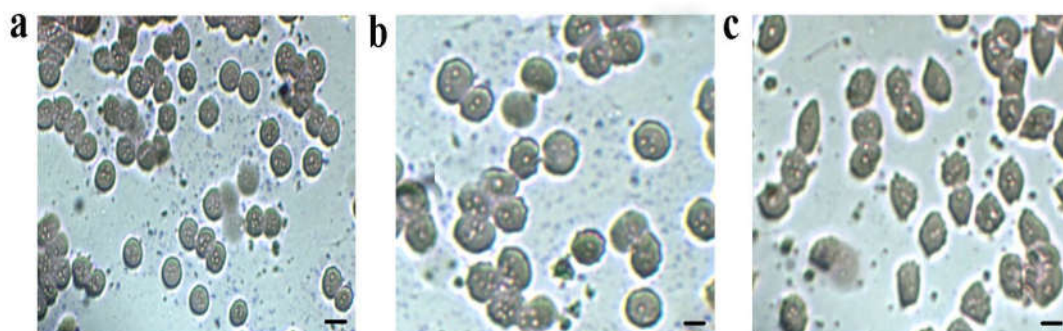


Fig. 4.38. Morphological evaluation of erythrocytes stained with Giemsa (a) untreated control cells (b) phyto-derived ZnONP (60 µg/mL) and (c) chemically derived cZnONP (60 µg/mL)treated cells. Scale bar represents 15 µm.

distortions were virtually absent in biogenic ZnONPs-treated red blood cells. A recent report by Babu et al. (2017) provided supportive evidence, wherein the presence of natural agent ferulic acid was found to reduce the hemolytic activity of ZnONPs resulting in better biocompatibility. It is quite tempting to speculate that the biogenic ZnONPs generated carrying infinitesimally small amounts of adsorbed phytoconstituents do not apparently affect the erythrocytes as evidenced by their normal cytomorphology.

4.5.11. Effect of ZnONPs on *Allium cepa* root-tips

A dose-dependent reduction in RMI value was observed in onion root tip cells treated with all of the five phyto-derived nanoparticles employed in the present study (Table 4.13). Treatment with AmSZnONPs resulted in the highest decrement of RMI (54 %). However, the plant cells exposed to cZnONPs exhibited signs of drastic cytogenotoxicity as evidenced by a near complete absence of mitotic phases and formation of ghost cells (Fig. 4.39). Previous reports on the cytogenetic toxicity of ZnONPs on onion root-tip cells mention the observation of extensive cell vacuolation along with ruptured nuclear and plasma membranes (Kumari et al., 2010; Ghosh et al., 2016).

Table 4.13. MI and RMI of phyto-derived/chemical ZnONPs treated *Allium cepa* root-tips

Type of nanoparticle	MI (%)			RMI (%)		
	Concentration (µg/mL)			Concentration (µg/mL)		
	20	60	100	20	60	100
AmFZnONPs	12.82 ± 0.46	11.6±0.69	9.9±0.4	90.9	82.2	70.2
AmRZnONPs	13±0.1	11.6±0.5	10±0.2	92.9	82.3	82.9
AmSZnONPs	10.6±0.5	9.2±0.5	7.6±1.2	75.7	65.7	54.3
SpLZnONPs	13.4±0.2	12.2±0.1	11.2	92.8	87.1	80
MzLZnONPs	12±0.5	11.2±0.1	9.8±0.5	87.1	80	70
cZnONPs	0.9±1.2	-	-	6.4	-	-

MI of untreated control cells (14.1 ± 1.03) was taken as 100% to compute the RMI values. Values are expressed as mean \pm SD, $P < 0.05$ compared to controls. Values shown in blue colour denote the lowest MI / RMI.

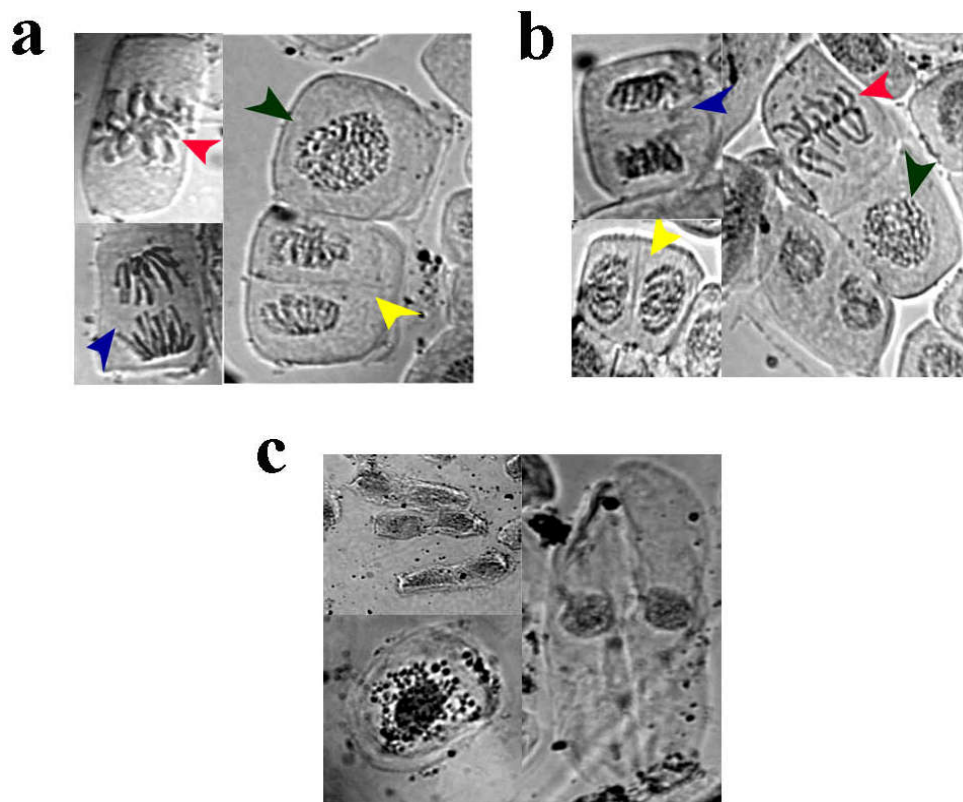


Fig. 4.39. Cytotoxicity of ZnONPs against *A. cepa* root-tip cells (a) untreated controls, cells treated with (b) phyto-derived ZnONP (60 µg/mL) and (c) chemically derived cZnONP (60 µg/mL). Arrowheads indicate mitotic phases observed: Green for prophase, red for metaphase, blue for anaphase and yellow for telophase.

Again, cells exposed to biogenic nanoparticles including AmSZnONPs, however, failed to display such cytological defects. These results were visually confirmed employing trypan blue vital staining assay. The root-tip cells, treated with chemically derived cZnONPs used as a control, were stained blue even at the lowest concentration tested (20 µg/mL) which was indicative of cell death. However, cells exposed to biogenic ZnONPs were found to be viable and bereft of stain due to exclusion of the vital dye and possession of intact cell membranes (Fig. 4.40).

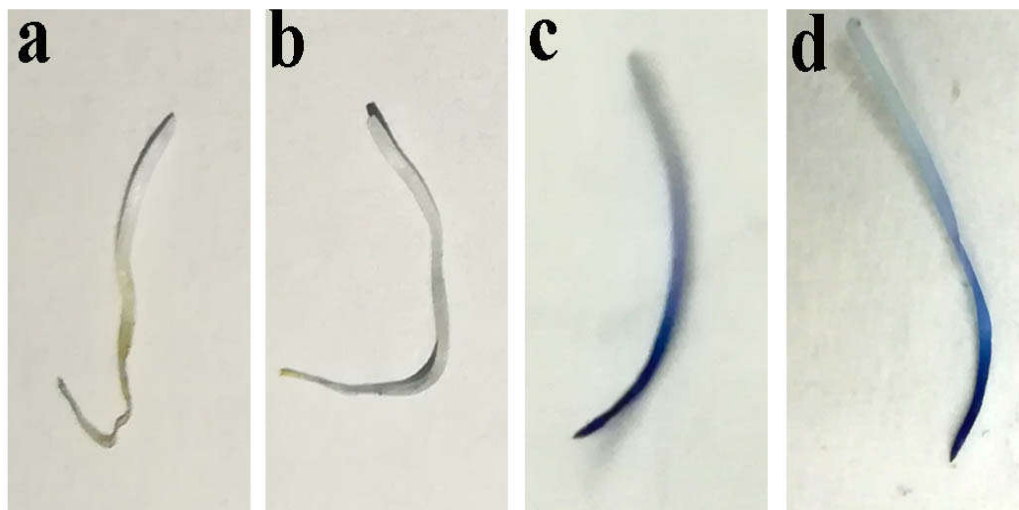


Fig. 4.40. *Trypan blue staining of A. cepa roots (a) untreated controls (b) treated with phyto-derived ZnONPs at 60 µg/mL (c) chemically derived cZnONPs at 20 µg/mL and (d) 60 µg/mL.*

Taken together, the present investigations have provided deeper insights into the selective toxicity of phyto-derived ZnONPs against cancer cells with no adverse effect on normal cells. On the contrary, the chemically-derived, commercially available version of ZnONPs was found to be toxic to two of the three cancer cell types tested. More importantly, the latter particle type caused extensive cellular damage to normal human and plant cell models studied. This study also sheds light on distinctive properties of these biogenic nanoparticles such as their surface chemistry owing to the presence of a subset of specific phytochemicals derived from the individual plant extracts. The results obtained clearly vouch for their overall biocompatibility with normal human and plant cells in addition to their cell-specific and superior anticancer activity.

The detailed cell and molecular biological analyses successfully unraveled the pathway affecting cellular behavior. The signs of ZnONP-induced apoptosis and necroptosis as revealed through microscopy and the evidence of DNA fragmentation on agarose gels are clear pointers to the activation of multiple pathways involved in cell death programmes. It has been established that ZnONP-mediated ROS responses orchestrate a series of pathological events which could be delineated in

the study. Based on these lines, a logical predictive model can be extrapolated. Cancer cells which usually carry high concentrations of anionic phospholipids and signaling molecules on their surface attract nanoparticles electrostatically, compared to normal cells. The particles are known to enter the cells directly through the lipid bilayer or by endocytosis into endosomes which merge with lysosomes leading to endosome destabilization. Release of soluble Zn ions triggered by decreasing pH in the early endosomes (pH 6.3) to late endosomes (pH 5.5) further decreasing to 4.7 in the lysosomal compartments culminates in ROS-mediated apoptosis (Bisht and Rayamajhi, 2016). Moreover, angiogenesis, a hallmark of cancer cells, leads to irregular and leaky walls with larger gaps than healthy blood vessels giving easy access to nanoparticle entry (Grossman et al., 2012). Arguably, this also provides a rationale for the selective killing of cancer cell observed in the obtained results.

EVALUATION OF MULTIFACETED PROPERTIES: PHOTOCATALYTIC, ANTIBACTERIAL AND DNA- INTERACTIVE POTENTIAL OF PHYTO-DERIVED AND THE CHEMICALLY SYNTHESIZED ZnONPs

5.1. Introduction

Green nanotechnology stands for the use and production of nature-friendly nanomaterials. It would be an added advantage if the nanomaterial so produced finds utility in applications for environmental remediation (Sivaraj et al., 2014; Das et al., 2018). For instance, in a scenario of contamination of water bodies with organic dye pollutants from textile and printing industries and with drug-resistant bacteria/mutated pathogens, it is worthwhile to explore novel remedial technologies. Nano-based functionalized surfaces, coatings and reagents offer better avenues for improved catalysis, adsorption, high reactivity and mobility enabling effective removal of heavy metals, inorganic/organic pollutants and harmful microbes making them useful for water and wastewater treatment (Gehrke et al., 2015; Guerra et al., 2018).

As per World Health Organization (WHO), the antimicrobial resistance was declared as one of the 'biggest threats to global health' (Davis et al., 2018). It is well established that development of drug resistance in microorganisms is a cause and consequence of the use of high drug doses, higher toxicity treatments, longer stays in hospitals and an increase in mortality. There are various factors which contribute towards antibiotic resistance in microorganisms, such as misuse and overuse of antibiotics, their extensive agricultural use and availability of fewer new antibiotics (Ventola, 2015). Since the antimicrobial action of nanoparticles is directly proportional to the surface area available for interaction with biological components, metallic nanoparticles have become one of the most promising choices to overcome the microbial resistance to drugs (Singh et al., 2018).

In yet other frontier/futuristic platforms, nanoparticle use continues to attain greater attraction for diverse applications of functionally integrating DNA/nucleic

acids for biosensing, labeling, targeted imaging, cellular delivery, diagnostics, therapeutics, bioelectronics, and biocomputing (Evans et al., 2016; Chamorro-Garcia and Merkoci., 2016; Kairdolf et al., 2017). The multifaceted versatility of inorganic metal oxide nanocrystals emanate from their optical, physical and electrochemical properties which facilitate functional combinations for specific end-uses (Samanta et al., 2016).

In view of the above, an evaluation of the multifaceted properties of the phyto-derived ZnONPs generated in the present study was deemed imperative and relevant. Interestingly, the physico-chemical characterization of the biosynthesized zinc oxide nanoparticles revealed their unique surface characteristics including the presence of adsorbed phytochemicals and peptides. Several reports were encountered during a literature scan which showed the multipronged potential of biogenic ZnONPs (Bhuyan et al., 2015; Pandimurugan and Thambidurai, 2016; Khalafi et al., 2019; Chemingui et al., 2019). This chapter highlights the findings obtained during a digressive exploration of their functions. In brief, a comparison has been made between biosynthesized ZnONPs versus their commercial chemical version in terms of (i) photocatalytic potential as evidenced by degradation of methylene blue, (ii) antibacterial activity against bacteria including MDR clinical strains and (iii) their interactions with DNA (plasmid / λ genome and 100 bp ladder). The overall results furnish a proof-of-principle of the superior nature of biofabricated zinc oxide nanoparticles over their chemical counterpart.

5.2. Materials and Methods

5.2.1. Photocatalytic dye degradation

The photocatalytic potential of AmFZnONPs, AmRZnONPs, AmSZnONPs, SpLZnONPs, MzLZnONPs and cZnONPs was assessed based on the reported ability of nanoparticles to catalytically reduce dyes such as methyl red, methylene blue and many others on exposure to light. Methylene blue (MB), for instance, can be reduced to its colourless leuco-form on exposure to direct sunlight (Bandekar et al., 2014; Kumar et al., 2014). The following is a brief outline of the experimental

procedure adopted in the present study. Aliquots of all types of ZnONPs, ranging from 50 µg - 2.0 mg/mL, were added individually to 50mL of methylene blue dye (1mg/100mL). The solutions were then magnetically stirred for 15 minutes, to achieve adsorption equilibrium of the photocatalyst with dye in the dark, and then exposed to direct sunlight for a period of 1, 3 and 5 h respectively. Aliquots from each sample were collected at the three designated time intervals for obtaining an absorption spectrum from 200 – 700 nm. An aliquot of methylene blue solution alone (without any ZnONPs) was also included in the analysis. The absorption at 665 nm was used to calculate percentage dye degradation, if any, using the equation,

$$\% \text{ dye degradation} = \frac{(A_0 - A_t)}{A_0} \times 100$$

where A_0 denoted initial absorption of dye in the presence of test samples and A_t represented absorption of the dye following the time 't' denoted in hours (h).

5.2.2. Antibacterial activity

The antibacterial potential of the different nanoparticles - AmFZnONPs, AmRZnONPs, AmSZnONPs, SpLZnONPs, MzLZnONPs and cZnONPs - was determined using four clinical bacterial isolates, *Escherichia coli*, *Klebsiella pneumoniae*, *Pseudomonas aeruginosa* and *Staphylococcus aureus*, obtained from a local tertiary care centre. Antibiotic profiling of these isolates was carried out using Kirby-Bauer disc-diffusion method according to CLSI (2017), employing the following antibiotic discs (HiMedia Mumbai, India) : imipenem (10 mcg), ciprofloxacin (5 mcg), cefepime (30 mcg), gentamicin (10 mcg), ampicillin (10 mcg), aztreonam (30 mcg), chloramphenicol (30 mcg), amikacin (30 mcg), meropenem (10 mcg), naldixic acid (30 mcg), polymixin B (300 units), ceftazidime (30 mcg) and ceftaxime (30 mcg).

5.2.2.1. Quantitative MIC-MBC determination

Exponentially growing cultures of clinical bacteria, serially diluted with Luria Bertani (LB) growth medium, were individually exposed to 100-1000 µg/mL

of AmFZnONPs, AmRZnONPs, AmSZnONPs, SpLZnONPs, MzLZnONPs and the chemically synthesized cZnONPs. In parallel, appropriate control cultures were treated simultaneously with equivalent volumes of the corresponding plant extracts (AmF, AmR, AmS, SpL and MzL). Following overnight growth at 37 °C, 0.1 mL each of the test cultures and the corresponding untreated controls were spread on LB-agar plates for determination of minimum inhibitory concentration (MIC) and minimum bacteriocidal concentration (MBC) (Reddy et al., 2014; Salem et al., 2015).

5.2.2.2. *Qualitative well diffusion assay*

Antibacterial activities of individual biogenic AmFZnONPs, AmRZnONPs, AmSZnONPs, SpLZnONPs, MzLZnONPs, their corresponding extracts and the chemical cZnONPs were then qualitatively confirmed using Kirby-Bauer method (Vani et al., 2011). Aliquots (75 µL) of each of the test samples containing concentrations equivalent to MIC were inoculated into 7 mm wells punched in LB agar plates swabbed previously with each of the four bacterial test strains. The zone of inhibition (in mm) of bacterial growth was measured following 16 h of incubation at 37 °C which was indicative of the susceptibility of the test organisms to the individual nanoparticles / extracts.

5.2.3. **Biogenic ZnO-DNA interactions**

The interaction of phyto-derived ZnONPs with molecular DNA was analyzed on the basis of *in vitro* experiments designed essentially as described by Wahab et al. (2009) with minor modifications. Briefly, in a 20 µL reaction volume, equal amounts of supercoiled plasmid DNA (pUC 18, 0.2 µg/µL), 100bp DNA ladder (0.5 µg/µL), and λ bacteriophage genomic DNA (0.3 µg/µL) were exposed to individual biogenic and chemical version of ZnONPs, ranging from 0.5 - 5.0 mg/mL. All test samples were then incubated at 37 °C for 90 min. Controls of each DNA type were also set, devoid of any nanoparticle treatment. Following incubation, the samples were snap-chilled to arrest the reaction. Equal volumes of the reaction products were gently loaded into the wells of a 2.0 % agarose gel for

electrophoretic separation followed by ethidium bromide staining for visualization and photography using an Alpha imagerTM 2200 (USA) gel documentation system.

5.2.4. Statistical analysis

All results have been expressed as mean values \pm standard deviation (S.D.) obtained from experiments carried out in triplicate. All data were subjected to one-way analysis of variance (ANOVA, SPSS version 20.0) by Dunnett's Multiple Comparison test. The difference was considered as statistically significant at $p < 0.05$ with respect to control.

5.3. Results and Discussion

5.3.1. Photocatalytic dye degradation

When a photocatalyst is illuminated by a light stronger than its band gap energy, electron migrates from valance band to conduction band thereby forming holes in the valance band. These holes can generate highly oxidative hydroxyl radicals, which can extract electrons from dye molecules leading to their degradation (Elamin and Elsanousi, 2013). Basic dyes such as methylene blue (MB) are organic in nature which contain benzene ring (s), a chromosphere and auxochrome group. It is a cationic thiazine dye of blue color, soluble in polar solvents, which has been used as a model system for photocatalytic studies in analytical chemistry, medicine and biology. Due to its solubility in water and ethanol, it can potentially pollute water bodies causing hazard to aquatic biota (Atchudan et al., 2016). Hence, degradation of this dye is of crucial importance for environmental protection. In this context, an assessment of the photocatalytic potential, if any, of the phyto-derived ZnONPs in comparison to the activity displayed by chemically derived nanoparticocles was carried out as described earlier in section 5.2.1.

Fig.5.1A. shows a pictorial representation of the visualized time-dependent photo-bleaching effects of biosynthesized ZnONPs in the presence of sunlight, whilst Fig. 5.1B. depicts the changes in the UV-vis absorption spectrum (200 – 700 nm) as a function of time. The reduction in the peak intensities in the absorption

spectrum are known to occur due to photo-assisted oxidative degradation of the large chromosphere group of methylene blue dye molecule (Zhang et al., 2014).

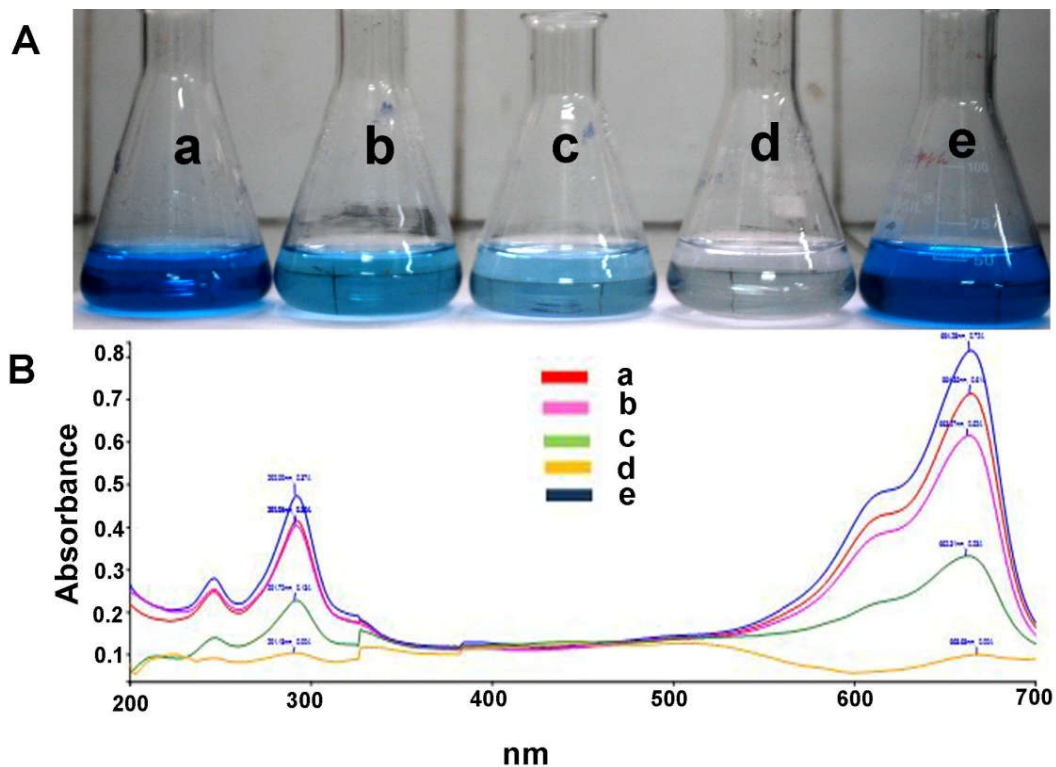


Fig. 5.1. (A) Pictorial and (B) graphical representation of photocatalytic dye degradation of methylene blue by biosynthesized ZnONPs following exposure to sunlight at (a) 0 h (b) 1 h (c) 3 h (d) 5 h and (e) 5 h (methylene blue control)

Based on the absorbance values obtained at 665 nm, a graphical representation of the results obtained with all nanoparticle types in a time and dose-dependent manner is given in Fig. 5.2. The highest rate of photocatalysis was exhibited by AmS-derived ZnONPs, wherein complete dye degradation was achieved at a concentration of 200 μ g/mL by 3 h; at a higher concentration of 400 μ g/mL, the time for complete degradation was effectively reduced to 1 h. Such an almost comparable inverse dose and time dependent relationship was also apparent in the case of SpLZnONPs. The lowest photocatalysis amongst the biosynthesized ZnONPs was exhibited by AmFZnONPs, wherein a minimum of 200 μ g/mL concentration was necessary to achieve 60 % degradation of the dye.

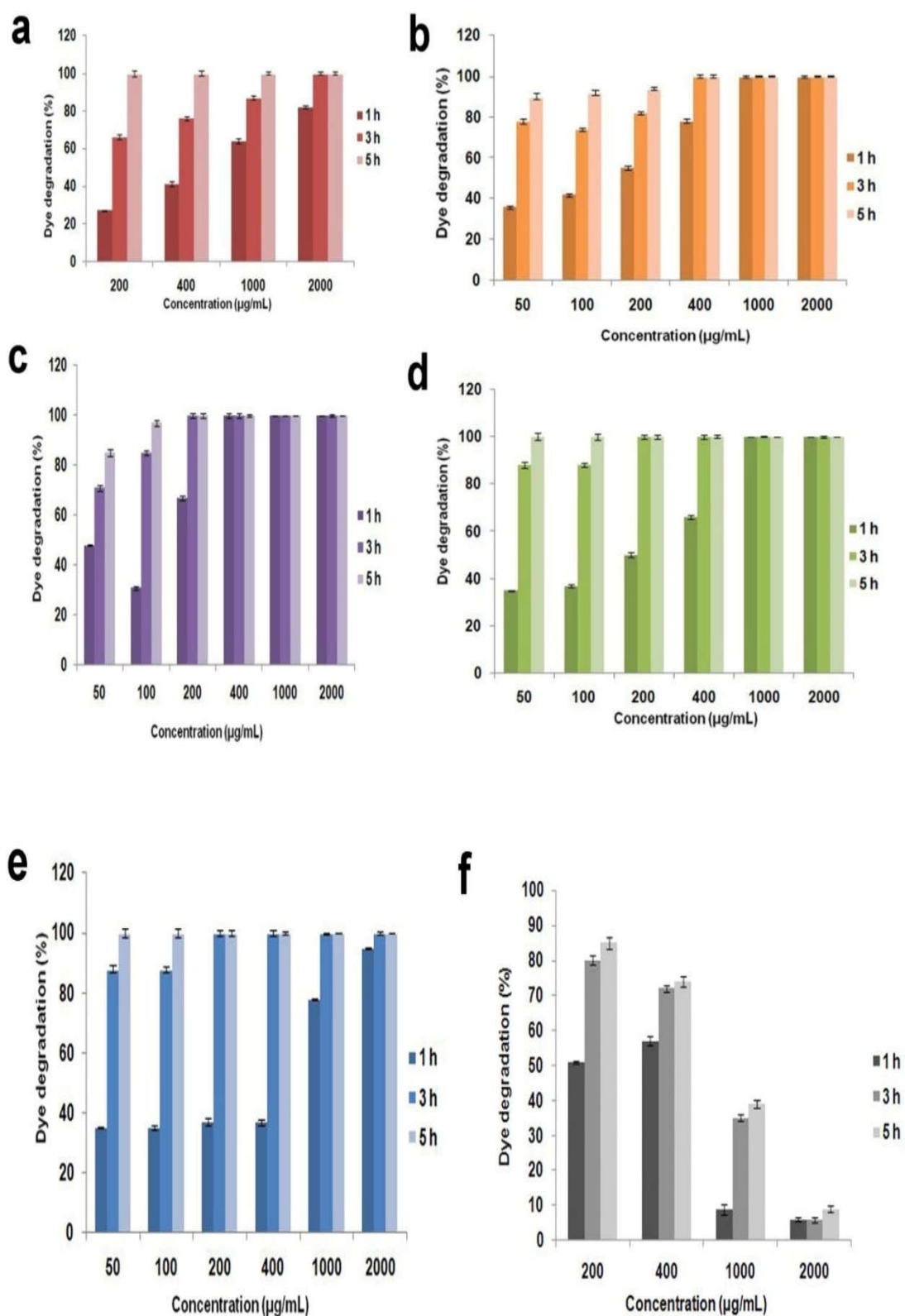


Fig. 5.2. Photocatalytic methylene blue dye degradation at time intervals of 1, 3 and 5 h by (a) AmFZnONPs (b) AmRZnONPs (c) AmSZnONPs (d) SpLZnONPs (e) MzLZnONPs and (f) cZnONPs

Incidentally, the chemically synthesized cZnONPs taken as control failed to achieve complete degradation within the maximum time and dose range tested. The maximum dye degradation observed was less than 90 % at 200 $\mu\text{g/mL}$ for 5 h. Strikingly, the inverse dose-time relationship (higher the dose, lesser the time required for photocatalytic dye degradation) observed with biosynthesized ZnONPs, was not applicable to the chemical version of zinc oxide nanoparticles. At higher doses, from 400 $\mu\text{g/mL}$ – 2.0 mg/mL within 1 – 5 h duration, the photocatalytic activity plummeted down drastically to < 10 %. The results clearly demonstrate the superior and dose-dependent photocatalytic potential of the phyto-derived zinc oxide nanoparticles. These findings are in agreement with the recent reports on MB degradation on exposure to sunlight using *Tabernaemontana divaricata* leaf extract and *Ulva lactuca* seaweed extract mediated ZnONPs (Ishwarya et al., 2018; Raja et al., 2018).

Previous studies have shown that zinc nanoparticles owe their photocatalytic dye degradation potential to the surface defects like oxygen vacancies, morphology and size (Davar et al., 2015). According to Raja et al.(2018) sunlight causes electrons and holes on nano-ZnO, which in turn, generate superoxide and hydroxyl radicals in the presence of water and oxygen molecules resulting in dye degradation. It is relevant to note here that solar irradiation is a good cost effective energy source compared to UV irradiation (Fatin et al., 2012). Nirmala et al. (2010) has pointed out that for better photocatalytic efficiency, ZnO must absorb not only UV but also visible light which accounts for the 45% of solar radiation. The red shift observed in the UV-vis absorption spectrum (section 3.3.2.4.) of phyto-assisted ZnONPs was likely due to the formation of defective energy levels between the valence and conduction bands resulting ultimately in improving catalytic activity (Yu et al., 2013). Further, surface modifications such as doping on ZnONPs have been found to increase its effectivity as a semiconductor photocatalyst compared to the unmodified version (Wang et al., 2012; Atchudan et al., 2016). The fact that phyto-derived ZnONPs displayed surface defects as evidenced by PL studies (sub-section 3.3.2.5.) as well as their decoration with phytomolecules as revealed by FTIR data (section 3.3.2.3.) confers enhanced photocatalytic potential to them. This also

provides a rational explanation to the low or poor activity exhibited by chemically generated ZnONPs.

5.3.2. Antibacterial potential

Based on the antibiotic profiling of the clinical bacterial isolates, carried out employing the Kirby-Bauer method (CLSI, 2017). *S.aureus* and *K. pneumoniae* were found to be multi-drug resistant, exhibiting resistance to antibiotic classes of beta-lactamases, quinolones, aminoglycosides and chloramphenicol. However, *E.coli* was found resistant only to beta-lactamases and quinolones, whilst *P.aeruginosa* displayed resistance against beta-lactamases and lipopeptides. Since the latter two strains showed resistance against only two classes of antibiotics, technically, they do not strictly fulfill the criteria to be classified as ‘multi-drug resistant’ (MDR) which requires display of resistance against three or more classes of antibiotics.

5.3.2.1. Quantitative MIC-MBC determination

MIC is the minimum inhibitory concentration of antimicrobial agent/compound capable of preventing bacterial growth whilst MBC is the minimum bacteriocidal concentration of the same which kills all bacteria. These two parameters are considered to be the ‘gold standard’ for determining *in vitro* susceptibility of microorganisms to antimicrobials. The procedure of determination of MIC- MBC values of the biosynthesized and the control ZnONPs is mentioned above in section 5.2.2.1. The values obtained in respect of each clinical strain are given in Table 5.1. The data clearly demonstrated superior antibacterial potential of biogenic ZnONPs against all tested strains in comparison to the chemical version. Notably, the chemical cZnONPs showed antibacterial activity only against *P.aeruginosa* at a very high concentration of 800µg/mL. Incidentally, *K. pneumoniae* was found to be most sensitive to MzL-derived ZnONPs with a MIC-MBC value of 124 and 136 µg/mL respectively. On the other hand, *P. aeruginosa* was found to be relatively the least sensitive toward biosynthetic ZnONPs as evidenced by the highest MICs ranging from 250 – 580 µg/mL. Since all plant derived ZnONPs were cytotoxic to both drug resistant (*K.pneumoniae* and *S. aureus*) and susceptible

pathogens (*E.coli* and *P. aeruginosa*), they can be exploited therapeutically as ‘nanobiotics’. The failure of occurrence of bacterial growth inhibition or cell killing by the corresponding phyto-derived extracts *per se* reinforces the view that the efficacy of these zinc oxide nanoparticles emanates solely due to the biosynthetic mode of generation. The poor antibacterial activity of the non-biogenic/chemical ZnONPs mentioned above also lends credence to this hypothesis.

Table 5.1. MIC and MBC values of phyto-/chemically derived ZnONPs

Types of ZnONPs	<i>E. coli</i>	<i>K. pneumoniae</i>	<i>P. aeruginosa</i>	<i>S. aureus</i>
MIC ($\mu\text{g/mL}$)				
AmFZnONPs	275 \pm 0.56	300 \pm 0.48	400 \pm 1.3	200 \pm 0.78
AmRZnONPs	337 \pm 1.6	225 \pm 0.54	250 \pm 2.4	175 \pm 1.4
AmSZnONPs	400 \pm 0.32	400 \pm 0.42	278 \pm 1.9	190 \pm 1.3
MzLZnONPs	260 \pm 2.4	124 \pm 1.2	580 \pm 1.7	210 \pm 0.5
SpLZnONPs	135 \pm 1.8	315 \pm 3.0	480 \pm 0.68	225 \pm 0.5
cZnONPs	0	0	800 \pm 1.1	0
MBC ($\mu\text{g/mL}$)				
AmFZnONPs	285 \pm 1.1	315 \pm 0.32	410 \pm 0.55	220 \pm 1.5
AmRZnONPs	352 \pm 0.32	250 \pm 1.25	284 \pm 2.0	220 \pm 0.58
AmSZnONPs	418 \pm 0.55	425 \pm 1.8	310 \pm 1.4	200 \pm 2.2
MzLZnONPs	277 \pm 0.87	136 \pm 0.90	589 \pm 3.5	220 \pm 2.7
SpLZnONPs	142 \pm 1.44	323 \pm 0.23	486 \pm 1.52	245 \pm 0.35
cZnONPs	0	0	822 \pm 0.81	0

Values are expressed as mean \pm S.D.; $p < 0.05$ compared to respective controls

5.3.2.2. Qualitative well diffusion assay

The inhibition zones obtained by the Kirby-Bauer well-diffusion method corroborated well with the overall inferences derived from the earlier set of experiments for determination of MIC-MBC values of ZnONPs (Fig.5.3, Table 5.2). A clear zone of bacterial growth inhibition was apparent around all wells containing biogenic ZnONPs against all four strains with cZnONPs showing an inhibition zone only against *P. aeruginosa*. The aqueous extracts *per se* also failed to inhibit growth of all test strains as previously observed.

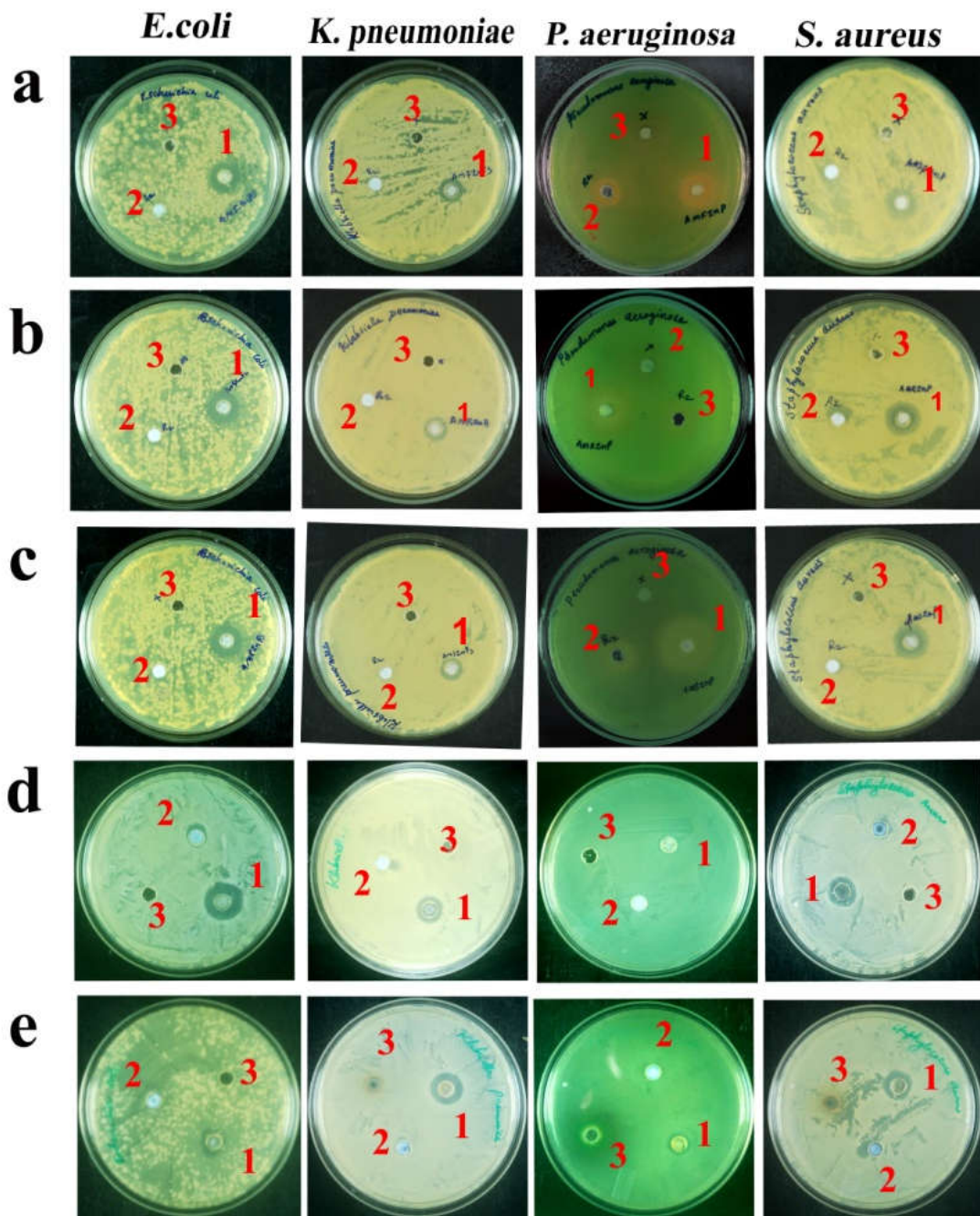


Fig. 5.3. Panels of images depicting antibacterial activity of (a) AmFZnONPs (b) AmRZnONPs (c) AmSZnONPs (d) SpLZnONPs and (e) MzLZnONPs against four clinical bacterial isolates employing Kirby-Bauer well diffusion assay. The numbers on the petriplates mark the wells loaded with 75 μ L of test samples containing concentrations equivalent to MIC : 1 - phyto-derived ZnONPs, 2- chemical ZnONPs and 3 - corresponding plant extracts.

In a recent report by Gupta et al. (2018) on nanoparticles biosynthesized using aqueous extract of *Catharanthus roseus*, the diameter of the inhibition zone obtained was 11 mm at a very high concentration of 1.5 mg/ mL against *E.coli*, *S. aureus* and *P. aeruginosa*. In comparison, the zone of inhibition obtained in the present study ranged from 13-27 mm at a concentration of 100 µg/mL to 1.0 mg/mL, revealing thereby the higher antibacterial activity of ZnONPs derived from aqueous extracts of *A.muricata*, *S.pinnata* and *M.zapota*.

Table 5.2. Zone of Inhibition (in mm) demonstrating antibacterial activity

Sample	<i>E. coli</i>	<i>K. pneumoniae</i>	<i>P. aeruginosa</i>	<i>S. aureus</i>
AmFZnONPs	20 ± 0.03	15±0.5	22±0.43	20±0.12
AmRZnONPs	17.58±1.3	13.39±0.08	22.24±1.1	20.41±0.75
AmSZnONPs	17.64±2.2	13.37±0.8	22.70±0.57	22.63±1.4
MzLZnONPs	17.50±2.6	22.86±1.3	15.67±0.38	22.20±1.5
SpLZnONPs	27.63±2.0	19.77±0.33	15.47±1.6	21.90±2.9
cZnONPs	0	0	15±0.6	0

Values are expressed as mean ± S.D., p < 0.05 compared to respective controls

Inhibition zone measurements in the present study also revealed that all biogenic ZnONPs were effective equally against both gram negative (*P.aeruginosa*) as well as gram positive (*S.aureus*) bacteria. The chemically synthesized control ZnONPs were also found to be active against the gram negative *P.aeruginosa* strain. These observations are in contrast with the results of a previous study by Premanathan et al. (2011), wherein the chemically synthesized ZnONPs were found to inhibit only gram positive strains. Notably, the present study showed that AmSZnONPs had higher antibacterial potential against *P.aeruginosa* and *S.aureus* despite their larger size (61 nm) compared to the lower activity displayed by AmFZnONP particles of smaller size (28 nm). This is perhaps indicative of the fact that surface properties of the nanoparticles are also crucial for the observed antibacterial effects. The findings also showed that *A. muricata* derived ZnONPs displayed better growth inhibition of *P. aeruginosa*, an opportunistic microbe

classified as ‘critical priority pathogen’ (WHO, 2017) involved mainly in nosocomial ICU infections (Pachori et al., 2019).

A mechanistic understanding of the antibacterial activity of nanoparticles is not fully clear. Studies have revealed that multiple factors - direct uptake of nanoparticles, ROS induction leading to impairment of cell membrane integrity and damage to cellular macromolecules such as DNA, RNA and protein - may all contribute towards bacterial death (Qidwai et al., 2018; Ali et al., 2018). According to Pati et al. (2014), the disruption of cell integrity by ZnONPs causes reduction of surface hydrophobicity and downregulation of oxidative stress-resistance gene expression thus inducing ROS production. Other factors /processes involved in cell killing by nanoparticles include extracellular dissolution and release of Zn^{2+} ions, dissolution at acidic pH in lysosomes, UV induced disruptive reactions, morphology and composition based aspects (Siddiqi et al. 2018).

5.3.3. Biogenic ZnO-DNA interactions

DNA with sugar-phosphate backbone is negatively charged in an aqueous environment. It can thus act like a molecular cage capable of recruiting/binding to various positively charged particles (Wahab et al., 2009). This interactive potential has been exploited for the development of biosensors and biomolecular targets. Selective bio-capture of thiolated probe DNA onto gold-seeded ZnO nanoflowers has found use as a biosensor of pathogenic *Leptospirosis*-causing strains (Perumal et al., 2015). Gold coated ZnO thin films are yet another low cost - high performance DNA biosensors with many applications in bio-diagnosis, food and forensic analysis (Foo et al., 2015). Interaction of ZnO and calf thymus DNA have recently been explored by means of conductivity and electrophoretic mobility studies by Das et al. (2018), giving insight into the surface defects of this inorganic metal oxide. Nanoparticles are also known to inhibit DNA replication based on their binding affinity to the molecule (Li et al., 2013). Binding of zinc ions onto DNA was observed to cause decrease in the absorption coefficient of purine bases resulting in decreased intensity in gel electrophoresis as well as reduction in absorption spectra and melting temperature (Nejdl et al., 2014).

The results of the *in vitro* experiments performed in the present study were found to be distinctive with respect to the type of particle as well as the DNA sample involved in the reactions. As already mentioned above, a total of six particle types (AmFZnONPs, AmRZnONPs, AmSZnONPs, SpLZnONPs, MzLZnONPs, cZnONPs) and three DNA samples (supercoiled pUC 18 plasmid DNA, genomic DNA of Lambda phage and a DNA ladder comprising of short DNA fragments of 0.1 to 1.0 kb in size) were employed for reactions incubated subsequently for 90 min at 37 °C. Aliquots of individual reaction products were analyzed by electrophoresis on 2.0 % agarose gels.

The plasmid pUC 18 DNA sample comprised of ~ 60 % in the supercoiled (sc) state and ~ 40 % in the open circular (oc) form according to the manufacturer's datasheet. These DNA samples when treated with AmFZnONPs and AmSZnONPs showed the occurrence of a dose-dependent change in the degree of relaxation of negative supercoiling as evidenced by the appearance of a discrete band between the supercoiled and relaxed open circular forms. This was evident only at concentrations of 4.0 and 5.0 mg/mL which was indicative that a definite concentration threshold for the phenomenon (Fig. 5.4. a and c in lanes 6, 7). However, DNA treated with SpLZnONPs and MzLZnONPs resulted in the formation of dose-dependent high molecular weight complexes with retarded mobility at concentrations beyond 2.0 mg/mL (Fig. 5.4. d and e in lanes 4-7).

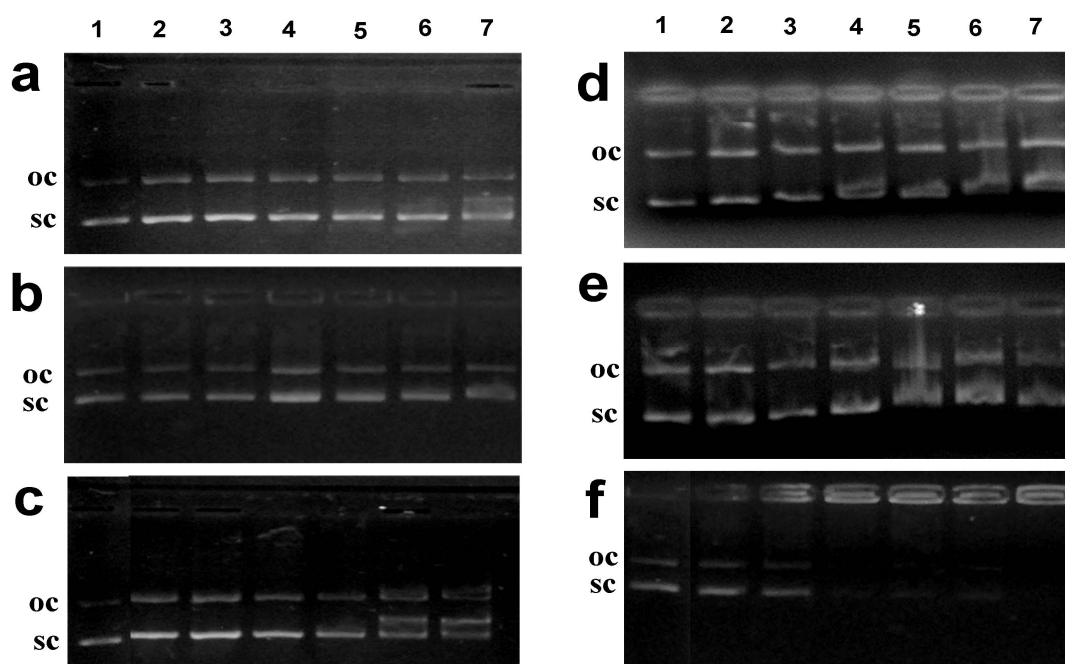


Fig. 5.4. *Interaction of Plasmid DNA-pUC18 (0.2 μ g/ μ L) with (a) AmFZnONPs (b) AmRZnONPs (c) AmSZnONPs (d) SpLZnONPs (e) MzLZnONPs and (f) cZnONPs : Untreated control DNA (Lane 1), DNA treated with 0.5 mg/mL (Lane 2), 1.0 mg/mL (Lane 3), 2.0 mg/mL (Lane 4), 3.0 mg/mL (Lane 5), 4.0 mg/mL (Lane 6) and 5.0 mg/mL (Lane 7). 'sc' and 'oc' denote supercoiled and open circular form of plasmid DNA respectively.*

The AmRZnONPs treated plasmid DNA failed to show any visible changes in the electrophoretic mobility which was suggestive of the absence of interactions of the particles with DNA. Strikingly, the chemically synthesized cZnONPs showed a dose-dependent formation of DNA complexes which failed to move out of the wells. The inhibited mobility apparently resulted from neutralization of negative charges on the sugar-phosphate backbone of DNA (Fig.5.4 f). In agreement with these observations, Makumire et al. (2014) have reported retardation of DNA mobility as a result of plasmid DNA interaction with ZnONPs. The electrostatic nature of interaction between ZnO tetrapod nanostructures and plasmid DNA has also been reported earlier (Nie et al., 2006). Likewise, Saha et al. (2014) have also observed that the surface nature of ZnONPs is critical for site-specific binding to nucleobases of the DNA.

In the case of interactions of SpLZnONPs and MzLZnONPs with the linear λ bacteriophage DNA, a decrease in the intensity of the bands (Fig.5.6) were observed

in samples treated with 2.0 – 4.0 mg/mL with slight increase in band intensity of samples treated with the highest concentration of nanoparticles (5.0 mg/mL). In samples treated with 3.0 and 4.0 mg/mL of AmF and AmR derived nanoparticles, the genomic DNA band was nearly invisible (Fig. 5.5. a and b in lanes 5, 6) but in samples exposed to 5.0 mg/mL, the band was found to reappear (Fig. 5.5 a and b in lane 7). Interestingly, this intriguing phenomenon of ‘fluorescence recovery after quenching’ has also been reported by Ma et al. (2016), wherein the basis of this effect is attributed to saturation by ZnO adsorption followed by its dissolution. Structural deformations in calf-thymus DNA following interactions with high concentration of chemically synthesized copper nanoparticles have also been recently reported (Bhar et al., 2017). However, none of the above mentioned changes were discernible in λ DNA samples treated with phyto-derived AmSZnONPs and chemically derived cZnONPs.

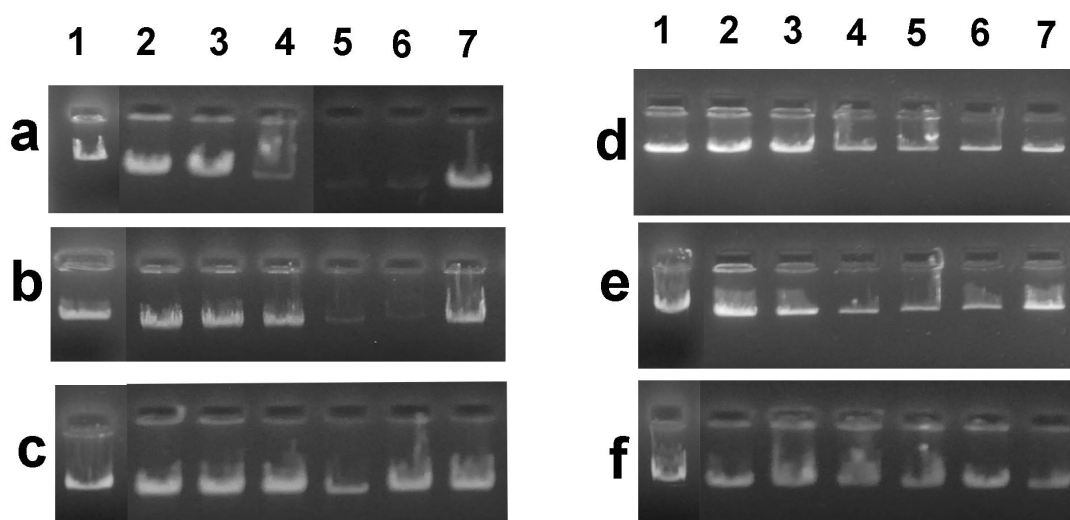


Fig. 5.5. Interaction of λ DNA (0.3 $\mu\text{g}/\mu\text{L}$) with (a) AmFZnONPs (b) AmRZnONPs (c) AmSZnONPs (d) SpLZnONPs (e) MzLZnONPs and (f) cZnONPs : Untreated control DNA (Lane 1), DNA treated with 0.5 mg/mL (Lane 2), 1.0 mg/mL (Lane 3), 2.0 mg/mL (Lane 4), 3.0 mg/mL (Lane 5), 4.0 mg/mL (Lane 6) and 5.0 mg/mL (Lane 7).

The interaction of biogenic and the chemical version of zinc oxide nanoparticles with 100bp DNA ladder was analyzed electrophoretically (Fig. 5.6.). The DNA ladder was found to be more or less unaffected when exposed to increasing concentrations of AmF-derived ZnONP apparently due to lack of affinity for DNA. In the case of interactions of higher concentrations of AmRZnONPs (3.0

– 5.0 mg/mL) with DNA, retardation of all bands accompanied with a smear of partially degraded DNA across the lane was evident (Fig. 5.6. b in lanes 5-7). Partial fluorescence quenching and upward band shifts due to retardation without any discernible DNA smearing was observed in DNA exposed to higher concentrations AmSZnONPs and SpLZnONPs (Fig. 5.6. c and d in lanes 6, 7). Increased fluorescence quenching and partial band shifts in a dose-dependent manner were apparent in DNA treated with chemical cZnONPs (Fig. 5.6. f in lanes 4-7). Since protein-free ‘naked DNA’ has been used in these studies, the resultant information should prove useful for future applications.

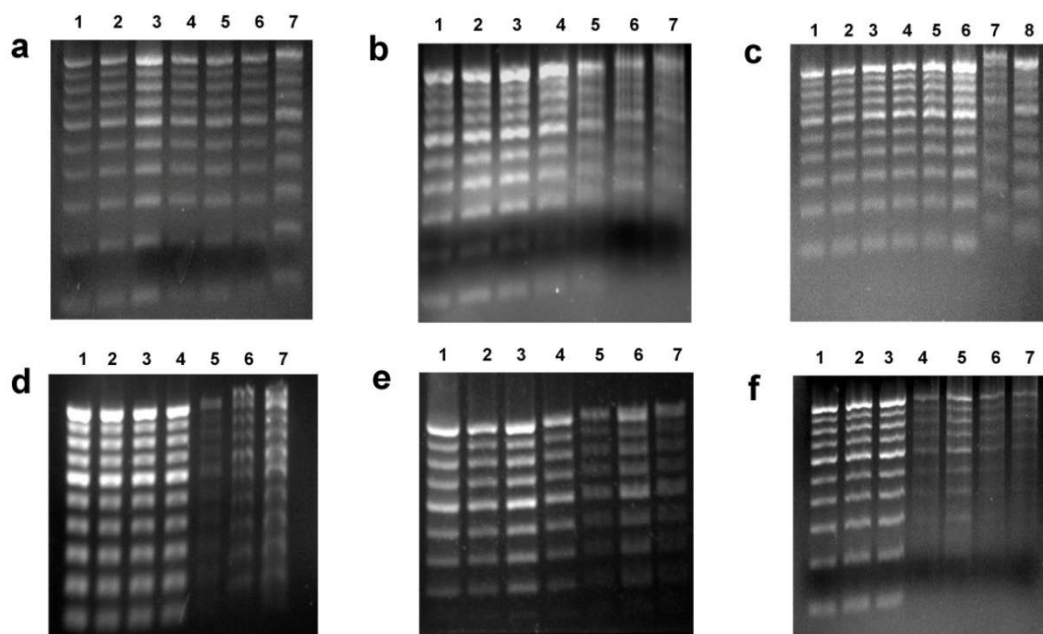


Fig. 5. 6. *Interaction of 100 bp ladder DNA (0.5 $\mu\text{g}/\mu\text{L}$) with (a) AmFZnONPs (b) AmRZnONPs (c) AmSZnONPs (d) SpLZnONPs (e) MzLZnONPs and (f) cZnONPs. Untreated control DNA (Lane 1), DNA treated with 0.5 mg/mL (Lane 2), 1.0 mg/mL (Lane 3), 2.0 mg/mL (Lane 4), 3.0 mg/mL (Lane 5), 4.0 mg/mL (Lane 6) and 5.0 mg/mL (Lane 7).*

Taken together the results presented in this chapter have been successful in highlighting multifaceted properties of the different phyto-derived ZnONPs in comparison with the chemical version of commercially available ZnONPs. The superiority of the phytogenic nanoparticles in terms of high photocatalytic, antibacterial and DNA interactive properties have been demonstrated.

SUMMARY AND CONCLUSIONS

Over the last decade, nanotechnology has been one of the fastest-growing areas of science and technology involved in the development of biocompatible, biodegradable, and functionalized nanomaterials. The unique physicochemical properties of nanomaterials allow creation of new nanoplatforms / systems / or devices with a wide variety of potential applications in various disciplines including biomedical sciences. Compared to other metal oxide nanoparticles, zinc oxide (ZnO) is inexpensive, biocompatible, and relatively less toxic making it an attractive candidate with drug potential. Moreover, ZnO is graded as a “GRAS” (generally recognized as safe) substance by the US Food and Drug Administration (FDA). ‘Green synthesis’ avoids production of unwanted or harmful by-products through the build-up of reliable, sustainable, and eco-friendly synthetic procedures. The use of ideal natural resources (such as organic systems) is essential to achieve this goal. Among the available green methods of synthesis, utilization of plant extracts is a rather simple and easy process to produce nanoparticles at large scale relative to bacteria and/or fungi-mediated synthesis.

The present study exploited the bioreduction and capping potential of phytoconstituents present in plant extracts for biosynthesis of zinc oxide nanoparticles. A total of 10 plants were chosen randomly, following a literature scan, ensuring that the selected plants had not been previously exploited for the purpose. Using a trial and error method, the factors affecting the phyto-mediated biosynthesis were empirically determined. Confirmation of successful generation of phyto-derived ZnONPs was ascertained by X-ray diffraction (XRD) and Field emission scanning electron microscopy (FESEM) techniques. Subsequently, optimization of parameters involved in the sol-gel method were fine-tuned for successful synthesis as demonstrated by the selection of specific conditions such as the use of 5 % (w/v) of zinc nitrate hexahydrate and calcination at 600 °C for 2 h. Incidentally, all these three parameters were found to be independent of external pH regulation. The aqueous extracts selected for fabrication of biogenic particles were

fruits, roots and seeds of *A.muricata*, leaves of *S.pinnata* and *M.zapota*. The abbreviations used to denote the respective nanoparticles were - AmFZnONPs, AmRZnONPs, AmSZnONPs, SpLZnONPs and MzLZnONPs. The commercially available, chemically synthesized zinc oxide nanoparticles (denoted as 'cZnONPs') purchased from Sigma-Aldrich (USA) was used as control nanoparticles. This was found necessary to provide a strict comparative evaluation of the cellular effects of biogenic nanoparticles versus their chemically synthesized counterparts.

XRD pattern obtained for all phyto-derived ZnONPs was indexed as ZnO wurtzite hexagonal structure with a crystalline mean size of 28 ± 2 nm for AmFZnONPs, 30 ± 1.4 nm for SpLZnONPs, 31 ± 0.5 nm for MzLZnONPs, 46 ± 2.5 nm for AmRZnONPs and 61 ± 3.5 nm for AmSZnONPs. The mean size as determined for the chemically-derived cZnONPs used as controls was 48.5 ± 2.1 nm. FESEM micrographs of individual preparations of the different ZnONPs clearly depicted the discrete/embedded/particle nature of ZnONPs with an average size close to that obtained with XRD computations. The fact that each particle type displayed specific shape(s) underscored the influence of specific cocktails of phyto-derived bioreductants in shaping and tuning of the nanoparticles. Interestingly, AmSZnONPs clearly showed formations of nanostructures such as hexagonal rods which were found to be the largest in size compared to all other biosynthesized and the control nanoparticles. The elemental composition(s) of the biosynthesized and the chemical ZnONPs determined by EDX analysis confirmed their purity as evidenced by the signals emanating from elemental zinc and oxygen in which the highest percentage of atomic Zn was found to be present in SpLZnONPs. FTIR spectral analysis revealed stretching vibrations of chemical bonds assigned to the presence of Zn-O in addition to phytochemicals such as flavonoids, terpenoids, aromatic aldehydes, carboxylic acids, phenolics and proteins. The evidence for the presence of plant derived compounds involved in bio-reduction, encapsulation and stabilization of the biosynthesized ZnONPs was thus confirmed. Notably, as expected, FTIR data obtained from the chemically derived cZnONPs failed to reveal the presence of such phytoconstituents. Sharp peaks in the range of 372-384 nm were obtained in the UV-Visible (UV-Vis) absorbance profile of both types of

ZnONPs corresponding to the characteristic absorption of monodisperse zinc oxide nanoparticles. The photoluminescence (PL) spectroscopy analysis revealed emission peaks at the visible range ascertaining defects on the particle surface. High resolution transmission electron microscopy (HRTEM) reconfirmed the monodispersed, polycrystalline and nano-sized nature of both types of ZnONPs. This study thus demonstrated successful *in situ* biosynthesis of pure and crystalline ZnONPs possessing structural properties similar to that of the chemically synthesized nanoparticles. A simple sol-gel procedure, aided by suitable aqueous plant extracts and metal precursor, devoid of any perilous chemicals, was utilized in an environment-friendly manner.

Detailed investigations were carried out to elucidate the dose-dependent cellular and molecular level effects of the the phyto-derived and the chemical versions of zinc oxide nanoparticles on cancer cells such as HCT 116 colon carcinoma, A549 lung adenocarcinoma and chronic myelogenous leukemic K562 cells. Cellular cytotoxicity of the nanoparticles was evaluated by MTT assay. Of the five phyto-derived ZnONPs, three particle types - AmRZnONPs, SpLZnONPs and MzLZnONPs – displayed cytotoxicity against all the three cancer cell lines tested in the study. These particles induced a drastic increase in cytotoxicity at the 48th hour of treatment with an IC₅₀ value around 60 and 40 µg/mL. Although the control nanoparticles, cZnONPs, only showed anticancer activity against two cell lines - HCT 116 and A549, it still served as a strict control for a comparative evaluation of cytotoxicity between the biosynthesized and the chemical derivative. Inhibition of colony forming capacity was observed in all cell types treated with ZnONPs. Light microscopic examination of HCT 116 cells revealed the cytomorphological changes induced by ZnONP treatment. The changes characteristic of both the programmed apoptotic and the necroptotic cell deaths were found to occur as evidenced by massive loss of cell anchorage ('anoikis') and the presence of many extensively swollen cells. A549 and K562, however, only showed apoptotic cellular deformations. Scanning electron microscopic analysis displayed membrane cavities and cell shrinkage in all three types of cancer cells exposed to ZnONPs thereby providing ample evidential support for the occurrence of both

necroptosis and apoptosis. Fluorescence imaging of ZnONP-treated HCT 116 cells following AO/EtBr staining also provided visual confirmation of the varied cellular death programmes. Molecular analysis of the oxidative stress-mediated cellular events such as Ca^{2+} release, ROS generation, loss of mitochondrial membrane potential and externalization of phosphatidylserine in all cell types enabled a deeper insight on the overlapping biochemical pathways affected by nanoparticle treatment. Interestingly, phyto-derived SpLZnONPs were found to be relatively more effective in bringing about the above-mentioned changes in the functioning of colon and leukemic cells whilst the chemical cZnONPs displayed better activity against lung cancer cells.

ZnONP-induced variations in the cell cycle distribution of each type of cancer cell population revealed critical information on the phase-specific sub-populations (sub -G₀, G₁, S and G₂/M) including induction of cell cycle arrest. A 3-fold increase in cell fraction in G₂/M phase was observed in HCT 116 cells exposed to SpL and MzL-derived ZnONPs whilst in A549 cells, treatment with all types of ZnONPs resulted in ~2 to ~3 - fold hike in the number of cells undergoing S and G₂/M phase. However, ZnONP-treated K562 cells displayed increase only in apoptotic sub-G₀ population. Assessment of genotoxicity was based on 'comet' as well as DNA fragmentation assay. ZnONP-treated HCT 116 and K562 cells displayed comet tails indicative of DNA damage by way of strand breaks as well as apoptotic oligonucleosomal DNA fragments together with varying levels of necrotic/necroptotic DNA smearing. A549 cells failed to display any such effects. Quantification of specific transcripts by RT-qPCR technique revealed upregulation of pro-apoptotic and downregulation of anti-apoptotic genes. In HCT 116, A549 and K562 cells treated with ZnONPs showed a dose-dependent elevation in the expression of Cyt *c*, cas-9, and cas-3, genes involved in mitochondrial (intrinsic) apoptotic pathway. Interestingly, phyto-derived ZnONP-treated A549 cells also showed upregulation of caspase-8 (~3-4 folds) thereby hinting at the involvement of extrinsic pathway. The expression levels of apoptosis-related genes based on western blot analysis corroborated well with the RT-qPCR and FACS data. A dose-dependent increase in expression of cytochrome *c*, cleaved caspase-3, cleaved-

PARP substantiated activation of intrinsic mitochondrial apoptotic pathway in ZnONP-treated HCT 116 and K562 cells whereas presence of cleaved caspase-8 in phyto-derived ZnONP treated A549 cells were suggestive of the involvement of the extrinsic death pathway. A dose-dependent decrease in cyclin B1 expression was also observed in cells arrested at G₂/M phase.

The biocompatibility of phyto-derived and chemical ZnONPs was further evaluated employing normal human lymphocytes/erythrocytes and plant root-tip cell models to assess their cytotoxicity in general. The results obtained from microscopic analysis, MTT assay, Mitotic Index calculation and hemolysis demonstrated the non-toxic nature of biogenic ZnONPs. Noticeably, lymphocytes and *A. cepa* root-tip cells exposed to chemically-derived cZnONPs showed extensive cellular damage and near complete absence of metaphase chromosomes. However, erythrocytes treated with cZnONPs showed minimal hemolysis but were found to be shrunken size-wise with sharp angular membrane distortions.

A comparative evaluation of the multifaceted properties of the biosynthesized, 'green' ZnONPs and their chemical counterparts revealed that the former possessed enhanced photocatalytic, antibacterial and DNA-interactive potential. All five types of phyto-derived ZnONPs were found to be capable of photocatalytic degradation of methylene blue whilst the chemically synthesized cZnONPs, taken as control, failed to achieve a time and dose dependent degradation of the dye. The highest rate of photocatalysis was exhibited by AmS-derived ZnONPs, wherein complete dye degradation was achieved at a concentration of 200 µg/mL by 3h. Biosynthesized ZnONPs displayed potent, dose-dependent antibacterial activity against both multidrug-resistant (*K.pneumoniae* and *S. aureus*) as well as susceptible (*E.coli* and *P. aeruginosa*) clinical pathogens underscoring their 'nanobiotic' potential. Chemical control cZnONPs, on the other hand, were found to be active only against *P.aeruginosa*, that too at a very high concentration of 800 µg/mL. The results of the *in vitro* experiments on interactions of both types of nanoparticles with plasmid DNA, λ DNA and 100 bp ladder revealed distinctive properties of the biogenic ZnONPs in altering the mobility of both linear phage

DNA as well as supercoiled plasmid DNA. However, both the biogenic and the chemical versions of ZnONPs displayed partial quenching of ethidium bromide based fluorescence and band shifts of 100 bp DNA ladder. These results also reconfirm that besides the size of the particle, their surface peculiarities also confer specific characteristics. Taken together, the results of the present study highlights the multifaceted properties of ‘green’, phyto-derived zinc oxide nanoparticles, which attest to their overall superior biocompatibilities and biotherapeutics, including anticancer potential.

FUTURE PROSPECTS

The present study successfully demonstrates that many more of such explorations in tailoring the ‘green’, biocompatible nanoparticles should prove worthwhile for biological, clinical and environment-friendly applications in future. India is a tropical country blessed with more than 50000 species of plants, including those with ethnomedicinal importance, enriched with diverse phyto-constituents, which are all exploitable for green synthesis of beneficial nanoparticles. Conjugation of highly pure bioactive compounds/drugs to a variety of nanoparticles, employing combinatorial therapeutic strategies in designing novel drugs including anti-neoplastic agents, is expected to overcome the major side-effects associated with conventional pharmaceuticals. Coupled with animal models and clinical trials, validation of their drug potential should prove beneficial for future applications in the emerging field of nanomedicine.

REFERENCES

- Abdul Rahman SNSA, Wahab NA, Malek SNA (2013) *In vitro* morphological assessment of apoptosis induced by antiproliferative constituents from the rhizomes of *Curcuma zedoaria*. Evid-based Compl Alt. <https://dx.doi.org/10.1155/2013/257108>
- Abdul Wahab SM, Jantan I, Md. Haque A, Arshad L (2018) Exploring the leaves of *Annona muricata* L. as a source of potential anti-inflammatory and anticancer agents. Front Pharmacol 9: Article 661
- Ahmed M, Akhtar MJ, Siddiqui MA, Ahmad J, Mussarat J, Al-Khedhairi AA, AlSalhi MS, Alrokayan SA (2011) Oxidative stress mediated apoptosis induced by nickel ferrite nanoparticles in cultured A549 cells. Toxicology 283: 101-108
- Ahmed S, Annu, Chaudhry SA, Ikram S (2017) A review on biogenic synthesis of ZnO nanoparticles using plant extracts and microbes: A prospect towards green chemistry. J Photoch Photobio B 166: 272–284
- Akbar A, Bilal Sadiq MB, Ali I, Muhammad N, Rehman Z, Khan MN, Muhammad J, Khan SA, Rehman FU, Anal AK (2019) Synthesis and antimicrobial activity of zinc oxide nanoparticles against foodborne pathogens *Salmonella typhimurium* and *Staphylococcus aureus*. Biocatalysis and Agricultural Biotechnology 17: 36–42
- Akhtar K, Zubair N, Ikram S, Khan Zu, Khalid H (2017) Synthesis and characterization of ZnO nanostructures with varying morphology. Bull Mater Sci 40(3): 459–466
- Akhtar MJ, Ahmad M, Kumar S, Khan MAM, Ahmad J, Alrokayan SA (2012) Zinc oxide nanoparticles selectively induce apoptosis in human cancer cells through reactive oxygen species. Int J Nanomedicine 7: 845-857

- Akhter SMH, Mahmood Z, Ahmad S, Mohammad F (2018) Plant-mediated green synthesis of zinc oxide nanoparticles using *Swertia chirayita* leaf extract, characterization and its antibacterial efficacy against some common pathogenic bacteria. *BioNanoScience*. <https://doi.org/10.1007/s12668-018-0549-9>
- Aladpoosh R, Montazer M (2015) The role of cellulosic chains of cotton in biosynthesis of ZnO nanorods producing multifunctional properties: Mechanism, characterizations and features. *Carbohydr Polym* 126(1): 122-129
- Alamri SAM, Hashem M, Nafady NA, Sayed MA, Alshehri AM, and El-Shaboury GA. (2018) Controllable Biogenic Synthesis of Intracellular Silver/Silver Chloride Nanoparticles by *Meyerozyma guilliermondii* KX008616. *J. Microbiol Biotechnol* 28(6): 917–930
- Alberts B, Johnson A, Lewis J, Morgan D, Raff M, Roberts K, Walter P (2015) *Cancer. Molecular biology of the cell*, Sixth edition, published by Garland Science, Taylor & Francis Group pp 1127-1129
- Al-Dhabi NA, Arasu MV (2018) Environmentally-friendly green approach for the production of zinc oxide nanoparticles and their anti-fungal, ovicidal, and larvicidal properties. *Nanomaterials*. <https://doi:10.3390/nano8070500>
- Al-Hada NM, Saion EB, Shaari AH, Kamarudin MA, Flaifel MH, Ahmad SH, Gene SA (2014) A facile thermal- treatment route to synthesize ZnO nanosheets and effect of calcination temperature. *PLoS ONE*. <https://doi.org/10.1371/journal.pone.0103134>
- Alhadhrami A, Almalki ASA, Adam AMA, Refat MS. (2018) Preparation of semiconductor zinc oxide nanoparticles as a photocatalyst to get rid of organic dyes existing factories in exchange for reuse in suitable purpose. *Int J Electrochem Sci* 13: 6503 – 6521

- Ali J, Irshad R, Li B, Tahir K, Ahmad A, Shakeel M, Khan NU, Khan ZUH. (2018) Synthesis and characterization of phytochemical fabricated zinc oxide nanoparticles with enhanced antibacterial and catalytic applications. *J Photoch Photobio B* 183: 349–356
- Ali K, Dwivedi S, Azam A, Saquib Q, Al-Said MS, Alkhedhairy AA, Musarrat J. (2016) Aloe vera extract functionalized zinc oxide nanoparticles as nanoantibiotics against multi-drug resistant clinical bacterial isolates. *Journal of Colloid and Interface Science* 472: 145–156
- Alkaladi A, Abdelazim AM, Afifi M (2014) Antidiabetic activity of zinc oxide and silver nanoparticles on streptozotocin-induced diabetic rats. *Int J Mol Sci* 15: 2015-2023
- Alshehri AA, Malik MA (2019) Biogenic fabrication of ZnO nanoparticles using *Trigonella foenum-graecum* (Fenugreek) for proficient photocatalytic degradation of methylene blue under UV irradiation. *J Mater Sci: Mater.* <https://doi.org/10.1007/s10854-019-01985-8>
- Alves MM, Andrade SM, Grenho L, Fernandes MH, Santos C, Montemor MF (2019) Influence of apple phytochemicals in ZnO nanoparticles formation, photoluminescence and biocompatibility for biomedical applications. *Mater Sci Eng C* 101: 76–87
- Amaral RG, dos Santos SA, Andrade LN, Severino P, Carvalho AA (2019) Natural Products as Treatment against Cancer: A Historical and Current Vision. *Clin Oncol* 4: 1562
- Amatori S, Persico G, Fanelli M (2017) Real-time quantitative PCR array to study drug-induced changes of gene expression in tumor cell lines. *J Cancer Metastasis Treat* 3: 90-99
- Ambika S, Sundrarajan M (2015) Green biosynthesis of ZnO nanoparticles using *Vitex negundo* L. extract: Spectroscopic investigation of interaction between

ZnO nanoparticles and human serum albumin. *J Photochem Photobiol B* 149: 143-148

Amin ARMR, Karpowicz PA, Carey TE, Arbiser J, Nahta R, Chen ZG, Dong JT, Kucuk O, Khan GN, Huang GS, Mi S, Lee HY, Reichrath J, Honoki K, Georgakilas AG, Amedei A, Amin A, Helferich B, Boosani CS, Ciriolo MR, Chen S, Mohammed SI, Azmi AS, Keith WN, Bhakta D, Halicka D, Niccolai E, Fujii H, Aquilano K, Ashraf SS, Newsheen S, Yang X, Bilsland A, Shin DM (2015) Evasion of anti-growth signaling: A key step in tumorigenesis and potential target for treatment and prophylaxis by natural compounds. *Semin cancer biol* 35: S55–S77

Anand P, Ajaikumar BK, Sundaram C, Kuzhuvelil BH, Sheeja TT, Oiki SL, Sung B, Aggarwal BB (2008) Cancer is a Preventable Disease that Requires Major Lifestyle Changes. *Pharm Res* 25(9). [https://dx.doi: 10.1007/s11095-008-9661-9](https://dx.doi.org/10.1007/s11095-008-9661-9)

Anbuvaran M, Ramesh M, Viruthagiri G, Shanmugam N, Kannadasan N (2015) *Anisochilus carnosus* leaf extract mediated synthesis of zinc oxide nanoparticles for antibacterial and photocatalytic activities. *Mat sci semicon proc* 39: 621-628

Anbuvaran M, Ramesh M, Viruthagiri G, Shanmugam N, Kannadasan N (2015) Synthesis, characterization and photocatalytic activity of ZnO nanoparticles prepared by biological method. *Spectrochimica Acta Part A: Molecular and Biomolecular Spectroscopy* 143, 304–308

Anitha R, Ramesh KV, Ravishankar TN, Sudheer Kumar KH, Ramakrishnappa T (2018) *Journal of Science: Advanced Materials and Devices* 3: 440–451.

Anjum DH (2016) Characterization of nanomaterials with transmission electron microscopy. *IOP Conf. Series: Materials Science and Engineering*. [https://dx.doi:10.1088/1757-899X/146/1/012001](https://dx.doi.org/10.1088/1757-899X/146/1/012001)

- Ansari SA, Khan MM, Ansari MO, Lee J, Cho MH (2013) Biogenic Synthesis, Photocatalytic, and Photoelectrochemical Performance of Ag–ZnO Nanocomposite. *J Phys Chem C* 117: 27023–27030
- Antwi SO, Eckert EC, Sabaque CV, Leof ER, Hawthorne KM, Bamlet WR, Chaffee KG, Oberg AL, Petersen GM (2015) Exposure to environmental chemicals and heavy metals, and risk of pancreatic cancer. *Cancer cause control* 26(11): 1583–1591
- Aoun F, Kourie HR, Carlos A, Thierry R. (2015) Next revolution in molecular theranostics: personalized medicine for urologic cancers. *Future Oncol* 11(15) : 2205–2219
- Aquib M, Farooq MA, Filli MS, Boakye-Yiadom KO, Kesse S, Maviah MBJ, Mavlyanova R, Wang B (2019) A review on the chemotherapeutic role of fucoidan in cancer as nanomedicine. *RJLBPCS* 512-539. <https://doi.org/10.26479/2019.0501.44>
- Archana B, Manjunath K, Nagaraju G, Sekhar KBC, Kottam N (2016) Enhanced photocatalytic hydrogen generation and photostability of ZnO nanoparticles obtained via green synthesis. *Int j hydrogen energy*. [https:// doi.org/10.1016/j.ijhydene.2016.11.099](https://doi.org/10.1016/j.ijhydene.2016.11.099)
- Arciniegas-Grijalba PA, Patin˜o-Portela MC, Mosquera-Sa´nchez LP, Guerrero-Vargas JA, Rodrı´guez-Pa´ez JER. (2017) ZnO nanoparticles (ZnO-NPs) and their antifungal activity against coffee fungus *Erythricium salmonicolor*. *Appl Nanosci* 7, 225–241
- Arole VM, Munde SV (2014) Fabrication of nanomaterials by top-down and bottom-up approaches – an overview. *JAAST: Material Science* 1(2) : 89-93
- Arruebo M, Vilaboa N, S´aez-Gutierrez B, Lambea J, Tres A, Valladares M, Gonz´alez-Fern´andez A (2011) Assessment of the Evolution of Cancer Treatment Therapies. *Cancers* 3: 3279-3330

- Artioli G, Angelini I, Polla A (2008) Crystals and phase transitions in protohistoric glass materials. *Phase Transitions* 81(2-3): 233–252
- Arvanag FM, Bayrami A, Habibi-Yangjeh A, Pouran SR (2019) A comprehensive study on antidiabetic and antibacterial activities of ZnO nanoparticles biosynthesized using *Silybum marianum* L seed extract. *Mater. Sci. Eng. C* 97: 397–405
- Asani SC, Umrani RD, Paknikar KM (2016) *In vitro* studies on the pleotropic antidiabetic effects of zinc oxide nanoparticles. *Nanomedicine (Lond.)* 11(13): 1671–168
- Ascierto PA, Dummer R (2018) Immunological effects of BRAF + MEK inhibition. *Oncoimmunology*. <https://doi.org/10.1080/2162402X.2018.1468955>
- Ashraf R, Riaz S, Kayani ZN, Naseem S (2015) Effect of calcination on properties of ZnO nanoparticles. *Materials Today: Proceedings* 2: 5468 – 5472
- Asik RM, Gowdhami B, Jaabir MSM, Archunan G, Suganthi N (2019) Anticancer potential of zinc oxide nanoparticles against cervical carcinoma cells synthesized via biogenic route using aqueous extract of *Gracilaria edulis*. *Mater. Sci. Eng. C* 103: 109840
- Askarinejad A, Alavi, MA, Morsali A (2011) Sonochemically Assisted Synthesis of ZnO Nanoparticles: A Novel Direct Method. *Iran J Chem Chem Eng* 30(3): 75-81
- Astirin O, Artanti A, Fitria M, Perwitasari E, Prayitno A (2013) *Annona muricata* Linn leaf induce apoptosis in cancer cause virus. *J Cancer Ther* 4: 1244-1250
- Aswathnarayan JB, Vittal RR, Muddegowda U (2018) Anticancer activity of metal nanoparticles and their peptide conjugates against human colon adenorectal carcinoma cells. *Artif cell nanomed B* 46(7):1444-1451
- Atchudan R, Edison TNJI, Perumal S, Karthikeyan D, Lee YR (2016) Facile synthesis of zinc oxide nanoparticles decorated graphene oxide composite

via simple solvothermal route and their photocatalytic activity on methylene blue degradation. *J photoch photobio b* 162: 500–510

Attanayake AP, Jayatilaka KAPW, Pathirana C, Mudduwa LKB (2015) Toxicological investigation of *Spondias pinnata* (Linn. F.) Kurz. (Family: Anacardiaceae) bark extract in Wistar rats. *Int.J. Green Pharm.* <https://doi.org/10.4103/0973-8258.150918>

Attia H, Nounou H, Shalaby M (2018) Zinc oxide nanoparticles induced oxidative dna damage, inflammation and apoptosis in rat's brain after oral exposure. *Toxics* 6: 29

Aviello G, Canadanovic-Brunet JM, Milic N, Capasso R, Fattorusso E, Tagliatella-Scafati O, Fasolino I, Izzo AA, Borrelli F (2011) Potent Antioxidant and Genoprotective Effects of Boeravinone G, a rotenoid Isolated from *Boerhaavia diffusa*. *PLoS ONE.* <https://doi.org/10.1371/journal.pone.0019628>

Awasare S, Bhujbal S, Nanda R (2012) *In vitro* cytotoxic activity of novel oleanane type of triterpenoid saponin from stem bark of *Manilkara zapota* Linn. *Asian J Pharm Clin Res* 5: 183 - 188.

Awwad RA, Sergina N, Yang H, et al. (2003) The role of transforming growth factor alpha in determining growth factor independence. *Cancer Res* 63:4731

Azizi S, Ahmad MB, Namvar F, Mohamad R (2014) Green biosynthesis and characterization of zinc oxide nanoparticles using brown marine macroalga *Sargassum muticum* aqueous extract. *Materials Letters* 116: 275-277

Azizi S, Mohamad R, Bahadoran A, Bayat S, Abdul Rahim R, Ariff A, Saad WZ (2016) Effect of annealing temperature on antimicrobial and structural properties of biosynthesized zinc oxide nanoparticles using flower extract of *Anchusa italic*. *J Photochem Photobiol B* 161: 441-449.

- Azmina MS, Nor RM, Rafea HA, Razak NSA, Sani SFA, Osman Z (2017) Enhanced photocatalytic activity of ZnO nanoparticles grown on porous silica microparticles. *Appl Nanosci* 7: 885–892
- Babu EP, Subastri AA, Suyavaran A, Premkumar K, Sujatha VB, Aristatile B, Alshammari GA, Dharuman V, Thirunavukkarasu C (2017) Size dependent uptake and hemolytic effect of zinc oxide nanoparticles on erythrocytes and biomedical potential of ZnO-Ferulic acid conjugates. *Scientific Reports*, 7 (4203): 1-12
- Baek M, Kim MK, Cho HJ, Lee JA, Yu J, Chung HE, Choi SJ (2011) Factors influencing the cytotoxicity of zinc oxide nanoparticles: particle size and surface charge. *J Phys: Conf. Ser.* <https://doi.org/10.1088/1742-6596/304/1/012044>
- Baharudin KB, Abdullah N, Derawi D (2018) Effect of calcination temperature on the physicochemical properties of zinc oxide nanoparticles synthesized by coprecipitation. *Mater Res Express.* <https://doi.org/10.1088/2053-1591/aae243>
- Bai D-P, Zhang X-F, Zhang G-L, Huang Y-F, Gurunathan S (2017) Zinc oxide nanoparticles induce apoptosis and autophagy in human ovarian cancer cells. *Int. J. Nanomed* 12: 6521-6535
- Bai KJ, Chuang KJ, Ma CM, Chang TY, Chuang HC (2017) Human lung adenocarcinoma cells with an EGFR mutation are sensitive to non-autophagic cell death induced by zinc oxide and aluminium-doped zinc oxide Nanoparticles. *J Toxicol Sci* 42(4): 437–444
- Bai L, Zhu W. (2006) p53: structure, function and therapeutic application. *J Cancer Mol* 2(4): 141-153
- Bai L, Wang S (2014) Targeting apoptosis pathways for new cancer therapeutics. *Annu Rev Med* 65: 139-155

- Bai X, Li L, Liu H, Tan L, Liu T, Meng X (2015) Solvothermal Synthesis of ZnO Nanoparticles and Anti-Infection Application in Vivo. *ACS Appl Mater Interfaces* 7: 1308–1317.
- Bakshi S, Zakharchenko A, Minko S, Kolpashchikov DM, Katz E (2019) Towards Nanomaterials for Cancer Theranostics: A System of DNA-Modified Magnetic Nanoparticles for Detection and Suppression of RNA Marker in Cancer Cells. *Magnetochemistry*. <https://doi.org/doi:10.3390/magnetochemistry5020024>
- Balabhadrapatruni VSKC, Nepal S, Varambally S. (2016) Genomic and epigenomic alterations in cancer. *Am J Pathol* 186(7): 1724-1735
- Ballout F, Habli Z, Rahal ON, Fatfat M, Muhtasib H-G (2018) Thymoquinone-based nanotechnology for cancer therapy: promises and challenges. *Drug Discov Today*. <https://doi.org/10.1016/j.drudis.2018.01.043>
- Balraj B, Senthilkumar N, Siva C, Krithikadevi R, Julie A, Potheher et al. (2017) Synthesis and characterization of zinc oxide nanoparticles using marine *Streptomyces* sp. with its investigations on anticancer and antibacterial activity. *Res Chem Intermed* 43: 2367–2376
- Bandekar G, Rajurkar NS, Mulla IS, Mulik UP, Amalnerkar DP, Adhyapak PV (2014) Synthesis, characterization and photocatalytic activity of PVP stabilized ZnO and modified ZnO nanostructures. *Appl Nanosci* 4: 199–208.
- Barenholz Y (2012) Doxil® -The first FDA-approved nano-drug: Lessons learned. *J Control Release* 160 (2): 117-134.
- Baracca A, Sgarbi G, Solaini G, Lenaz G (2003) Rhodamine 123 as a probe of mitochondrial membrane potential: evaluation of proton flux through F₀ during ATP synthesis. *Biochimica et Biophysica Acta* 1606: 137– 146
- Barnum KJ, O’Connell MJ (2014) Cell Cycle Regulation by Checkpoints. *Methods Mol Biol* 1170: 29–40

- Barthlott W, Neinhuis C (1997) Purity of the sacred lotus, or escape from contamination in biological surfaces. *Planta* 202: 1–8
- Bashir S (2019) Pharmacological importance of *Manilkara zapota* and its bioactive constituents. *Bol Latinoam Caribe Plant Med Aromat* 18 (4): 347 – 358
- Basnet P, Chanu TI, Samanta D, Chatterjee S (2018) A review on bio-synthesized zinc oxide nanoparticles using plant extracts as reductants and stabilizing agents. *J Photochem Photobiol B* 183: 201–221
- Bayrami A, Parvinroo S, Habibi-Yangjeh A, Pouran SR (2018) Bio-extract-mediated ZnO nanoparticles: microwave-assisted synthesis, characterization and antidiabetic activity evaluation. *Artif Cells Nanomed Biotechnol* 46(4): 730-739
- Beaudouin J, Liesche C, Aschenbrenner S, Hörner M, Eils R (2013) Caspase-8 cleaves its substrates from the plasma membrane upon CD95-induced apoptosis. *Cell Death Differ* 20: 599–610
- Belay A, Bekele B, Reddy ARC (2018) Effects of Temperature and Polyvinyl Alcohol Concentrations in the Synthesis of Zinc Oxide Nanoparticles. *J Nanotechnol Material Sci* 5(1): 44-50
- Berghe TV, Linkermann A, Jouan-Lanhouet S, Walczak H, Vandenabeele P (2014) Regulated necrosis: the expanding network of non-apoptotic cell death pathways. *Nature Reviews* 10: 135-146
- Bhagyanathan NK, Thoppil JE (2016) Pre-apoptotic activity of aqueous extracts of *Cynanchum sarcomedium* Mieve & Liede on cells of *Allium cepa* and human erythrocytes. *Protoplasma* 253: 1433–1438.
- Bhar R, Kaur G, Mehta SK (2017) Experimental validation of DNA interactions with nanoparticles derived from metal coupled amphiphiles. *J Biomol Struct Dyn* [https:// doi.org/10.1080/07391102.2017.1398682](https://doi.org/10.1080/07391102.2017.1398682)

- Bhatia S, Verma N (2017) Photocatalytic activity of ZnO nanoparticles with optimization of defects. *Mater Res Bull* 95: 468-476
- Bhattacharyya A, Duraisamy P, Govindarajan M, Buhroo AA, Prasad R (2016) Nano-Biofungicides: Emerging Trend in Insect Pest Control. In: Prasad R. (eds) *Advances and Applications Through Fungal Nanobiotechnology. Fungal Biology*. Springer, Cham. 307-319
- Bhuyan T, Mishra K, Khanuja M, Prasad R, Varma A (2015) Biosynthesis of zinc oxide nanoparticles from *Azadirachta indica* for antibacterial and photocatalytic applications. *Mat Sci Semicon Proc* 32: 55-61
- Bindu P, Thomas S (2014) Estimation of lattice strain in ZnO nanoparticles: X-ray peak profile analysis. *J Theor Appl Phys* 8 (4): 123–134.
- Biplab KC, Paudel SN, Rayamajhi S, Karna D, Adhikari S, Shrestha BG, Bisht G. (2016) Enhanced preferential cytotoxicity through surface modification: synthesis, characterization and comparative in vitro evaluation of TritonX-100 modified and unmodified zinc oxide nanoparticles in human breast cancer cell (MDA-MB-231). *Chem Cent J* 10: 16
- Birge RB, Boeltz S, Kumar S, Carlson J, Wanderley J, Calianese D, Barcinski M, Brekken RA, Huang X, Hutchins JT, Freimark B, Empig C, Mercer J, Schroit AJ, Schett G, Herrmann M (2016) Phosphatidylserine is a global immunosuppressive signal in efferocytosis, infectious disease, and cancer. *Cell Death Differ* 23: 962–978
- Birusanti AB, Mallavarapu U, Nayakanti D, Espenti CS (2018) Plant-mediated ZnO nanoparticles using *Ficus racemosa* leaf extract and their characterization, antibacterial activity. *Asian J Pharm Clin Res* 11(9): 463–467
- Bisht G, Rayamajhi S (2016) ZnO nanoparticles: a promising anticancer agent. *Nanobiomedicine* 3(9):1-11

- Bitar RM, Fahmi RR, Borjac JM. (2018) *Annona muricata* extract reduces inflammation via inactivation of nalp3 inflammasome. *Journal of Natural Remedies* 19(1): 12 – 23
- Björnmalm M, Thurecht KJ, Michael M, Scott AM, Caruso F (2017) Bridging bio–nano science and cancer nanomedicine. *ACS Nano* 11: 9594-9613
- Bor G, Azmi DM, Yaghmur A (2019) Nanomedicines for cancer therapy: current status, challenges and future prospects. *Ther Deliv.* <https://doi.org/10.4155/tde-2018-0062>
- Bora NS, Kakoti BB, Gogoi B, Goswami AK (2014) Ethno-medicinal claims, phytochemistry and pharmacology of *spondias pinnata*: a review. *IJPSR* 5(4): 1138-1145.
- Brigger I, Dubernet C, Couvreur P (2012) Nanoparticles in cancer therapy and diagnosis. *Adv. Drug Deliv Rev* 64: 24-36
- Brintha SR, Ajitha M (2015) Synthesis and characterization of ZnO nanoparticles via aqueous solution, sol-gel and hydrothermal methods. *IOSR Journal of Applied Chemistry (IOSR-JAC)* 8(11): 66-72
- Brun N, Mazerolles L, Pernot M (1991) Microstructure of opaque red glass containing copper. *J Mater Sci Lett* 10: 1418–1420
- Calixto GMF, Bernegossi J, de Freitas LM, Fontana CR, Chorilli M (2016) Nanotechnology-Based Drug Delivery Systems for Photodynamic Therapy of Cancer: A Review. *Molecules.* <https://doi.org/10.3390/molecules21030342>
- Cao D, Gong S, Shu X, Zhu D, Liang S. (2019) Preparation of ZnO nanoparticles with high dispersibility based on oriented attachment (OA) process. *Nanoscale Res Lett.* <https://doi.org/10.1186/s11671-019-3038-3>
- Cao J-J, Tan C-P, Chen M-H, Wu N, Yao D-Y, Liu X-G, Ji L-N, Mao Z-W (2017) Targeting cancer cell metabolism with mitochondria-immobilized

- phosphorescent cyclometalated iridium(III) complexes. *Chem Sci* 8: 631–640
- Cao Y, Long J, Liu L, He T, Jiang L, Zhao C, Li Z (2017) A review of endoplasmic reticulum (ER) stress and nanoparticle (NP) exposure. *Life Sciences* 186: 33–42
- Cao Y, Roursgaard M, Kermanizadeh A, Loft S, Moller P (2015) Synergistic effects of zinc oxide nanoparticles and fatty acids on toxicity to Caco-2 cells. *Int J Toxicol* 34(1): 67–76
- Chamorro-Garcia A, Merkoci A (2016) Nanobiosensors in diagnostics. *Nanobiomedicine* 3: 1–26
- Chan K-S, Koh C-G, Li H-Y (2012) Mitosis-targeted anti-cancer therapies: where they stand. *Cell Death and Disease* 3: e411
- Chandra D, Liu JW, Tang DG (2002) Early mitochondrial activation and cytochrome c up-regulation during apoptosis. *J Biol Chem* 277(52): 50842–50854
- Chang Y, Moore PS, Weiss RA (2017) Human oncogenic viruses: nature and discovery. *Phil Trans R Soc B*. <https://dx.doi.org/10.1098/rstb.2016.0264>
- Chaudhary A, Kumar N, Kumar R, Salar RK (2019) Antimicrobial activity of zinc oxide nanoparticles synthesized from *Aloe vera* peel extract. *SN Applied Sciences*. <https://doi.org/10.1007/s42452-018-0144-2>
- Chaudhuri D, Ghate NB, Panja S, Basu T, Shendge AK, Mandal N (2016) Glycoside rich fraction from *Spondias pinnata* bark ameliorate iron overload induced oxidative stress and hepatic damage in Swiss albino mice. *BMC Complement Altern Med* 16: 262.
- Chaudhuri D, Ghate NB, Singh SS, Mandal N (2015) Methyl gallate isolated from *Spondias pinnata* exhibits anticancer activity against human glioblastoma by

induction of apoptosis and sustained extracellular signal regulated kinase 1/2 activation. *Pharmacogn Mag* 11(42): 269–276.

Chauhan R, Reddy A, Abraham J (2015) Biosynthesis of silver and zinc oxide nanoparticles using *Pichia fermentans* JA2 and their antimicrobial property. *Appl Nanosci*. <https://doi.org/10.1007/s13204-014-0292-7>

Chemingui H, Missaoui T, Mzali JC, Yildiz T, Konyar M, Smiri M, Saidi N, Hafiane A, Yatmaz HC (2019) Facile green synthesis of Zinc oxide nanoparticles (ZnO NPs): antibacterial and photocatalytic activities. *Mater. Res. Express*. <https://doi.org/10.1088/2053-1591/ab3cd6>

Chen G, Li S-Y, Malik HT, Ma Y-G, Xu H, Sun L-K (2016) Organic two-photon nanoparticles modulate reactive oxygen species, intracellular calcium concentration, and mitochondrial membrane potential during apoptosis of human gastric carcinoma SGC-7901 cells. *Biotechnol Lett* 38: 1269–1276

Chen W, Ouyang J, Liu H, Chen M, Zeng K, Sheng J, Liu Z, Han Y, Wang L, Li J, Deng L, Liu YN, Guo S (2017) Black phosphorus nanosheet-based drug delivery system for synergistic photodynamic/photothermal/chemotherapy of Cancer *Adv Mater* 29:1603864

Chen Y, Gao D-Y, Huang L (2015) In vivo delivery of miRNAs for cancer therapy: challenges and strategies. *Advanced Drug Delivery Reviews* 81: 128–141

Chiang MF, Chou PY, Wang WJ, Sze CI and Chang NS (2013) Tumor Suppressor WWOX and p53 Alterations and Drug Resistance in Glioblastomas. *Front Oncol*. <https://doi.org/10.3389/fonc.2013.00043>

Choudhary MK, Kataria J, Bhardwaj VK, Sharma S (2019) Green biomimetic preparation of efficient Ag–ZnO heterojunctions with excellent photocatalytic performance under solar light irradiation: a novel biogenic-deposition-precipitation approach. *Nanoscale Adv* 1: 1035–1044

Chowdhury D, Lieberman J (2008) Death by a Thousand Cuts: Granzyme Pathways of Programmed Cell Death. *Annu Rev Immunol* 26: 389–420

- Chung I-M, Rahuman AA, Marimuthu S, Kirthi AV, Anbarasan K, Rajakumar G (2015) An investigation of the cytotoxicity and caspase-mediated apoptotic effect of green synthesized zinc oxide nanoparticles using *Eclipta prostrata* on human liver carcinoma cells. *Nanomaterials* 5: 1317-1330
- Chunhui Y, Hong C, Xiuxiang M (2016) Polyphyllin D induces apoptosis and differentiation in K562 human leukemia cells. *Int Immunopharmacol* 36: 17–22
- Coleman ML, Sahai EA, Yeo M, Bosch M, Dewar A, Olson MF (2001) Membrane blebbing during apoptosis results from caspase-mediated activation of ROCK I *Nature Cell Biology* 3: 339-345
- Colomban P, Gouadec G (2005) The ideal ceramic fiber/oxide matrix composite : how to conciliate antagonist physical and chemical requirements ?. *Ann Chim Sci Mater* 30 (6): 1-16
- Cook JW, Hewett CL, Hieger I (1933) The isolation of a cancer-producing hydrocarbon from coal tar. Parts I, II, and III. *J Chem Soc (Resumed)* 395–405
- Cooper JR, Abdullatif MB, Burnett EC, Kempbell KE, Conforti F, Tolley H, Collins JE, Davies DE (2016) Long term culture of the A549 cancer cell line promotes multilamellar body formation and differentiation towards an alveolar type II pneumocyte phenotype. *PLoS One* <https://doi.org/10.1371/journal.pone.0164438>
- Cortez AP, Menezes EGP, Benfica PL, Santos AP, Cleres LM, Ribeiro HO, Lima EM, Kato MJ, Valadares MC (2017) Grandisin induces apoptosis in leukemic K562 cells. *Brazilian Journal of Pharmaceutical Sciences* 53(1):1-9.
- Cragg GM, Pezzuto JM (2016) Natural products as a vital source for the discovery of cancer chemotherapeutic and chemopreventive agents. *Med Princ Pract* 25(2): 41–59

- Ćurčić MG, Stanković MS, Mrkalić EM, Matović ZD, Banković DD, Cvetković DM, Đačić DS, Marković SD (2012) Antiproliferative and proapoptotic activities of methanolic extracts from *Ligustrum vulgare* L. as an individual treatment and in combination with palladium complex. *Int J Mol Sci* 13: 2521-2534
- Curigliano G, Criscitiello C (2014) Successes and Limitations of Targeted Cancer Therapy in Breast Cancer. *Prog Tumor Res* 41: 15–35
- da Silva BL, Caetano BL, Chiari-Andr'eo BG, Pietro RCLR, Chiavacci LA (2019) Increased antibacterial activity of zno nanoparticles: influence of size and surface modification. *Colloids and Surfaces B: Biointerfaces* <https://doi.org/10.1016/j.colsurfb.2019.02.013>
- Damyanov CA, Maslev IK, Pavlov VS, Avramov L (2018) Conventional Treatment of Cancer Realities and Problems. *Annals of Complementary and Alternative* 1(1): Article 1002.
- Danks AE, Hall SR, Schnepf Z (2016) The evolution of 'sol-gel' chemistry as a technique for materials synthesis. *Mater Horiz* 3: 91-112
- Darroudi M, Sabouri Z, Oskuee RK, Zak AK, Kargar H, Hamid MHNAH (2013) Sol-gel synthesis, characterization and neurotoxicity effect of zinc oxide nanoparticles using *gum tragacanth*. *Ceram Int* 39: 9195–9199
- Das J, Mannan A, Md. Rahman M, Md. Dinar AM, Uddin ME, Khan IN, Md. Habib R, Hasan N (2011) Chloroform and ethanol extract of *Spondias pinnata* and its different pharmacological activity like- antioxidant, cytotoxic, antibacterial potential and phytochemical screening through in-vitro method. *Int j pharm biomed res* 2(4):1805 – 1812
- Das MP, Rebecca LJ (2017) Evaluation of antibacterial efficacy of biogenic zinc oxide nanoparticles on cotton fabrics. *J Pharm Sci & Res* 9(12): 2553-2557

- Das S, Chakraborty J, Chatterjee S, Kumar H (2018) Prospects of biosynthesized nanomaterials for the remediation of organic and inorganic environmental contaminants. *Environ Sci: Nano* 5: 2784-2808
- Das S, Chakraborty T (2018) A review on green synthesis of silver nanoparticle and zinc oxide nanoparticle from different plants extract and their antibacterial activity against multi-drug resistant bacteria. *JIPBS* 5(4): 63-73
- Das S, Chatterjee S, Pramanik S, Devi PS, Kumar GS. (2018) A new insight into the interaction of ZnO with calf thymus DNA through surface defects. *J Photochem Photobiol B* 178: 339–347
- Das D, Nath BC, Phukon P, Kalita A, and Dolui SK (2013) Synthesis of ZnO nanoparticles and evaluation of antioxidant and cytotoxic activity. *Colloids Surf B Biointerfaces* 111:556-560.
- Dasgupta N, Ranjan S, Ramalingam C (2017) Applications of nanotechnology in agriculture and water quality management. *Environ Chem Lett* 15: 591–605
- Davar F, Majedi A, Mirzaei A (2015) Green synthesis of ZnO nanoparticles and its application in the degradation of some dyes. *J Am Ceram Soc* 98: 1739–1746
- Davis M, Whittaker A, Lindgren M, Djerf-Pierre M, Manderson L, Flowers P (2018) Understanding media publics and the antimicrobial resistance crisis. *Glob. Public Health* 13: 1158–1168
- De Angelis I, Barone F, Zijno A, Bizzari L, Russo MT, Pozzi R, Franchini F, Giudetti G, Uboldi C, Pondi J, Rossi F, De Berardis B (2013) Comparative study of ZnO and TiO₂ nanoparticles: physicochemical characterization and toxicological effects on human colon carcinoma cells. *Nanotoxicology* 7(8): 1361–1372.
- de Sousa OV, Vieira GD, de Jesus RG, de Pinho J, Yamamoto CH, Alves MS (2010) Antinociceptive and anti-inflammatory activities of the ethanol

- extract of *Annona muricata* L. leaves in animal models. *Int J Mol Sci* 11: 2067-78.
- Demicheli R, Retsky MW, Hrushesky WJM, Baum M, Gukas ID (2008) The effects of surgery on tumor growth: a century of investigations. *Annals of Oncology* 19: 1821–1828.
- Deng Y, Zhang H (2013) The synergistic effect and mechanism of doxorubicin-ZnO nanocomplexes as a multimodal agent integrating diverse anticancer therapeutics. *International Journal of Nanomedicine* 8: 1835–1841.
- Dhandapani P, Siddarth AS, Kamalasekaran S, Maruthamuthu S, Rajagopal G (2014) Bio-approach: ureolytic bacteria mediated synthesis of ZnO nanocrystals on cotton fabric and evaluation of their antibacterial properties *Carbohydr. Polym* 103: 448–455
- Dhivya R, Ranjani J, Bowen PK, Rajendhran J, Mayandi J, Annaraj (2017) Biocompatible curcumin loaded PMMA-PEG/ZnO nanocomposite induce apoptosis and cytotoxicity in human gastric cancer cells. *Materials Science and Engineering: C* 80: 59–68.
- Dhivya R, Ranjani J, Rajendhran J, Mayandi J, Annaraj J (2018) Enhancing the anti-gastric cancer activity of curcumin with biocompatible and pH sensitive PMMA-AA/ZnO nanoparticles. *Materials Science and Engineering: C* 82: 182–189.
- Ding Y, He C, Lu S, Wang X, Wang C, Wang L, Zhang J, Piao M, Chi G, Luo Y, Sai K, Ge P (2019) MLKL contributes to shikonin-induced glioma cell necroptosis via promotion of chromatinolysis. *Cancer Letters*, 467, 58–71.
- Ding Y, Wang ZL. (2009) Structures of planar defects in ZnO nanobelts and nanowires. *Micron* 40, 335–342
- Djurišić AB, Leung YH, Ng AMC. (2014) Strategies for improving the efficiency of semiconductor metal oxide photocatalysis. *Mater. Horiz.*, DOI: 10.1039/c4mh00031e

- Dobrucka R, Długaszewska J, Kaczmarek M. (2018) Cytotoxic and antimicrobial effects of biosynthesized ZnO nanoparticles using of *Chelidonium majus* extract. *Biomed Microdevices*, 20, 5.
- Dobrucka R, Długaszewska J. (2016) Biosynthesis and antibacterial activity of ZnO nanoparticles using *Trifolium pratense* flower extract. *Saudi J Biol Sci* 23: 517–523
- Dorostkar R, Ghalavand M, Nazarizadeh A, Tat M, Hashemzadeh MS (2017) Anthelmintic effects of zinc oxide and iron oxide nanoparticles against *Toxocara vitulorum*. *Int Nano Lett* 7: 157–164
- Dorrnian D, Solati E, Dejam L (2012) Photoluminescence of ZnO nanoparticles generated by laser ablation in deionized water. *Appl Phys A* 109:307–314
- Drexler HG (2000) *The leukemia-lymphoma cell line facts book*, San Diego: Academic Press
- Du H, Che G. (2017) Genetic alterations and epigenetic alterations of cancer-associated fibroblasts (Review). *Oncology letters* 13: 3–12.
- Duraimurugan J, Suresh Kumar G, Maadeswaran P, Shanavas S, Anbarasan PM, Vasudevan V (2018) Structural, optical and photocatalytic properties of zinc oxide nanoparticles obtained by simple plant extract mediated synthesis. *J Mater Sci: Mater Electron*. <https://doi.org/10.1007/s10854-018-0466-2>
- Ebadi M, Zolfaghari MR, Aghaei SS, Zargar M, Shafiei M, Zahiri HS, Noghabi KA (2019) A bio-inspired strategy for the synthesis of zinc oxide nanoparticles (ZnO NPs) using the cell extract of cyanobacterium *Nostoc* sp. EA03: from biological function to toxicity evaluation. *RSC Adv* 9: 23508–23525
- Elamin N, Elsanousi A (2013) Synthesis of ZnO nanostructures and their photocatalytic activity. *Journal of Applied and Industrial Sciences* 1(1): 32-35

- Elmore S (2007) Apoptosis: a review of programmed cell death. *Toxicol Pathol.* 35(4): 495–516
- Elsayed EM, Shalan AE, Rashad MM (2014) Preparation of ZnO nanoparticles using electrodeposition and co-precipitation techniques for dye-sensitized solar cells applications. *J Mater Sci: Mater Electron* 25: 3412–3419
- Elumalai K, Velmurugan S, Ravi S, Kathiravan V, Ashokkumar S (2015) Green synthesis of zinc oxide nanoparticles using *Moringa oleifera* leaf extract and evaluation of its antimicrobial activity. *Spectrochimica Acta Part A: Molecular and Biomolecular Spectroscopy* 143: 158–164
- Elumalai K, Velmurugan S (2015) Green synthesis, characterization and antimicrobial activities of zinc oxide nanoparticles from the leaf extract of *Azadirachta indica*. *Appl Surf Sci* 345: 329–336
- Eruslanov E, Kusmartsev S (2009) Identification of ROS Using Oxidized DCFDA and Flow-Cytometry. *Advanced Protocols in Oxidative Stress II, Methods in Molecular Biology*. https://doi.org/10.1007/978-1-60761-411-1_4
- Esteban-Tejeda L, Prado C, Cabal B, Sanz J, Torrecillas R, Moya JS (2015) Antibacterial and Antifungal Activity of ZnO Containing Glasses. *PLoS ONE* 10(7): e0132709. <https://doi.org/10.1371/journal.pone.0132709>
- Evans AC, Thadani NN, Suh J (2016) Biocomputing nanoplatforms as therapeutics and diagnostics. *J Control Release* 28(240): 387–393
- Ezealisiji KM, Siwe-Noundou X, Maduelosi B, Nwachukwu N, Krause RWM (2019) Green synthesis of zinc oxide nanoparticles using *Solanum torvum* (L) leaf extract and evaluation of the toxicological profile of the ZnO nanoparticles–hydrogel composite in Wistar albino rats. *International Nano Letters* 9: 99–107
- Fadaka A, Ajiboye B, Ojo O, Adewale O, Olayide I, Emuowhochere R (2017) Biology of glucose metabolism in cancer cells. *Journal of Oncological Sciences* 3: 45-51

- Fakhari S, Jamzad M, Fard HK (2019) Green synthesis of zinc oxide nanoparticles: a comparison. *Green Chemistry Letters and Reviews* 12(1): 19-24
- Fan B, Shi S, Shen X, Yang X, Liu N, Wu G, Guo X, Huang N (2019) Effect of HMGN2 on proliferation and apoptosis of MCF-7 breast cancer cells. *Oncology Letters* 17: 1160-1166
- Fang X, Jiang L, Gong Y, Li J, Liu L, Cao Y (2017) The presence of oleate stabilized ZnO nanoparticles (NPs) and reduced the toxicity of aged NPs to Caco-2 and HepG2 cells. *Chemico-Biological Interactions* 278: 40–47.
- Farasat M, Niazvand F, Khorsandi L (2019) Zinc oxide nanoparticles induce necroptosis and inhibit autophagy in MCF-7 human breast cancer cells. *Biologia*. <https://doi.org/10.2478/s11756-019-00325-9>
- Farouk F, Shebl RI (2018) Comparing surface chemical modifications of zinc oxide nanoparticles for modulating their antiviral activity against Herpes simplex virus type-1. *Int J Nanoparticles Nanotech* 4. ISSN: 2631-5084
- Fatin SO, Lim HN, Tan WT, Huang NM (2012) comparison of photocatalytic activity and cyclic voltammetry of zinc oxide and titanium dioxide nanoparticles toward degradation of methylene blue. *Int. J. Electrochem. Sci.* 7: 9074- 9084
- Fawcett D, Verduin JJ, Shah M, Sharma SB, Poinern GEJ (2017) A review of current research into the biogenic synthesis of metal and metal oxide nanoparticles via marine algae and seagrasses. *Journal of Nanoscience*. <https://doi.org/10.1155/2017/8013850>
- Fayek NM, Azza R, Monem A, Mossa MY, Meselhy MR, Shazly AH (2012). Chemical and biological study of *Manilkara zapota* (L.) Van Royen leaves (*Sapotaceae*) cultivated in Egypt. *Phcog Res* 4: 85 - 91.
- Federal Drug Administration: USA, 2011; Considering whether an FDA-regulated product involves the application of nanotechnology. <https://www.fda.gov/RegulatoryInformation/Guidances/ucm257698.html>

- Feitelson MA, Arzumanyan A, Kulathinal RJ, Blain SW, Holcombe RF, Mahajna J, Marino M, Martinez-Chantar ML, Nawroth R, Sanchez-Garcia I, Sharma D, Saxena NK, Singh N, Vlachostergios PJ, Guo S, Honoki K, Fujii H, Georgakilas AG, Bilsland A, Amedei A, Niccolai E, Amin A, Ashraf SS, Boosani CS, Guha G, Ciriolo MR, Aquilano K, Chen S, Mohammed SI, Azmi AS, Bhakta D, Halicka D, Keith WN, Nowsheen S (2015) Sustained proliferation in cancer: Mechanisms and novel therapeutic targets. *Seminars in Cancer Biology* 35: 25–54
- Ferreira AJ, Cemlyn-Jones J, Cordeiro CR (2013) Nanoparticles, nanotechnology and pulmonary nanotoxicology. *Rev Port Pneumol* 19(1): 28–37
- Ferreira L, Castro P, Chagas A, Franca S, Beleboni R (2013) In vitro anthelmintic activity of aqueous leaf extract of *Annona muricata* L. (Annonaceae) against *Haemonchus contortus* from sheep. *Exp. Parasitol* 134:327-332.
- Filho RAE, Nicolas A, Castro TLDP, Deplanche M, Azevedo VADC, Goossens PL, Taieb FT, Gerard Lina G, Loir YL, Berkova N (2017) Heterogeneous family of cyclomodulins: smart weapons that allow bacteria to hijack the eukaryotic cell cycle and promote infections. *Front. Cell. Infect. Microbiol.* <https://doi.org/10.3389/fcimb.2017.00208>
- Florento L, Matias R, Tuaño E, Santiago K, Cruz Fd, Tuazon A (2012) Comparison of cytotoxic activity of anticancer drugs against various human tumor cell lines using *in vitro* cell-based approach. *Int J Biomed Sci* 8(1): 76-80
- Folorunso A , Akintelu S, Oyebamiji AK , Ajayi S, Abiola B, Abdusalam I, Morakinyo A (2019) Biosynthesis, characterization and antimicrobial activity of gold nanoparticles from leaf extracts of *Annona muricata*. *Journal of Nanostructure in Chemistry* 9: 111–117
- Foo KL, Hashim U, Voon CH, Kashif M, Ali ME (2015) Au decorated ZnO thin film: application to DNA sensing. *Microsyst Technol.* <https://doi.org/10.1007/s00542-015-2572-x>

- Fowsiya J, Asharani IV, Mohapatra S, Eshapula A, Mohi P, Thakar N, Monad S, Madhumitha G (2019) *Aegle marmelos* phytochemical stabilized synthesis and characterization of ZnO nanoparticles and their role against agriculture and food pathogen. *Green Process Synth* 8: 488–495
- Franken NAP, Rodermond HM, Stap J, Haveman J, van Bree C (2006) Clonogenic assay of cells *in vitro*. *Nat Protoc* 1(5):2315-9.
- Frisch SM, Francis H (1994) Disruption of epithelial cell-matrix interactions induces apoptosis. *The Journal of Cell Biology* 124(4): 619-626.
- Fu L, Fu Z (2015) *Plectranthus amboinicus* leaf extract–assisted biosynthesis of ZnO nanoparticles and their photocatalytic activity. *Ceramics International* 41(2A): 2492-2496
- Gajbhiye S, Sakharwade S (2016) Silver nanoparticles in cosmetics. *Journal of Cosmetics, Dermatological Sciences and Applications* 6: 48-53
- Galstyan V, Comini E, Ponzoni A, Sberveglieri V, Sberveglieri G (2016) ZnO Quasi-1D nanostructures: synthesis, modeling and properties for applications in conductometric chemical sensors chemosensors 4(6): 1–21
- Gandhi L, Rodriguez-Abreu D, Gadgeel S, Esteban E, Felip E, De Angelis F, Domine M, Clingan P, Hochmair MJ, Powell SF, Cheng SYS, Bischoff HG, Peled N, Grossi F, Jennens RR, Reck M, Hui R, Garon EB, Boyer M, Rubio-Viqueira B, Novello S, Kurata T, Gray JE, Vida J, Wei Z, Yang J, Raftopoulos H, Pietanza MC, Garassino MC (2018) Pembrolizumab plus Chemotherapy in Metastatic Non–Small-Cell Lung Cancer. *N Engl J Med* <https://doi.org/10.1056/NEJMoa1801005>
- Ganguly A, Al Mahmud Z, Nasir Uddin MM, Rahman SMA (2013). *In-vivo* anti-inflammatory and anti-pyretic activities of *Manilkara zapota* leaves in albino Wistar rats. *Asian Pac J Trop Dis* 3 : 301 - 307

- Ganguly A, Al Mahmud Z, Saha SK, Rahman SMA. (2016) Evaluation of antinociceptive and antidiarrhoeal properties of *Manilkara zapota* leaves in Swiss albino mice. *Pharm Biol* 54 : 1413 - 1419
- Gao F, Ma N, Zhou H, Wang Q, Zhang H, Wang P, Hou H, Wen H, Li L (2016) Zinc oxide nanoparticles-induced epigenetic change and G2/M arrest are associated with apoptosis in human epidermal keratinocytes. *International Journal of Nanomedicine* 11: 3859–3874
- Gavamukulya Y, Maina EN, Meroka AM, Madivoli ES, El-Shemy HA, Wamunyokoli F, Magoma G (2019) Green Synthesis and Characterization of Highly Stable Silver Nanoparticles from Ethanolic Extracts of Fruits of *Annona muricata*. *Journal of Inorganic and Organometallic Polymers and Materials*. <https://doi.org/10.1007/s10904-019-01262-5>.
- Geetha R, Ashokkumar T, Tamilselvan S, Govindaraju K, Sadiq M, Singaravelu G (2013) Green synthesis of gold nanoparticles and their anticancer activity. *Cancer nano* 4: 91-98
- Gehrke I, Geiser A, Somborn-Schulz A (2015) Innovations in nanotechnology for water treatment. *Nanotechnology, Science and Applications* 8: 1–17
- George BPA, Abrahamse H. (2016) A review on novel breast cancer therapies: photodynamic therapy and plant derived agent induced cell death mechanisms. *Anti-Cancer Agents in Medicinal Chemistry* 16: 793-801
- Ghasemzadeh A, Bivalacqua TJ, Hahn NM, Drake CG (2015) New strategies in bladder cancer: a second coming for immunotherapy. *Clin Cancer Res* 22(4): 793-801
- Ghosh D, Venkataramani P, Nandi S, Bhattacharjee S (2019) CRISPR–Cas9 a boon or bane: the bumpy road ahead to cancer therapeutics. *Cancer Cell Int* 19:12
- Ghosh M, Jana A, Sinha S, Jothiramajayam M, Nag A, Chakraborty, Mukherjee A, Mukherjee A (2016) Effect of ZnO nanoparticles in plants: Cytotoxicity,

genotoxicity, deregulation of antioxidant defenses and cell cycle arrest. *Mutat res-gen tox en* 807: 25-32

Giard DJ, Aaronson SA, Todaro GJ, Arnstein P, Kersey JH, Dosik H, Parks WP (1973) In vitro cultivation of human tumors: establishment of cell lines derived from a series of solid tumors. *Journal of the National Cancer Institute* 51(5): 1417–1423

Gnanasangeetha D, SaralaThambavani D (2014) Biogenic production of Zinc oxide nanoparticles using *Acalypha indica*. *Journal of Chemical, Biological and Physical Sciences* 4(1): 238-246

Goldstein MR, Mascitelli L. (2011) Surgery and cancer promotion: are we trading beauty for Cancer? *Q J Med* 104: 811–815

Golsheikh AM, Kamali KZ, Huang NM, Zak AK. (2018) Effect of calcination temperature on performance of ZnO nanoparticles for dye-sensitized solar cells. *Powder Technology* 329: 282–287

Gou Y, Miao D, Zhou M, Wang L, Zhou H and Su G (2018) Bio-inspired protein-based nanoformulations for cancer theranostics. *Front Pharmacol* <https://doi.org/10.3389/fphar.2018.00421>

Gregersen LH, Jacobsen AB, Frankel LB, Wen J, Krogh A, Lund AH (2010) MicroRNA-145 targets YES and STAT1 in colon cancer cells. *PLoS One* 21 5(1):e8836. <https://doi.org/10.1371/journal.pone.0008836>.

Grossman HJ, McNeil SE (2012) Nanotechnology in cancer medicine. *ACS Nano* 4(10): 5641-5646.

Gu C, Wilson MSC, Jessen HJ, Saiardi A, Shears SB (2016) Inositol pyrophosphate profiling of two HCT 116 cell lines uncovers variation in InsP₈ levels. *PLoS One*. <https://doi.org/10.1371/journal.pone.0165286>

Guan X (2015) Cancer metastases: challenges and opportunities *Acta Pharmaceutica Sinica B* 5(5): 402–418

- Guerra FD, Attia MF, Whitehead DC, Alexis F (2018) Nanotechnology for environmental remediation: materials and applications. *Molecules*. <https://doi.org/10.3390/molecules23071760>
- Guha D, Saha T, Bose S, Chakraborty S, Dhar S, Khan P, Adhikary A, Das T, Sa G (2019) Integrin-EGFR interaction regulates anoikis resistance in colon cancer cells. *Apoptosis*. <https://doi.org/10.1007/s10495-019-01573-5>
- Gümüř D, Berber AA, Ada K, Aksoy H (2014) *In vitro* genotoxic effects of ZnO nanomaterials in human peripheral lymphocytes. *Cytotechnology*, 66: 317-325.
- Gunalan S, Sivaraj R, Rajendran V (2012) Green synthesized ZnO nanoparticles against bacterial and fungal pathogens. *Progress in Natural Science: Materials International* 22(6): 693–700
- Guo D, Bi H, Wang D, Wu Q (2013) Zinc oxide nanoparticles decrease the expression and activity of plasma membrane calcium ATPase, disrupt the intracellular calcium homeostasis in rat retinal ganglion cells. *The International Journal of Biochemistry & Cell Biology* 45(8): 1849–1859
- Guo J, Peng C (2014) Synthesis of ZnO nanoparticles with a novel combustion method and their C₂H₅OH gas sensing properties. *Ceramics International* 41: 2180–2186
- Guo KW (2017) Property of zinc oxide (ZnO) nanostructures potential for biomedical system and its common growth mechanism. *J Appl Biotechnol Bioeng* 2(5):197–202
- Gupta M, Tomar RS, Kaushik S, Mishra RK, Sharma D (2018) Effective antimicrobial activity of green ZnO nano particles of *Catharanthus roseus*. *Front Microbiol*. <https://doi.org/10.3389/fmicb.2018.02030>

- Haas BK, Osborne CRC, Vukelja SJ, Selman J, Davis T, Kimmel GT (2019) Effect of exercise during adjuvant chemotherapy for breast cancer. *Journal of clinical oncology* 37(15): 6524-6524
- Habib SS (2009) Synthesis of ZnO nanoparticles using Ball milling method. *Material Science Research India* 6(1): 79-82
- Hamdy FC, Donovan JL, Lane JA, Mason M, Metcalfe C, Holding P, Davis M, Peters TJ, Turner EL, Martin RM, Oxley J, Robinson M, Staffurth J, Walsh E, Bollina P, Catto J, Doble A, Doherty A, Gillatt D, Kockelbergh R, Kynaston H, Paul A, Powell P, Prescott S, Rosario DJ, Rowe E, Neal DE. (2016) 10-Year Outcomes after Monitoring, Surgery, or Radiotherapy for Localized Prostate Cancer. *N Engl J Med* DOI: 10.1056/NEJMoa1606220
- Hamed AR, Abdel-Azim NS, Shams KA, Hammouda FM. (2019) Targeting multidrug resistance in cancer by natural chemosensitizers. *Bulletin of the National Research Centre*. <https://doi.org/10.1186/s42269-019-0043-8>
- Hamizah S, Roslida AH, Fezah O, Tan KL, Tor YS, Tan CI (2012) Chemopreventive potential of *Annona muricata* L leaves on chemically-induced skin papillomagenesis in mice. *Asian Pac J Cancer Prev* 13: 2533-9.
- Han B-I, Lee M (2015) Paclitaxel-induced G2/M arrest via different mechanism of actions in glioma cell lines with differing p53 mutational status. *International Journal of Pharmacology* 12: 19-27.
- Han J, Su H, Xu J, Song W, Gu Y, Chen Y, Moon W-J, Zhang D (2012) Silk mediated synthesis and modification of photoluminescent ZnO nanoparticles. *Journal of Nanoparticle Research* 14(2): 726
- Han Q, Ma Y, Wang H, Dai Y, Chen C, Liu Y, Jing L, Sun X (2018) Resibufogenin suppresses colorectal cancer growth and metastasis through RIP3-mediated necroptosis. *16: 201.*

- Han B, Wang TD, Shen SM, Yu Y, Mao C, Yao ZJ, Wang LS (2015), Annonaceous acetogenin mimic AA005 induces cancer cell death via apoptosis inducing factor through a caspase -3- independent mechanisms. BMC Cancer 15:139
- Hanahan D, Weinberg RA (2000) The hallmarks of cancer. Cell 100: 57–70
- Hanahan D, Weinberg RA (2011) Hallmarks of Cancer: The next generation. Cell 144: 646-676.
- Happy A, Soumya M, Kumar SV, Rajeshkumar S, Sheba RD, Lakshmi T, Nallaswamy VD (2019) Phyto-assisted synthesis of zinc oxide nanoparticles using *Cassia alata* and its antibacterial activity against *Escherichia coli*. Biochemistry and Biophysics Reports 17: 208–211
- Haque S, Md S , Fazil M, Kumar M, Sahni JK , Ali J, Baboota S (2012) Venlafaxine loaded chitosan NPs for brain targeting: Pharmacokinetic and pharmacodynamic evaluation. Carbohydrate Polymers 89: 72– 79
- Hare JJ, Lammers T, Ashford MB, Puri S, Storm G, Barry ST (2017) Challenges and strategies in anti-cancer nanomedicine development: An industry perspective. Advanced Drug Delivery Reviews 108: 25–38
- Harifi T, Montazer M (2015) Application of nanotechnology in sports clothing and flooring for enhanced sport activities, performance, efficiency and comfort: a review. Journal of Industrial Textiles. <https://doi.dx/10.1177/1528083715601512>
- Hariharan R, Senthilkumar S, Suganthi A, Rajarajan M (2012) Synthesis and characterization of doxorubicin modified ZnO/PEG nanomaterials and its photodynamic action. Journal of Photochemistry and Photobiology B: Biology 116: 56–65.
- Hattori N, Yamada S, Torii K, Takeda S, Nakamura K, Tanaka H, Kajiyama H, Kanda M, Fujii T, Nakayama G, Sugimoto H, Koike M, Nomoto S, Fujiwara

- M, Mizuno M, Hori M, Kodera Y (2015) Effectiveness of plasma treatment on pancreatic cancer cells. *International Journal Of Oncology* 47: 1655-1662
- Haun F, Neumann S, Peintner L, Wieland K, Habicht J, Schwan C, Østevold K, Koczorowska MM, Binossek M, Kist M, Busch H, Boerries M, Davis RJ, Maurer U, Schilling O, Aktories K, Borner C (2018) Identification of a novel anoikis signalling pathway using the fungal virulence factor gliotoxin. *Nature Communications* 9: 3524
- Hazra C, Kundu D, Chaudhari A, Jana T (2012) Biogenic synthesis, characterization, toxicity and photocatalysis of zinc sulfide nanoparticles using rhamnolipids from *Pseudomonas aeruginosa* BS01 as capping and stabilizing agent. *J Chem Technol Biotechnol* 88: 1039–1048
- He L, Liu Y, Mustapha A, Lin M (2011) Antifungal activity of zinc oxide nanoparticles against *Botrytis cinerea* and *Penicillium expansum*. *Microbiological Research* 166: 207—215
- Health effects test guidelines (1998), United States Environmental Protection Agency. Prevention, Pesticides and Toxic Substances (7101), EPA 712-C-98-223
- Heiligtag FJ, Niederberger M (2013) The fascinating world of nanoparticle research. *Materials Today* 16(7/8): 262-271
- Helfinger V, Schröder K. (2018) Redox control in cancer development and progression. *Molecular Aspects of Medicine* 63: 88–98
- Hernández-Vargas H, Palacios, J Moreno-Bueno G (2007) Molecular profiling of docetaxel cytotoxicity in breast cancer cells: uncoupling of aberrant mitosis and apoptosis. *Oncogene*, 26: 2902–2913
- Hessler JA, Budor A, Putchakayala K, Mecke A, Rieger D, Holl MMB, Orr BG (2005) Atomic force microscopy study of early morphological changes during apoptosis. *Langmuir* 21: 9280-9286

- Hientz K, Mohr A, Bhakta-Guha D, Efferth T. (2016) The role of p53 in cancer drug resistance and targeted chemotherapy. *Oncotarget* 8(5), 8921-8946
- Hiremath S, Vidya C, Antonyraj MAL, Chandraprabha MN, Gandhi P, Jain A, Anand K. Biosynthesis of ZnO nano particles assisted by *Euphorbia tirucalli* (Pencil Cactus) (2013). *International Journal of Current Engineering and Technology* (special issue 1) 176-179
- Hodi FS, O'Day SJ, McDermott DF, Weber RW, Sosman JA, Haanen JB, Gonzalez R, Robert C, Schadendorf D, Hassel JC, Akerley W, van den Eertwegh AJ, Lutzky J, Lorigan P, Vaubel JM, Linette GP, Hogg D, Ottensmeier CH, Lebbé C, Peschel C, Quirt I, Clark JI, Wolchok JD, Weber JS, Tian J, Yellin MJ, Nichol GM, Hoos A, Urba WJ (2010) Improved survival with ipilimumab in patients with metastatic melanoma. *N Engl J Med* 363: 711–723
- Hofseth LJ, Hussain SP, Harris CC (2004) p53: 25 years after its discovery. *Trends Pharmacol Sci.* 25(4): 177-181
- Hong H, Wang F, Zhang Y, Graves SA, Eddine SBZ, Yang Y, Theuer CP, Nickles RJ, Wang X, Cai W (2015) Red fluorescent Zinc oxide nanoparticle: A novel platform for cancer targeting. *ACS Appl Mater Interfaces* <https://doi.org/10.1021/am508440j>
- Hong SN (2018) Genetic and epigenetic alterations of colorectal cancer. *Intest Res* 16(3): 327-337
- Hongmei Z (2012) Extrinsic and Intrinsic Apoptosis Signal Pathway Review. *Apoptosis and Medicine*. <https://dx.doi.org/10.5772/50129>.
- Horie M, Fujita K (2011) Chapter four-toxicity of metal oxides nanoparticles. *Adv. Mol. Toxicol*, 5:145-178
- Hossain H, Howlader MSI, Dey SK, Hira A, Ahmed A (2012) Antinociceptive and antidiarrheal properties of the ethanolic extract of *Manilkara zapota* (Linn.) bark. *Int J Pharm Sci Res* 3: 4791 - 4795

- Hosseinahli N, Aghapour M, Duijf PHG, Baradaran B (2018) Treating cancer with microRNA replacement therapy: a literature review. *Journal of Cellular Physiology* 233(8): 5574–5588
- Howell GM, Humphrey LE, Ziober BL, Awwad R, Periyasamy B, Koterba A, Li W, Willson JK, Coleman K, Carboni J, Lynch M, Brattain MG (1998) Regulation of transforming growth factor alpha expression in a growth factor-independent cell line. *Mol Cell Biol* 18(1): 303-313
- Hu D, Si W, Qin W, Jiao J, Li XL, Gu XP, Hao YF (2019) *Cucurbita pepo* leaf extract induced synthesis of zinc oxide nanoparticles, characterization for the treatment of femoral fracture, *Journal of Photochemistry & Photobiology, B: Biology*. <https://doi.org/10.1016/j.jphotobiol.2019.04.001>
- Hu Q, Li H, Wang L, Gu H, Fan C (2019) DNA nanotechnology-enabled drug delivery systems. *Chem. Rev.* 119: 6459–6506
- Huang, X., Schwind, S., Yu, B., Santhanam, R., Wang, H., Hoellerbauer, P., Mims A, Klisovic R, Walker AR, Chan KK, Blum W, Perrotti D, Byrd JC, Bloomfield CD, Caligiuri MA, Lee RJ, Garzon R, Muthusamy N, Lee LJ, Marcucci, G (2013) Targeted delivery of microRNA-29b by transferrin-conjugated anionic lipopolyplex nanoparticles: A novel therapeutic strategy in acute myeloid leukemia. *Clinical Cancer Research*, 19(9): 2355–2367
- Hussain A, Oves M, Alajmi MF, Hussain I, Amir S, Ahmed J, Rehman MT, El-Seedi HR, Ali I (2019) Biogenesis of ZnO nanoparticles using *Pandanus odorifer* leaf extract: anticancer and antimicrobial activities. *RSC Adv.* 9:15357–15369
- Hüttemann M, Pecina P, Rainbolt M, Thomas H. Sanderson, Kagan VE, Samavati L, Doan JW, Lee I (2011) The multiple functions of cytochrome *c* and their regulation in life and death decisions of the mammalian cell: from respiration to apoptosis. *Mitochondrion* 11(3): 369–381.

- Irimie AL, Sonea L, Jurj A, Mehterov N, Zimta AA, Budisan L, Braicu C, Berindan-Neagoe L (2017) Future trends and emerging issues for nanodelivery systems in oral and oropharyngeal cancer. *International Journal of Nanomedicine* 12:4593-4606
- Ishola IO, Awodele O, Olusayero AM, Ochieng CO (2014) Mechanisms of analgesic and anti-inflammatory properties of *Annona muricata* Linn. (Annonaceae) fruit extract in rodents. *J. Med. Food* 17: 1375-82
- Ishwarya R, Vaseeharan B, Kalyani S, Banumathi B, Govindarajan M, Alharbi NS, Kadaikunnan S, Al-anbr MN, Khaled JM, Benelli G (2018) Facile green synthesis of zinc oxide nanoparticles using *Ulva lactuca* seaweed extract and evaluation of their photocatalytic, antibiofilm and insecticidal activity. *Journal of Photochemistry & Photobiology, B: Biology* 178: 249–258
- Itroutwar PD, Govindaraju K, Tamilselvan S, Kannan M, Raja K, Subramanian KS (2019) Seaweed-Based Biogenic ZnO Nanoparticles for Improving Agro-morphological Characteristics of Rice (*Oryza sativa* L.). *Journal of Plant Growth Regulation*. <https://doi.org/10.1007/s00344-019-10012-3>
- Jahanban-Esfahlan R, de la Guardia M, Ahmadi D, Yousefi B (2017) Modulating tumor hypoxia by nanomedicine for effective cancer therapy. *Journal of Cellular Physiology* 233(3): 2019–2031
- Jain AK, Singh D, Dubey K, Maurya R, Pandey AK (2019) Zinc oxide nanoparticles induced gene mutation at the HGPRT locus and cell cycle arrest associated with apoptosis in V-79 cells. *J Appl Toxicol* 1–16
- Jaiswal PK, Goel A, Mittal RD (2015) Survivin: A molecular biomarker in cancer. *Indian J Med Res* 141(4): 389–397
- Jamdagni P, Khatri P, Rana JS (2018) Green synthesis of zinc oxide nanoparticles using flower extract of *Nyctanthes arbor-tristis* and their antifungal activity. *Journal of King Saud University – Science* 30: 168–175

- Jampílek J, Kráľová K (2015) Application of nanotechnology in agriculture and food industry, its prospects and risks. *Ecol Chem Eng S.* 22(3): 321-361
- Janaki AC, Sailatha E, Gunasekaran S (2015) Synthesis, characteristics and antimicrobial activity of ZnO nanoparticles. *Spectrochimica Acta Part A: Molecular and Biomolecular Spectroscopy* 144: 17–22
- Jang JS, Yu CJ, Choi SH, Ji SM, Kim ES, Lee JS (2008) Topotactic synthesis of mesoporous ZnS and ZnO nanoplates and their photocatalytic activity. *J Catal* 254: 144–155
- Janotti A, de Walle CGV (2009) Fundamentals of zinc oxide as a semiconductor. *Rep. Prog. Phys.* <https://doi.org/10.1088/0034-4885/72/12/126501>
- Jarrar A, Lotti F, Devecchio J, Ferrandon S, Gantt G, Mace A, Karagkounis G, Orloff M, Venere M, Hitomi M, Lathia J, Jeremy N, Rich JN, Matthew F, Kalady MF (2018) Poly(ADP-Ribose) polymerase inhibition sensitizes colorectal cancer-initiating cells to chemotherapy. *Stem cells* 37: 42–53
- Jayaseelan C, Abdul Rahuman A, Vishnu Kirthi A, Marimuthu S, Santhoshkumar T, Bagavan A, Gaurav K, Karthik L, Bhaskara Rao KV (2012) Novel microbial route to synthesize ZnO nanoparticles using *Aeromonas hydrophila* and their activity against pathogenic bacteria and fungi. *Spectrochimica Acta Part A* 90:78–84
- Jeevanandam J, Barhoum A, Chan YS, Dufresne A, Danquah MK (2018) Review on nanoparticles and nanostructured materials: history, sources, toxicity and regulations. *Beilstein J Nanotechnol* 9: 1050–1074
- Jiang D, Yang H, Willson JKV, Liang J, Humphrey LE, Zborowska E, Wang D, Foster J, Fan R, Brattain MG (1998) Autocrine transforming growth factor alpha provides a growth advantage to malignant cells by facilitating re entry into the cell cycle from suboptimal growth states. *J Biol Chem* 273: 31471-31479

- Jiang J, Pi J, Cai J (2018) The Advancing of Zinc Oxide Nanoparticles for Biomedical Applications. *Bioinorganic Chemistry and Applications*. <https://doi.org/10.1155/2018/1062562>
- Jiang R-D, Shen H, Piao Y-J (2010) The morphometrical analysis on the ultrastructure of A549 cells. *Romanian Journal of Morphology and Embryology* 51(4): 663–667
- Jin Z, El-Deiry W. (2005) Overview of cell death signaling pathways. *Cancer Biology & Therapy* 4(2): 147-171
- Joghee S, Ganeshan P, Vincent A, Hong SI (2018) Ecofriendly biosynthesis of Zinc oxide and Magnesium Oxide particles from medicinal plant *Pisonia grandis* R.Br. leaf extract and their antimicrobial activity. *BioNanoScience*. <https://doi.org/10.1007/s12668-018-0573-9>
- Johnson LA, June CH (2017) Driving gene-engineered T cell immunotherapy of cancer. *Cell Research* 27: 38-58
- Johnson VL, Ko SCW, Holmstrom TH, Eriksson JE, Chow SC (2000) Effector caspases are dispensable for the early nuclear morphological changes during chemical-induced apoptosis. *Journal of Cell Science* 113:2941-2953
- Jongen-Lavrencic M (2005) BCR/ABL-mediated downregulation of genes implicated in cell adhesion and motility leads to impaired migration toward CCR7 ligands CCL19 and CCL21 in primary BCR/ABL-positive cells. *Leukemia* 19(3): 373–380.
- Joruiz SM, Bourdon JC (2015) p53 Isoforms: Key Regulators of the Cell Fate Decision. *Cold Spring Harb Perspect* 6: a026039
- Joung J, Konermann S, Gootenberg JS, Abudayyeh OO, Platt RJ, Brigham MD, Sanjana NE, Zhang F (2017) Genome-scale CRISPR-Cas9 knockout and transcriptional activation screening. *Nat. Protoc* 12: 828–863

- Junqueira LC, Carneiro J (2004) *Histologia basica*. Guanabara Koogan, Rio de Janeiro, 8: 285–300
- Jurj A, Braicu C, Pop LA, Tomuleasa C, Gherman CD, Berindan-Neagoe I (2017) The new era of nanotechnology, an alternative to change cancer treatment. *Drug Design, Development and Therapy* 11: 2871–2890
- Justino AB, Miranda NC, Franco RR, Martins MM, da Silva NM, Espindola FS (2018) *Annona muricata* Linn. leaf as a source of antioxidant compounds with in vitro antidiabetic and inhibitory potential against α -amylase, α -glucosidase, lipase, non-enzymatic glycation and lipid peroxidation. *Biomedicine & Pharmacotherapy* 100: 83–92
- Kabir J, Lobo M, Zachary L (2002) Staurosporine induces endothelial cell apoptosis via focal adhesion kinase dephosphorylation and focal adhesion disassembly independent of focal adhesion kinase proteolysis. *Biochem. J* 367: 145 - 155
- Kadam VV, Ettiyappan JP, Balakrishnan RM (2019) Mechanistic insight into the endophytic fungus mediated synthesis of protein capped ZnO nanoparticles. *Materials Science & Engineering B* 243; 214–221
- Kadhem HA, Ibraheem SA, Jabir MS, Kadhim AA, Taqi ZJ, Florin MD (2019) Zinc oxide nanoparticles induce apoptosis in human breast cancer cells via caspase-8 and P53 pathway. *Nano Biomed Eng* 11(1): 35-43
- Kadiyala U, Turali-Emre ES, Bahng JH, Kotov NA, VanEpps JS. (2018) Unexpected insights into antibacterial activity of zinc oxide nanoparticles against methicillin resistant *Staphylococcus aureus* (MRSA). *Nanoscale* 10(10): 4927–4939
- Kairdolf BA, Qian X, and Nie S (2017) Bioconjugated nanoparticles for biosensing, in vivo imaging, and medical diagnostics. *Anal Chem* 89:1015–1031
- Kajstura M, Halicka HD, Pryjma J, Darzynkiewicz Z (2007) Discontinuous fragmentation of nuclear DNA during apoptosis revealed by discrete “Sub-G1” peaks on DNA content histograms. *Cytometry Part A* 71A: 125–131

- Kakiuchi K, Hosono E, Kimura T, Imai H, Fujihara S (2006) Fabrication of mesoporous ZnO nanosheets from precursor templates grown in aqueous solutions. *J Sol-Gel Sci Technol* 39: 63–72
- Kalpana VN, Kataru BAS, Sravani N, Vigneshwari T, Panneerselvam A, Rajeswari VD (2018) Biosynthesis of zinc oxide nanoparticles using culture filtrates of *Aspergillus niger*: antimicrobial textiles and dye degradation studies. *OpenNano* 3: 48–55
- Kalpana VN, Rajeswari D. (2018) A review on green synthesis, biomedical applications, and toxicity studies of ZnO NPs. *Bioinorganic Chemistry and Applications*. <https://doi.org/10.1155/2018/3569758>
- Kamal S, Akhter R, Tithi NA, Md. Abdul Wadud, Narjish SN, Shahriar M, Bhuiyan MA (2015) Biological investigations of the leaf extract of *spondias pinnata*. *International Journal of Pharmaceutical Sciences and Research* 6(8): 3351-3358
- Kang T, Guan R, Song Y, Lyu F, Ye X, Jiang H (2015) Cytotoxicity of zinc oxide nanoparticles and silver nanoparticles in human epithelial colorectal adenocarcinoma cells. *LWT - Food Science and Technology* 60: 1143-1148
- Kanthan R, Senger JL, Kanthan SC (2012) Molecular events in primary and metastatic colorectal carcinoma: a review. *Pathology Research International*. <https://doi.org/10.1155/2012/597497>
- Kashif M, Akhtar N (2017) Determination of sun protection factor and physical remanence of dermocosmetic emulgels formulated with *Manilkara zapota* (L.) fruit extract. *Tropical Journal of Pharmaceutical Research*, 18 (4): 809-816
- Katifelis H, Lyberopoulou A, Mukha I, Vityuk N, Grodzyuk G, Theodoropoulos GE, Efsthopoulos EP, Gazouli M (2018) Ag/Au bimetallic nanoparticles induce apoptosis in human cancer cell lines via P53, CASPASE-3 and

BAX/BCL-2 pathways. *Artificial Cells, Nanomedicine And Biotechnology* 46(S3):S389–S398

Kavithaa K, Paulpandi M, Ponraj T, Murugan K, Sumathi S (2016) Induction of intrinsic apoptotic pathway in human breast cancer (MCF-7) cells through facile biosynthesized zinc oxide nanorods. *Karbala International Journal of Modern Science* 2:46-55

Kayani ZN, Saleemi F, Batool I (2015) Effect of calcination temperature on the properties of ZnO nanoparticles. *Appl. Phys. A*. <https://doi.org/10.1007/s00339-015-9019-1>

Khalafi T, Buazar F, Ghanemi K (2019) Phycosynthesis and enhanced photocatalytic activity of zinc oxide nanoparticles toward organosulfur pollutants. *Scientific Reports*. <https://doi.org/10.1038/s41598-019-43368-3>

Khalil MI, Al-Qunaibit MM, Al-zahem AM, Labis JP (2014) Synthesis and characterization of ZnO nanoparticles by thermal decomposition of a curcumin zinc complex. *Arabian Journal of Chemistry* 7: 1178–1184

Khan I, Saeed K, Khan I (2017) Nanoparticles: properties, applications and toxicities. *Arabian Journal of Chemistry*. <https://dx.doi.org/10.1016/j.arabjc.2017.05.011>

Khan MF, Ansari AH, Hameedullah M, Ahmad E, Husain FM, Zia Q, Baig U, Zaheer MR, Alam MM, Khan AM, AlOthman ZA, Ahmad I, Ashraf GM, Aliev G (2016) Sol-gel synthesis of thorn-like ZnO nanoparticles endorsing mechanical stirring effect and their antimicrobial activities: potential role as nano-antibiotics. *Scientific Reports*. <https://doi.org/10.1038/srep27689>

Khan SA, Noreen F, Kanwal S, Iqbal A, Hussain G (2018) Green synthesis of ZnO and Cu-doped ZnO nanoparticles from leaf extracts of *Abutilon indicum*, *Clerodendrum infortunatum*, *Clerodendrum inerme* and investigation of their biological and photocatalytic activities. *Materials Science and Engineering: C* 82: 46–59

- Khan YA, Singh BR, Ullah R, Shoeb M, Naqvi AH, Abidi SMA. (2015) Anthelmintic Effect of Biocompatible Zinc Oxide Nanoparticles (ZnO NPs) on *Gigantocotyle explanatum*, a Neglected Parasite of Indian Water Buffalo. PLoS ONE 10(7), e0133086, doi:10.1371/journal.pone.0133086.
- Khan M, Naqvi AH, Ahmad M (2015) Comparative study of the cytotoxic and genotoxic potentials of zinc oxide and titanium dioxide nanoparticles. Toxicol. Rep 2: 765-774
- Khana MM, Saadaha NH, Khan ME, Harunsania MH, Tana AL, Cho MH (2019) Potentials of *Costus woodsonii* leaf extract in producing narrow band gap ZnO nanoparticles. Materials Science in Semiconductor Processing 91: 194–200
- Khandel P, Yadaw RK, Soni DK, Kanwar L, Shahi SK. (2018) Biogenesis of metal nanoparticles and their pharmacological applications: present status and application prospects. Journal of Nanostructure in Chemistry 8: 217–254
- Khatami M, Alijani HQ, Heli H, Sharifi I (2018) Rectangular shaped zinc oxide nanoparticles: Green synthesis by Stevia and its biomedical efficiency. Ceramics International. <https://doi.org/10.1016/j.ceramint.2018.05.224>
- Khazaei S, Esa NM, Ramachandran V, Hamid RA, Pandurangan AK, Etemad A, Ismail P (2017) *In vitro* Antiproliferative and Apoptosis Inducing Effect of *Allium atrovioleaceum* Bulb Extract on Breast, Cervical, and Liver Cancer Cells. Front Pharmacol 5:8
- Khomdram S, Arambam S, Shantibal G. (2014) Nutritional profiling of two underutilized wild edible fruits *Elaeagnus pyriformis* and *Spondias pinnata*. Ann Agric Res New Series 35(2):129-135
- Kim J-H, Jeong MS, Kim D-Y, Her S, Wie M-B (2015) Zinc Oxide Nanoparticles Induce Lipoxygenase-mediated Apoptosis and Necrosis in Human Neuroblastoma SHSY5Y Cells. Neurochemistry International 90: 204-14

- Kim KK, Kim D, Kim SK, Park SM, Song JK (2011) Formation of ZnO nanoparticles by laser ablation in neat water. *Chemical Physics Letters* 511: 116–120
- Kim-Campbell N, Gomez H, Bayir H (2019) Cell death pathways: apoptosis and regulated necrosis. *Humoral and cellular mechanisms of kidney damage* 20(5):113-120e2
- Klein E, Vanky F, Ben-Bassa H, Neuman TH, Ralph NP, Zeuthen J, Polliack A (1976) Properties of the k562 cell line, derived from a patient with chronic myeloid leukemia. *Int J Cancer* 18: 421-431
- Koeffler HP, Golde DW (1980) Human myeloid leukemia cell lines: a review. *Blood* 56(3), 344-350
- Kondo H, Miyoshi K, Sakiyama S, Tangoku A, Noma T (2015) Differential regulation of gene expression of alveolar epithelial cell markers in human lung adenocarcinoma-derived A549 clones stem cells international. <https://dx.doi.org/10.1155/2015/165867>
- Kosmider B, Zyner E, Osiecka R, Ochocki J (2004) Induction of apoptosis and necrosis in A549 cells by the *cis*-Pt(II) complex of 3-aminoflavone in comparison with *cis*-DDP. *Mutation Research* 563: 61–70
- Kripal R, Gupta AK, Srivastava RK, Mishra SK (2011) Photoconductivity and photoluminescence of ZnO nanoparticles synthesized via co-precipitation method. *Spectrochimica Acta Part A* 79: 1605– 1612
- Krupa, Vimala R (2016) Evaluation of tetraethoxysilane (TEOS) sol–gel coatings, modified with green synthesized zinc oxide nanoparticles for combating microfouling. *Materials Science and Engineering: C* 61(1): 728-735
- Kumar A, Dixit CK (2017) Methods for characterization of nanoparticles. *Advances in Nanomedicine for the Delivery of Therapeutic Nucleic Acids* : 43-58. <https://dx.doi.org/10.1016/B978-0-08-100557-6.00003-1>

- Kumar B, Smita K, Cumbal L, Debut A (2014) Green approach for fabrication and applications of zinc oxide nanoparticles. *Bioinorganic Chemistry and Applications*. <https://dx.doi.org/10.1155/2014/523869>
- Kumar BV, Naik HSB, Girija D, Kumar BJ (2011) ZnO nanoparticle as catalyst for efficient green one-pot synthesis of coumarins through Knoevenagel condensation. *J Chem Sci* 123(5): 615–621
- Kumar DRY, Vurivihema, Agrawal M, Sruthy CP, Vedamurthy AB, Krishna V, Hoskeri HJ (2012) *Manilkara zapota* seed embryo extract a potent anthelmintic agent. *Asian J Pharm Clin Res* 5: 159 - 161
- Kumar HKN, Mohana NC, Nuthan BR, Ramesha KP, Rakshith D, Geetha N, Satish S (2019) Phyto-mediated synthesis of zinc oxide nanoparticles using aqueous plant extract of *Ocimum americanum* and evaluation of its bioactivity. *SN Applied Sciences* 1:651
- Kumaravel TS, Vilhar B, Faux SP, Jha AN (2009) Comet Assay measurements: a perspective. *Cell Biol Toxicol* 25: 53–64
- Kumari M, Khan SS, Pakrashi S, Mukherjee A, Chandrasekaran N (2011) Cytogenetic and genotoxic effects of zinc oxide nanoparticles on root cells of *Allium cepa*. *J Hazard mater* 190: 613-621
- Kundu D, Hazra C, Chatterjee A, Chaudhari A, Mishra S (2014) Extracellular biosynthesis of zinc oxide nanoparticles using *Rhodococcus pyridinivorans* NT2: multifunctional textile finishing, biosafety evaluation and in vitro drug delivery in colon carcinoma. *J Photochem Photobiol. B Biol* 140: 194–204
- Kuppusamy P, Ichwan SJ, AlZikri PN, Suriyah WH, Soundharrajan I, Govindan N, Maniam GP, Yusoff MM (2016) *In vitro* anticancer activity of Au, Ag nanoparticles synthesized using *Commelina nudiflora* L. aqueous extract against HCT 116 colon cancer cells. *Biol Trace Elem Res* 173(2): 297-305

- Kuskovsky IL, Neumark GF, and Gong Y (2006) Doping Aspects Of Zn-Based Wide-Band-Gap Semiconductors, in Springer Handbook of Electronic and Photonic Materials, S. Kasap, P. Capper (Eds.) Springer-Verlag, Part D, 843.
- Kyriakopoulos CE, Chen YH, Carducci MA, Liu G, Jarrard DF, Hahn NM, Shevrin DH, Dreicer R, Hussain M, Eisenberger M, Kohli M, Plimack ER, Vogelzang NJ, Picus J, Cooney MM, Garcia JA, DiPaola RS, Sweeney CJ (2018) Chemohormonal Therapy in Metastatic Hormone-Sensitive Prostate Cancer: Long-Term Survival Analysis of the Randomized Phase III E3805 CHAARTED Trial. *J Clin Oncol* 36:1080-1087
- Lakshmipriya T, Soumya T, Jayasree PR, Manish Kumar PR (2018) Selective induction of DNA damage, G2 abrogation, and mitochondrial apoptosis by leaf extract of traditional medicinal plant *Wrightia arborea* in K562 cells. *Protoplasma* 255: 203–216
- Lan FF, Wang H, Chen YC, Chan CY, Ng SS, Li K, Xie D, He ML, Lin MC, Kung HF (2011) Hsa-let-7g inhibits proliferation of hepatocellular carcinoma cells by downregulation of c-Myc and upregulation of p16(INK4A). *Int J Cancer* 128(2): 319–331
- Larsen BD, Sørensen CS (2017) The caspase-activated DNase: apoptosis and beyond. *FEBS J* 284(8) : 1160-1170.
- Lee J, Jang H-J, Chun H, Pham T-H, Bak Y, Shin J-W, Jin H, Kim Y-I, Ryu H W, Oh SR, Yoon D-Y (2019) *Calotropis gigantea* extract induces apoptosis through extrinsic/intrinsic pathways and reactive oxygen species generation in A549 and NCI-H1299 nonsmall cell lung cancer cells. *BMC Complementary and Alternative Medicine* 19:134
- Lee SD, Nam SH, Kim MH, Boo JH (2012) Synthesis and photocatalytic property of ZnO nanoparticles prepared by spray-pyrolysis method. *Physics Procedia* 32: 320 – 326

- Leonhardt U (2007) Optical metamaterials: Invisibility cup. *Nat. Photonics* 1: 207–208
- Lettieri-Barbato D, Aquilano K (2018) Pushing the limits of cancer therapy: the nutrient game. *Front Oncol.* <https://doi.org/10.3389/fonc.2018.00148>
- Li K, Zhao X, Hammer BK, Du S, Chen Y (2013) Nanoparticles Inhibit DNA Replication by Binding to DNA: Modeling and Experimental Validation. *ACSNANO* 7(11) : 9664–9674
- Li X, Wang L, Fan Y, Feng Q, Cui F-Z, Watari F (2013) Nanostructured scaffolds for bone tissue engineering. *J Biomed Mater Res Part A* 101: 2424–2435
- Li X, Xu H, Chen ZS, Chen GJ (2011) Biosynthesis of nanoparticles by microorganisms and their applications. *Nanomater* <https://doi.org/10.1155/2011/270974>
- Li Y, Yu H, Han F, Wang M, Luo Y, Guo X (2018) Biochanin A induces S phase arrest and apoptosis in lung cancer cells. *BioMed Research International.* <https://doi.org/10.1155/2018/3545376>
- Liao H, Ji F, Helleday T, Ying S (2018) Mechanisms for stalled replication fork stabilization: new targets for synthetic lethality strategies in cancer treatments. *EMBO Reports.* <https://doi.org/10.15252/embr.201846263>
- Lim S, Kaldis P (2013) Cdks, cyclins and CKIs: roles beyond cell cycle regulation. *Development* 140: 3079-3093
- Limo MJ, Sola-Rabada A, Boix E, Thota V, Westcott ZC, Puddu V, Perry CC (2018) Interactions between metal oxides and biomolecules: from fundamental understanding to applications. *Chem. Rev.* 118: 11118–11193
- Lin C-Y, Chang T-W, Hsieh W-H, Hung M-C, Lin I-H, Lai S-C, Tzeng Y-J (2016) Simultaneous induction of apoptosis and necroptosis by Tanshinone IIA in human hepatocellular carcinoma HepG2 cells. *Cell Death Discovery* 2, 16065

- Lin W, Xu Y, Huang C, Ma Y, Shannon KB, Chen D, Huang Y (2009) Toxicity of nano-and micro-sized zinc oxide particles in human lung epithelial cells. *J Nanopart Res* 11: 25-39
- Lingaraju K, Raja Naika H, Manjunath K, Basavaraj RB, Nagabhushana H, Nagaraju G, Suresh D (2015) Biogenic synthesis of zinc oxide nanoparticles using *Ruta graveolens* (L.) and their antibacterial and antioxidant activities. *Appl Nanosci*. doi 10.1007/s13204-015-0487-6
- Liu J, Chen Q, Feng L, Liu Z (2018) Nanomedicine for tumor microenvironment modulation and cancer treatment enhancement. *Nano Today* 21: 55–73
- Liu K, Liu P-c, Liu R, Wu X (2015) Dual AO/EB Staining to Detect Apoptosis in Osteosarcoma Cells Compared with Flow Cytometry. *Med Sci Monit Basic Res* 21: 15-20
- Liu N, Yang HL, Wang P, Lu YC, Yang YJ, Wang L, Lee SC (2016) Functional proteomic analysis reveals that the ethanol extract of *Annona muricata* L. induces liver cancer cell apoptosis through endoplasmic reticulum stress pathway. *Journal of ethnopharmacology* 189: 210–217
- Lokesh Shastri, M. S. Qureshi and M. M. Malik (2014) Synthesis and luminescence properties of ZnO nanoparticles produced by the sol gel method. *J Pure Appl & Ind Phys* 4(3): 119-125
- Lombardo D, Kiselev MA, Caccamo MT (2019) Smart nanoparticles for drug delivery application: development of versatile nanocarrier platforms in biotechnology and nanomedicine. *Journal of Nanomaterials*. <https://doi.org/10.1155/2019/3702518>
- Lozzio CB, Lozzio BB (1975) Human chronic myelogenous leukemia cell-line with positive Philadelphia chromosome. *Blood* 45 (3): 321–334
- Luchetti F, Gregorini A, Papa S, Burattini S, Canonico B, Valentini M, Falcieri E (1998) The K562 chronic myeloid leukemia cell line undergoes apoptosis in response to interferon- α . *Haematologica* 83: 974-980

- Lukman AL, Gong B, Marjo CE, Roessner U, Harris AT (2011) Facile synthesis, stabilization, and anti-bacterial performance of discrete Ag nanoparticles using *Medicago sativa* seed exudates. *J. Colloid Interface Sci.* 353: 433–444
- Lund AH, van Lohuizen M (2004) Epigenetics and cancer. *Genes Dev* 18: 2315-2335
- Luo J (2016) CRISPR/Cas9: From genome engineering to cancer drug discovery. *Trends Cancer* 2, 313–324
- López-Cuenca S, Carrillo PLA, Velasco MR, de León RD, Saade H, López RG, Mendizábal E, Puig JE (2011) High-yield synthesis of zinc oxide nanoparticles from bicontinuous microemulsions. *Journal of Nanomaterials* Article ID 431382
- Ma DD, Yang WX (2016) Engineered nanoparticles induce cell apoptosis: potential for cancer therapy. *Oncotarget* 7(26): 40882-40903.
- Ma L, Liu B, Huang, P -JJ, Zhang X, Liu J (2016). DNA adsorption by ZnO nanoparticles near its solubility limit: implications for DNA fluorescence quenching and DNAzyme activity assays. *Langmuir* 32(22): 5672–5680
- Mahamuni PP, Patil PM, Dhanavade MJ, Badiger MV, Shadija PG, Lokhande AC, Bohara RA (2019) Synthesis and characterization of zinc oxide nanoparticles by using polyol chemistry for their antimicrobial and antibiofilm activity. *Biochemistry and Biophysics Reports* 17: 71–80
- Mahendiran D, Subash G, Selvan DA, Rehana D, Kumar RS, Rahiman AK (2017) Biosynthesis of zinc oxide nanoparticles using plant extracts of *Aloe vera* and *Hibiscus sabdariffa*: phytochemical, antibacterial, antioxidant and anti-proliferative studies. *BioNanoSci.* <https://doi.org/10.1007/s12668-017-0418-y>
- Maiworm AI, Presta GA, Santos-Filho SD, Paoli SD, Giani TS, Fonseca AS, Bernardo-Filho M (2008) Osmotic and morphological effects on red blood

- cell membrane: Action of an aqueous extract of *Lantana camara*. Braz J. Pharmacog 18: 42-46
- Makarov VV, A. J. Love AJ, Sinitsyna OV, Makarova SS, Yaminsky IV, Taliansky ME, Kalinina NO (2014) “Green” nanotechnologies: synthesis of metal nanoparticles using plants. Acta naturae 6(1): 35-44
- Makumire S, Chakravadhanula VSK, Kollisch G, Redel E, Shonhai A(2014) Immunomodulatory activity of zinc peroxide (ZnO₂) and titanium dioxide (TiO₂) nanoparticles and their effects on DNA and protein Integrity. Toxicology Letters 227: 56–64
- Malik P, Shankar R, Malik V, Sharma N, Mukherjee TK (2014) Green chemistry based benign routes for nanoparticle synthesis. Journal of Nanoparticles. <https://dx.doi.org/10.1155/2014/302429>
- Mameneh R, Shafiei M, Aidi A, Karimi E, Badakhsh B, Abbasi N (2019) Toxicity study of silver nanoparticles synthesized from aqueous flower extract of *Scrophularia striata* on MCF-7 human breast cancer cell line. Phcog Mag 15: 66-72
- Mansoori B, Mohammadi A, Davudian S, Shirjang S, Baradaran B (2017) The different mechanisms of cancer drug resistance: a brief review. Adv Pharm Bull 7(3): 339-348
- Marcazzan S, Varoni EM, Blanco E, Lodi G, Ferrari M (2018) Nanomedicine, an emerging therapeutic strategy for oral cancer therapy. Oral Oncology 76: 1–7
- Maret W. (2012) New perspectives of zinc coordination environments in proteins. Journal of Inorganic Biochemistry 111 (2012) 110–116
- Maret W (2013) Zinc Biochemistry: From a Single Zinc Enzyme to a Key Element of Life. Adv. Nutr. 4: 82–91

- Martinez-Lage M, Puig-Serra P, Menendez P, Torres-Ruiz R, Rodriguez-Perales S (2018) CRISPR/Cas9 for cancer therapy: hopes and challenges. *Biomedicines* 6: 105
- Martin valet D, Zhu P, Lieberman J (2005) Granzyme A induces caspase-independent mitochondrial damage, a required first step for apoptosis. *Immunity* 22: 355–370
- Matassov D , Kagan T, Leblanc J, Sikorska M, Zakeri Z (2004) Measurement of apoptosis by DNA fragmentation. *Methods Mol Biol* 282: 1-17
- Mathuram TL, Ravikumar V, Reece LM, Karthik S, Sasikumar CS, Cherian KM (2016) Tideglusib induces apoptosis in human neuroblastoma IMR32 cells,provoking sub-G0/G1accumulation and ROS generation. *Environmental Toxicology and Pharmacology* 46: 194–205
- Matinise N, Fuku XG, Kaviyarasu K, Mayedwa N, Maaza M (2017) ZnO nanoparticles via *Moringa oleifera* green synthesis: Physical properties & mechanism of formation. *Applied Surface Science* 406 : 339–347
- McDermott DF, Drake CG, Sznol M, Choueiri TK, Powderly JD, Smith DC, Brahmer JR, Carvajal RD, Hammers HJ, Puzanov I, Hodi FS, Kluger HM, Topalian SL, Pardoll DM, Wigginton JM, Kollia GD, Gupta A, McDonald D, Sankar V, Sosman JA, Atkins MB (2015) Survival, durable response, and long-term safety in patients with previously treated advanced renal cell carcinoma receiving nivolumab. *J Clin Oncol* 33(18): 2013–2020
- Milind P, Preethi. (2015) Chickoo: A wonderful gift from nature. *Int.J.Res. Ayurveda Pharm* 6(4): 544 – 550
- Mills CD, Lenz LL, and Harris RA (2016) A breakthrough: macrophage-directed cancer immunotherapy. *Cancer Res* 76(3): 513-6
- Mirza AZ, Siddiqui FA (2014) Nanomedicine and drug delivery: a mini review. *Int Nano Lett.* <https://doi.org/10.1007/s40089-014-0094-7>

- Moazzam M, Mehboob T, Bashir I, Aslam R, Tabassam N, Jamshaid M (2018) Constituents of Cosmeceuticals and Implication of Nanotechnology in Cosmetics. *RADS J. Pharm. Pharm. Sci.* 6(4): 270-281
- Moezzi A, Cortie M, McDonagh A (2011) Aqueous pathways for the formation of zinc oxide nanoparticles. *Dalton Trans* 40: 4871–4878
- Moghadamtousi SZ, Fadaeinasab M, Nikzad S, Mohan G, Ali HM, Kadir, HA (2015) *Annona muricata* (Annonaceae): a review of its traditional uses, isolated acetogenins and biological activities. *Int J Mol Sci* 16:15625-15658
- Moghaddam AB, Moniri M, Azizi S, Rahim RA, Ariff AB, Navaderi M, Mohamad R (2017) Eco-friendly formulated zinc oxide nanoparticles: induction of cell cycle arrest and apoptosis in the MCF-7 cancer cell line. *Genes* 8: 281
- Moghaddam AB, Moniri M, Azizi S, Rahim RA, Ariff AB, Saad WZ, Namvar F, Navaderi M. (2017) Biosynthesis of ZnO nanoparticles by a new *Pichia kudriavzevii* yeast strain and evaluation of their antimicrobial and antioxidant activities. *Molecules*. <https://doi.org/10.3390/molecules22060872>
- Mohammadi FM, Ghasemi N (2018) Influence of temperature and concentration on biosynthesis and characterization of zinc oxide nanoparticles using cherry extract. *Journal of Nanostructure in Chemistry* 8: 93–102
- Mohammadinejad R, Karimi S, Iravani S, Varma RS (2016) Plant-derived nanostructures: types and applications. *Green Chem* 18: 20–52
- Montero-Muñoz M, Ramos-Ibarra JE, Rodríguez-Páez JE, Ramirez A, J A Huamaní-Coaquira JA. (2017) Shape-control of Zinc Oxide nanoparticles: enhancing photocatalytic activity under UV irradiation. *IOP Conf. Series: Journal of Physics: Conf. Series*. <https://doi.org/10.1088/1742-6596/792/1/012068>
- Montoro A, Soriano JM, Barquinero JF (2012) Assessment in vitro of cytogenetic and genotoxic effects of propolis on human lymphocytes. *Food Chem Toxicol* 50: 216-21

- Moon SH, Choi WJ, Choi S-C, Kim EH, Kim J, Lee J-O, Kim SH (2016) Anti-cancer activity of ZnO chips by sustained zinc ion release. *Toxicology Reports* 3: 430–438
- Moreira AF, Dias DR, Correia IJ (2016) Stimuli-responsive mesoporous silica nanoparticles for cancer therapy: a review. *Microporous and Mesoporous Materials* 236: 141–157
- Mornani EG, Mosayebian P, Dorrnian D, Behzad K (2016) Effect of calcination temperature on the size and optical properties of synthesized zno nanoparticles. *Journal of Ovonic Research* 12(2): 75 - 80
- Mourdikoudis S, Pallares RM, Thanh NTK (2018) Characterization techniques for nanoparticles: comparison and complementarity upon studying nanoparticle properties. *Nanoscale* 10: 12871–12934
- Mozdoori N, Safarian S, Sheibani N (2017) Augmentation of the cytotoxic effects of zinc oxide nanoparticles by MTCP conjugation: Non-canonical apoptosis and autophagy induction in human adenocarcinoma breast cancer cell lines *Materials Science and Engineering C* 78: 949–959
- Munshi GH, Ibrahim AM, Al-Harbi LM (2018) Inspired preparation of Zinc oxide nanocatalyst and the photocatalytic activity in the treatment of methyl orange dye and paraquat herbicide. *International Journal of Photoenergy*. <https://doi.org/10.1155/2018/5094741>
- Musa I, Qamhieh N, Mahmoud ST (2017) Synthesis and length dependent photoluminescence property of Zinc oxide nanorods. *Results in Physics* 7: 3552–3556
- Mussarat J, Saquib Q, Azam A, Naqvi SAH (2009) Zinc oxide nanoparticles induced-DNA damage in human lymphocytes. *Int J Nanoparticles* 2: 402-414

- Nagajyothi PC, Minh An TN, Sreekanth TVM, Lee J, Lee DJ, Lee KD (2013) Green route biosynthesis: Characterization and catalytic activity of ZnO nanoparticles. *Materials Letters* 108: 160–163
- Nagajyothi PC, Sreekanth TVM, Tetey CO, Jun YI, Mook SH (2014) Characterization, antibacterial, antioxidant, and cytotoxic activities of ZnO nanoparticles using *Coptidis Rhizoma*. *Bioorg. Med. Chem. Lett* 24: 4298–4303
- Nagarajan S, Kuppusamy KA (2013) Extracellular synthesis of zinc oxide nanoparticle using seaweeds of gulf of Mannar, India. *Journal of Nanobiotechnology* <https://www.jnanobiotechnology.com/content/11/1/39>
- Namvar F, Azizi, S Rahman HS, Mohamad R, Rasedee A, Soltani, M Rahim RA (2016) Green synthesis, characterization, and anticancer activity of hyaluronan/zinc oxide nanocomposite. *Onco Targets Ther.*; 9: 4549
- Namvar F, Rahman HS, Mohamad R, Azizi S, Tahir PM, Chartrand MS, Yeap SK. (2015) Cytotoxic effects of biosynthesized zinc oxide nanoparticles on murine cell lines. *Evidence-Based Complementary and Alternative Medicine*. <https://dx.doi.org/10.1155/2015/593014>
- Nasrollahzadeh M, Sajadi SM, Sajjadi M, Issaabadi Z. (2019) Chapter 4 - Applications of Nanotechnology in Daily Life. *Interface Science and Technology* 28: 113-143
- National Toxicology Program (NTP). 2016. Report on Carcinogens, Fourteenth Edition.; Research Triangle Park, NC: U.S. Department of Health and Human Services, Public Health Service. <https://ntp.niehs.nih.gov/go/roc14>
- Nava OJ, Soto-Robles CA, Gomez-Gutierrez CM, Vilchis-Nestor AR, Castro-Beltran A, Olivas A, Luque PA. (2017) Fruit peel extract mediated green synthesis of zinc oxide nanoparticles. *Journal of Molecular Structure* 1147: 1-6

- Naveed Ul Haq A, Nadhman A, Ullah I, Mustafa G, Yasinzai M, Imran Khan I. (2017) Synthesis approaches of zinc oxide nanoparticles: the dilemma of ecotoxicity. *Journal of Nanomaterials*. <https://doi.org/10.1155/2017/8510342>
- Negrini S, Gorgoulis VG, Halazonetis TD (2010) Genomic instability - an evolving hallmark of cancer *Nature Reviews* 11: 220-228.
- Nejdl L, Ruttkay-Nedecky B, Kudr J, Krizkova S, Smerkova K, Dostalova S, Vaculovicova M, Kopel P, Zehnalek J, Trnkova L, Babula P, Adam V, Kizek R. (2014) DNA interaction with zinc(II) ions. *International Journal of Biological Macromolecules* 64:281– 287
- Nethravathi PC, Shruthi GS, Suresh D, Udayabhanu, Nagabhushana H, Sharma SC. (2015) *Garcinia xanthochymus* mediated green synthesis of ZnO nanoparticles: photoluminescence, photocatalytic and antioxidant activity studies. *Ceramics International* 41: 8680–8687
- Neumark YGI, Kuskovsky (2007) *Springer Handbook of Electronic and Photonic Materials: Doping Aspects of Zn-Based Wide-Band-Gap Semiconductors*, ed. by P.C. Safa Kasap (Springer, 2007), pp 843–854
- Ng CT, Yong LQ, Hande MP, Ong CN, Liya EY, Bay BH, Baeg GH (2017) Zinc oxide nanoparticles exhibit cytotoxicity and genotoxicity through oxidative stress responses in human lung fibroblasts and *Drosophila melanogaster*. *International Journal of Nanomedicine* 12: 1621–1637
- Ngoepe NM, Mbita Z, Mathipa M, Mketi N, Ntsendwana B, Hintsho-Mbita NC. (2018) Biogenic synthesis of ZnO nanoparticles using *Monsonia burkeana* for use in photocatalytic, antibacterial and anticancer applications. *Ceramics International* 44(14): 16999–17006
- Nguyen SH, Webb HK, Mahon PJ, Crawford RJ, Ivanova EP (2014) Natural insect and plant micro-/nanostructured surfaces: an excellent selection of valuable templates with superhydrophobic and self-cleaning properties. *Molecules* 19: 13614–13630

- Niaz K, Maqbool F, Khan F, Bahadar H, Hassan FI, Abdollahi M (2017) Smokeless tobacco (*paan* and *gutkha*) consumption, prevalence, and contribution to oral cancer. *Epidemiol Health*. <https://doi.org/10.4178/epih.e2017009>
- Nie L, Gao L, Feng P, Zhang J, Fu X, Liu Y, Yan X, Wang T (2006) Three-dimensional functionalized tetrapodlike ZnO nanostructures for plasmid DNA delivery. *small* 2(5): 621 – 625
- Nirmala M, Nair MG, Rekha K, Anukaliani A, Samdarshi SK, Nair RG (2010) Photocatalytic activity of ZnO nanopowders synthesized by DC thermal plasma. *African Journal of Basic & Applied Sciences* 2(5-6) : 161-166
- Nouroozi F, Farzaneh F (2011) Synthesis and characterization of brush-like ZnO nanorods using albumen as biotemplate. *J Braz Chem Soc* 22(3): 484–488
- Nuruzzaman M, Rahman MM, Liu Y, Naidu R (2016) Nanoencapsulation, Nano-guard for Pesticides: A New Window for Safe Application. *J Agric Food Chem* 64(7): 1447-83
- Obute GC, Ekeke C, Izuka DC (2016) Genotoxicity assessment of refined petroleum products and popular local soft drink (Zobo) in daily use in Nigeria. *Res J Mut* 6: 22-30
- Ochieng PE, Iwuoha E, Michira I, Masikini M, Ondiek J, Githira P, Kamau GN (2015) Green route synthesis and characterization of ZnO nanoparticles using *Spathodea campanulata*. *International Journal of BioChemiPhysics* 23: 53-61
- Ogunyemi SO, Abdallah Y, Zhang M, Fouad H, Hong X, Ibrahim E, Masum MMI, Hossain A, Mo J, Li B (2019) Green synthesis of zinc oxide nanoparticles using different plant extracts and their antibacterial activity against *Xanthomonas oryzae* pv. *oryzae*. *Artificial Cells, Nanomedicine, And Biotechnology* 47(1): 341–352
- Othman BA, Greenwood C, Abuelela AF, Bharath AA, Chen S, Theodorou I, Douglas T, Uchida M, Ryan M, Merzaban JS, Porter AE. (2016)

Correlative light-electron microscopy shows RGD-targeted ZnO nanoparticles dissolve in the intracellular environment of triple negative breast cancer cells and cause apoptosis with intratumor heterogeneity
Advanced Healthcare Materials

Pacheco SOS, Pacheco FJ, Zapata GMJ, Garcia JME, Previale CA, Cura HE, Craig WJ (2016) Food habits, lifestyle factors, and risk of prostate cancer in central Argentina: a case control study involving self-motivated health behaviour modifications after diagnosis. *Nutrients*. <https://doi.org/10.3390/nu8070419>

Pachori P, Gothwal R, Gandhi P (2019) Emergence of antibiotic resistance *Pseudomonas aeruginosa* in intensive care unit; a critical review. *Genes & Diseases* 6:109-119

Padalia H, Chanda S (2017) Characterization, antifungal and cytotoxic evaluation of green synthesized zinc oxide nanoparticles using *Ziziphus nummularia* leaf extract. *Artificial cells, nanomedicine, and biotechnology* 45(8): 1751–1761

Paino IMM, Gonçalves FJ, Souza FL, Zucolotto V (2016) Zinc oxide flower-like nanostructures that exhibit enhanced toxicology effects in cancer cells. *ACS Appl. Mater. Interfaces*, 8: 32699–32705

Pan S, Lin H, Deng J, Chen P, Chen X, Yang Z, Peng H (2014) Novel wearable energy devices based on aligned Carbon nanotube fiber textiles. *Adv. Energy Mater.* <https://doi.org/10.1002/aenm.201401438>

Panda KK, Golari D, Venugopal A, Achary VMM, Phaomei G, Parinandi NL, Sahu HK, Panda BB (2017) Green synthesized zinc oxide (ZnO) nanoparticles induce oxidative stress and DNA damage in *Lathyrus sativus* L. root bioassay system. *Antioxidants*. <https://doi.org/10.3390/antiox6020035>

Pandey H, Kumar V, Roy BK (2014) Assessment of genotoxicity of some common food preservatives using *Allium cepa* L. as a test plant. *Toxicol Rep* 1: 300-308.

- Pandimurugan R, Thambidurai S (2016) Novel seaweed capped ZnO nanoparticles for effective dye photodegradation and antibacterial activity. *Advanced Powder Technology* 27(4): 1062–1072
- Pandurangan M, Enkhtaivan G, Kim DH (2016) Anticancer studies of synthesized ZnO nanoparticles against human cervical carcinoma cells. *Journal of Photochemistry and Photobiology B: Biology* 158: 206–211.
- Papazoglou ES, Parthasarathy A (2007) *Bionanotechnology Synth. Lect. Biomed. Eng.* 2: 1–139. <https://doi.dx/2200/S00051ED1V01Y200610BME007>
- Parthasarathy G, Saroja M, Venkatachalam M, Evanjelene VK (2017) Biological Synthesis of Zinc Oxide Nanoparticles from Leaf Extract of *Curcuma neilgherrensis* Wight. *International Journal of Materials Science* 12(1): 73-86
- Parthasarathi V, Thilagavathi G (2011) Synthesis and characterization of zinc oxide nanopartilce and its application on fabrics for microbe resistant defence clothing. *Int J Pharm Pharm Sci* 3(4):392-398
- Parthiban C, Sundaramurthy N (2015) Biosynthesis, characterization of ZnO nanoparticles by using *Pyrus Pyrifolia* leaf extract and their photocatalytic activity. *IJRSET* 4(10) : 9710-9718
- Patel P, Kansara K, Senapati VA, Shanker R, Dhawan A, Kumar A (2016) Cell cycle dependent cellular uptake of zinc oxide nanoparticles in human epidermal cells. *Mutagenesis* 31: 481–490
- Patel S Patel JK (2016) A review on a miracle fruits of *Annona muricata*. *J. Pharmacogn. Phytochem* 5: 137-148.
- Pathakoti K , Manubolu M , Hwang H-M (2017) Nanostructures: Current uses and future applications in food science. *Journal of food and drug analysis* 25:245-253.

- Pati R, Das I, Mehta RM, Sahu R, Sonawane A (2016) Zinc-oxide nanoparticles exhibit genotoxic, clastogenic, cytotoxic and actin depolymerization effects by inducing oxidative stress responses in macrophages and adult mice. *Toxicological Sciences* 150(2):454–472
- Pati R, Mehta RK, Mohanty S, Padhi A, Sengupta M, Vaseeharan B, Goswami C, Sonawane A (2014) Topical application of zinc oxide nanoparticles reduces bacterial skin infection in mice and exhibits antibacterial activity by inducing oxidative stress response and cell membrane disintegration in macrophages. *Nanomedicine: Nanotechnology, Biology and Medicine* 10(6): 1195-1208
- Patra JK, Das G, Fraceto LF, Campos EVR, Rodriguez-Torres MdP, Acosta-Torres LS, Diaz-Torres LA, Grillo R, Swamy MK, Sharma S, Habtemariam S, Shin H-S (2018) Nano based drug delivery systems: recent developments and future prospects. *J Nanobiotechnol.* <https://doi.org/10.1186/s12951-018-0392-8>
- Perez-Herrero E, Fernandez-Medarde A. (2015) Advanced targeted therapies in cancer: Drug nanocarriers, the future of chemotherapy. *Eur. J. Pharm. Biopharm.* <https://dx.doi.org/10.1016/j.ejpb.2015.03.018>
- Perumal V, Hashim U, Gopinath SCB, Haarindraprasad R, Foo KL, Balakrishnan SR, Poopalan P (2015) ‘Spotted nanoflowers’: goldseeded zinc oxide nanohybrid for selective bio-capture. *Scientific Reports.* <https://dx.doi.org/10.1038/srep12231>
- Pfeffer CM, Singh ATK. (2018) Apoptosis: a target for anticancer therapy. *Int. J. Mol. Sci.* 19: 448.
- Phaniendra A, Jestadi DB, Periyasamy L (2015) Free Radicals: Properties, Sources, Targets, and Their Implication in Various Diseases. *Ind J Clin Biochem* 30 (1):11–26
- Piccinini F, Tesei A, Arienti C, Bevilacqua A (2017) Cell counting and viability assessment of 2D and 3D cell cultures: expected reliability of the trypan blue

- assay. Biological Procedures Online. <https://dx.doi.org/10.1186/s12575-017-0056-3>
- Pierce BA (2012) Cancer genetics. Genetics: A conceptual approach. 4th edition, 637.
- Pitot HC (1993) The molecular biology of carcinogenesis. Cancer 72(3): 962-970
- Ponarulselvam S, Panneerselvam C, Murugan K, Aarthi N, Kalimuthu K, Thangamani S (2012) Synthesis of silver nanoparticles using leaves of *Catharanthus roseus* Linn. G. Don and their antiplasmodial activities. Asian Pac J Trop Biomed 2(7): 574-580
- Poon SL, McPherson JR, Tan P, Teh BT, Rozen SG (2014) Mutation signatures of carcinogen exposure: genome-wide detection and new opportunities for cancer prevention. Genome Medicine 6:24.
- Porter AG, Janicke RU (1999) Emerging roles of caspase-3 in apoptosis. Cell Death and Differentiation 6: 99-104
- Pott P (1775) Chirurgical Observations Relative to the Cataract, the Polypus of the Nose, Cancer of the Scrotum, Different Kinds of Ruptures, and the Mortification of the Toes and Feet. Cancer Scrot. In. London: Hawes, Clarke, Collins
- Powles T, Eder JP, Fine GD, Braiteh FS, Loriot Y, Cruz C, Bellmunt J, Burrell HA, Petrylak DP, Teng SL, Shen X, Boyd Z, Hegde PS, Chen DS, Vogelzang NJ (2014) MPDL3280A (anti-PD-L1) treatment leads to clinical activity in metastatic bladder cancer. Nature 515: 558–562
- Prasad K, Jha AK (2009) ZnO nanoparticles: synthesis and adsorption study. Nat. Sci 1: 129–135
- Prasad N, Sabarwal A, Yadav UCS, Singh RP (2018) Lupeol induces S-phase arrest and mitochondria-mediated apoptosis in cervical cancer cells. J Biosci 43(2):249–261

- Prashanth GK, Prashanth PA, Nagabhushana BM, Ananda S, Krishnaiah GM, Nagendra HG, Sathyananda HM, Singh CR, Yogisha S, Anand S, Tejabhiram Y (2017) Comparison of anticancer activity of biocompatible ZnO nanoparticles prepared by solution combustion synthesis using aqueous leaf extracts of *Abutilon indicum*, *Melia azedarach* and *Indigofera tinctoria* as biofuels. *Artificial Cells, Nanomedicine, and Biotechnology* 46(5): 968-979
- Prathna TC, Mathew L, Chandrasekaran N, Raichur AM, Mukherjee A (2010) Biomimetic synthesis of nanoparticles: science, technology & applicability. *Biomimetics learning from nature*. Intech Open edited by Amithav Mukherjee. <https://doi.org/10.5772/198>
- Premanathan M, Karthikeyan K, Jeyasubramanian K, Manivannan G (2011) Selective toxicity of ZnO nanoparticles toward Gram-positive bacteria and cancer cells by apoptosis through lipid peroxidation. *Nanomedicine: Nanotechnology, Biology, and Medicine* 7:184–192
- Priya P, Shoba FG, Parimala M, Sathya J (2014) Antioxidant and antibacterial properties of *Manilkara zapota* (L.) Royen flower. *Int J Pharm Clin Res* 6: 174 - 178.
- Purkait PK, Roy J, Maitra S, Choudhuri MG (2015) Green synthesis of Zinc oxide nanoparticles – A Review. *Scientific voyage* 1(2): 32-46
- Puvvada N, Rajput S, Kumar BN, Sarkar S, Konar S, Brunt KR, Rao RR, Mazumdar A, Das SK, Basu R, Fisher PB, Mandal M, Pathak A (2015) Novel ZnO hollow-nanocarriers containing paclitaxel targeting folate receptors in a malignant pH-microenvironment for effective monitoring and promoting breast tumor regression. *Scientific Reports* 5(1): 11760.
- Qidwai A, Pandey A, Kumar R, Shukla SK, Dikshit A (2018) Advances in biogenic nanoparticles and the mechanisms of antimicrobial effects. *Indian J Pharm Sci* 80(4) : 592-603

- Qin JJ, Wang W, Zhang R (2017) Experimental Therapy of Advanced Breast Cancer: Targeting NFAT1–MDM2–p53 Pathway. *Prog Mol Biol Transl Sci.* 151: 195–216.
- Quail DF, Dannenberg AJ (2019) The obese adipose tissue microenvironment in cancer development and progression. *Nature Reviews Endocrinology* 15: 139–154
- Rady I, Bloch MB, Chamcheu R-CN, Mbeumi SB, Md Anwar R, Mohamed H, Babatunde AS, Kuate J-R, Noubissi FK, El Sayed KA, Whitfield GK, Chamcheu JC (2018) Anticancer Properties of Graviola (*Annona muricata*): A Comprehensive Mechanistic Review. *Oxidative Medicine and Cellular Longevity.* Article ID 1826170.
- Raghupathi KR, Koodali RT, Manna AC (2011) Size-dependent bacterial growth inhibition and mechanism of antibacterial activity of zinc oxide nanoparticles. *Langmuir* 27:4020–4028
- Raguvaran R, Manuja A, Singh S, Chopra M, Manuja BK, Dimri U (2015) Zinc oxide nanoparticles induced hemolytic cytotoxicity in horse red blood cells. *Int J Pharm Sci Res*, 6: 1166-69
- Raja A, Ashokkumar S, Marthandam PR, Jayachandiran J, Khatiwada CP, Kaviyarasu K, Raman GR, Swaminathan M (2018). Eco-friendly preparation of zinc oxide nanoparticles using *Tabernaemontana divaricata* and its photocatalytic and antimicrobial activity. *Journal of Photochemistry and Photobiology B: Biology* 181: 53–58
- Rajabairavi N, Raju CS, Karthikeyan C, Varutharaju K, Nethaji S, Hameed ASH, et al (2017) Biosynthesis of novel zinc oxide nanoparticles (ZnO NPs) using endophytic bacteria *Sphingobacterium thalpophilum*. *Springer Proc Phys.* 189: 245–254.
- Rajakumar G, Thiruvengadam M, Mydhili G, Gomathi T, Chung I-M (2017) Green approach for synthesis of zinc oxide nanoparticles from *Andrographis*

- paniculata* leaf extract and evaluation of their antioxidant, anti-diabetic, and anti-inflammatory activities. *Bioprocess Biosyst Eng* 41: 21–30
- Rajendran SP, Sengodan K (2017) Synthesis and characterization of Zinc oxide and Iron Oxide nanoparticles using *Sesbania grandiflora* leaf extract as reducing agent. *Journal of Nanoscience*. <https://doi.org/10.1155/2017/8348507>.
- Rajeshkumar S, Venkat Kumar S, Ramaiah A, Agarwal H, Lakshmi T, Roopan SM (2018) Biosynthesis of zinc oxide nanoparticles using *Mangifera indica* leaves and evaluation of their antioxidant and cytotoxic properties in lung cancer (A549) cells. *Enzyme and Microbial Technology* 117: 91-95
- Raji R, Gopchandran KG (2017) ZnO nanostructures with tunable visible luminescence: Effects of kinetics of chemical reduction and annealing. *Journal of Science: Advanced Materials and Devices* 2: 51-58
- Rajiv P, Vanathi P, Thangamani A (2018) An investigation of phytotoxicity using Eichhornia mediated zinc oxide nanoparticles on *Helianthus annuus* *Biocatalysis and Agricultural Biotechnology* 16: 419-424
- Rajput A, Martin IDS, Rose R, Beko A, LeVea C, Sharratt E, Mazurchuk R, Hoffman RM, Brattain MG, Wang J (2008) Characterization of HCT 116 human colon cancer cells in an orthotopic model. *Journal of Surgical Research* 147: 276–281
- Ramalingam V, Revathidevi S, Shanmuganayagam T, Muthulakshmi L, Rajaram R (2016) Biogenic gold nanoparticles induce cell cycle arrest through oxidative stress and sensitize mitochondrial membranes in A549 lung cancer cells. *RSC Advances* 6(25): 20598–20608
- Ramesh MM, Anbuvaran G, Viruthagiri (2015) Green synthesis of ZnO nanoparticles using *Solanum nigrum* leaf extract and their antibacterial activity. *Spectrochimica Acta Part A: Molecular and Biomolecular Spectroscopy*. 136(B5):864-870

- Ramimoghadam D, Hussein MZB, Taufiq-Yap YH (2013) Hydrothermal synthesis of zinc oxide nanoparticles using rice as soft biotemplate. *Chemistry Central Journal* 7:136
- Rao US, Srinivas G, Rao TP (2015) Influence of precursors on morphology and spectroscopic properties of ZnO nanoparticles. *Procedia Materials Science* 10: 90 – 96
- Rasmussen JW, Martinez E, Louka P, Wingett DG (2010) Zinc oxide nanoparticles for selective destruction of tumor cells and potential for drug delivery applications. *Expert Opin. Drug. Deliv.* 7:1063–1077
- Rathore P, Chittora Ak, Ameta R, Sharma S (2015) Enhancement of photocatalytic activity of zinc oxide by doping with nitrogen. *Sci. Revs. Chem. Commun.* 5(4): 113-124
- Ratney YJJJ, David SB (2017) Evaluation of *in-vitro* anticancer and antioxidant activity of zinc oxide nanoparticle by chemical and green method. *International Journal of Latest Trends in Engineering and Technology (Special Issue - International Conference on Nanotechnology: The Fruition of Science-2017)*: 10-15.
- Rauf MA, Oves M, Rehman FU, Khan AR, Husain N (2019) Bougainvillea flower extract mediated zinc oxide's nanomaterials for antimicrobial and anticancer activity. *Biomedicine & Pharmacotherapy*. <https://doi.org/10.1016/j.biopha.2019.108983>
- Rauf MA, Owais M, Rajpoot R, Ahmad F, Khan N, Zubair S (2017) Biomimetically synthesized ZnO nanoparticles attain potent antibacterial activity against less susceptible: *S. aureus* skin infection in experimental animals. *RSC Adv.* 7:36361–36373
- Raut S, Thorat PV, Thakre R (2015) Green Synthesis of Zinc Oxide (ZnO) Nanoparticles Using *Ocimum Tenuiflorum* Leaves. *International Journal of Science and Research* 4(5): 1225-1228.

- Rauwel P, Salumaa M, Aasna A, Galeckas A, Rauwel E (2016) A review of the synthesis and photoluminescence properties of hybrid ZnO and carbon nanomaterials. *Journal of Nanomaterials* <https://dx.doi.org/10.1155/2016/5320625>
- Reddy LS, Nisha MM, Joice M, Shilpa PN. (2014) Antimicrobial activity of zinc oxide (ZnO) nanoparticle against *Klebsiella pneumoniae*. *Pharmaceutical Biology* 52(11): 1388-1397
- Rehana D, Mahendiran D, Kumar RS, Rahiman AK (2017) In vitro antioxidant and antidiabetic activities of zinc oxide nanoparticles synthesized using different plant extracts. *Bioprocess Biosyst Eng.* <https://dx.doi.org/10.1007/s00449-017-1758-2>
- Rello S, Stockert JC, Moreno V, G´amez A., Pacheco M, Juarranz A, Cañete M, Villanueva A (2005) Morphological criteria to distinguish cell death induced by apoptotic and necrotic treatments. *Apoptosis* 10: 201-208
- Rikans LE, Hornbrook, KR (1997) Lipid peroxidation, antioxidant protection and aging. *Biochem Biophys Acta* 1362:116-127
- Roberti A, Valdes AF, Torrecillas R, Fraga MF, Fernandez AF (2019) Epigenetics in cancer therapy and nanomedicine. *Clinical Epigenetics.* <https://doi.org/10.1186/s13148-019-0675-4>
- Roos WP, Thomas AD, Kaina B (2016) DNA damage and the balance between survival and death in cancer biology. *Nature Reviews Cancer* 16: 20–33
- Ruoslahti E, Reed JC (1994) Anchorage dependence, Integrins and apoptosis. *Cell* 77: 477-478.
- Rupprecht JK, Hui YH, McLaughlin JL (1990) Annonaceous acetogenins: a review. *J. Nat. Prod* 53: 237–278

- Ryu W-I, Park Y-H, Bae HC, Kim JH, Jeong SH, Lee H, Son SW (2014) ZnO nanoparticle induces apoptosis by ROS triggered mitochondrial pathway in human keratinocytes. *Mol Cell Toxicol* 10: 387-391.
- Safta TB, Ziani L, Favre L, Lamendour L, Gros G, Mami-Chouaib F, Martinvalet D, Chouaib S, Thiery J (2014) Granzyme B-activated p53 interacts with Bcl-2 to promote cytotoxic lymphocyte-mediated apoptosis. *J Immunol* 194: 418-428
- Sagadevan S, Raj KP, Aziz FA, Chowdhury ZZ, Johan MRB, Podder J (2018) Structure, properties, photocatalytic and antibacterial activity and applications of zinc oxide nanoparticles—an overview. *Journal of Bionanoscience* 12:457–468
- Saha R, Karthik S, Balu KS, Suriyaprabha R, Siva P, Rajendran V. (2018) Influence of the various synthesis methods on the ZnO nanoparticles property made using the bark extract of *Terminalia arjuna*. *Mater. Chem. Phys.* <https://doi.org/10.1016/j.matchemphys.2018.01.023>
- Saha S, Sarkar P (2014) Understanding the interaction of DNA–RNA nucleobases with different ZnO nanomaterials. *Phys Chem Chem Phys* 16: 15355-15366
- Sahu D, Kannan GM, Vijayaraghavan R, Anand T, Khanum F. (2013) Nanosized zinc oxide induces toxicity in human lung cells. *ISRN Toxicology* <https://dx.doi.org/10.1155/2013/316075>
- Salah N, Habib SS, Khan ZH, Memic A, Azam A, Alarfaj E, Zahed N, Al-Hamedi S (2011) High-energy ball milling technique for ZnO nanoparticles as antibacterial material. *International Journal of Nanomedicine* 6: 863–869
- Salari Z, Ameri A, Forootanfar H, Adeli-Sardou M, Jafari M, Mehrabani M, Shakibaie M (2017) Microwave-assisted biosynthesis of zinc nanoparticles and their cytotoxic and antioxidant activity. *Journal of Trace Elements in Medicine and Biology* 39: 116–123

- Salem W, Leitner DR, Zingl FG (2015) Antibacterial activity of zinc and silver nanoparticles against *Vibrio cholera* and enterotoxigenic *Escherichia coli*. Int. J. Med. Microbiol 305: 85-95
- Salvadores M, Mas-Ponte D, Supek F (2019) Passenger mutations accurately classify human tumors. PLOS Computational Biology. <https://doi.org/10.1371/journal.pcbi.1006953>
- Samà J, Prades J D, Casals O, Barth S, Gracia I, Cané C, Domènech-Gil G, Hernández-Ramírez F, Romano-Rodríguez A (2015) Low-cost fabrication of zero-power metal oxide nanowire gas sensors: trends and challenges. Procedia Engineering 120: 488 – 491.
- Samanta A, Medintz IL (2016) Nanoparticles and DNA – a powerful and growing functional combination in bionanotechnology. Nanoscale 8: 9037–9095
- Samat NA, Nor RM (2013) Sol–gel synthesis of zinc oxide nanoparticles using *Citrus aurantifolia* extracts. Ceramics International 39: 545–548
- Samuel SM, Bose L, George KC (2009) Optical properties of ZnO nanoparticles. SB Academic Review 16: 57-65
- Samzadeh-Kermani A, Izadpanah F, Mirzaee M (2016) The improvements in the size distribution of zinc oxide nanoparticles by the addition of a plant extract to the synthesis. Cogent Chemistry. <https://dx.doi.org/10.1080/23312009.2016.1150389>
- Sanad F, Nabih S, Goda MA (2018) A Lot of Promise for ZnO-5FU Nanoparticles Cytotoxicity against Breast Cancer Cell Lines. J Nanomed Nanotechnol 9:1.
- Sanaeimehr Z, Javadi I, Namvar F (2018) Antiangiogenic and antiapoptotic effects of green synthesized zinc oxide nanoparticles using *Sargassum muticum* algae extraction. Cancer Nano. <https://doi.org/10.1186/s12645-018-0037-5>

- Sangappa M, Vandana SP, Bharath AU, Thiagarajan P (2013) Mycobiosynthesis of novel non toxic zinc oxide nanoparticles by a new soil fungus *Aspergillus terreus* VIT 2013. *J. Chem. Pharm. Res.* 5(12): 1155-1161
- Sangeetha G, Rajeshwari S, Venckatesh R (2011) Green synthesis of zinc oxide nanoparticles by aloe barbadensis miller leaf extract: structure and optical properties. *Materials Research Bulletin* 46: 2560–2566
- Santarelli A, Mascitti M, Russo LL, Sartini D, Troiano G, Emanuelli M, Muzio LL. (2018) Survivin-based treatment strategies for squamous cell carcinoma. *Int. J Mol Sci* 19: 971
- Saunders K, Sainsbury F, Lomonosoff, GP (2009) Efficient generation of cowpea mosaic virus empty virus-like particles by the proteolytic processing of precursors in insect cells and plants. *Virology* 393: 329–337
- Sawhney RS, Zhou GH, Humphrey LE, et al (2002) Differences in sensitivity of biological functions mediated by epidermal growth factor receptor activation with respect to endogenous and exogenous ligands. *J Biol Chem* 277:75.
- Schaefer H-E (2010) *Nanoscience: The science of the small in physics, engineering, chemistry, biology and medicine.* Springer-Verlag Berlin Heidelberg, <https://doi.org/10.1007/978-3-642-10559-3>.
- Schwanhäusser B, Busse D, Li N, Dittmar G, Schuchhardt J, Wolf J, Chen W, Selbach M (2011) Global quantification of mammalian gene expression control. *Nature* 473: 337–342
- Scimeca M, Bischetti S, Lamsira HK, Bonfiglio R, Bonanno E (2018) Energy Dispersive X-ray (EDX) microanalysis: A powerful tool in biomedical research and diagnosis. *European Journal of Histochemistry*
- Seca AML, Pinto DCGA (2018) plant secondary metabolites as anticancer agents: successes in clinical trials and therapeutic application. *Int. J. Mol. Sci.* <https://doi.org/10.3390/ijms19010263>

- Senese S, Lo YC, Huang D, Zangle TA, Gholkar AA, Robert L, Homet B, Ribas A, Summers MK, Teitell MA, Damoiseaux R, Torres JZ . (2014) Chemical dissection of the cell cycle: probes for cell biology and anti-cancer drug development. *Cell Death and Disease* 5: e1462 <https://doi.org/10.1038/cddis.2014.420>.
- Senthilkumar SR, Sivakumar T (2014) Green tea (*Camellia sinensis*) mediated synthesis of zinc oxide (ZnO) nanoparticles and studies on their antimicrobial activities. *Int J Pharm Pharm Sci* 6(6): 461-465
- Setyawati MI, Tay CT, Leong DT (2013) Effect of zinc oxide nanomaterials-induced oxidative stress on the p53 pathway. *Biomaterials* 34: 10133-10142
- Shafii ZA, Basri M, Malek EA, Ismail M (2017) Phytochemical and antioxidant properties of *Manilkara zapota* (L.) P Royen fruit extracts and its formulation for cosmeceutical application. *Asian Journal of Plant Science and Research* 7(3):29-41.
- Shah M, Fawcett D, Sharma S, Tripathy SK, Poinern GEJ (2015) Green Synthesis of Metallic Nanoparticles via Biological Entities. *Materials* 8: 7278–7308
- Shalem O, Sanjana NE, Hartenian E, Shi X, Scott DA, Mikkelson T, Heckl D, Ebert BL, Root DE, Doench JG, Zhang F (2014) Genome-scale CRISPR-Cas9 knockout screening in human cells. *Science* 343: 84–87
- Shamhari NM, Wee BS, Chin SF, Kok KY (2018) Synthesis and characterization of zinc oxide nanoparticles with small particle size distribution. *Acta Chim Slov* 65: 578–585
- Shamsuzzaman, Mashrai A, Khanam H, Aljawfi RN (2017) Biological synthesis of ZnO nanoparticles using *C. albicans* and studying their catalytic performance in the synthesis of steroidal pyrazolines. *Arabian Journal of Chemistry* 10:S1530–S1536
- Shaniba VS, Aziz AA, Jayasree PR, Manish Kumar PR (2019) *Manilkara zapota* (L.) P. Royen Leaf Extract Derived Silver Nanoparticles Induce Apoptosis in

Human Colorectal Carcinoma Cells Without Affecting Human Lymphocytes or Erythrocytes. Biological trace element research. <https://doi.org/10.1007/s12011-019-1653-6>.

Shanmugapriya K, Saravana PS, Payal H, Mohammed SP, Bennai W (2011) A comparative study of antimicrobial potential and phytochemical analysis of *Artocarpus heterophyllus* and *Manilkara zapota* seed extracts. **J Pharm Res** 4: 2587 - 2589.

Sharifi S, Barar J, Hejazi MS, Samadi N (2015) Doxorubicin changes Bax /Bcl-xL Ratio, Caspase-8 and 9 in breast cancer cells. *Adv Pharm Bull.* 5(3): 351-359

Sharma V, Anderson D, Dhawan A (2012) Zinc oxide nanoparticles induce oxidative DNA damage and ROS triggered mitochondria mediated apoptosis in human liver cells (HepG2). *Apoptosis* 17 (8): 852–870.

Sharma A, Goyal AK, Rath G (2018) Recent advances in metal nanoparticles in cancer therapy. *Journal of Drug Targeting* 26:8, 617- 632, <https://doi.org/10.1080/1061186X.2017.1400553>

Sharmila G, Muthukumaran C, Sandiya K, Santhiya S, Sakthi Pradeep R, Manoj Kumar N, Suriyanarayanan N, Thirumarimurugan M (2018) Biosynthesis, characterization, and antibacterial activity of Zinc oxide nanoparticles derived from *Bauhinia tomentosa* leaf extract. *Journal of Nanostructure in Chemistry* 8: 293–299

Sharmila G, Thirumarimurugan M, Muthukumaran C (2019) Green synthesis of ZnO nanoparticles using *Tecoma castanifolia* leaf extract: Characterization and evaluation of its antioxidant, bactericidal and anticancer activities. *Microchemical Journal* 145: 578-587

Shastri L, Qureshi MS, Malik MM (2014) Synthesis and Luminescence Properties of ZnONanoparticles Produced by the Sol Gel Method. *Journal of pure applied and industrial physics.* 4(3):119-125.

- Shen J, Xiao Z, Zhao Q, Li M, Wu X, Zhang L, Hu W, Cho CH (2017) Anti-cancer therapy with TNF α and IFN γ : A comprehensive review. Cell proliferation <https://doi.org/10.1111/cpr.12441>
- Shirsekar PP Kanhe NS, Mathe VL (2016) Interaction of zinc oxide nanoparticles with human red blood cells. Bionano Frontier 9:99-104
- Shobha N, Nanda N, Giresha AS, Manjappa P, Dharmappa KK, Nagabhushana, BM (2018) Synthesis and characterization of Zinc oxide nanoparticles utilizing seed source of *Ricinus communis* and study of its antioxidant, antifungal and anticancer activity. Materials Science and Engineering: C. <https://doi.org/10.1016/j.msec.2018.12.023>
- Siddiqi KS, ur Rahman A, Tajuddin, Husen A (2018) Properties of zinc oxide nanoparticles and their activity against microbes. Nanoscale Research Letters <https://doi.org/10.1186/s11671-018-2532-3>
- Siddiquah A, Hashmi SS, Mushtaq S, Renouard S, Blondeau JP, Abbasi R, Hano C, Abbasi BH (2018) Exploiting in vitro potential and characterization of surface modified zinc oxide nanoparticles of *Isodon rugosus* extract: their clinical potential towards HEPG2 cell line and human pathogenic bacteria. EXCLI Journal 17: 671-687
- Siemann W, Keng C (1986) Cell cycle specific toxicity of the Hoechst 33342 stain in untreated or irradiated murine tumor cells. Cancer Research 46: 3556-3559
- Sinden RR (2012) DNA structure and function; Academic Press, Inc.: Cambridge, MA. U.S.A
- Sing T, Shukla S, Kumar P, Wahla V, Bajpai VK, Rather IA (2017) Corrigendum: application of nanotechnology in food science: perception and overview. Front Microbiol <https://doi.org/10.3389/fmicb.2017.02517>

- Singh BN, Rawat AKS, Khan W, Naqvi AH, Singh BR. (2014) Biosynthesis of stable antioxidant ZnO nanoparticles by *Pseudomonas aeruginosa* Rhamnolipids. PLoS One <https://doi.org/10.1371/journal.pone.0106937>
- Singh J, Dutta T, Kim K-H, Rawat M, Samddar P, Kumar P. (2018) ‘Green’ synthesis of metals and their oxide nanoparticles: applications for environmental remediation. Nanobiotechnol. <https://doi.org/10.1186/s12951-018-0408-4>
- Singh J, Kaur S, Kaur G, Basu S, Rawat M (2019) Biogenic ZnO nanoparticles: a study of blueshift of optical band gap and photocatalytic degradation of reactive yellow 186 dye under direct sunlight. Green Process Synth 8: 272–280
- Singh K, Singh J, Rawa M (2019) Green synthesis of zinc oxide nanoparticles using *Punica Granatum* leaf extract and its application towards photocatalytic degradation of Coomassie brilliant blue R-250 dye. SN Applied Sciences <https://doi.org/10.1007/s42452-019-0610-5>
- Singh NA (2017) Nanotechnology innovations, industrial applications and patents. Environ Chem Lett 15: 185–191
- Singh P, Garg A, Pandit S, Mokkapati VRSS, Mijakovic I (2018) Antimicrobial effects of biogenic nanoparticles. Nanomaterials. <https://doi.org/10.3390/nano8121009>
- Singh P, Pandit S, Mokkapati VRSS, Garg A, Ravikumar V, Mijakovic I (2018) Gold nanoparticles in diagnostics and therapeutics for human cancer. Int. J. Mol. Sci. <https://doi.org/10.3390/ijms19071979>
- Singh RP, Shukla VK, Yadav RS, Sharma, Singh PK, Pandey AC (2011) Biological approach of zinc oxide nanoparticles formation and its characterization. Adv. Mat. Lett. 2(4): 313-317

- Singh T, Shukla S, Kumar P, Wahla V, Bajpai VK and Rather IA (2017) Application of nanotechnology in food science: perception and overview. *Front. Microbiol.* 8:1501.
- Sirelkhatim A, Mahmud S, Seeni A, Kaus NHM, Ann LC, Bakhori SKM, Hasan H, Mohamad D (2015) Review on zinc oxide nanoparticles : antibacterial activity and toxicity mechanism. *Nano-Micro Lett* 7: 219–242
- Sivakumar P, Lee M, Kim Y, Shim MS (2018) Photo-triggered antibacterial and anticancer activities of zinc oxide nanoparticles *J. Mater. Chem. B.* <https://doi.org/10.1039/C8TB00948A>
- Sivaraj R, Salam HA, Rajiv P, Rajendran V (2014) Green nanotechnology: the solution to sustainable development of environment. *Environmental Sustainability* 311-324
- Smaili SS, Hsu YT, Carvalho ACP, Rosenstock TR, Sharpe JC, Youle RJ (2003) Mitochondria, calcium and pro-apoptotic proteins as mediators in cell death signaling. *Brazilian Journal of Medical and Biological Research* 36: 183-190
- Song G, Cheng L, Chao Y, Yang K, Liu Z (2017) Emerging nanotechnology and advanced materials for cancer radiation therapy. *Adv. Mater.* <https://doi.org/10.1002/adma.201700996>
- Soto F and Chrostowski R (2018) Frontiers of medical micro/nanorobotics: *in vivo* applications and commercialization perspectives toward clinical uses. *Front. Bioeng. Biotechnol.* <https://doi.org/10.3389/fbioe.2018.00170>
- Sparano JA, Gray RJ, Makower DF, Pritchard KI, Albain KS, Hayes DF, Geyer Jr CE, Dees EC, Goetz MP, Olson Jr JA, Lively T, Badve SS, Saphner TJ, Wagner LI, Whelann TJ, Ellis MJ, Paik S, Wood WC, Ravdin PM, Keane MM, Moreno HLG, Reddy PS, Goggins TF, Mayer IA, Brufsky AM, Toppmeyer DL, Kaklamani VG, Berenberg JL, Abrams J, Sledge Jr GW.

- (2018) Adjuvant chemotherapy guided by a 21-gene expression assay in breast cancer. *N Engl J Med*. <https://doi.org/10.1056/NEJMoa1804710>
- Sposito AJ, Kurdekar A, Zhao J, Hewlett I (2018) Application of nanotechnology in biosensors for enhancing pathogen detection. *Nanomed Nanobiotechnol* <https://doi.org/10.1002/wnan.1512>
- Spratt DE, Dess RT, Zumsteg ZS, Lin DW, Tran PT, Morgan TM, Antonarakis ES, Nguyen PL, Ryan CJ, Sandler HM, Cooperberg MR, Posadas E, Feng FY (2017) A Systematic Review and Framework for the Use of Hormone Therapy with Salvage Radiation Therapy for Recurrent Prostate Cancer. *Eur Urol*. <https://dx.doi.org/10.1016/j.eururo.2017.06.027>
- Sreekanth D, Arunasree MK, Roy KR, Chandramohan Reddy T, Reddy GV, Reddanna P (2007) Betanin a betacyanin pigment purified from fruits of *Opuntia ficus-indica* induces apoptosis in human chronic myeloid leukemia Cell line-K562. *Phytomedicine* 14(11): 739-746
- Sri Sindhura K, Prasad TNVKV, Panner Selvam P, Hussain OM (2013) Synthesis, characterization and evaluation of effect of phytogenic Zinc nanoparticles on soil exo-enzymes. *Appl Nanosci*. <https://doi.org/10.1007/s13204-013-0263-4>
- Steffy K, Shanthi G, Maroky AS, Selvakumar S (2018) Enhanced antibacterial effects of green synthesized ZnO NPs using *Aristolochia indica* against Multi-drug resistant bacterial pathogens from Diabetic Foot Ulcer. *Journal of Infection and Public Health* 11: 463–471
- Su S, Zou Z, Chen F, Ding N, Du J, Shao J, Li L, Fu Y, Hu B, Yang Y, Sha H, Meng F, Wei J, Huang X, Liu B (2017) CRISPR-Cas9-mediated disruption of PD-1 on human T cells for adoptive cellular therapies of EBV positive gastric cancer. *OncoImmunology*. <https://dx.doi.org/10.1080/2162402X.2016.1249558>.

- Sudheer Kumar KH, Dhananjaya N, Reddy Yadav LS (2018) E. tirucalli plant latex mediated green combustion synthesis of ZnO nanoparticles: Structure, photoluminescence and photo-catalytic activities. *Journal of Science: Advanced Materials and Devices* 3: 303-309
- Sujarwo W, Saraswaty V, Keim AP, Caneva G, Tofani D (2017) Ethnobotanical uses of ‘cemcem’ (*Spondias pinnata* (L. f.) kurz; anacardiaceae) leaves in bali (indonesia) and its antioxidant activity, *PhOL* 1: 113-123.
- Sukri SNAM, Shameli K, Wong MM-T, Teow S-Y, Chew J, Ismail NA (2019) Cytotoxicity and antibacterial activities of plant-mediated synthesized zinc oxide (ZnO) nanoparticles using *Punica granatum* (pomegranate) fruit peels extract. *Journal of Molecular Structure* <https://doi.org/10.1016/j.molstruc.2019.04.026>
- Sun H, Gao D (2018) Propofol suppresses growth, migration and invasion of A549 cells by down-regulation of miR-372. *BMC Cancer*. <https://doi.org/10.1186/s12885-018-5175-y>
- Sundrarajan M, Ambika S, Bharathi K (2015) Plant-extract mediated synthesis of ZnO nanoparticles using *Pongamia pinnata* and their activity against pathogenic bacteria. *Advanced Powder Technology* 26: 1294–1299
- Sunoqrot S, Abujamous L (2019) pH-sensitive polymeric nanoparticles of quercetin as a potential colon cancer-targeted nanomedicine. *Journal of Drug Delivery Science and Technology* 52: 670–676.
- Suresh D, Nethravathi PC, Udayabhanu, Rajanaika H, Nagabhushana H, Sharma SC. (2015) Green synthesis of multifunctional zinc oxide (ZnO) nanoparticles using *Cassia fistula* plant extract and their photodegradative, antioxidant and antibacterial activities. *Materials Science in Semiconductor Processing* 31: 446–454
- Suresh J, Pradheesh G, Alexramani V, Sundrarajan M, Hong SI (2018) Green synthesis and characterization of zinc oxide nanoparticle using insulin plant

(*Costus pictus* D. Don) and investigation of its antimicrobial as well as anticancer activities. Adv Nat Sci: Nanosci Nanotechnol. <https://doi.org/10.1088/2043-6254/aaa6f1>

Suresh S, Karthikeyan S, Jayamoorthy K (2016) Spectral investigations to the effect of bulk and nano ZnO on peanut plant leaves. Karbala International Journal of Modern Science 2: 69-77

Sutradhar P, Saha M (2016) Green synthesis of Zinc oxide nanoparticles using tomato (*Lycopersicon esculentum*) extract and its photovoltaic application. Journal of Experimental Nanoscience 11(5): 314-327

Sztandera K, Gorzkiewicz M, Klajnert-Maculewicz B (2019) Gold Nanoparticles in Cancer Treatment. Mol. Pharmaceutics 16: 1–23

Talam S, Karumuri SR, Gunnam N. (2012) Synthesis, Characterization, and Spectroscopic Properties of ZnO Nanoparticles. ISRN Nanotechnology. <https://doi.org/10.5402/2012/372505>

Tan BL, Norhaizan ME, Chan LC (2018) Apoptosis in the modulation of caspase activation and EGFR/NF- κ B activities of hela human cervical cancer cells. Evidence-Based Complementary and Alternative Medicine. Article ID 6578648

Taranath TC, Bheemanagouda NP, Santosh TU, Sharath BS (2015) Cytotoxicity of zinc nanoparticles fabricated by *Justicia adathoda* L. on root tips of *Allium cepa* L.- a model approach. Environ Sci Pollut Res 22: 8611-8617.

Taunk PB, Das R, Bisen DP, Tamrakar RK (2015) Structural characterization and photoluminescence properties of zinc oxide nano particles synthesized by chemical route method. Journal of Radiation Research and Applied Sciences 8: 433-438

Thatoi P, Kerry RG, Gouda S, Das G, Pramanik K, Thatoi H, Patra JK (2016) Photo-mediated green synthesis of silver and zinc oxide nanoparticles using aqueous extracts of two mangrove plant species, *Heritiera fomes* and

- Sonneratia apetala* and investigation of their biomedical applications. *Journal of Photochemistry and Photobiology B: Biology* 163: 311–318
- Thema FT, Manikandan E, Dhlamini MS, Maaza M (2015) Green synthesis of ZnO nanoparticles via *Agathosma betulina* natural extract. *Mater Lett* 161: 124–127
- Thuret G, Chiquet C, Herrag S, Dumollard J-M, Boudard D, Bednarz Z, Campos L, Gain P (2003) Mechanisms of staurosporine induced apoptosis in a human corneal endothelial cell line. *Br J Ophthalmol* 87: 346-352
- Tian X, Gu T, Patel S, Bode AM, Lee MH, Dong Z (2019) CRISPR/Cas9 – An evolving biological tool kit for cancer biology and oncology. *NPJ Precis. Oncol* 3: 8
- Ting AH, McGarvey KM, Baylin SB (2006) The cancer epigenome-components and functional correlates. *Genes Dev* 20: 3215-3231
- Tivnan A, Orr WS, Gubala V, Nooney R, Williams DE, McDonagh C, Prenter S, Harvey H, Domingo-Fernández R, Bray IM, Piskareva O, Ng CY, Lode HN, Davidoff AM, Stallings RL (2012) Inhibition of neuroblastoma tumor growth by targeted delivery of microRNA-34a using anti-disialoganglioside GD2 coated nanoparticles. *PLoS One* 7(5): e38129 <https://doi.org/10.1371/journal.pone.0038129>
- Tiwari V, Mishra N, Gadani K, Solanki PS, Shah NA and Tiwari M (2018) Mechanism of anti-bacterial activity of zinc oxide nanoparticle against carbapenem-resistant *Acinetobacter baumannii*. *Front. Microbiol.* <https://doi.org/10.3389/fmicb.2018.01218>
- Tomicic MT, Christmann M, Kaina B (2010) Topotecan triggers apoptosis in p53-deficient cells by forcing degradation of XIAP and Survivin thereby activating Caspase-3-mediated Bid cleavage. *JPET* 332(1): 316-325

- Tran S, DeGiovanni P-J, Piel B, Rai P (2017) Cancer nanomedicine: a review of recent success in drug delivery. *Clin Trans Med* <https://doi.org/10.1186/s40169-017-0175-0>
- Tripathi RM, Bhadwal AS, Gupta RK, Singh P, Shrivastav A, Shrivastav BR (2014) ZnO nanoflowers: novel biogenic synthesis and enhanced photocatalytic activity. *J Photochem Photobiol B Biol* 141: 288–295
- Tripathy N, Ahmad R, Ko HA, Khang G, Hahn YB (2015) Enhanced anticancer potency using an acid-responsive ZnO-incorporated liposomal drug-delivery system. *Nanoscale*, (9): 4088–4096
- Tso C, Zhung C, Shih Y, Tseng Y, Wu S, Doong R (2010) Stability of metal oxide nanoparticles in aqueous solutions. *Water Science & Technology* 61(1):127-133
- Uchida S, Kobayashi K, Ohno S, Sakagami H, Kohase H, Nagasaka H (2019) Induction of non-apoptotic cell death by adrenergic agonists in human oral squamous cell carcinoma cell lines. *Anticancer research* 39: 3519-3529.
- Uekane TM, Nicolotti L, Griglione A, Bizzo HR, Rubiolo P, Bicchi C, Rocha-Leão MHM, Rezende CM (2017) Studies on the volatile fraction composition of three native Amazonian-Brazilian fruits: Murici (*Byrsonima crassifolia* L., Malpighiaceae), bacuri (*Platonia insignis* M., Clusiaceae), and sapodilla (*Manilkara zapota* L., Sapotaceae). *Food Chem* 219: 13 - 22
- Ugurel S, Röhmel J, Ascierio PA, Flaherty KT, Grob JJ, Hauschild A, Larkin J, Long GV, Lorigan P, McArthur GA, Ribas A, Robert C, Schadendorf D, Garbe C (2017) Survival of patients with advanced metastatic melanoma: the impact of novel therapies-update. *Eur J Cancer* 83: 247–257
- Umar H, Kavaz D, Rizaner N (2019) Synthesis, characterization, and spectroscopic properties of ZnO nanoparticles. *International Journal of Nanomedicine* 1: 87–100

- United Nations. Questions About Nanotechnology. 2012 <https://www.epa.gov/chemical-research/research-nanomaterials>
- Vallabani NVS, Sengupta S, Shukla RK, Kumar A (2019) ZnO nanoparticles-associated mitochondrial stress-induced apoptosis and G2/M arrest in HaCaT cells: a mechanistic approach. *Mutagenesis*, 34: 265–277.
- Vanathi P, Rajiv P, Narendhran S, Rajeshwari S, Rahman PKSM, Venckatesh R. (2014) Biosynthesis and characterization of phyto mediated zinc oxide nanoparticles: a green chemistry approach. *Materials Letters* 134: 13–15.
- Van Driel WJ, Koole SN, Sikorska K, vanLeeuwen JHS, Schreuder HWR, Hermans RHM, de Hingh IHJT, van der Velden J, Arts HJ, Massuger LFAG, Aalbers AGJ, Verwaal VJ, Kieffer JM, deVijver KKV, vanTinteren H, Aaronson NK, Sonke GS (2018) Hyperthermic intraperitoneal chemotherapy in ovarian cancer. *N Engl J Med*. <https://doi.org/10.1056/NEJMoa1708618>
- Vani C, Sergin GK, Annamalai A (2011) A study on the effect of zinc oxide nanoparticles in *Staphylococcus aureus*. *Int J Pharma Bio Sci* 2: 326-335
- Vasileiou I, Xanthos T, Koudouna E, Perrea D, Klonaris C, Katsargyris A, Papadimitriou L (2009) Propofol: a review of its non-anaesthetic effects. *Eur J Pharmacol*. 605(1–3): 1–8
- Velsankar K, Sudhakar S, Parvathy G, Kaliammal R (2020) Effect of cytotoxicity and Antibacterial activity of biosynthesis of ZnO hexagonal shaped nanoparticles by *Echinochloa frumentacea* grains extract as a reducing agent. *Materials Chemistry and Physics*. <https://doi.org/10.1016/j.matchemphys.2019.121976>
- Venkatesan J, Kim SK, Shim MS (2016) Antimicrobial, antioxidant and anticancer activities of biosynthesized silver nanoparticles using algae *Ecklonia cava*. *Nanomaterials* 6: 235
- Ventola CL (2015) The antibiotic resistance crisis: Part 1: Causes and threats. *P T Peer-Rev J Formul Manag* 40: 277–283

- Vijayakumara S, Krishnakumara C, Arulmozhia P, Mahadevana S, Parameswari N (2018) Biosynthesis, characterization and antimicrobial activities of zinc oxide nanoparticles from leaf extract of *Glycosmis pentaphylla* (Retz.) DC. *Microbial Pathogenesis* 116: 44–48
- Vimala K, Sundarraaj S, Paulpandi M, Vengatesan S, Kannan S (2014) Green synthesized doxorubicin loaded zinc oxide nanoparticles regulates the Bax and Bcl-2 expression in breast and colon carcinoma. *Process Biochemistry* 49: 160–172
- Vinotha V, Iswarya A, Thaya R, Govindarajan M, Alharbie NS, Kadaikunnane S, Khalede JM, Al-Anbr MN, Vaseeharan B (2019) Synthesis of ZnO nanoparticles using insulin-rich leaf extract: Anti-diabetic, antibiofilm and anti-oxidant properties. *Journal of Photochemistry & Photobiology, B: Biology*. <https://doi.org/10.1016/j.jphotobiol.2019.111541>
- Vogelstein B, Lane D, Levine AJ (2000) Surfing the p53 network. *Nature* 408(6810): 307-310
- Von Roemeling C, Jiang W, Chan CK, Weissman IL, Kim BYS (2017) Breaking down the barriers to precision cancer nanomedicine. *Trends in Biotechnology* 35(2): 159–171
- Wahab R, Ansari SG, Kim YS, Khang G, Shin HS (2008) Effect of hydroxylamine hydrochloride on the floral decoration of zinc oxide synthesized by solution method. *Applied Surface Science* 254: 2037–2042
- Wahab R, Ansari SG, Kim YS, Seo HK, Kim GS, Khang G, Shin H-S (2007) Low temperature solution synthesis and characterization of ZnO nano-flowers. *Materials Research Bulletin* 42: 1640–1648
- Wahab R, Ansari SG, Seo H-K, Kim YS, Suh E-K, Shin HS (2009) Low temperature synthesis and characterization of rosette-like nanostructures of ZnO using solution process. *Solid State Sciences* 11: 439–443

- Wahab R, Hwang IH, Kim Y-S, Shin H-S (2011) Photocatalytic activity of zinc oxide micro-flowers synthesized via solution method. *Chemical Engineering Journal* 168: 359–366
- Wahab R, Kim YS, Hwang IH, Shin H-S (2009) A non-aqueous synthesis, characterization of zinc oxide nanoparticles and their interaction with DNA. *Synthetic Metals* 159: 2443–2452
- Wakaskar RR (2017) Cancer therapy with drug delivery systems. *J Pharmacogenomics Pharmacoproteomics*. <https://doi.org/10.4172/2153-0645.100e158>
- Wakaskar RR (2017) Brief overview of nanoparticulate therapy in cancer. *Journal of Drug Targeting*. <https://doi.org/10.1080/1061186X.2017.1347175>
- Walter P, Welcomme E, Hallégot P, Zaluzec NJ, Deeb C, Castaing J, Veysseyre P, Bréniaux R, Lévêque J-L, Tsoucaris G (2006) Early Use of PbS Nanotechnology for an Ancient Hair Dyeing Formula. *Nano Lett* 6: 2215–2219
- Wang F, Xue X, Wei J, An Y, Yao J, Cai H, Wu J, Dai C, Qian Z, Xu Z, Miao Y (2010) HsamiR-520h downregulates ABCG2 in pancreatic cancer cells to inhibit migration, invasion, and side populations. *British Journal of Cancer* 103(4): 567–574
- Wang G, Wang JJ, Yin PH, Xu K, Wang YZ, Shi F, Gao J, Fu XL (2019) New strategies for targeting glucose metabolism-mediated acidosis for colorectal cancer therapy. *J Cell Physiol* 234:348–368
- Wang H, Zhang T, Sun W, Wang Z, Zuo D, Zhou Z, Li S, Xu J, Yin F, Hua Y, Cai Z (2016) Erianin induces G2/M-phase arrest, apoptosis, and autophagy via the ROS/JNK signaling pathway in human osteosarcoma cells in vitro and in vivo. *Cell Death and Disease* 7: 2247
- Wang L, Chen C, Guo L, Li Q, Ding H, Bi H, Guo D (2018) Zinc oxide nanoparticles induce murine photoreceptor cell death via mitochondria-

- related signaling pathway. *Artificial cells, nanomedicine, and biotechnology* 46(S1): S1102–S1113.
- Wang M, Thanou M (2010) Targeting nanoparticles to cancer. *Pharmacological Research* 62(2): 90-99
- Wang MM, Wang J, Cao R, Si Y, Wang SY, Du H (2017) Natural transformation of zinc oxide nanoparticles and their cytotoxicity and mutagenicity. *Journal of Nanomaterials*. <https://doi.org/10.1155/2017/8457960>
- Wang P, Yang HL, Yang YJ, Wang L, Lee SC (2015) Overcome cancer cell drug resistance using natural products. *Evidence-Based Complementary and Alternative Medicine*. <https://dx.doi.org/10.1155/2015/767136>
- Wang Y, Liu J, Liu L, Sun DD (2012) Enhancing stability and photocatalytic activity of ZnO nanoparticles by surface modification of graphene oxide. *Journal of Nanoscience and Nanotechnology* 12: 1–7
- Wang Y, Zhang Y, Guo Y, Lu J, Yu X, Veeraraghavan VP, Mohan SK, Wang C, Yu X (2019) Synthesis of Zinc oxide nanoparticles from *Marsdenia tenacissima* inhibits the cell proliferation and induces apoptosis in laryngeal cancer cells (Hep-2). *Journal of Photochemistry & Photobiology, B: Biology*. <https://doi.org/10.1016/j.jphotobiol.2019.111624>
- Wang ZL (2004) Zinc oxide nanostructures: growth, properties and applications. *J. Phys.: Condens. Matter* 16(25) : R829–R858
- Weight CJ, Xiao S, Guo J, Hwa B, Villalta P, Tejpaul R, Krishna S, Murugan P, Turesky R (2017) Physiological evidence of DNA damage by carcinogens known to be present in charred and processed meats (PhIP DNA adducts) in a small cohort of patients with prostate cancer. *Journal of Clinical Oncology* 35(6): 580
- Wenzel ES, Singh ATK (2018) Cell-cycle Checkpoints and Aneuploidy on the Path to Cancer. *in vivo* 32: 1-5

- WHO (2017) Global priority list of antibiotic-resistant bacteria to guide research, discovery, and development of new antibiotics.accessible on https://www.who.int/medicines/publications/WHO-PPL_Short_Summary_25Feb-ET_NM_WHO.pdf.
- WHO (2018) International agency for research on cancer, Latest global cancer data accessible on https://www.iarc.fr/wp-content/uploads/2018/09/pr263_E.pdf
- WHO (2016) Quality control of Giemsa stock solution and buffered water. https://www.wpro.who.int/mvp/lab_quality/2096_oms_gmp_sop_03c_rev.pdf f 1-11., Accessed 11 February 2018.
- Wodarz D, Newell AC, Komarova NL (2018) Passenger mutations can accelerate tumour suppressor gene inactivation in cancer evolution. *J. R. Soc. Interface* <https://dx.doi.org/10.1098/rsif.2017.0967>
- Wolfram J, Ferrari M (2019) Clinical cancer nanomedicine. *Nano Today* <https://doi.org/10.1016/j.nantod.2019.02.005>
- Wong RSY (2011) Apoptosis in cancer: from pathogenesis to treatment. *Journal of Experimental & Clinical Cancer Research* 30: 87.
- Xia D, Ji W, Xu C, Lin X, Wang X, Xia Y, Lv P, Song Q, Ma D, Chen Y (2017) Knockout of MARCH2 inhibits the growth of HCT 116 colon cancer cells by inducing endoplasmic reticulum stress. *Cell Death and Disease*. <https://doi.org/10.1038/cddis.2017.347>
- Xie Y, He Y, Irwin PL, Jin T, Shi X (2011) Antibacterial activity and mechanism of action of zinc oxide nanoparticles against *Campylobacter jejuni*. *Applied And Environmental Microbiology* 77(7): 2325–2331
- Xu X, Ho W, Zhang X, Bertrand N, Farokhzad O (2015) Cancer nanomedicine: from targeted delivery to combination therapy. *Trends in Molecular Medicine* 21(4): 223–232

- Xu Y, Ren H, Liu J, Wang Y, Meng Z, He Z, Miao W, Chen G, Li X (2019) Switchable NO-releasing nanomedicine for enhanced cancer therapy and inhibition of metastasis. *Nanoscale*. <https://doi.org/10.1039/C9NR00732F>
- Yadav LSR, Pratibha S, Manjunath K, Shivanna M, Ramakrishnappa T, Dhananjaya N, Nagaraju G. (2019) Green synthesis of Ag - ZnO nanoparticles: structural analysis, hydrogen generation, formylation and biodiesel applications. *J Sci Adv Mater Dev* <https://doi.org/10.1016/j.jsamd.2019.03.001>.
- Yajid AI, Ab Rahman HS, Wong MPK, Wan Zain WZ (2018) Potential benefits of *Annona muricata* in combating cancer: a review. *Malays J Med Sci* 25(1): 5–15
- Yao Y, Dai W (2014) Genomic Instability and Cancer. *J Carcinog Mutagen* <https://doi.org/10.4172/2157-2518.1000165>
- Yeang CH, Beckman RA (2016) Long range personalized cancer treatment strategies incorporating evolutionary dynamics. *Biology Direct*. <https://doi.org/10.1186/s13062-016-0153-2>
- Yetisen AK, Qu H, Manbachi A, Butt H, Dokmeci MR, Hinstroza JP, Skorobogatiy M, Khademhosseini A, Yun SH (2016) Nanotechnology in textiles. *ACS Nano* 10: 3042–3068
- Yin X, Li Q, Wei H, Chen N, Wu S, Yuan Y, Liu B, Chen C, Bi H, Guo D (2019) Zinc oxide nanoparticles ameliorate collagen lattice contraction in human tenon fibroblasts. *Archives of Biochemistry and Biophysics* 669:1-10.
- Yoshinari GH, Jr, Fassoni AC, Mello LF, Rego EM (2019) Modeling dynamics and alternative treatment strategies in acute promyelocytic leukemia. *PLoS One*. <https://doi.org/10.1371/journal.pone.0221011>
- Youn YS, Bae YH (2018) Perspectives on the past, present, and future of cancer nanomedicine. *Advanced Drug Delivery Reviews* 130: 3-1

- Yousef MI, Mutar TF, Kamel MAE (2019) Hepato-renal toxicity of oral sub-chronic exposure to aluminum oxide and/or zinc oxide nanoparticles in rats. *Toxicology Reports* 6: 336–346
- Yu C, Tang H, Guo Y, Bian Z, Yang L, Chen Y, Tang A, Zhou X, Yang X, Chen J, Chen Z, Lv J, Li L (2018) Hot tea consumption and its interactions with alcohol and tobacco use on the risk for esophageal cancer: a population-based cohort study. *Ann Intern Med* 168(7): 489-497
- Yu D, Trad T, McLeskey Jr JT, Craciun V, Taylor CR (2010) ZnO nanowires synthesized by vapor phase transport deposition on transparent oxide substrates. *Nanoscale Res Lett* 5: 1333–1339
- Yu K-S, Shi J-Y, Zhang Z-L, Liang Y-M, Liu W (2013) Synthesis, characterization, and photocatalysis of ZnO and Er-doped ZnO. *Journal of Nanomaterials*. <https://doi.org/10.1155/2013/372951>
- Yuan Y-G, Zhang S, Hwang J-Y, Kong I-K (2018) Silver nanoparticles potentiates cytotoxicity and apoptotic potential of camptothecin in human cervical cancer cells. *Oxidative Medicine and Cellular Longevity*. <https://doi.org/10.1155/2018/6121328>
- Yusof HM, Mohamad R, Zaidan UH, Rahman NAA (2019) Microbial synthesis of Zinc oxide nanoparticles and their potential application as an antimicrobial agent and a feed supplement in animal industry: a review. *Journal of Animal Science and Biotechnology*. <https://doi.org/10.1186/s40104-019-0368-z>
- Yuvakkumar R, Suresh J, Nathanael AJ, Sundrarajan M, S.I. Hong (2014) Novel green synthetic strategy to prepare ZnO nanocrystals using rambutan (*Nephelium lappaceum* L.) peel extract and its antibacterial applications. *Materials Science and Engineering C* 41: 17–27
- Yuvakkumar R, Suresh J, Saravanakumar B, Nathanael AJ, Hong SI, Rajendran V (2015) Rambutan peels promoted biomimetic synthesis of bioinspired zinc

oxide nanochains for biomedical applications. *Spectrochimica Acta Part A: Molecular and Biomolecular Spectroscopy* 137: 250–258

Zak AK, Razali R, Majid WHA, Darroudi M (2011) Synthesis and characterization of a narrow size distribution of zinc oxide nanoparticles. *International Journal of Nanomedicine* 6: 1399–1403

Zhan T, Rindtorff N, Betge J, Ebert MP, Michael Boutros M (2019) CRISPR/Cas9 for cancer research and therapy. *Seminars in Cancer Biology* 55: 106–119

Zhang J, Ding M, Xu K, Mao L, Zheng J (2016) shRNA-armed conditionally replicative adenoviruses: a promising approach for cancer therapy. *Oncotarget* 7(20): 29824–29834

Zhang J, Qin X, Wang B, Xu G, Qin Z, Wang J, Wu L, Ju X, Bose DD, Qiu F, Zhou H, Zou Z (2017) Zinc oxide nanoparticles harness autophagy to induce cell death in lung epithelial cells. *Cell Death and Disease*. <https://doi.org/10.1038/cddis.2017.337>

Zhang R, Piao MJ, Kim KC, Kim AD, Choi J-Y, Choi J, Hyun JW. (2012) Endoplasmic reticulum stress signaling is involved in silver nanoparticles-induced apoptosis. *The International Journal of Biochemistry & Cell Biology* 44: 224–232.

Zhang X, Qin J, Xue Y, P Yu, Zhang B, Wang L, Liu R (2014) Effect of aspect ratio and surface defects on the photocatalytic activity of ZnO nanorods. *Scientific reports* 4: 4596.

Zhang X-F, Shen W, Gurunathan S (2016) Silver nanoparticle-mediated cellular responses in various cell lines: an *in vitro* model. *Int J Mol Sci* <https://doi.org/10.3390/ijms17101603>

Zhang Y, M.K. Ram, E.K. Stefanakos, D.Y. Goswami (2012) Synthesis, characterization, and applications of ZnO nanowires. *J Nanomater* <https://doi.org/10.1155/2012/624520>

- Zhang Y, Yang JM (2013) Altered energy metabolism in cancer. *Cancer Biology & Therapy* 14(2) : 81-89
- Zhao C-Y, Cheng R, Yang Z, Tian Z-M (2018) Nanotechnology for cancer therapy based on chemotherapy. *Molecules*. <https://doi.org/10.3390/molecules23040826>
- Zhao Y, Cao J, Melamed A, Worley M, Gockley A, Jones D, Nia HT, Zhang Y, Stylianopoulos T, Kumar AS, Mpekris F, Datta M, Sun Y, Wu L, Gao X, Yeku O, del Carmen MG, Spriggs DR, Jain RK, Xu L. (2019) Losartan treatment enhances chemotherapy efficacy and reduces ascites in ovarian cancer models by normalizing the tumor stroma. *PNAS* 116(6): 2210-2219
- Zhou C, Zhu Y, Lu B, Zhao W, Zhao X (2017) Survivin expression modulates the sensitivity of A549 lung cancer cells resistance to vincristine. *Oncology Letters* 16: 5466-5472
- Zhou J, Wang Y, Zhao F, Wang Y, Zhang Y, Yang L (2006) Photoluminescence of ZnO nanoparticles prepared by a novel gel-template combustion process. *Journal of Luminescence* 119(120): 248–252
- Zhou Z , Song J, Tian R, Yang Z, Yu G, Lin L, Zhang G, Fan W, Zhang F, Niu G, Nie L, Chen X. (2017) Activatable singlet oxygen generation from lipid hydroperoxide nanoparticles for cancer therapy. *Angew. Chem. Int. Ed.* 56: 6492 –6496
- Zhu P, Zhao N, Sheng D, Hou J, Hao C, Yang X, Zhu B, Zhang S, Han Z, Wei L, Zhang L. (2016) Inhibition of growth and metastasis of colon cancer by delivering 5-Fluorouracil-loaded pluronic P85 copolymer micelles. *Scientific Reports*. <https://doi.org/10.1038/srep20896>